SAMPLING AND PHARMACOKINETICS OF SKIN INTERSTITIAL FLUID FOR THERAPEUTICALLY MONITORED DRUGS

by

Veronika Schmitt

R.Ph., Ludwig-Maximilians University, 2010

A THESIS SUBMITTED IN PARTIAL FULFILLMENT OF

THE REQUIREMENTS FOR THE DEGREE OF

DOCTOR OF PHILOSOPHY

in

THE FACULTY OF GRADUATE AND POSTDOCTORAL STUDIES

(Pharmaceutical Sciences)

THE UNIVERSITY OF BRITISH COLUMBIA

(Vancouver)

December 2015

Abstract

To guide therapeutic decision making, the pharmacokinetics (PK) of certain toxic drugs are typically studied in blood. A drug's blood concentration is thus acting as a surrogate for its target site concentration. However, a drug's target is often extravascular and measuring tissue concentrations would be more meaningful. Furthermore, blood sampling is painful and can be challenging for some patients such as children, seriously ill, and old patients; it is, however, currently the standard method for drug testing.

Current research suggests that a tissue fluid called interstitial fluid (ISF) can be sampled in minimal amounts without pain and can be used to quantify certain drugs. However, to successfully use this fluid for therapeutic drug monitoring, researchers still face three main challenges: sampling ISF, determining the concentrations and PK of drugs in ISF and their relation to blood concentrations, and quantifying drugs in very small volumes.

To improve these challenges, we studied all three areas. First, we reviewed and evaluated methods of extracting ISF. Second, we studied ISF and blood concentrations of 13 drugs in a rabbit model to evaluate their PK. And third, we developed a method for quantifying a drug in just 2 µL of serum from rabbits. Currently available methods need larger sample volumes, whereas ISF is only available in small amounts.

We found that many of the drugs we tested in a single-dose study were readily detectable in ISF (vancomycin, gentamicin, methotrexate, cisplatin, carboplatin, valproic acid, phenobarbital, mycophenolic acid and theophylline) and their PK parameters were determined using non-compartmental analysis. Furthermore, steady-state concentrations were predicted from the single-dose study for blood and ISF. At equilibrium, ISF drug concentrations were higher (vancomycin and gentamicin) and more stable compared to blood concentrations. For

vancomycin these predictions were confirmed in an additional *in vivo* study. We further found that the concentration *vs*. time course of some drugs (vancomycin, gentamicin, methotrexate, valproic acid, phenobarbital, mycophenolic acid, digoxin and theophylline) could be well described by compartmental models.

This study shows that ISF can be a valuable matrix for therapeutic drug monitoring and merits further studies to ascertain its clinical utility.

Preface

The work presented was conducted in the Faculty of Pharmaceutical Sciences at the University of British Columbia. Animal studies were conducted at the Centre for Comparative Medicine at the University of British Columbia.

At the time of writing, parts of chapter 2 and 3 have been published in the following manuscripts:

1. [Kiang TKL, Schmitt V, Ensom MHH, Chua B, and Häfeli UO. Therapeutic Drug Monitoring in Interstitial Fluid: A Feasibility Study Using a Comprehensive Panel of Drugs. Journal of Pharmaceutical Sciences. 2012. Vol. 101 (4642-4652).] I was the second author responsible for collecting most of the data and some of the data analysis. I wrote part of the manuscript.

2. [Häfeli UO, Ensom MHH, Kiang TKL, Stoeber B, Chua B, Pudek M, and Schmitt V. Comparison of Vancomycin Concentrations in Blood and Interstitial Fluid: A Possible Model for Less Invasive Therapeutic Drug Monitoring. Clinical Chemistry and Laboratory Medicine. 2011. Vol. 49 (2123-2125).] I am last author of this paper and was responsible for the generation of a small amount of data.

Two more papers will be submitted before the publication of the thesis:

1. Part of Chapter 3 that has not been published before will be submitted as a single manuscript. The authors are Veronika Schmitt who generated most experimental data and performed all data analysis, Dr. Leonid Kagan who will help with further analysis and Dr. Urs O. Häfeli, supervisor and principal investigator on the grant that funded this project.

2. Chapter 5 will be submitted as a short communication. The authors are Veronika Schmitt who generated all experimental data and performed all data analysis. András Szeitz, who helped with the method development and was the technical advisor on the mass spectrometer, and Dr. Urs O. Häfeli, supervisor and principal investigator on the grant that funded this project.

All protocols involving *in vivo* research described in this thesis were reviewed and approved by the University of British Columbia Animal Care Committee (Certificate number of originally approved version A10-0149) and adhered to the guide to the care and use of experimental animals [1].

Table of Contents

List of Tables

List of Figures

List of Abbreviations

ABC	ATP-Binding Cassette
AUC	Area Under the Curve
AUMC	Area Under the First Moment Curve
C_0	Concentration at Time Zero
CA	Compartmental Analysis
C_{BLOOD}	Concentration in Blood/Serum/Plasma
CE	Collision Energy
C_{ISF}	Concentration in ISF
CL	Clearance
C_{max}	Maximum Concentration
C_{min}	Minimum Concentration (in multiple dosing schedules usually called $C_{trough)}$
CNS	Central Nervous System
C_{trough}	Concentration before next dose
CV	Coefficient of Variation
CXE	Collision Cell Exit Potential
D_L	Loading Dose
D_M	Maintenance Dose
DNA	Deoxyribonucleic acid
DP	Declustering Potential
ECF	Extracellular Fluid
EDTA	Ethylenediaminetetraacidic acid
F	Bioavailability
FDA	Food and Drug Administration
FPIA	Fluorescence Polarization Immunoassay
GABA	Gamma-Amino Butyric Acid
GHP	Polypropylene, hydrophilic
ICF	Intracellular Fluid
ICP-AES	Inductively Coupled Plasma Atomic Emission Spectroscopy
ISF	Interstitial Fluid
LADME	Liberation Absorption Distribution Metabolism Excretion
λ_Z	Terminal Elimination Constant
LCMS	Liquid Chromatography Mass Spectrometry
LCMS	Liquid Chromatography Mass Spectrometry
LLOQ	Lower Limit of Quantitation

LOC	Lab on a Chip
LogD	Octanol Water Distribution Coefficient
LogP	Octanol Water Partition Coefficient
LSS	Limited Sampling Strategies
ME	Mixed Esters
MEDA	Mini-Erosion Dermal Access
MEIA	Microparticle Enzyme Immunoassay
MF	Microfiltration
MIC	Minimal Inhibitory Concentration
mLSI	Microfluidic Large Scale Integration
MRM	Multiple Reaction Monitoring
MRT	Mean Residence Time
MW	Molecular Weight
MWCO	Molecular Weight Cutoff
NCA	Non-Compartmental Analysis
PAES	Polyarylethersulfone
PAN	Polyacrylonitrile
PBS	Phosphate Buffered Saline
PDMS	Polydimethylsiloxane
PE	Polyethylene
PES	Polyethersulfone
PETINIA	Particle Enhanced Turbidimetric Inhibition Immunoassay
PK	Pharmacokinetic(s)
POC	Point of Care
PTFE	Polytetrafluorethylene
PVC	Polyvinylchloride
PVDF	Polyvinylidene fluoride
QC	Quality Control
QH	Quality Control (High Range)
QL	Quality Control (Low Range)
QM	Quality Control (Mid Range)
R	Recovery Factor: $(1/\text{Recovery in \%}) \cdot 100$
RBC	Red Blood Cell
RNA	Ribonucleic acid
RSD	Relative Standard Deviation
S	Serum
SCF	Spontaneous Capillary Flow

SD	Standard Deviation
$T_{1/2}$	Half Life
TDM	Therapeutic Drug Monitoring
T_{max}	Time of Maximum Concentration
TPSA	Topological Polar Surface Area
T_S	Tacrolimus dissolved in serum
T_W	Tacrolimus dissolved in water
T_{WM}	Tacrolimus dissolved in water/methanol
UF	Ultrafiltration
UHPLC-MS/MS	Ultra High Performance Liquid Chromatography-Tandem Mass Spectrometry
UHPLC-UV	Ultra High Performance Liquid Chromatography-Ultraviolet Spectroscopy
ULOQ	Upper Limit of Quantitation
USP	United States Pharmacopeia
VEGF	Vascular Endothelial Growth Factor
V_D	Volume of Distribution
W	Water
WM	50% water/methanol mixture

Acknowledgements

I would like to thank my supervisor Dr. Urs Häfeli for his efforts to turn me into an independent and organized researcher. I also thank my advisory committee Dr. Mary HH Ensom, Dr. Benjamin Jung, Dr. Wayne Riggs, Dr. Boris Stoeber and the committee chair Dr. Judy Wong for their endurance, intellectual and moral support and guidance throughout graduate school.

I would also like to thank all members of the Häfeli lab for their support and other members of the Faculty of Pharmaceutical Sciences, who made my time a positive experience, most prominently Rachel Wu.

Specific individuals deserve a special mention for making the past couple of years in Vancouver particularly valuable. Christian always provides logical and humorous feedback to my scientific and non-scientific questions and, like me, can indulge in extensive discussions about almost anything. Todd always finds the shortest and most rational explanation for my many worries without having to indulge in discussions for more than five minutes, and taught me how to spend my free time outdoors. Ankur inspired me through his calm rational approachable personality and sarcasm. John is my idol.

I am also thankful to my friends and family in Germany: to my family, for continuously asking when I finally will be done with my degree and for providing some necessary funding; to my friends, predominantly Maren and Christiane, for never questioning how long I am planning to stay in Vancouver.

To Chester

Chapter 1: Introduction

Until the late 19th century, it was common practice to remove large amounts of blood from the human body in hopes of remedying most diseases. The basis for bloodletting was the medical theory of humorism, whose origins date back to the ancient Greek medicine around 400 years BC. The human body was thought to consist of four humors, namely blood, yellow and black bile, and phlegm, which are in balance for a healthy person. The sick person was thought to have an excess or deficit of one or more body fluids and bloodletting was the number one therapeutic choice (with the others being induced vomiting or urination). Most patients got weaker and never recovered, but as nobody had a better explanation of the human body or was accused of witchcraft for a better idea, bloodletting continued on well into the late 19th century. Nowadays, we know that only a few diseases can be treated with bloodletting, such as chronic iron overload and a pathologically elevated hematocrit. We also know that blood transports everything our body needs to function and that analyzing blood components can give us an idea of a patient's health status. In fact, many doctors' visits involve having a blood sample taken for analysis. Medicine has become so advanced that even a small amount of blood can give us information about our genetic makeup, diseases that we had, currently have or might develop in the future. Biomolecules or drug concentrations can be measured in blood with great accuracy, and are interesting to study, regardless if the drug was taken for recreational use or therapy. Monitoring of drug concentrations usually aims to improve a patient's drug therapy by early recognition of drug concentrations that are too low (sub-therapeutic) or too high (toxic). This is known as therapeutic drug monitoring (TDM). Beginning in the late 1960s and early 1970s, the monitoring of drug concentrations was found to have a positive impact on patient health by reducing drug-related toxicities [2]. For example, drug-related toxicities in patients taking

1

digoxin were monitored in two hospitals over two years. In hospital A, 10% of 272 patients suffered from adverse drug reactions but in hospital B only 4% of 291 patients did. Closer analysis revealed that hospital B performed three times as many digoxin assays as hospital A. The overall drug levels were lower and better controlled in hospital B due to better monitoring of drug concentrations. The conclusion was that closer monitoring of drug concentrations can reduce the number of adverse reactions to digoxin, most prominently cardiac dysrhythmias. Ongoing research on TDM has resulted in an updated list of drugs which can be monitored and how that monitoring is best achieved (i.e., what concentration range is best targeted and at what time after administration [3-8]). Drugs for which monitoring is often recommended usually have a narrow therapeutic index and show high inter-patient variability in drug concentrations. Many aspects of TDM, however, remain debatable including the concomitant administration of other drugs [9], the correct interpretation of results and the cost-effectiveness of TDM [10].

The choice of biological fluid to be used for monitoring is also ripe for investigation. For drugs that do not show an easily measureable physiological effect (e.g., blood pressure), often blood concentrations are better predictors of the drug effect than just the dose. However, concentrations of a drug outside the blood vessel (e.g., in tissues) could also be valuable, since most drugs have to leave the blood circulation to reach the site of action.

We studied drug concentrations outside the blood vessels to gain a better understanding of the PK of drugs in tissues, thereby contributing to the future effectiveness of therapeutic drug monitoring.

1.1 Body Fluids and Endothelial Barrier Function

1.1.1 Fluids of the Human Body

In simple terms, the human body consists of water, solutes and water insoluble material. Body fluids have been described in great detail in Peter A. Stewart's Textbook of Acid-Base [11]. To summarize, the human body is usually about 60% water, which is equivalent to 42 L aqueous solution in a standard male adult of 70 kg. The aqueous component can be subdivided into 25 L of intracellular fluid (ICF), of which 2 L are contained in red blood cells, and 17 L extracellular fluid (ECF). There are many different cell and tissue types in the human body that perform specific tasks and therefore need a specific composition, so ICF and ECF are two separate entities that are inhomogeneous among themselves. However, a major difference in ion concentrations justifies viewing them as separate extracellular and intracellular aggregates. ICF is high in potassium and magnesium and low in sodium and chloride, whereas ECF contains low amounts of potassium and magnesium and high concentrations of sodium and chloride. Furthermore ICF is high in organic acids whereas ECF contains negligible amounts of it.

Both the ICF and ECF aggregates can be further separated into subdivisions as sketched in Figure 1. ECF is found outside the cells and can be subdivided into blood plasma (3 L), interstitial fluid (13.5 L) and others (0.5 L). These other fluids are sometimes called transcellular fluids and consist of aqueous humor, synovial and bursal fluid, bile, saliva, gastric and pancreatic juice. ICF is, as the name implies, all fluid that resides within a cell.
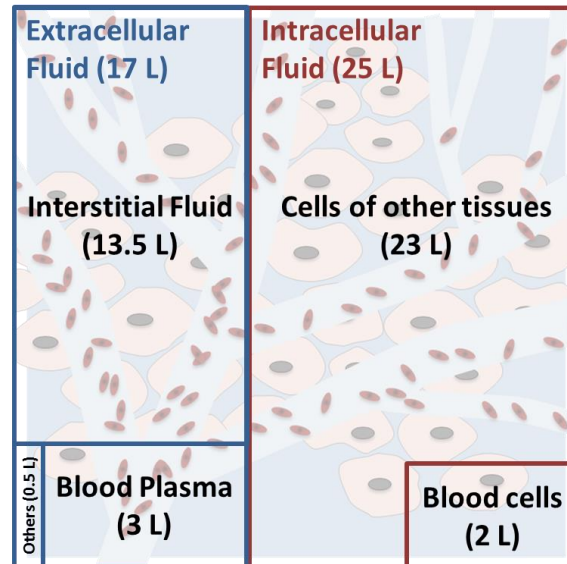
Figure 1. Subdivisions of fluids in the human body as given by [11].

The largest fluid unit is ICF (25 L) and the second largest is interstitial fluid (ISF, 13.5 L). Both ICF and ISF are usually referred to as pooled entities (idealized fluid), even though ISF consists of small pockets and ICF of many tiny drops. Only blood plasma, the third largest fluid unit (3 L), is an actual pooled entity and is therefore most conveniently sampled for medical purposes.

Regarding volume and distribution of body fluids, other researchers came to conclusions similar to Stewart's. According to Levitt, water makes up 43% of the total body water of 17.2 L and skin and connective tissue hold 70% of the total extracellular water fraction (12 L) [12]. According to John E. Hall and Arthur C. Guyton the adult body is 60% water [13]. One third of this water is present in the extracellular space (plasma, ISF and transcellular fluid) and four fifths of it is ISF (=11 L). The Clinician's Pocket Reference gives numbers for ICF of 28 L, ECF 14 L, plasma 3.5 L and ISF 10.5 L [14].

To summarize, estimates of ISF volume are from 9 to 12 L [15], depending on age and health status. Although these estimates vary, the volume of ISF is still much greater than the volume of blood plasma and thus sampling ISF instead of blood might be possible in the future for

diagnostic and therapeutic measures. The largest amounts of ISF are found in the skin [12, 15], so a minimally invasive extraction of ISF from the epidermis is feasible. Changes in ISF reflect changes in a patient's water balance, which can be affected, for example, by hydration, certain diseases, drugs or inflammation. We therefore suggest that ISF reflects a patient's health status at least as well as blood.

1.1.2 Blood and Plasma

The total blood volume makes up 8% of human body weight: about 5.2 L for an average women of 65 kg and 5.6 L for an average male of 70 kg [14]. Blood consists of a cellular part (and therefore ~2 L ICF) and a non-cellular aqueous part of 3 L and is restricted to our cardiovascular system. For medical purposes, blood often needs to be treated and separated into its cellular and non-cellular parts for further analysis.

Separation of blood by centrifugation into its cellular and non-cellular parts results in 45% red blood cells, < 1% white blood cells and platelets, and 55% plasma or serum. On average, the male's red blood cell mass (20-36 mL/kg) is slightly higher than the female's (19-31 mL/kg) [14]. Depending on how the blood has been treated before centrifugation, the aqueous part is called serum or plasma. Untreated clotted blood produces serum without clotting factors (most prominently Factor I: fibrinogen), whereas treated non-clotted blood (e.g., with sodium citrate, sodium or lithium heparin, potassium EDTA, potassium oxalate and sodium fluoride) produces plasma, still containing all clotting factors. Recommended centrifugation speeds for serum and plasma are 1000-2000 x g for 10 min at 4°C and for plasma without platelets: 2000 x g for 15 min at 4°C [16]. After centrifugation, it is often therapeutically relevant to know the approximate number of certain blood cell populations (e.g., lymphocytes, erythrocytes), whereas the non-cellular liquid is needed for drug analysis.

5

The cell-free liquid plasma or serum consists of 90% water and 10% solutes. The solutes include electrolytes (e.g., sodium, chloride, potassium, calcium, magnesium, bicarbonate, and phosphate), protein (e.g., albumin, α_1-, α_2-, β-, and γ- globulins), hormones, nutrients (e.g., glucose) and metabolites (e.g., lactate, pyruvate, creatinine, creatine, uric acid). Blood and its solutes circulate rapidly and there is a diffusion equilibrium for many solutes into ISF except for macromolecules [11] and specific ions that are transported actively against a concentration gradient.

1.1.3   Interstitial Fluid: Location and Volume

ISF is the major part of extracellular fluid (13.5 L) and "bathes" [11] most cells in the body. It is divided from blood plasma by a single layer of endothelial cells and is well distributed in the interstitial space (interstitium). The interstitium is defined as the space between the capillary wall and the cell [17] and represents a matrix for cellular nutrition, hydration and communication. Aukland and Nicolaysen [15] write that ISF provides a framework for parenchymal cells and is also the transport medium for nutrients and waste products between cells and capillary blood. ISF is called a fluid; however, the sizes of the liquid filled spaces are micrometer-thin layers or filled pockets in the interstitium. Those liquid spaces are so small that the whole entity of the interstitial matrix and ISF is better described as a gel-like structure. The gel consists of the interstitial matrix made of collagen fibers, glycosaminoglycans, and elastin [15, 17] with the occasional ISF pocket distributed throughout. Apart from a small amount of plasma proteins and hyaluronan (a glycosaminoglycan), ISF is supposed to contain negligible amounts of protein and other organic acids [11]. Some sources even described the presence of proteins in the interstitial space as a slow "leak" from the vasculature [18]. From our measurements in rabbits, an ISF protein content of 7.9 ± 5.5 g/L (n = 5) and a serum protein content of 55.9 ± 3.0 g/L (n = 5) was

6

determined (normalized to BSA). For this measurement, microfiltration (pore size 0.2 µm) was used to extract ISF.

However, more recent studies that used hemodilution to indirectly determine the amount of protein in ISF found higher amounts of protein in humans: as high as 20.6 g/L in comparison to plasma at ~ 70 g/L [19] (Table 1).

Table 1. The mean plasma concentrations of proteins and salts in 20 subjects during standing and after 10 min in supine positions; Concentrations in ISF (mmol/L) have been estimated based on hemodilution from standing to supine and differences have been confirmed by paired t-tests [19].

	Standing	Supine	Interstitial Fluid
Total Protein (g/L)	73.7	68.6	20.6
Albumin	0.676	0.630	0.188
Total Calcium	2.365	2.288	1.551
Ca2+ (at pH 7.4)	1.257	1.250	1.183
Total Magnesium	0.887	0.866	0.666
Mg2+ (at pH 7.4)	0.532	0.530	0.506
Total Sodium	138.8	138.4	134.6
Total Potassium	4.28	4.17	3.17
Total CO2	29.7	29.2	23.9
Phosphates	1.177	1.123	0.610

1.1.4   Fluid Movement between Plasma and ISF and Filtration Pressure

From the plasma compartment, fluid moves continuously through the endothelial cells to the ISF compartment, then to the lymph compartment to finally return to the circulation again [18]. Plasma, ISF and lymph are different forms of the same liquid, varying in composition, but travelling through the same compartments over and over again. With the exception of plasma proteins, the plasma volume is completely turned over every nine hours [18], thereby moving water and electrolytes as well as other molecules throughout the body.

The main driving forces for fluid movement are colloid osmotic absorption pressure (caused by plasma proteins) and capillary hydraulic pressure that is due to the heart beat [18]. These oncotic and hydrostatic forces are known as the Starling forces and are part of the classic Starling

7

principle which describes the net driving force for fluid filtration of a solvent through a capillary

bed (Figure 2). On the arterial end of the blood capillary, the hydrostatic pressure is larger than

the osmotic pressure so tissue fluid is formed at the arterial end of the vessel. At the venous end,

most of the tissue fluid (90%) will return to the small veins due to the higher oncotic pressure

(mostly created by the plasma proteins) and negligible hydrostatic pressure inside the vessel.

Only some (10%) of the tissue fluid will be taken up by lymph vessels. If there is an imbalance

in pressure differences (high pressure in vasculature, protein deficiency), leaky vasculature

(inflammation) or problems in the lymphatic back-transport of fluids and protein, more tissue

fluid can accumulate (edema).

A Revised Starling Principle

$$F = (P_c - P_g) - \sigma(\pi_p - \pi_g)$$

B Classic Starling Principle

$$F = (P_c - P_i) - \sigma(\pi_p - \pi_i)$$
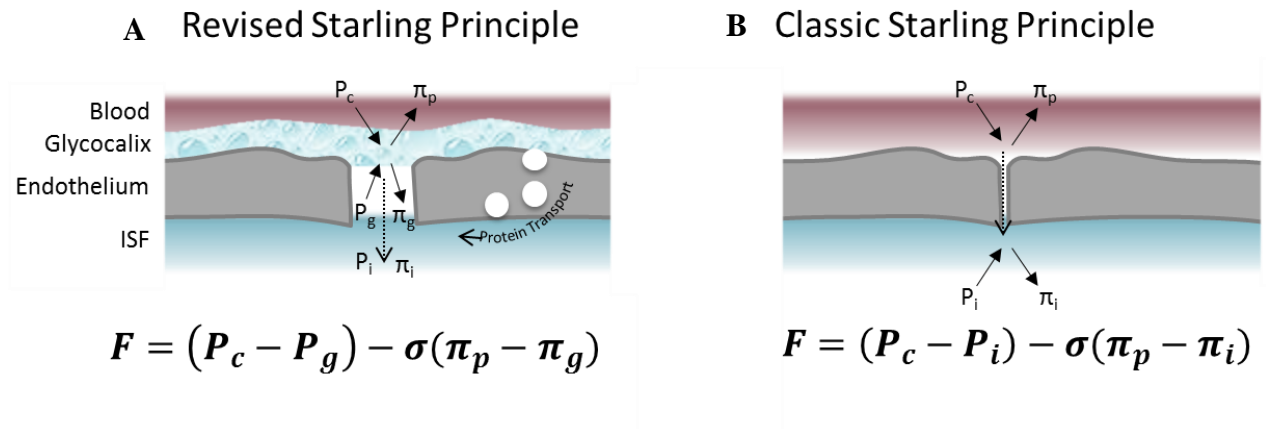
Figure 2. Distribution of forces across the continuous endothelium, paracellular space in A is enlarged for clarity. A) the revised and B) the classic Starling principle. F is the sum of forces across the membrane, P_c is the capillary pressure, P_i is the interstitial pressure, P_g is the pressure in the subglycocalix space, σ is the reflection coefficient, π_p is the plasma protein osmotic pressure, π_i is the interstitial protein osmotic pressure, π_g is the osmotic pressure in the subglycocalix space. Adapted from [18].

This classic Starling equation has been accepted for decades, but it has recently been revised and

is now often referred to as the glycocalix model of transvascular fluid exchange [18, 20]. Two

major concerns were connected to the Starling principle. First, it was experimentally confirmed

that a reabsorption of liquid into the vasculature cannot be maintained over time, likely due to an

increase of the interstitial osmotic pressure π_i. Second, the capillary filtration rate calculated from the Starling forces is much greater than the actual lymph production [21, 22].

The revised model views the filtration barrier as a gap between cells (= paracellular) that is covered with a glycoprotein layer instead of the long accepted "small pore theory of the endothelium". The glycoprotein layer (glycocalix) serves as an ultrafiltration space. The protein content and pressure inside the gap is separate and different from ISF (bulk osmotic pressure of ISF π_i > osmotic pressure in gap π_g). The protein content of ISF is much higher than in the subglycocalix space as it is transported through a different pathway and would have to diffuse into the paracellular space against a current of fluid. In addition to this osmotic asymmetry in continuous endothelium, another important finding is that tissue fluid balance is not managed by venular absorption. During reabsorption of liquids, π_g would increase drastically and hinder further absorption, and therefore most fluids are transported back to the circulation via the lymph.

Lymph is part of the ISF entity and has been described as the overflow tissue fluid that plays an important role in protein transport back to the circulation [11]. Lymph is collected via blind-ended lymphatic vasculature and transported via the thoracic duct and the right lymphatic trunk. These major lymphatic vessels drain into the left and right subclavian vein and return lymph to the venous system at a rate of 1-2 L/day with a protein concentration of 20-30 g/L [23]. This connection back to blood lets the fluid travel through the body again, with its total volume and partitioning guided by pressure and concentration differences.

Total extracellular fluid (plasma, lymph and ISF) volume is maintained practically constant [15, 17], which is important for an adequate perfusion and hydration of tissues and organs. A recent commentary focused on interstitial fluid pressure, the importance of constant ISF volume as well

as the relation of ISF pressure to kidney disease [24]. Interstitial fluid pressure is negative in healthy controls (- 0.9 mm Hg) whereas patients with chronic kidney disease have elevated ISF pressures (4.6 mm Hg) [25]. Although it is not clear how ISF pressure and contents are adjusted in humans, several recent articles have contributed to our understanding of ISF homeostasis. In animals, a volume adjustment of ISF takes place locally through β1-integrin mediated contraction of collagen fibrils [26]. Furthermore, macrophages play an important role in the electrolyte adjustment of skin interstitial fluid: high sodium levels have been measured in the tissues during salt-sensitive hypertension, surprisingly without retention of water in the interstitial space. Instead, hyperplasia of the lymph-capillary network through a macrophage-mediated secretion of VEGF-C has been observed [27]. Lymph capillary electrolyte clearance is also coupled with systemic blood pressure control.

Together, intravascular (blood) and extravascular (ISF, lymph) pressure, volume and the compartment's contents of endogenous molecules play an important role in diseases. Furthermore, the distribution of exogenous drug molecules is also of interest and can increase the understanding of diseases.

1.1.5   Microvascular Exchange

Microvascular exchange describes how molecules travel across barriers in the human body. A large number of reviews on the transport processes guiding microvascular exchange and on endothelial permeability are available [18, 28-33]. Fluids in the body do not travel freely but are restricted by selectively permeable barriers formed by linings of interconnected cells. Two important types of linings are epithelial and endothelial cells.

Epithelial cells are multiple layers of interconnected cells that rest on a basal lamina, a type of extracellular matrix, and cover surfaces of the body. These organized tissues are in contact with the outside environment in the form of skin, airways and the digestive tract.

Endothelial cells are a specific type of epithelium that lines the inside of the vasculature, such as blood vessels and lymph vessels, as an interconnected cell layer sitting on a basement membrane. The characteristics and thickness of the endothelium vary with body site and function. Arterioles with diameters of up to 100 µm have also a layer of smooth muscle. However, the thin endothelium of the peripheral capillaries, which are 5 to 10 µm in diameter, is only one cell-layer thick and attached to a basement membrane by integrins [28]. These capillaries are very important for drug exchange and will be discussed in the following paragraphs.

Capillaries can be highly specialized and divided into different groups depending on their permeability, usually guided by the continuity of the cell lining, the number of cell-cell connections (adherens junctions, tight junctions, gap junctions) and the integrity and specialization of the basement membrane. There are sinusoidal, fenestrated and continuous capillaries. Sinusoidal capillaries are found in the bone marrow and have large clefts between the endothelial cells and a discontinuous basement membrane resulting in pores of 30-40 µm that allow whole cells to squeeze through. Fenestrated capillaries of the glomerulus of the kidney are extremely leaky (pores of 60-80 nm) but generally will not allow proteins to pass. Continuous capillaries are found in most body parts and are permeable to water and solutes, but also allow the exchange of oxygen, carbon dioxide and other nutrients. There is a specialized form of continuous capillary, found in the central nervous system (CNS) which is often referred to as the blood-brain barrier. It is almost impermeable to molecules and sealed through tight junctions surrounded by the basal membrane and another cell layer of glia cells (Figure 3).
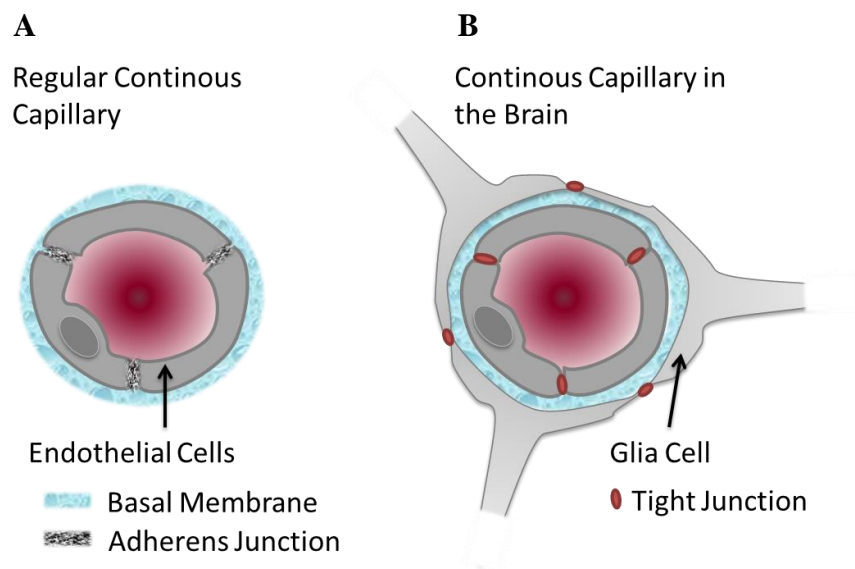
Figure 3. Two types of continuous capillaries, A: regular continuous capillary, B: continuous capillary in the brain, adapted from [34].

As mentioned, continuous peripheral capillaries are important anatomical barriers for drug exchange. Drug exchange happens in the continuous capillaries through a single layer of endothelium cells surrounded by a network of glycans and protein. This network is called the basal membrane (glycocalix). There are different ways a molecule can get from one side of the endothelial cells to the other and the basal membrane plays an important role.

The basal membrane spans the gaps between the endothelial cells like a microdialysis membrane only allowing molecules smaller than 10 kDa to pass freely [34]. The number and extent of cell-cell junctions varies between continuous capillaries. Adherent junctions in the capillary bed usually exclude molecules larger than 3 nm in diameter (e.g., albumin with a molecular weight (or MW) of 69 kDa, and a molecular radius of 3.6 nm) whereas tight junctions result in mean pore sizes of 1 nm [32].

Molecules cannot only pass between the endothelial cells (inter/paracellular route) but also through the cell body (transcellular route) [28]. The transcellular route is important for the

transport of macromolecules and usually happens by the formation of vesicles (diameter 70 nm) or tunnel-like structures through the endothelial cell. It is reported that vesicle formation (caveolae) and endocytosis is triggered by albumin binding to glycoprotein 60 receptors (gp60) on the apical endothelial membrane and by Src-kinase mediated phosphorylation of caveolin-1 at the endothelial luminal membrane. Vesicles shuttle molecules from the apical to the basolateral membrane (transcytosis) to deliver them into the interstitial fluid by exocytosis. In addition, clusters of interconnected vesiculo-vacuolar organelles can form a tunnel-like structure of 80 to 200 nm [28], allowing macromolecules to pass.

In order to use any of the above described mechanisms, molecules first have to reach the area of interest. While blood transports molecules to all areas in the body, the rate of blood perfusion depends on the organ.

1.1.6 Rate of Blood Perfusion

The rate of blood perfusion plays an important role for the accumulation and distribution of molecules throughout the body. Skin receives about 6% of the total cardiac output (Table 2) which equals 300 mL/min. Therefore, when comparing blood concentrations of certain drugs to ISF concentrations, this perfusion limitation can be reflected in the total drug measured in skin ISF. If the drug exposure is very short term and the drug does not cross the endothelial cells easily, ISF concentrations can be low or undetectable. However, if the drug exposure is extended, which is often the case (e.g. multiple doses), or the drug can leave the circulation easily, extravascular drug concentrations can be high despite a limited perfusion. How easily molecules can permeate membranes is related to their physicochemical properties, which are described in more detail in the next chapter.

13

Table 2. Blood flow to different organs and tissues under basal conditions [35].

Organ	%	mL/min	mL/min/100 g
Brain	14	700	50
Heart	4	200	70
Bronchi	2	100	25
Kidney	22	1100	360
Liver (total)	27	1350	95
Portal	(21)	1050	-
Arterial	(6)	300	-
Muscle (inactive state)	15	750	4
Bone	5	250	3
Skin (cold weather)	6	300	3
Thyroid glands	1	50	160
Adrenal glands	0.5	25	300
Other tissues	3.5	175	1.3
Total	**100**	**5000**	

1.1.7   Physicochemical Properties of Drugs and Microvascular Exchange

A drug molecule administered to the human body has to find its target quickly. This is a difficult task. Many obstacles such as cellular barriers, possible binding partners and the molecule's own properties determine its ultimate fate. The molecule's own properties are discussed further in the following paragraphs.

Most drugs are below 500 Da and are referred to as "small molecules". Their targets are often proteins (enzymes, receptors, ion channels, transporters, cytoskeletal proteins), but can also be DNA, as for anticancer drugs, RNA, as for antibiotics, or lipid membranes as for antibiotics and narcotics [34]. How a drug, that has been administered intravenously, interacts with blood components or permeates biological barriers depends on its physicochemical properties, including size (molecular weight), solubility (water solubility), lipophilicity (octanol/water partition coefficient or logP), polarity (polar surface area, H-donor groups, H-acceptor groups),

14

acidity (pKa) and flexibility (rotable bonds). Using some of these properties, rules have been derived to estimate a drugs behavior in a biological system.
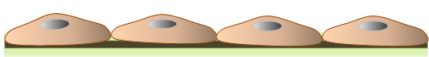
A popular rule is Lipinski's rule of 5 (Ro5) which is used to estimate the solubility, absorption and permeation characteristics of drugs. It is often applied to oral bioavailability and focuses on properties such as the number of H-donors and acceptors, the molecular weight and the logP value. According to the Ro5 a drug molecule is more easily absorbed in the gastrointestinal tract through the epithelial cell lining if there are less than 5 H-bond donors (expressed as the sum of –OH and –NH groups), the molecular weight is smaller than 500 Da, the logP is smaller than 5 and if there are less than 10 H-bond acceptors (expressed as the sum of N's and O's). The rule is based on a distribution of calculated properties among several thousand drugs. Antibiotics, antifungals, vitamins and cardiac glycosides are orally active but lie outside the rule of 5 [36]. Substrates for biological transporters are exceptions to the rule as well.

Rules like the Ro5 could be applied or constructed for other environments, such as for the crossing of drugs into ISF. The distribution of drugs into ISF would be important for drugs that have their target in the tissue but also for the understanding of extravascular drug distribution in general. Such a rule would be different than the Ro5, but some similarities might be seen and drugs with good oral bioavailability might also be useful for ISF detection. The following paragraph outlines the differences and commonalities in epithelial linings to support this supposition (see also chapter 1.1.5 for epithelial and specifically endothelial cells).

Epithelial cells line body surfaces. Based on their shape and the arrangement of cells (layering), they are divided into groups [37]. Epithelial cells are anchored on a basal lamina that together with connective tissue forms the basement membrane. It is an important supporting and nourishing sheet of fibrous extracellular matrix [38]. Both the lining of blood vessels and the

intestinal lining are types of simple epithelia that are one cell layer thick. Drug permeation
through these linings is therefore similar. But differences exist between the epithelium that lines
blood vessels (simple squamous epithelium) and the lining of the small intestinal walls (simple
columnar epithelium) (Table 3). Most prominently the cells differ in shape and apical
differentiations and therefore in their surface area. Furthermore, the intestinal epithelium is
spiked with P-glycoprotein 1 (Pgp-1) transporters of the ATP-binding cassette (ABC)
continuously pumping drugs back into the intestinal lumen which makes absorption through the
intestinal wall much more difficult than "just" crossing an epithelial cell barrier of a blood
vessel.

Table 3. Comparison of simple squamous and simple columnar epithelium of blood vessel and intestinal lumen.

	Simple squamous epithelium (=endothelium)	Simple columnar epithelium
Location (example)	Lining of blood vessels	Intestinal lining
Cell shape	Flattened	Taller than wide
Apical differentiations	None	Microvilli
Function	Diffusion and filtration barrier, secretion	Absorption barrier, transport, secretion
Transporters of the ATP-binding cassette (ABC)	None	P-glycoprotein 1 (Pgp-1) transporters

The binding of a drug to cellular structures or proteins plays an important role on its way to the
site of action. Most drugs have to leave the circulation to get to the site of action and regardless
of whether a drug is in the blood or ISF, we can divide its concentrations always into two
overarching groups: protein/cell/tissue bound and free drug. The free drug which passes the

endothelial cells easier is often referred to as the active drug, whereas the bound drug acts as a drug reservoir, from which drug can be released.

Knowing the amount of free and protein bound drug in the tissue can be interesting for therapy, because for many drugs, the interstitial space is closer to the site of action than blood.

To summarize, it is challenging for a drug to reach its target due to many obstacles. But how much drug crosses membrane barriers to the site of action, how long drug stays there and how much of it can be detected is an interesting field of study. It depends on many factors, some of which have been discussed here, such as the molecules' physicochemical properties, organ blood perfusion, membrane properties and protein binding. All these factors determine how the molecule will be treated by the body, which is the main concept of PK and will be briefly discussed in the next chapter.

1.2 A Very Short History of Pharmacokinetics

In Germany in 1953, the term pharmacokinetics was first used. In particular, in his publication "Der Blutspiegel: Kinetik der Konzentrationsabläufe in der Kreislaufflüssigkeit"[1], F. H. Dost described blood levels, kinetics and concentration changes in circulating body fluid [39]. Some of the concepts currently used in the field of PK were published much earlier than 1953 though, including the description of the Michaelis-Menten Equation by Leonor Michaelis and Maud Menten in 1913 [40].

In simple terms, PK describes the movement of a molecule in the body and how the body treats the molecule. More specifically, PK studies are related to the absorption, the distribution, the metabolism and the excretion (ADME) of substances that have been administered to the body.

---

[1]Translation: "The Blood Level: The Kinetics of Concentration Changes in the Circulation"

As formulated by Gibaldi and Levy in 1976, "the relationship of these processes (ADME) to the intensity and time course of therapeutic and adverse effects of drugs" is the main purpose of PK and it "involves the application of mathematical and biochemical techniques in a physiologic and pharmacologic context" [41]. Milo Gibaldi, Gerhard Levy and Donald Perrier are pioneers and founders of some of the mathematical concepts of PKs. Their seminal publication "Pharmacokinetics" from 1982 [42] summarizes most important concepts to that date and is a well-known textbook of basic PKs.

1.2.1   Pharmacokinetic Parameters

PK parameters describe the fate of a drug in the human body. Their derivation can be tedious and often requires rich data sets of drug concentration *vs.* time data. Some parameters, such as the dose (D) and the dosing interval (τ), are fixed design parameters while others, such as the maximum and minimum concentration (C_{max} and C_{min}) and the time of maximum concentration (t_{max}), can be directly measured. Other parameters can be estimated from the PK data set, such as the elimination rate constant (λ_z or k_{el}), the terminal-phase half-life ($t_{1/2}$), the area under the concentration *vs.* time curve (AUC), drug clearance (CL) and the volume of distribution (V_d). V_d is often called the apparent volume of distribution because it is not a physical space but a proportionality constant between the plasma concentration and the amount of drug in the body. Therefore the volume of distribution can be larger than the total body volume but it is not smaller than the plasma volume. Factors determining the value of V_d for a specific drug are the physiologic properties of the body (e.g., CL) and the physicochemical properties of the drug (e.g. drug partitioning, protein binding). There are three types of V_d that are often determined for a drug: the initial volume of distribution (V_c), the terminal volume of distribution for plasma concentrations measured at pseudo-equilibrium (V_z or V_{area}) and the volume of distribution when

18

plasma concentrations are measured in steady-state conditions (V_{ss}) [43]. If the plasma concentration is measured during the phase of drug distribution, the ratio of the drug amount to plasma concentration is a time dependent variable.

To determine PK parameters multiple approaches can be taken. Some approaches see the whole body as one single space where drug goes in and out and some approaches divide the body into logical subdivisions (compartments) that interact with each other.

1.2.2   Pharmacokinetic Data Analysis

A first approach to PK data analysis is called non-compartmental or statistical moment analysis. In this approach, no model assumptions are made and the PK parameters are directly read and calculated from the given data. PK parameters of the non-compartmental approach are:

- C_{max}, the maximum concentration measured or maximum exposure [e.g., in mg/mL],

- t_{max}, the time when the maximum concentration was reached [e.g., in h],

- CL, the clearance or amount of fluid that is cleared from drug per time [e.g., in mL/h],

- F, the bioavailability or the fraction of administered drug that reaches the systemic circulation [in %],

- AUC, the area under the concentration *vs.* time curve [e.g., in mg·h/L],

- AUMC, the area under the first moment curve or the area under the concentration ·time *vs.* time curve [e.g., in mg·h·h/L],

- V_d, the volume(s) of distribution or proportionality constant(s) between total amount of drug in the body and plasma concentrations [e.g., in mL/kg],

- $t_{1/2}$, the terminal half-life or the time it takes for the concentration to drop to half the concentration [e.g., in h],

19

- MRT, the mean residence time or the mean time every drug molecule resides in the body [e.g., in h].

Using the non-compartmental approach and assuming linear PK, it is possible to predict specific concentrations using non-parametric superposition. However, for the prediction of full concentration time courses in blood and other tissues, a model that describes the data set is necessary. This is called the compartmental approach and it sees the body as being made up of different compartments with transfer rates between the compartments. Using differential equations, exponential equations can be derived to describe the data and PK parameters calculated.

1.3 Therapeutic Drug Monitoring

1.3.1 Definition of Therapeutic Drug Monitoring

Therapeutic drug monitoring (TDM) is the measurement of specific drug concentrations in serum, plasma or whole blood in order to determine the correct individual drug dose and/or to check for a patient's compliance. Even better than knowing a single concentration is to know the area under the concentration vs. time curve (AUC) for a drug. The AUC is an important parameter because it represents a patient's total exposure to a drug. Directly related to the drug exposure is the patient's chance of being treated successfully or of experiencing toxic effects. Unfortunately, the more accurate determination of the AUC is difficult as its computation relies on 10 to 15 data points over a dosing interval. Taking 10 to 15 blood samples after the administration of a drug to the patient is clearly problematic, so the AUC is either estimated from a limited number of samples or specific single sample concentrations are used and compared to a reference range.

Luckily it is not necessary for most drugs to know the exact AUC or blood concentrations. Most drugs do not require monitoring because they do not show serious side effects even in higher concentrations and their physiological effect (e.g., absence of pain, decrease of blood pressure) can be monitored non-invasively. Most drugs have a large therapeutic window, which means that the effective concentration is much lower than the toxic concentration.

The drugs that are most likely to be monitored are those which exhibit a narrow therapeutic window (Figure 4), show a high inter-patient variability of PK parameters representing absorption, distribution, metabolism and excretion and show no clear physical measure to determine drug efficacy (e.g., blood pressure). TDM is thus regularly performed for several anticonvulsants (e.g., valproic acid, phenobarbital, phenytoin), cardioactive drugs (e.g., amiodarone and other antiarrhythmics), immunosuppressants (e.g., tacrolimus, cyclosporine, mycophenolic acid), some antibiotics (e.g., vancomycin, gentamicin), theophylline, psychoactive agents (e.g., tricyclic antidepressants, lithium) and antineoplastic drugs (e.g., methotrexate) and it has been suggested for antiretroviral drugs [44]. The establishment of target concentration ranges (Table 4) is not trivial and has led to recommendations that are accepted, but might not be optimal, particularly not for patients who suffer from multiple medical conditions, or for children [45]. In addition, tethering patients to a target range is only useful if the drug concentration correlates with the effect in a known relationship. Monitoring should protect the patient from low-dose treatment failures (efficiency) and high-dose toxicities (safety), and should minimize costs related to drug therapy and hospitalization.
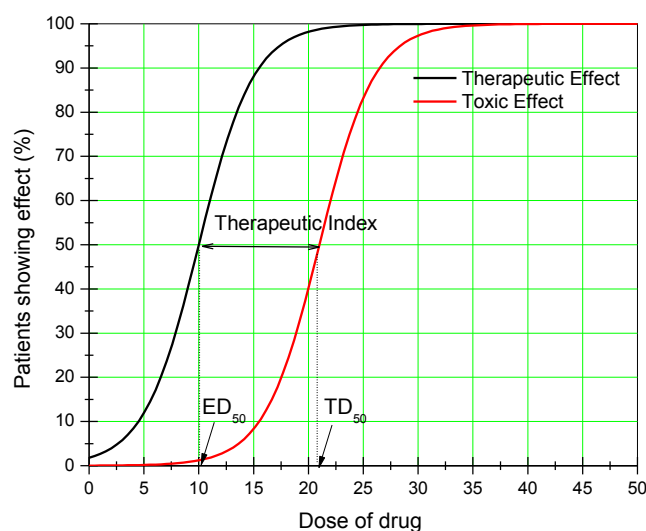
Figure 4. Therapeutic index for a drug.
ED_{50} = Dose where 50% of the patients show an effect, TD_{50} = Dose where 50% of the patients show toxicity.

Table 4. Suggested therapeutic ranges for selected drugs after intravenous administration.

Drug	Target Range
Vancomycin	T: 10-20 µg/mL
Gentamicin	T: 0.5-2 µg/mL, P: 3-10 µg/mL
Cyclosporine	T: 100-400 ng/mL
Mycophenolic acid	12 h AUC ≥ 40 µg/mL/h
Tacrolimus	T: 5-20 ng/mL
Valproic acid	T: 30-100 µg/mL or 200-700 µmol/L
Phenytoin	T: 10-20 µg/mL or 40-80 µmol/L (total), free: 0.75-1.25 µg/mL or 3-5 µmol/L
Phenobarbital	10-35 µg/mL or 43-150 µmol/L
Methotrexate	0.1 to 1 µmol/L 24 to 72 hours after drug infusion
Digoxin	0.5-0.9 ng/mL
Theophylline	5-15 µg/mL

T: Trough concentration just before next dose is given
P: Peak concentration

1.3.2 Clinical challenges of Therapeutic Drug Monitoring

Patient safety and well-being is the focus of drug therapy and clinical procedures. Different patients have different needs and having a small blood sample taken can be a triviality for one patient and a big problem for another. While TDM is recommended for many drugs in the clinic, in practice it can be a problem. Already sick patients, as well as geriatric and pediatric patients, are subjected to repeated blood draws. Infants only have 250 to 800 mL of blood and repeated blood draws can become challenging. Older patients can have thin and fragile veins that make blood sampling hard and often result in puncturing through the vein and more pain for the patient. Using a small amount of blood (finger poke) instead of intravenous blood sampling could be one way of making TDM simpler, if quantification methods are validated for smaller volumes. Instead of blood, other biological fluids, such as saliva and sweat, have been suggested for TDM and extracellular fluid from the skin, if possible to extract could be a valuable alternative for TDM as well.

The incorporation of extravascular fluid in PK and pharmacodynamic studies can help us to understand the relationship between drug concentration and effect [46]. Drug outside the blood vessel is sometimes described as free drug or unbound drug, but this might not be adequate as even protein bound drug is transported through the endothelium via transcytosis [47], although this process is slower than passive diffusion. Protein bound or not, usually drugs can move outside the blood vessel as long as the glycoprotein 60 (gp60) mediated transport mechanism for the protein albumin is functional. Once outside, it might bind to tissue proteins again, therefore escape from a direct interaction with the target or serve as a reservoir.

Extravascular fluid could not only help to understand the relationship between drug concentration and effect better, but might be superior to blood regarding pre-analysis factors that

can vary the drug concentration measured. Mistakes during blood sampling (e.g. leading to hemolysis) and storage (e.g., temperature, time of blood separation into plasma or serum) can possibly influence the concentration of drug measured and further influence the therapeutic decision and dose adjustment. Extravascular fluid is simpler regarding its contents (e.g., no blood cells) and such pre-analysis factors are therefore less influential.

1.3.3   Trends in Therapeutic Drug Monitoring

Ideally, TDM would be pain-free and convenient as well as guiding a patient's drug treatment. Although this ideal has not been reached, efforts are being made to minimize patient discomfort and maximize therapeutic outcomes thus preventing treatment failures and severe side effects that lead to further hospitalization. There is no doubt that therapeutic outcomes would be maximized if the drug concentration were known at all times during the therapy. Unfortunately, this is not possible as it would result in patient discomfort and a great expense. To minimize patient discomfort while maximizing therapeutic outcomes, the number of samples needed for therapeutic decision making can be reduced (e.g., less frequently monitoring) and the sampling technique improved.

To sample as little as possible is currently accomplished by two approaches: concentration time-point monitoring and predictive AUC monitoring. For concentration time-point monitoring, a blood level is taken at a specific time and is compared to a previously established blood concentration reference range. For AUC monitoring, one to four blood levels are taken at a specific time and the total drug exposure (AUC) is predicted from the concentrations using a previously established equation. Some drugs like vancomycin are monitored using a single concentration, whereas for other drugs like cyclosporine better outcomes have been reported using AUC monitoring [48]. Concentrations that have shown promise for monitoring are steady-

state trough concentrations (C_0 or C_{trough}) measured just before the next dose is given. However, any concentration c_x where x = number of hours after dose can be useful in informing therapeutic choices. The exact time should likely be determined for each drug and formulation individually. As an example, trough concentrations can be similar for two different formulations (e.g., cyclosporine Sandimmune[®] and Neoral[®] [49]) but their peak concentration can be very different and different toxicities could be observed. Guidelines for TDM can vary between clinics and are continuously updated. With new recommendations being published constantly, one can easily lose track of the current "best practice".

Regarding AUC-monitoring, a process called limited sampling strategies (LSS) or regression limited sampling strategies (r-LSS) is often applied to predict a patient's total drug exposure from a limited number of samples (e.g., one to four time-point samples). To determine the time points that will allow for the best AUC prediction, it is necessary to perform a full PK study (e.g., 10-15 samples) in a specific patient population followed by a multiple regression analysis or Bayesian analyses. To evaluate the error associated with the prediction, the equation has to be tested on a data set different from the one it was derived. This is not always done. It is often claimed that such equations (LSS) are only valid for a specific patient population and that they are center-specific. David and Johnston [50], however, have tested several scenarios and shown for transplant patients that LSS fit across different transplant types and that there might not be any center specificity. According to their studies, it is important to consider the analytical technique that is used to quantify the drug. In a different study [48], the impact of sampling time deviations for LSS AUC predictions was studied. It was suggested that "robustness" towards sampling time deviations should be added as a selection criterion for LSS. AUC predictions are

25

especially affected or misleading if sampling is done at times where the concentration-time relationship is steep.

The perfect robust estimator for the AUC and therefore drug exposure has not yet been found or does not exist, despite hundreds of articles (Medline search for limited sampling strategies shows at least 147) that describe limited sampling strategies and the method of LSS development [51]. An approach to estimate AUC has been recently suggested by Jawien [52]. It differs from the widely applied methods of AUC determinations that include regression analysis, the trapezoidal rule and standard numerical approaches. The author explains that "in a standard limiting sampling approach one starts from a set of arbitrary chosen times and selects from it a small subset that provides the best linear regression between concentrations measured at this subset and AUC estimated from the full set. The criterion is based on the sum of squares of differences between predicted and observed AUCs. In my approach there is no predefined set of times to choose from, the criterion is a minimum of maximal expected difference between predicted and true AUC not estimated by trapezoid rule but calculated from the model. Thus some modeling results are needed." When a limited amount of only two samples is used, the optimal sampling schedule and optimal quadrature determined by this minimax algorithm were superior to those determined by the trapezoid and standard numerical estimations. In simple words, minimax aims at minimizing the possible loss for a maximum loss scenario. It is often used in game theory and statistics, but details cannot be described here.

In summary, TDM is advancing every day and more and more researchers from different fields are trying to find the best method to maximize therapeutic outcomes for drugs that are not considered safe for the patient without monitoring. Many aspects have to be considered in the

field of TDM for advancements including clinical patient data, mathematical and statistical analysis, timing of sampling, sample analysis and the biological matrix.

1.4 Hypothesis and Research Objectives

The aim of this work is to determine the PK of drugs in ISF and to compare concentrations in blood and ISF after a single dose or multiple doses of certain drugs.

We believed interesting relationships will be discovered, that can contribute to the clinical understanding of drug therapy. In addition, we hope to inspire other researchers to look for newer techniques to measure drug concentrations in body fluids other than blood. Although blood is one of the most important liquids in the human body, other body fluids have to be taken into account to explain the body's complex functioning. In situations where blood might not be a good representative of the target tissue concentrations or where further blood loss is unbearable for the patient, an alternative fluid should be taken. Such situations might be especially salient when the target is outside the blood vessel and extravascular drug distribution is erratic, when unexplained treatment difficulties occur, in cancer, during tissue inflammation and skin diseases. There is a significant amount of information that cannot be "drawn" from blood so the inclusion of information from other liquids and the knowledge of their relationship to blood concentrations are important. ISF might be one of the biological fluids that can contribute significantly to explain drug action, side effects and/or resistance.

The hypothesis of this work is that ISF is a valuable sampling matrix for TDM. This hypothesis will be evaluated in the following objectives.

1.4.1   Objective 1

Determine a method of accessing interstitial fluid reliably.

1.4.2   Objective 2

Determine the PK of TDM drugs in ISF and compare them to blood levels.

1.4.3   Objective 3

Quantify the example TDM drug vancomycin in microvolumes of biological samples like ISF to improve small-sample drug analysis and make drug quantification in small samples of ISF possible.

Chapter 2: Sampling of Interstitial Fluid from Skin

In this chapter we would like to summarize current sampling techniques for ISF, point out challenges and suggest directions for future ISF sampling.

2.1   Background

2.1.1   Common Techniques for Sampling of ISF: Microdialysis and Ultrafiltration
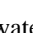
Endogenous and exogenous molecules are measured in blood as a surrogate for diagnostic and therapeutic decision making [53-57], "despite the knowledge that biochemical events and pharmacological effects usually take place in the tissue rather than in the blood stream" [55]. Ideally the tissue fluid of interest would be directly sampled instead of using the surrogate blood compartment, especially if the distribution of drug into the tissue is not immediate. Skin tissue fluid could be such a tissue fluid that might be closer to the site of action because it is extravascular and therefore closer to a drug target that is located extravascular. Sampling of tissue fluid or ISF from the skin is performed rarely, because current techniques are rather difficult to perform. To determine and study the concentration of biomolecules or drugs in tissues, researchers have to implant a sampling device into the tissue of interest, that will remain in place throughout the study and allows for the continuous extraction of small amounts of tissue fluid. While many researchers are interested in finding new techniques that are easier to perform, pain-free and fast, so far this has been only moderately successful and concentrations of drugs in tissue fluids are still most commonly determined using microdialysis or ultrafiltration [55, 58], techniques that are similarly invasive than blood sampling.

Developed in the 1960s for brain research, microdialysis remains active in the field of research and for specific clinical studies but is not used a tool for everyday therapeutic drug monitoring.

Similarly, ultrafiltration is also mainly used for specific research studies, often in larger animal species and not only implanted in the subcutaneous tissue [59] but also in other tissues of interest like the intestinal tract [60]. For both microdialysis and ultrafiltration, a semipermeable membrane is implanted in the tissue of study and fluid is either extracted through the application of suction (filtration) or the tissue is continuously perfused with a carrier liquid to extract drug by passive diffusion into the perfusate (dialysis) (Figure 5).
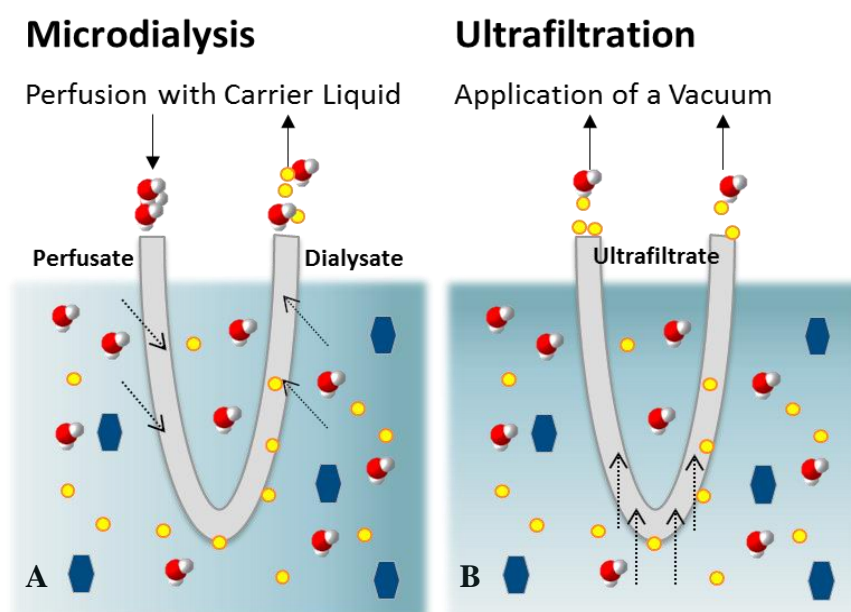
Figure 5. Schematic depiction of the difference between microdialysis and ultrafiltration adapted from [61]. A semipermeable membrane loop is immersed in a drug containing solution, A: Microdialysis: drug extraction through diffusion of drug molecules across the membrane, B: Ultrafiltration: drug extraction through filtration. water molecule, ○ small drug molecule, ⬣ large drug molecule.

In both cases the pore size and material of the membrane will determine which molecules can pass and which ones are retained by size or physicochemical interactions with the membrane material. Microdialysis and ultrafiltration usually use membrane materials like polyacrylonitrile (PAN), polyarylethersulfone (PAES), polyethersulfone (PES), polyethylene (PE) or artificial

cellulose (Cuprophane) and have a molecular weight cutoff (MWCO) between 6 kDa to 1 MDa [61-63]. Analytes that reach the MWCO are usually to 80% prevented from passing the membrane. Although there is no direct conversion between a 3-dimensional unit (Da) to a metric length, 1 MDa approximately corresponds to a pore size of 100 nm, roughly the size of the human pentameric immunoglobulin M [64]. Microdialysis will yield larger but diluted samples depending on the probe length used and flow rate of the perfusate [65]. Probe lengths are usually between 1 and 10 mm and flow rates can, depending on the syringe pump used, be as low as 1 nL/mL (CMA 400 Syringe Pump, CMA microdialysis, Kista, Sweden) but are often around 1 µL/min [65]. There are two types of microdialysis devices, flow through with inlet and outlet on opposite sites, and one with inlet and outlet on the same side.

Compared to microdialysis, ultrafiltration will usually yield a smaller but undiluted sample. The total amount that can be extracted and the achievable flow rate depend on the tissue's hydration status and its possibility of replacing depleted liquid. From our own experience, a flow rate between 2.4-3.9 µL/min could be reached using a subcutaneously implanted PAN ultrafiltration probe (30 kDa MWCO) connected to an evacuated blood collection container (Vacutainers®).

2.1.2   Other ISF sampling techniques: Microperfusion, Blister Fluid, Skin Erosion, Wick, Tissue Cage Reservoir and Skin Windows

Methods that are less commonly described for the sampling of tissue fluid are open flow microperfusion [66], sampling of blister fluid or skin mini-erosion technique [67-69], the implantation of an absorbent material (wick) [70, 71] in the tissue of interest, and the application of tissue cage reservoirs or windows. Open flow microperfusion is similar to microdialysis but instead of a semipermeable membrane, a material with macroscopic holes (500 µm) is used.

Open flow microperfusion has been recently popular for insulin determination in adipose tissue [72].

Blister fluid can be sampled from the skin after the epidermis has been separated from the dermis with the help of suction [69, 73, 74] or a blister creating agent like cantharidin [75]. Suction can be applied to the skin using special suction cups and a vacuum of ~4.3 psi for usually 1-2 hours. More specifically, a block that contains ~ 5-8 mm diameter holes can be applied to the inner surface of the forearm to raise blisters containing 0.1 to 0.2 mL of fluid [76] similarly to the blisters shown in Figure 6. The technique has been reported in the literature as early as 1968 [68], has found some sampling applications in the late 1990's [67, 73] and is also used for skin graft applications [77, 78].
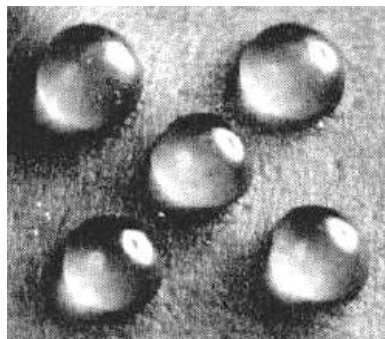
Figure 6. Suction blisters of 0.5 cm diameter from Kiistala [68]

The wick technique goes back to the 1970s and refers to an implantation of nylon filaments either within a hypodermic needle or directly into the skin and has been mostly used to determine interstitial fluid pressures [24].

The tissue cage reservoir technique uses subcutaneously implanted silicone elastomer tubing closed on both sides but with perforations. Perforations of 0-2 mm in diameter leave about 45% of the surface open and, after sufficient time (e.g., days to weeks), ISF will accumulate in the tissue cage and can be sampled with a needle [79].

Another technique to access ISF is called skin-window technique. For this technique, the epidermis of the forearm is scraped without causing severe bleeding and a sterile tissue-culture chamber is applied to the exposed dermis. The tissue culture chamber is a round glass slide with a rim and a rubber gasket. After the injection of 1 mL saline into the chamber, the subsequent removal of 0.2 mL creates a negative pressure so that extracellular fluid components will diffuse into the chamber after applying a transparent tape over the window [80].

2.1.3   Newer ISF Extraction Techniques: Microneedles and Microfluidics

2.1.3.1   State of the Art: Microneedles

When the word microneedles is mentioned, tiny sharp mechanical structures come into mind, ideally small enough that they are barely visible with the naked eye, but fascinating when observed under the microscope. Many microneedles are in the order of 50-700 µm in length and usually below 100 µm in diameter. They can be hollow or solid and they can emerge vertically from a baseplate (out-of plane) or be fabricated parallel to the baseplate (in-plane). Furthermore microneedles can be designed to dissolve in the skin, they can have special coatings (e.g., for biocompatibility, drug delivery), or specially shaped tips (e.g., mosquito tip [81]) and they can even form a gel through swelling of the microneedle material [82]. Fabrication involves the use of sophisticated micromachining techniques. Micromachining includes a series of depositions (e.g., evaporation, sputtering, electroplating, chemical vapor deposition), etching (e.g., wet etching in chemical solutions, dry etching through gases or reactive ions) and pattern transfers (e.g., photolithography) of materials on substrates. Materials for micromachining of tiny needle structures include silicon, glass, metals and polymers [82-84].

Research areas that profit from such small needles and first come into mind when considering microneedles are drug delivery [82], specifically gene delivery [85], injections, skin permeability

and vaccinations [86]. Other areas that are equally fascinating, but usually less clearly connected to microneedles are the removal of body fluids, sensing and drug analysis. The reason for an explosion of ideas in the field of delivery and a less successful exploration of the opposite extraction might originate from the technical problems and the multidisciplinary nature of devices that are necessary for the extraction of liquid. A device that is designed to deliver a substance needs a liquid storing unit and a delivery unit, which is usually operated manually similar to a normal syringe using a plunger or a mechanical spring device. An extraction device, however, needs an extraction unit, a liquid storage unit, and an analytical unit or allow for the easy transfer of the fluid to an external analytical platform. The extraction unit is less easy to power manually and often relies on complicated valve structures and actuation mechanisms (e.g., a self-recovery actuator [87]) and is much harder to fabricate and integrate into the device. How difficult the extraction is, depends also on the body fluid that is desired. Blood is much easier to extract than tissue fluids from the skin, as the vascular system is under "pressure" whereas the tissue fluids are well retained by the connective tissue. Researchers report some promising results for the extraction of ISF and the use a combination of microneedles, microfluidics and ultrasound. Often, the term extraction is used but in fact no real extraction takes place in the way that needle- like structures perforate the skin and directly take up liquid from the skin with a possibility to collect the liquid and analyze it like blood. More often, skin permeability is first increased by piercing of the skin with microneedles and then either a vacuum is applied over the pierced skin after the microneedles have been removed [88] or a subsequent "extraction" is merely a diffusion of compounds into an acceptor liquid similar to a Franz diffusion cell [89]. In a comparable scenario the diffusion cell is used as a coupling liquid for the application of ultrasound and subsequent diffusion of analytes across the epidermis [90, 91]. Devices for the

sensing or extraction of ISF are reported and patented, but mostly simulations have been done, with a real extraction from skin often pending [92, 93]. A direct extraction has so far only been reported in minimal amounts using microneedles and microchannels [94]. It is expected that with the advent and progression of microfabrication and lab on a chip (LOC) technologies, researchers will soon tackle the current difficulties of ISF extraction and analysis using integrated devices.

2.1.3.2   Microfluidic Devices

A microfluidic LOC device (also known as micro total analysis system - µTAS) is a small device that can handle, store and analyze small volumes of biological matrix. In combination with a method of sampling, like microneedles, such devices can be valuable for TDM. If used outside the clinic, they would be called point-of care (POC) devices and simplified versions of them already exist for glucose monitoring, urine testing, pregnancy and fertility testing, and infection confirmation with streptococcus, flu and HIV [95].

The main advantage of microfluidic devices is the handling and the manipulation of small volumes of fluids in channels typically between 1 and 100 µm. This makes them very promising for ISF storage and further analysis and they are therefore shortly discussed in the next chapters.

2.1.3.2.1   Fabrication of Microfluidic Devices

The fabrication of microfluidic devices uses micromachining technologies, which derived from the knowledge used to fabricate integrated circuits in the field of microelectronics. A recent review [83] summarizes key features for the design, fabrication and characterization of LOC devices. In short, micromachining consists of a series of depositions (e.g., evaporation, sputtering, electroplating, chemical vapor deposition), etching (e.g., wet etching in chemical

35

solutions, dry etching through gases or reactive ions) and pattern transfers (e.g.,

photolithography) of materials on substrates. Materials for micromachining include silicon,

glass, metals and polymers. Plenty of platforms that can also integrate assays are reported in the

literature, namely, capillary microfluidics, centrifugal microfluidics, the ''microfluidic large

scale integration'' (mLSI), the electrokinetic platform, pressure driven droplet-based

microfluidics, electrowetting based microfluidics, surface acoustic waves driven microfluidics

and free scalable non-contact dispensing [96].

2.1.3.2.2   Materials for Microfluidic Devices

Materials for micromachining include silicon, glass, metals and polymers. By far the most often

used polymer is polydimethylsiloxane (PDMS), a transparent and elastomeric polymer. PDMS

can be modified and manipulated by a fabrication technique called soft lithography, which has

been described in detail in 1998 by Xia and Whitesides [97], and provides greater flexibility and

convenience (no clean-room required) for patterning than photolithography. Soft lithography

describes an "integrated set of techniques for fabricating microstructures in an elastomeric

material, for modifying the chemical properties of surfaces and for controlling flows of fluid

adjacent to surfaces" [98]. Manufactured devices (e.g., mLSI) are monolithic multilayer PDMS

devices, with the lower layer containing the fluidic channels and the upper layer integrating

pneumatic control channels. To make the key component of an mLSI, the on-chip valve, a

pneumatic control channel has to cross a fluidic channel while both are separated by a

membrane. An external actuation mechanism is needed to operate the valve. The applied

pressure to the upper layer's ducts can expand the elastomeric membrane to block the channel

and liquid flow below. In a similar way, peristaltic pumps and mixers can be fabricated [96].

2.1.3.2.3   Fluid Flow in Microfluidic Devices

Fluid flow in microfluidic devices is important, because the flow profile and design will ultimately determine where liquid accumulates, is stored and analyzed.

In a closed microfluidic channel, two flow profiles are known for the laminar capillary flow, the pressure driven flow and the surface tension driven flow. The movement of liquids in microfluidic chips is quite often pressure driven and includes pumps, valves, chambers and intersections. For simpler devices, which are made of porous membrane materials, flow is surface tension driven and relies on intermolecular forces. The pressure driven unit operations are complex and require an external actuation mechanism whereas pumping independent mechanisms that depend on surface tension are passive and easy to perform.

A microfluidic device for specific applications has to be carefully designed and fluid flow has to be considered. Merging the passive liquid handling (passive microfluidics) or pumping-independent mechanisms with the advanced fabrication technology of LOC devices can form microfluidic hybrids. Such hybrids can be used for the extraction of ISF in a fast and convenient way. A self-recovery actuator can be included instead of external actuation mechanisms similar to the self-recovery actuator for blood extraction [87]. Such technologies would also be helpful for mixing of liquids or assay components after the extraction of biological fluid.

Many microfluidic systems are enclosed and transparent with only inlet and outlet, making them suitable for a protected assay procedure. However, not all microfluidic platforms are closed and it has been reported very recently that open microfluidics or "suspended microfluidics" are also possible [99]. Spontaneous capillary flow (SCF) is surface tension driven and can happen in a channel with specific dimensions even if there is no ceiling or floor. SCF occurs when it is energetically favourable (unfavourable increase liquid-air interface *vs.* favourable increase in

37

liquid-solid interface), which can happen for different channel geometries. Such an open device "enables accessible, multiplexed systems for biochemical and cell-based assays" [99]. For ISF extraction closed microfluidics might be better as the evaporation surface for open microfluidics would be detrimental for the small volumes of ISF.

2.1.4   Challenges of Liquid Capture Using Microneedles

The volume of ISF in the human body is larger than the blood volume (12 L *vs*. 5 L, see chapter 1.1.1). Removing a small amount (< 0.1 mL) of this liquid would not interfere with the health of the patient. It is in general agreement that the skin and connective tissue, with around 70% of the total volume, contains the largest amounts of ISF [12, 15], so that a minimally invasive extraction of ISF from the epidermis is feasible. However, the epidermis is unfortunately known to be densely packed with cells, so that there is little room for free liquid to be extracted. The deeper dermal layer (reticular region), which might be the most defining layer for the mechanics of skin, is a dense fibrous structure (elastin, collagen, reticulin) in a jelly amorphous ground substance. ISF is not freely available there either and it is mostly bound water by glycosaminoglycans (mostly hyaluronate) forming a gel like ground substance [100]. Nevertheless, it has been reported by several authors [101-104] that there is some free moveable fluid available and this is exactly the fluid we are interested in getting.

Microneedles are promising for the extraction of small amounts of liquid from the skin, but there are several problems that have prevented the development of a viable solution so far. Firstly, ISF is bound to the tissue and well distributed. If available as tiny drops of freely moving liquid it adds up to a very small volume. As soon as microneedles are pressed on the skin, it is possible that this liquid is squeezed out of the way or that the skin layers are compressed in a way that makes the extraction impossible. Secondly, although microneedles are very small features and

38

seem ideal to capture small amounts of liquid, it is often impossible to see the liquid in the microneedles unless another microdevice is attached to the needle in a way that the liquid can be seen. If the amount of liquid is so small that it cannot be seen with the naked eye even with microchannels or reservoirs attached to it, then it is necessary to develop a sensing platform (e.g., electrochemically) that proves the successful extraction or directly analyzes the amount of extract and possible drug molecules. A very recent popular, versatile and cheap method of direct analysis is paper-based sensing [105, 106] . A third complication is the method of attaching sensing devices to the extraction device. The connection should likely be airtight to prevent evaporation or leakage of extract. Many types of glue do not work with microneedle materials and are not resistant to high pressures in small channels. The testing of microneedles offers further challenges as *in vitro* conditions (e.g., hydration and elasticity) of excised skin is hard to maintain constant and dead skin is unlike living tissue, especially if previously frozen.

The ultimate goal is to extract minute amounts of undiluted and unfiltered ISF without pain for the patient. While the extraction with microneedles is not as straightforward as expected at the start of this project, various other approaches (ultrafiltration, microfiltration, skin-blistering, electroporation) have been studied to access ISF. Understanding the distribution and accessibility of ISF, knowing the amount of drug that is present in ISF and studying the PKs in ISF (Chapter 3) are important in order to eventually include TDM in tissue fluids into clinical practice.

2.2 Materials and Methods

Four different filtration techniques and direct extraction techniques were investigated for the extraction of ISF. The first, ultrafiltration (2.2.1) was used to create most data sets for further PK analysis, as ultrafiltration membranes are commercially available and less complicated to apply than microdialysis (no pump needed). Ultrafiltration also does not dilute the sample. We also

39

used and developed several microfiltration devices (2.2.2) that can use variable capillary filter membranes, which is potentially useful for drugs that are not easily extracted with ultrafiltration due to interactions with the specific ultrafiltration material and for the study of protein bound drug. Furthermore, using membranes with larger pore sizes can improve the collection speed compared to ultrafiltration and sample collection would be more similar to blood sampling. In small studies, we studied rabbit skin using blistering (2.2.2) and electroporation (2.2.3) in order to access undiluted ISF directly from the very base of the epidermis.

2.2.1   Ultrafiltration

Ultrafiltration [58] is a sampling technique that relies on the implantation of a small sampling probe into the specific tissue of study and a subsequent application of a vacuum to extract extracellular fluids. It is invasive but it can give information on which molecules leave the circulation and what accumulates in tissues.

2.2.1.1   Ultrafiltration: *In Vitro* Experiment

In our studies, we used the ultrafiltration "Reinforced *In Vivo* Ultrafiltration Sampling Probe" from Bioanalytical Systems (West Lafayette, IN, US) made of polyacrylonitrile with a molecular weight cutoff of 30 kDa *in vivo* and *in vitro*.

The *in vivo* experiment aimed to reveal the PK of certain drugs in the ISF tissue in rabbits and will be discussed in detail in the next chapter (Chapter 3). The *in vitro* recovery experiment was used to determine possible drug interactions of drugs with the probe material (membrane: polyacrylonitrile, tubing: fluorinated ethylene propylene). Drug solutions of vancomycin, gentamicin, tacrolimus, cyclosporine, mycophenolic acid, valproic acid, phenytoin, phenobarbital, digoxin and theophylline were prepared in PBS 7.4 (Gibco™ Phosphate Buffered Saline Solution, pH 7.4, Fisher Scientific, CA). To mimic the experimental conditions *in vivo*,

drug concentrations for the recovery experiment were chosen close to the maximum

concentration detected in blood/serum or plasma for each drug (Table 5). The UF probes were

soaked overnight in distilled water and washed with PBS pH 7.4 the next day. After connecting

the probe to a 21G × ¾" winged infusion set, the probe was immersed in a drug solution of

known concentration at room temperature. The first 150 µL of extract was discarded to

completely purge the remaining PBS in the probe. Three consecutive extracts of 150 µL each

were then collected in vacuum tubes (over 5-10 min) and quantified using the analytical assays

that are used in clinical practice (Table 5). To calculate drug recovery, drug concentrations of all

extracts were compared with the initial drug solution (also quantified with the same analytical

techniques) and expressed as percentage of recovery.

$$\text{Recovery}(\%) = \frac{\text{concentration (after passing UF probe)}}{\text{concentration (before passing UF probe)}} \times 100 \qquad\qquad (1)$$

Table 5. Summary table for *in vitro* ultrafiltration experiment. The quantification methods were PETINIA = Particle Enhanced Turbidimetric Inhibition Immunoassay, LCMS = Liquid Chromatography Mass Spectrometry, FPIA = Fluorescence Polarization Immunoassay, ICP-AES = Inductively Coupled Plasma Atomic Emission Spectroscopy, MEIA = Microparticle Enzyme Immunoassay.

Drug	Maximum concentration detected *in vivo* ultrafiltration experiment	Concentration tested *in vitro*	Drug Quantification Assay
Vancomycin	72.1 μg/mL	45.9 and 90.9 μg/mL	PETINIA (Vancouver General Hospital, CA), Siemens
Gentamicin	144.5 μg/mL	149.6 μg/mL	PETINIA (Vancouver General Hospital, CA), Siemens
Tacrolimus	67.5 μg/mL	28.6 and 23.1 μg/mL	LCMS (Vancouver General Hospital, CA), Waters Quattro Micro API MS
Cyclosporine	1994.6 μg/L	1249 and 565 μg/L	LCMS (Vancouver General Hospital, CA), Waters Quattro Micro API MS
Mycophenolic acid mofetil	45.7 μg/mL	76.9 μg/mL	LCMS (Vancouver General Hospital, CA), Waters Quattro Micro API MS
Valproic Acid	1219.1 μmol/L	1331.9 and 2260.9 μmol/L	FPIA (Children's & Women's Health Centre of BC, Vancouver), Abbott
Phenobarbital	230.0 μmol/L	179.7 and 249.3 μmol/L	PETINIA (Vancouver General Hospital, CA), Siemens
Phenytoin	68.5 μmol/L	26.2 and 45.1 μmol/L	PETINIA (Vancouver General Hospital, CA), Siemens
Carboplatin	6625.8 μg/L	2071.4 and 51.6 μg/L	ICP-AES (Exova, Vancouver, CA)
Cisplatin	3384.8 μg/L	4670.4 and 83.3 μg/L	ICP-AES (Exova, Vancouver, CA)
Methotrexate	51.75 μmol/L	69.25 and 121.9 μmol/L	FPIA (Children's & Women's Health Centre of BC, Vancouver, CA), Abbott
Theophylline	123.3 μmol/L	152 μmol/L	PETINIA (Vancouver General Hospital, CA), Siemens
Digoxin	10.6 nmol/L	10.2 and 10.7 nmol/L	MEIA (Vancouver General Hospital, CA), Siemens

2.2.1.2   Ultrafiltration: *In Vivo* Experiment

The *in vivo* experiment will be discussed in detail in the next chapter (3.2.4). In short, the ultrafiltration probes were implanted into the necks of rabbits and ISF was extracted after the rabbits received a single dose of various drugs. Blood samples were collected concomitantly to compare ISF and blood concentrations.

2.2.2   Skin Blistering

2.2.2.1   Methodology

Skin blistering or mini-erosion techniques have been reported useful to access ISF without the need of any implantation or filtration steps, but by using a suction cup [67, 69, 73, 74]. After the application of a pressure of several hundred (100-300) mm Hg below atmospheric pressure, the epidermis separates from the dermis [68] forming an epidermal vesicle after 1-2 h [77]. The fluid in the vesicle is comparable to ISF [107-109] and can then be aspirated. Mini-erosion dermal access (MEDA) was successfully used to determine glucose concentrations in adults [69] and for the serial sampling of ISF in newborns [73].

Creating blisters using suction on rabbit skin was studied here experimentally. Furthermore, the application of heat and extreme cold for creating blisters was used as well. The goal for all methods was to detach the epidermis from the dermal layer and form a blister filled with ISF or to completely remove the detached skin layer and extract ISF using mild suction. The removal of a small amount of epidermis can expose the dermal layer and give direct access to ISF (Figure 7).
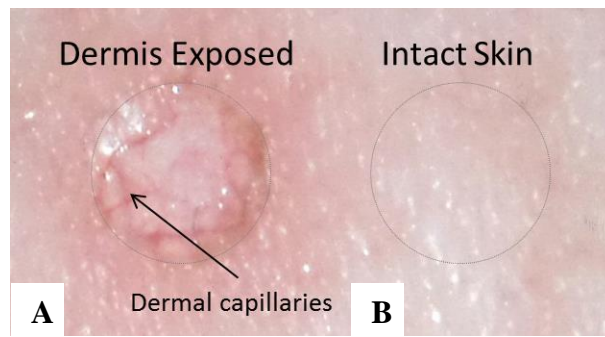
Figure 7. Example picture of a skin erosion created by the removal of epidermis through liquid nitrogen. A: dermis exposed and blood vessels visible, B: intact skin.

2.2.2.2   Skin Blistering: *In Vivo* Experiment

To prepare for skin blistering and subsequent ISF extraction, the rabbit's lateral abdomen was shaved and depilatory cream was applied. Bupivacaine was injected subcutaneously. Three different approaches were tried to create blisters on different days with an appropriate rest for the animal in-between.

In one experiment, a suction cup connected to syringe was applied to the skin and a vacuum was created over several minutes. A disposable syringe attached through a rubber tube to a 3-way tab and another disposable syringe (50 mL) to create a vacuum was described by Gupta *et al.* [77]. Depending on the volume of aspirated air, variable negative pressures can be created.

Figure 8. Suction device: syringe 30 mL, three-way stopcock, silicone tubing and glass suction cup.

In a second experiment, liquid nitrogen was applied to the rabbit skin with a cotton swab in four different spots. In the medical field, a therapy using extreme cold (liquid nitrogen, -196 °C) to

destroy tissue is called cryotherapy. Liquid nitrogen is used in the treatment of actinic keratoses [110] and for the removal of cutaneous warts [111]. After the application of liquid nitrogen with a cotton swab for 20-30 seconds, the skin usually turns white and can be peeled off after two days.

In a third experiment, a stainless steel spatula was heated in a flame for 30 seconds and then quickly applied to the skin to form a small burn blister. It is known from burn-injury patients that blisters formed after the application of heat will expose the dermis. If the area of burn is small, the risk of dehydration and other complications is very low.

2.2.3   Electroporation (InvaFree HMS[®])

2.2.3.1   Methodology

An electroporation suction device (InvaFreeHMS[®], Figure 9) that has been patented for the continuous extraction of ISF [112] was studied after the instrument was provided to us by the inventors Abdeltif Essalik and André Dussault. The manufacturers claim that the device is an extractor system for animals that extracts ISF continuously and in an almost pain-free way.
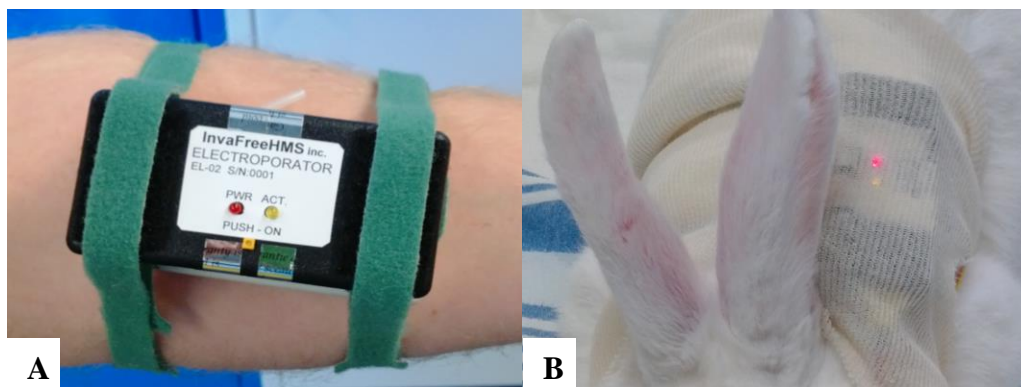
Figure 9. A: The ISF extractor (grey box directly on skin) and electroporator (black box on top) installed on the inside forearm, B: The same instrument installed on the back skin of the rabbit.

2.2.3.2 *In Vivo* Electroporation Experiment

The device, which consists of two parts, the extractor instrument and the electroporation supply, was installed on the rabbit skin as recommended by the inventors. In short, the neck of the rabbit was closely shaved and cleaned with isopropanol. The protective paper from the adhesive on the extractor surface was removed and the device applied onto the wrinkle free rabbit skin. There was a small sparing (~1cm) in the adhesive tape so that the extraction chamber and the electrodes protruding into the extraction chamber were able to touch the skin. The extractor was secured by two Velcro straps, a tubular band aid and a rabbits' jacket (Figure 10).

Figure 10. Rabbit with InvaFreeHMS® and rabbits' jacket.

The extractor was turned on and a vacuum evolved as indicated by the control light turning off. The electroporation device was then connected to the extractor using the supplied cable and retained by further Velcro straps. Connecting the electroporator to the extraction device turned the device on. The electrodes were lowered until they touched the skin and electroporation started. After electroporation, the electroporator was disconnected and extraction started automatically using a vacuum. The instructions of the inventor's manual were closely followed with the exception of using three cycles of electroporation instead of the suggested five. The tubing on the side of the device was connected to a small tube for the collection of ISF.

2.2.4 Microfiltration

Using the ultrafiltration device described in 2.2.1.1, proteins, protein-bound molecules and large drug molecules are usually excluded from the extract due to the molecular weight cutoff of 30 kDa. The most abundant blood and tissue protein that drug molecules prominently bind to is albumin with a molecular weight of more than 60 kDa. Some drug molecules can also interact with the membrane material that is used for ultrafiltration. PAN is structurally similar to polyvinyl chloride (PVC), so that some drugs that adsorb to PVC likely also adsorb to PAN. The only difference between the two polymers is that instead of a halogen ion in PVC, PAN contains a pseudo-halogenide, a cyanide. The polymeric membrane materials used for microfiltration are structurally very different polyethersulfones (Figure 11).

We wanted to manufacture microfiltration devices that use different materials than ultrafiltration devices and that have larger pore sizes to possibly speed up the extraction process and include proteins in the extract. Large-pore microfiltration probes are not commonly commercially available, so we obtained various capillary membrane tubing materials as the starting material to manufacture microfiltration probes in the lab with pore sizes of up to 0.5 µm. The chosen membranes had larger pore sizes than 30 kDa (0.2 µm, 0.5 µm), but were still significantly smaller than the size of a red blood cell (approximately 8 µm). After implantation into the desired tissue, ISF can be extracted without blood.
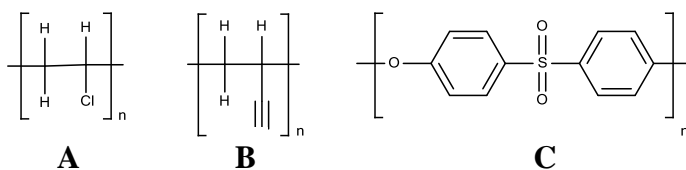
Figure 11. A: polyvinylchloride (PVC), B: polyacrylonitrile (PAN), C: polyethersulfone (PES).

2.2.4.1 Manufacture of the Microfiltration Device

Capillary membrane material was obtained from Spectrum Laboratories (Rancho Dominguez, CA, US) and included PES (polyethersulfone), ME (mixed esters) and mPES (modified polyethersulfone) membranes.

To assemble a microfiltration probe three materials were necessary: tubing material that can connect to a syringe for extraction, the semipermeable membrane that will be implanted into the tissue and a connector that holds both pieces together (Figure 12).
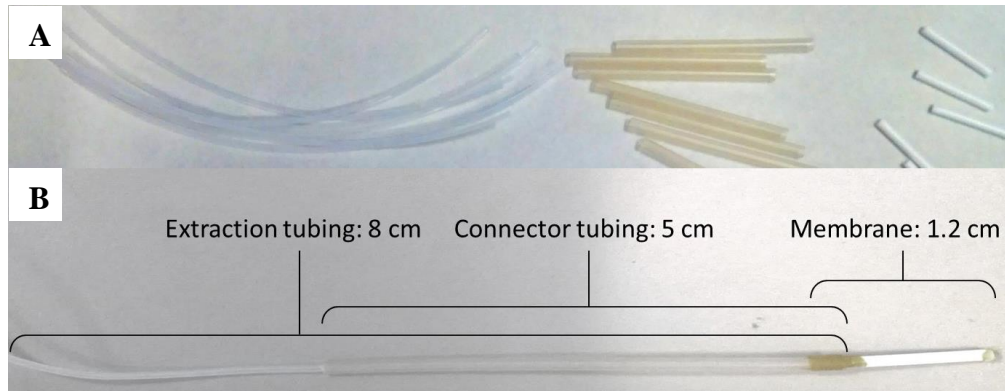
Figure 12. A: Microfiltration probe pieces, B: assembled microfiltration probe.

Generic PTFE tubing (outer diameter 0.03 ", inner diameter 0.016") was cut to 8 cm pieces. The connector tubing was transparent heat shrink tubing (Qualtek, heatshrink, PVDF 3/64", Digikey Electronics Corp, CA) and cut to 5 cm pieces and the capillary membrane was cut to 1.2 cm pieces. One side of the PTFE tubing was perforated with a 30G needle and inserted into the membrane. This would later increase the strength of the membrane and prevent a collapse when applying a vacuum. The overlap and 2/3 of the PTFE tubing were coated with transparent epoxy glue (UHU plus schnellfest, 2-K-Epoxidharzkleber, UHU GmbH & Co KG, Bühl, DE). The transparent heat shrink tubing was then put over the PTFE tubing and the connection to the

membrane. It was heated until tightly melted around the connection and to the rest of the PTFE tubing. PTFE tubing cannot be glued with epoxy permanently but the heat-shrink tubing made the connection tight. To close the other end of the membrane, a drop of transparent epoxy glue was used.

2.2.4.2   Microfiltration: *In Vitro* experiment

The assembled microfiltration probes were manufactured to be used later *in vivo* for a steady-state drug study of vancomycin. Before performing *in vivo* experiments, the different membrane materials were tested for vancomycin permeability *in vitro*. A simple spectrophotometric measurement at 229 nm was used to determine the vancomycin concentration in the solution before and after passing the different capillary membrane materials. Therefore, a calibration curve of vancomycin (Vancomycin hydrochloride, Sigma Aldrich, Oakville, ON, CA) in water (Milli-Q Synthesis system, Millipore, Billerica, MA) was prepared over a range of 0-100 µg/mL. A vancomycin solution of 30 µg/mL was used as the extraction solution. Three times 50 µL were extracted through the membrane materials and subsequently quantified.

2.2.4.3   Microfiltration: *In Vivo* experiment

In a preliminary experiment, the ethylene-oxide sterilized microfiltration membrane was implanted in one rabbit through a 14G catheter to check if an extraction is possible. The procedure was performed after shaving of the rabbits' neck and under local anesthesia with 0.3 mL bupivacaine (Marcaine® 0.50%; Hospira, QC, CA).

2.2.5   Microneedle Experiments

2.2.5.1   Background

Ongoing research suggests that microneedles are useful tools to deliver small amounts of liquid into the upper skin layer without causing pain to the patient. This is useful for drug delivery,

gene delivery and skin vaccinations [113, 114]. If the delivery of liquid is possible, then the removal of liquid in small quantities should be possible as well, but the needles and channel geometry might have to be different than for injection devices. In fact, researchers report that the removal of liquid from the skin could be useful for the analysis of glucose, biomarkers and therapeutic drug monitoring [88, 91, 115-118] (see 2.1.3.1). However, the direct extraction of ISF using microneedles is challenging due to multiple reasons discussed previously (2.1.4). To capture, transfer or quantify ISF and molecules within, microneedles have to be attached to another microdevice, which is not a trivial task.

In order to remove fluid from the skin, it is important to know where the fluid is available and where it is distributed. To study the interstitial space of the upper skin layer, we visualized it through injection of a dye mixture containing sulforhodamine B and potassium ferrocyanide. The spreading depends on many parameters including the dyes properties, needle geometry, injection depth, pressure and volume injected, and is quite complicated. However, in our proof of concept experiment we only tested one type of microneedle under constant conditions (pressure, volume) together with a special dye mixture. It proved to be reasonably challenging to inject liquid into a skin sample using minimal laboratory equipment without force and pressure measurements and microscopes. Many studies are in fact done in human subjects [119] instead of a model test stage or use fairly complicated set-ups [120]. After multiple trials, we applied vibrational forces [121] to make the injection and penetration of the microneedles easier on our test stage and successfully delivered the liquid to visualize the ISF space.

2.2.5.2   Microneedles Used for Our Experiment

For our experiment, we were granted pyramid shaped 3-needle array hollow silicon microneedles of 600 µm length from Nanopass (NanoPass Technologies Ltd., Nes Ziona, IL) (Figure 13).
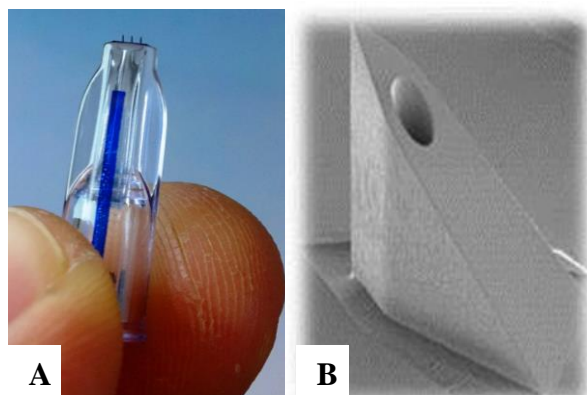
Figure 13. A: Nanopass MicronJet microneedle array on Luer hub with 3 microneedles, needle length: 600 μm, B: pyramidal tip shape under electron microscope (picture courtesy NanoPass Technologies Ltd.).

The needle arrays are designed for injections (e.g., skin vaccinations), for which the amount of volume that is needed to first fill the needle hub and needles before delivery does not necessarily have to be in the low microliter range (1- 5 μL). Volumes delivered to the skin are usually around 100 and 200 μL and if the Luer hub holds 10-20 μL mL after injection, then the delivered dose is still sufficient, despite the 10-20% dead volume left over in the Luer hub. However, for more precise applications like the extraction of very small volumes in the sub- 50 μL range, the dead volume in the Luer hub must be as small as possible and it is advantageous to see liquid close to the needle tips. We reduced the dead volume to < 1 μL with PTFE tubing glued inside the needle hub. A small hole was drilled in one side of the needle hub to insert small PTFE tubing all the way to the base of the microneedles. The hub was filled with transparent epoxy and cured overnight at room temperature. The end of the PTFE tubing that emerged on the other side of the whole was cut to an appropriate working length (~ 5 cm) and connected to a precision dispensing tip (30 Gauge, EFD Nordson Corporation, East Providence, RI, US). To accomplish this, a stainless steel squeeze ring (cut from a 16 Gauge hypodermic needle) was put over the tubing, the tubing was then slid over the dispensing tip and a small amount of epoxy glue was

applied. The ring was squeezed tight. Using this modified needle device (Figure 14) allowed for the exact monitoring of 1-5 µL of liquid in the tubing instead of the ~ 40 µL dead volume in the Luer hub, which is especially important for the extraction of liquid.
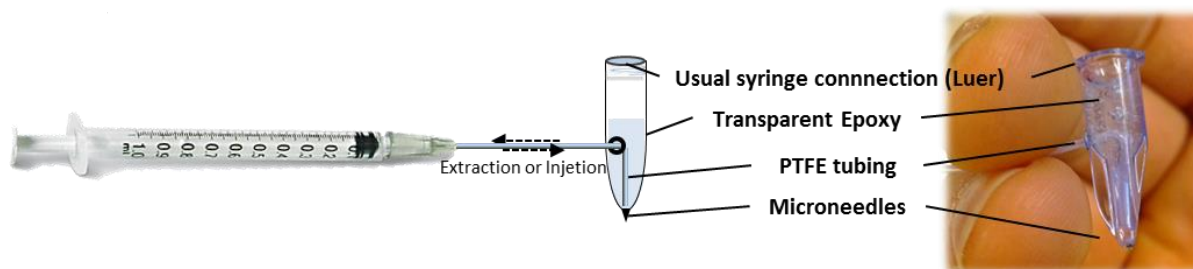
Figure 14. Modified injection/extraction device.

2.2.5.3   Skin Samples

In preclinical pharmaceutical research, it is often necessary to study the delivery or permeation of drugs into skin, to test the penetration of needles or to study the mechanical properties of skin upon application of forces. There are several possibilities for researchers to choose from for their studies including real human skin samples, animal skin and artificial skin simulants.

Some companies (Genoskin, Toulouse, FR) have specialized in the supply of human skin for research in the cosmetic, chemical and pharmaceutical industry. Human skin from donors can be delivered either frozen or as a native biopsy sample that has been kept alive in an appropriate medium. Ethics approval has been obtained by the company and is not necessary for the individual researcher. However, these skin models are usually used for the testing of drug penetration, absorption, metabolism and toxicity. To test needles and injection patterns or mechanical properties, researchers often look for a cheap and plentiful alternative like animal skin. Pig skin has been studied and identified as a good representative of human skin regarding the thickness of stratum corneum, epidermis and dermis. Values obtained for human skin stratum corneum are 6-19 µm [122, 123] and for epidermis are 70-82 µm [123] and were measured on

52

the dorsal aspect of the forearm, shoulder and buttock. Human dermis has been reported to be between 1-1.9 mm [124]. Porcine skin stratum corneum and epidermis has a thickness of 26-80 μm and 34-56 μm respectively [125]. Especially, the dorsal site of the pig ear has recently been reported to be a suitable model for human skin with stratum corneum, epidermal and dermal thicknesses of 17-28 μm, 60-85 μm and 1.86 mm, respectively [124]. If the biological characteristics (e.g., cell and tissue behavior) are not necessary for a project and the researcher is only interested in the mechanical characteristics, an artificial model could be used. An artificial skin model has elasticity properties similar to real skin and is often desired for a mechanical characterization of certain microneedle designs and their insertion and fracture forces, and will not be discussed in detail here.

The decision on a suitable model for research depends mostly on the application. While the viability and thickness of the skin is most important for permeability studies and drug absorption, mechanical skin properties are most important for penetration testing of needles, whereas the delivery of substances or the study of extracellular space merely requires a suitable cell network. For our study, we decided to use abdominal pig skin from a local butcher. Abdominal skin is thinner and less hairy than skin from the dorsal site and allowed the microneedles to penetrate and deposit dye into the epidermal and dermal region. The skin was a fresh and unfrozen sheet of abdomen and chest and was cut into 3 cm x 8 cm pieces after removing the hypodermis and muscle tissue. The skin sheets were 1-5 mm thick and flat frozen to – 80 °C until the experiment.

2.2.5.4 Injection Test Stage

To deliver a special dye into the upper skin layers to visualize ISF space, the modified needle device (Figure 14) was mounted on a test stage. The test stage consists of a needle holder (height adjustable), a syringe holder for the injection liquid and a skin holder loop connected to a

vibrating motor and a Plexiglas test stage. The skin was thawed under running warm water, wiped with ethanol (70% v/v) to remove any oily residues from the epidermis and covered with a moist paper towel to keep it hydrated. Just before the injection, the skin was placed on a slice of sponge (0.8 cm thick) and placed under the skin holder loop attached to the vibration motor. The skin holder loop is made of stiff wire and transfers the vibrations onto the skin. A triangular Styrofoam block cut at a 45 °C angle was slid under the skin to press it against the skin holder and the acrylic test stage was tightened against the block from below. The microneedles were attached to a 20 mL syringe Luer holder and placed into the needle holder over the skin. The small tubing was connected to a 1 mL syringe, which was put horizontally into a syringe holder (Figure 15).
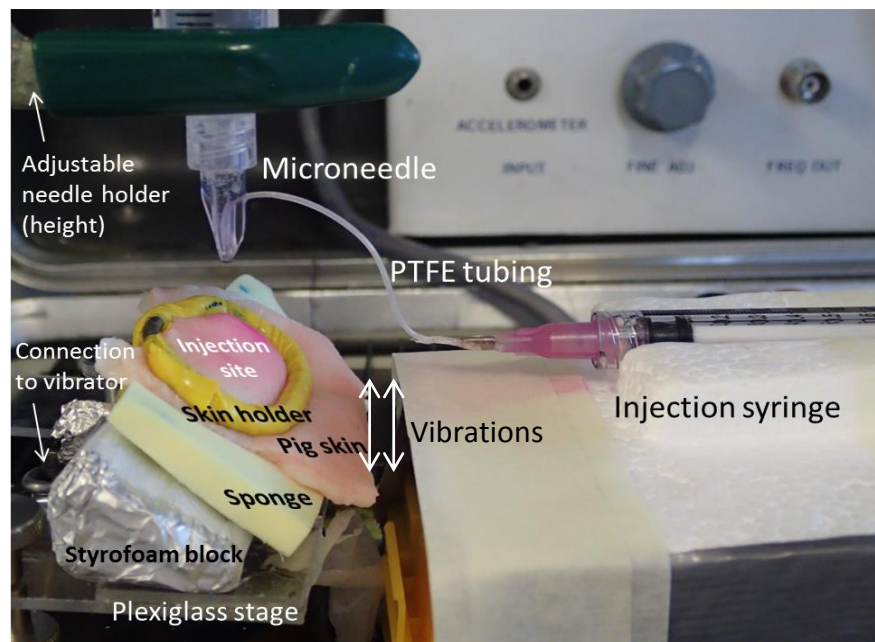
Figure 15. Injection/extraction test stage.

2.2.5.5 Dual-Dye Delivery to the Skin to Locate ISF Space

A solution of two model dyes was delivered into excised pig skin samples with microneedles of 600 μm length using the described test stage and vibrations of 50 Hz and an amplitude of ~ 1 mm.

The injection solution contained two dyes to potentially visualize different regions of the interstitial space. For the injection solution, 150 μL of a 4.7 mg/mL sulforhodamine B (Sodium salt, Sigma Aldrich, Oakville, ON, CA) solution in water were diluted to 1050 μL and then mixed 1:1 with a solution of 53 mg/mL potassium ferrocyanide trihydrate $(K_4[Fe(II)(CN)_6]\cdot 3\ H_2O$, Sigma Aldrich, Oakville, ON, CA) in water. Sulforhodamine is an organic red fluorescent dye (Absorption 565 nm/Emission 585 nm) and used as a polar tracer in cell biology (Figure 16).
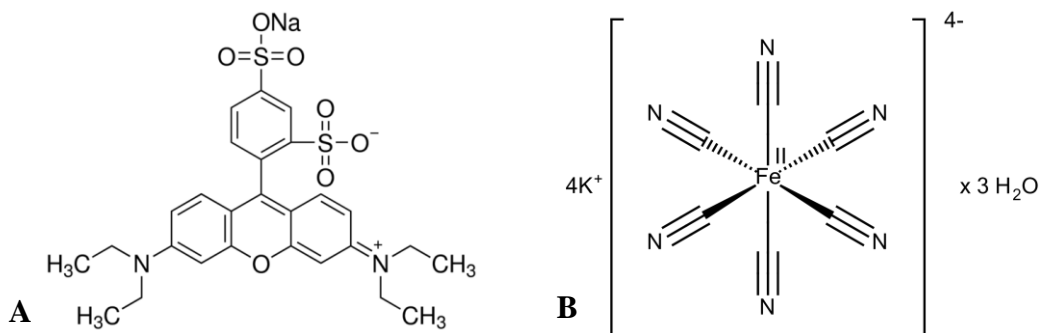
Figure 16. Structures of the delivered dyes;
A: Sulforhodamine B (M = 580.65 g/mol) , B: Potassium ferrocyanide trihydrate (M = 422.39 g/mol).

Potassium ferrocyanide is a yellow salt that is almost colorless when dissolved in water but precipitates as a dark blue inorganic pigment (Prussian Blue) when it comes into contact with Fe (III) (Figure 17).
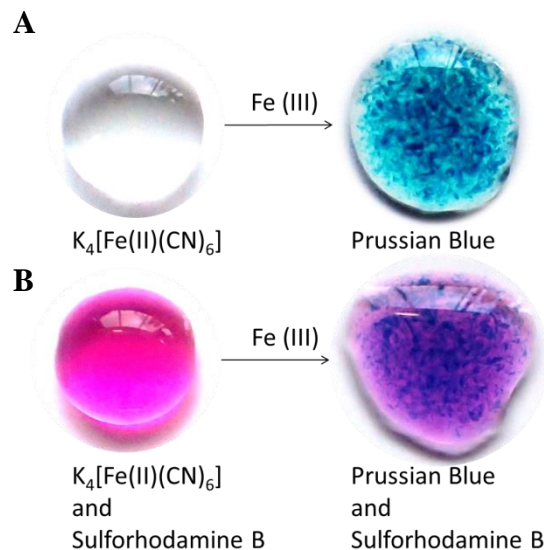
Figure 17. A: An aqueous solution of potassium ferrocyanide precipitates to a dark blue pigment (Prussian Blue) when a solution of Fe (III) is added, B: The dual dye solution before and after addition of Fe (III).

Sulforhodamine B is a polar pink fluorescent dye that is easily visible in the skin after injection and potassium ferrocyanide has been reported as an extracellular tracer. According to a 1960s publication [126], the "ferrocyanide method" is a vital stain for the less dense part of the interstitial space, which is the part that is most likely to contain free movable liquid. The negatively charged coordination complex ferrocyanide ($[Fe(CN)_6]^{4-}$) preferably accumulates in regions of the interstitium that is looser compared to the denser highly negative charged regions. Potassium ferrocyanide can mark the looser part of the negatively charged glycosaminoglycan ground substance of the interstitial space [126] as droplets of 0.1 μm [15] after its precipitation. While potassium ferrocyanide itself is colorless when injected, after injection and sectioning, it can be precipitated by the addition of Fe (III) and therefore made insoluble. Mixing both dyes for injection allows for the coloring and visual examination of different parts of the interstitial space. For the injection, the microneedle was lowered onto the skin tightly allowing a skin fold wrap around the needles (Figure 18), then vibration was turned on and while retracting the needle

56

slowly in vertical direction, the plunger of the injection syringe was held pushed. Retracting the

needle slowly allowed for determining the lowest position of the needle where the injection of

liquid can take place. An injection was possible when the resistance in the skin suddenly dropped

and the plunger could be pressed easily. After the injection, the vibrations were turned off and

the needle was left in place for another 30 s before retracting it fully.
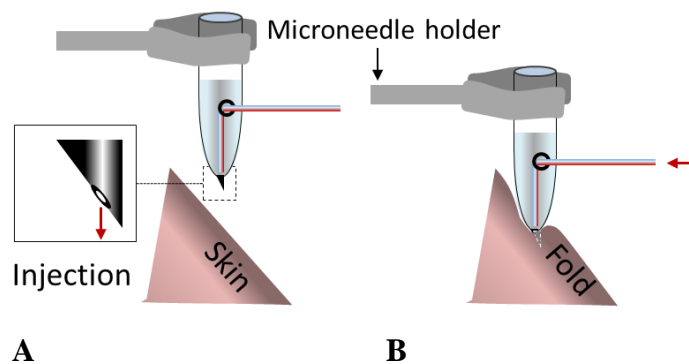
Figure 18. A: Detailed schematic of the needle tip and the direction of the opening towards the skin, B: Needle in injection position, skin fold wrapped around needle hub.

2.2.5.6 Histologic Preparation of Skin Sections

Skin samples were injected and frozen between two glass slides at –80 °C within 45 minutes.

Freezing between glass slides flattened the skin sections appropriately and allowed for better

cutting of longitudinal sections later on. For sectioning, skin samples were removed from the

glass slides, cut to appropriate dimensions for slicing (~ 2 cm × 2 cm) and fixed on the sample

holder using Cryomatrix (Thermo Fisher, Kalamazoo, MI, US). Cross sections and longitudinal

sections of 60 μm thickness each were prepared using a cryotome at –25 °C and collected on

glass slides. When the glass slides were brought to room temperature, the section automatically

adhered to the glass slides. For staining, every second cut slice was covered with 50-100 μL Fe

(III) solution (~ 50 mg/mL). The solution was aspirated after 10 s and the corner of the section

lightly tapped with KimWipe® tissue to not disturb the precipitated dye. Slices were observed under the microscope (Motic AE31, at $40 \times$ magnification). To conserve the slides, a 10:1 mixture of PDMS base: PDMS curing agent (Sylgard ® 184 Elastomer Kit, Dow Corning, Midland, MI) was degassed and poured over the slides and cured in 2 days at room temperature.

2.3 Results and Discussion

2.3.1 Ultrafiltration: *In Vitro* Experiment

All 13 tested drugs have significantly smaller molecular weights ($0.18 - 1.45$ kDa) than the MWCO of the UF probes (30 kDa) so that a decrease in recovery could point towards drug adsorption to the membrane material.

The ultrafiltration experiment resulted in mean recovery rates of $3.4 - 100.5$ %. A two sample t-test assuming unequal variances was performed to determine if drug recovery was significantly different from 100% for each drug ($\alpha = 0.05$). As only one drug measurement was performed for the drug solution before passing the membrane, 10 random numbers were generated with a standard deviation (SD) of 10% as a comparison data pool for 100% recovery. An SD of 10% seemed an appropriate value for the precision of the drug assay as a similar value has been reported for one of the used assays [127]. Furthermore, the SD seen in the recovery measurements was on average 10%.

The decrease in drug concentration after passing the UF membrane was significant for phenobarbital, digoxin, gentamicin, mycophenolic acid, tacrolimus, cyclosporine and methotrexate. Therefore, adjustments to drug concentrations in ISF have been made before further data analysis for the mentioned drugs using the calculated factor R (Table 6).

Table 6. Drug recovery for UF probe (PAN 30 kDa); Factor R = (1/Mean)·100.

In PBS 7.4	Recovery 1 (%)	Recovery 2 (%)	Recovery 3 (%)	Recovery 4 (%)	Mean (%)	SD (%)	R	Difference significant
Phenobarbital	76.7	90.9	88.8	89.0	86.4	6.5	1.16	Yes
Phenytoin	92.4	(123.3)[2]	51.7	68.3	70.8	20.5	1.41	No
Digoxin	68.1	84.8	90.8	91.4	83.8	10.8	1.19	Yes
Gentamicin	-[1]	25.4	0.8	9.1	11.8	12.5	8.47	Yes
Vancomycin	65.4	(147.3)[2]	70.0	92.1	75.8	14.3	1.32	No
Theophylline	-[1]	101.0	101.6	98.8	100.5	1.5	1.00	No
Mycophenolic Acid	-[1]	69.3	37.1	61.0	55.8	16.7	1.79	Yes
Tacrolimus	2.8	3.9	3.2	3.7	3.4	0.5	29.4	Yes
Cyclosporine	2.9	2.7	17.5	24.2	11.8	10.8	8.47	Yes
Valproic Acid	91.9	114.9	99.8	95.5	100.5	10.1	1.00	No
Methotrexate	80.7	95.4	92.2	93.0	90.3	6.6	1.11	Yes
Cisplatin	71.9	84.4	97.5	101.9	88.9	13.5	1.12	No
Carboplatin	93.6	106.9	98.6	96.5	98.9	5.7	1.01	No

[1] only three measurements available for this drug
[2] value excluded (possible measurement error)

2.3.2 Blistering

In the first experiment, using suction for the creation of blisters, no blisters were created. After several minutes of suctioning, a hematoma formed under the suction cup and the experiment was terminated.

Using the liquid nitrogen blistering method, no ISF could be extracted from the rabbits' lateral back. After the application of liquid nitrogen with a cotton swab, the skin turned white as expected but the epidermis did not detach from the dermis. The skin could not be removed with tweezers. On a previously performed experiment on human skin, a very thin layer of skin could be removed almost directly after the application of liquid nitrogen for 20 seconds and ISF could

be extracted using mild suction (Figure 19). On rabbit skin, the skin just turned white and healed

and scabbed without complications over the next days (Figure 19).

Figure 19. A: Human skin, epidermis removed from a Ø 5 mm skin erosion after the application of liquid nitrogen, B: Human skin, ISF extraction after the application of mild suction, C: Rabbit skin, skin scabbing of the Ø 7 mm skin erosion 2 days after the application of liquid nitrogen.

Using heat for the creation of skin blisters, no ISF could be extracted. It was expected that a

blister would be created immediately after the application of heat, but the skin turned slightly

yellow and no blister was created. After the removal of parts of the epidermis the erosions started

bleeding and it was clear that heat does not create appropriate skin blisters for the extraction of

ISF.
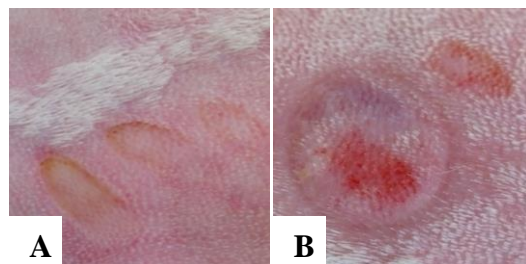
Figure 20. A: Rabbit skin after the application of heat with a spatula, B: Rabbit skin after the removal of small pieces of skin and the application of suction.

It was concluded that the main reason for being unable to create a blister with any of the

methods and detach the epidermis was the high density of hair in rabbit skin. The hair anchors

the epidermis to the dermis and does not allow for a detachment of epidermis. Rabbit skin was

found to be more elastic and thinner and provided less rigidity than human skin when applying

suction cups and it therefore bruised easily. Furthermore, all skin erosions on rabbit skin were very prone to bleeding after treatments.

2.3.3 Electroporation

Electroporation usually refers to the application of an electrical field to a biological system to reorganize lipid bilayers of the cell membrane. A reorganization can lead to the creation of conductive pathways or water- filled holes that allow large molecules (like DNA) to pass the cell membrane to the inside of the cell. The disruption of the cell membrane can be irreversible or reversible and is discussed in detail elsewhere [128].

In our experiment, electroporation led to an irreversible disruption of cellular structures, although it is unclear if this has been intended by the developers of the electroporation device or not. After 24 hours, a red liquid was found in the tube (Figure 21). After removing the device the extraction site looked bloody and slightly inflamed. The sticky rubber on the device was disintegrating and the small tube contained blood as confirmed microscopically (Figure 21). The electroporation device had to be characterized as unsuitable for the extraction of ISF in rabbits.
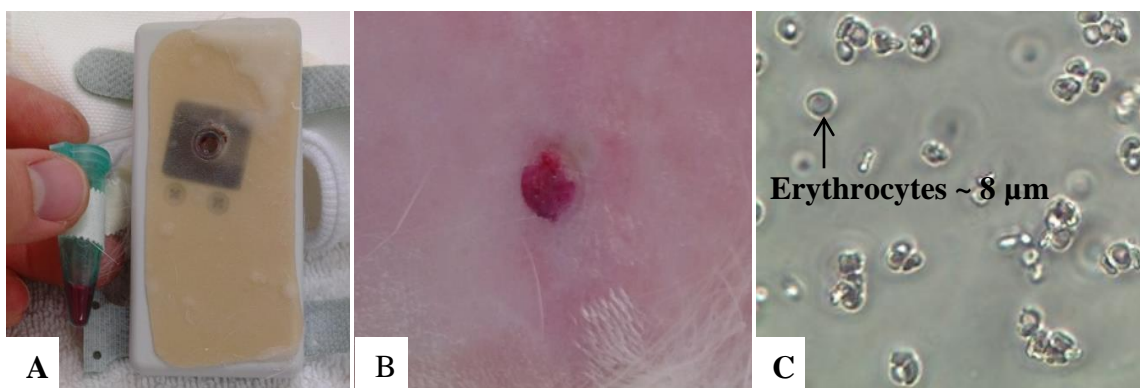
Figure 21. A: InfaFree HMS® device when removed from rabbit skin.
The small tube contains blood, B: Rabbit skin where the electroporator was attached, C: Red blood cells in extract.

Similar to the blistering methods, rabbit skin was unsuitable for the electroporation device. The skin of the rabbits is thin and starts to bleed faster than human skin. The device was also too

heavy and uncomfortable to carry for rabbits as their movements and behavior can hardly be

controlled. Furthermore, the use of the device creates fairly deep wounds of 0.5 cm in diameter,

which heal very slowly.

2.3.4   Microfiltration: *In Vitro* Experiment

Drug recovery through different microfiltration capillary membranes was determined in order to

decide which membrane is most appropriate for the *in vivo* microfiltration study (next chapter

2.3.5). The calibration curve for the spectrophotometric quantification of vancomycin

(0-100 µg/mL) at 229 nm is displayed in Figure 22.
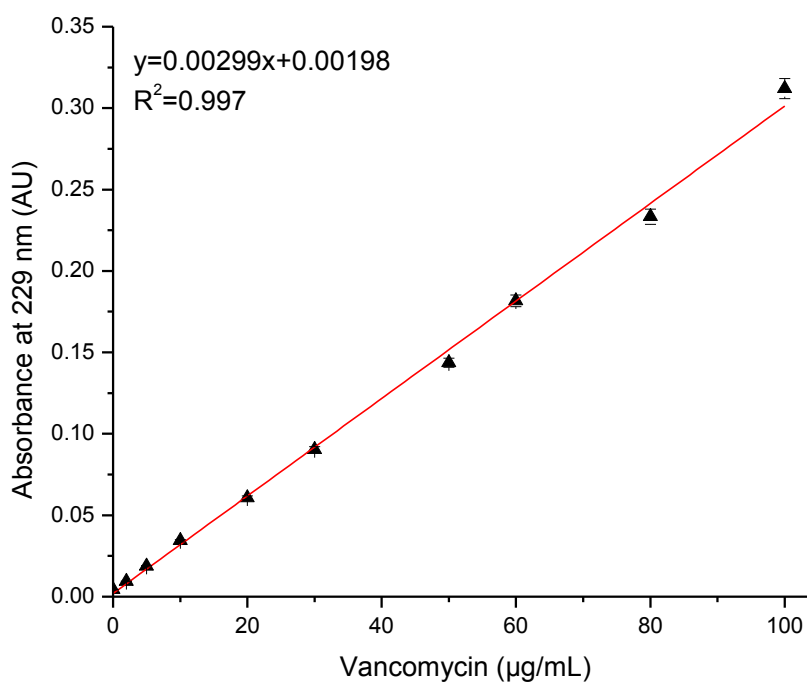
Figure 22. Standard curve of vancomycin in water 0-100 µg/mL.
The Nanodrop2000 Reproducibility Data Sheet [129] mentions a CV of 2%.

Recovery rates for modified polyethersulfone (mPES, 30 kDa), polyethersulfone (PES, 0.2 µm), polyethersulfone (PES, 0.5 µm) and mixed ester (ME, 0.2 µm) were 92.6, 108.2, 105.9, and 104.0%, respectively.

Table 7. Recovery rates for 4 membrane materials using a vancomycin solution of 30 μg/mL (n = 3).

Membrane	Drug Concentration Before Pass (µg/mL)	Drug Concentration After Pass (µg/mL)	Recovery (%)
mPES	30.11 ± 0.03	27.89 ± 0.16	92.62 ± 0.56
PES 0.2	28.56 ± 0.03	30.89 ± 0.30	108.17 ± 0.96
PES 0.5	26.33 ± 0.33	27.89 ± 0.03	105.91 ± 0.10
ME	27.78 ± 0.03	28.89 ± 0.16	104.00 ± 0.55

While recovery rates were acceptable for all membranes, ME was chosen as the final material for the microfiltration probe because of its stiffness and large diameter (1 mm). A stiffer probe material makes the implantation easier and a large diameter can result in the extraction of larger volumes per length of probe.

2.3.5   Microfiltration: *In Vivo* Experiment

The microfiltration probes manufactured according to chapter 2.2.4.1 were gas sterilized by ethylene oxide. In a preliminary experiment (see detailed procedure in 3.2.4.2), one probe was implanted in a single rabbit and tested for its performance. The extraction of ISF was possible and comparable to the extraction procedure using ultrafiltration. The microfiltration units could be superior to the ultrafiltration probe as the probe is smaller and therefore easier to be implanted. Furthermore, the extraction is simpler and uses a syringe for point extraction instead of vacuum blood collection tubes over time intervals.
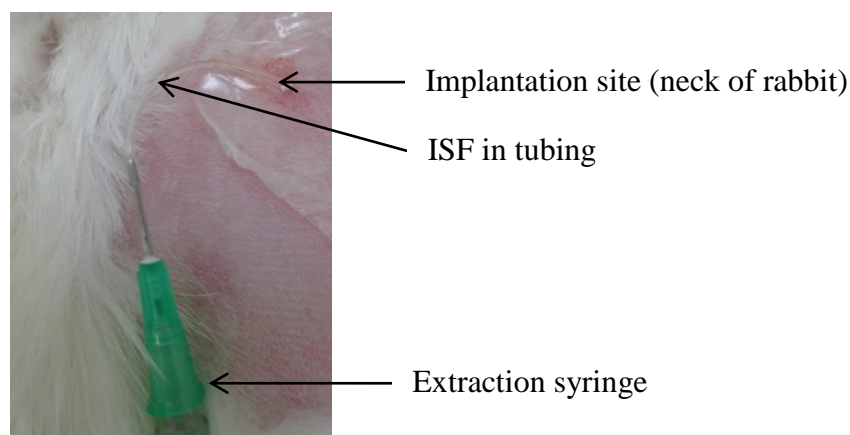
Figure 23. Microfiltration membrane implanted in rabbit's neck.
ISF visible in tubing after < 10 min of suction with 1 mL syringe.

The study was expanded to 5 rabbits for the detection of vancomycin concentrations in a steady-state experiment (Chapters 3.2.4.2 and 3.3.6).

2.3.6 Microneedle Injection Pattern

Several observations were made after the injection of a dye mixture into pig skin with microneedles.

- Vibrations and angle: The injection of 50-100 µL of the dye mixture was successful but only possible if the skin was vibrated at 50 Hz and angled at roughly 45°. The insertion of these needles at an angle resembles the insertion of in plane needles parallel to the skin surface. The sharp needle tip "slices" into the skin during insertion rather than puncturing the skin through compression. If the needles are lowered onto the skin perpendicularly, the insertion force can compress the tissue below and can hinder the delivery of liquids.

- Skin stretching: it is important that the skin is not stretched too much or the delivery of liquid is impossible. To minimize stretching, it is best to use a soft sponge as a bed for the

skin. The soft sponge will retreat in the area where liquid is injected and allow the skin to

expand. This seems to mimic the behavior of the dermal skin layer.

- Dyes: it was obvious that the two dyes differed greatly in the amount they spread out
  around the injection site. This is displayed in Figure 24 - 27. The injection solution
  contained sulforhodamine B and ferrocyanide, but only every other skin slice has been
  treated with Fe (III) to precipitate ferrocyanide as Prussian Blue and make the spreading
  of it visible. Ferrocyanide spreads out much further under the experimental conditions
  than sulforhodamine and the border is sharper and better visible.
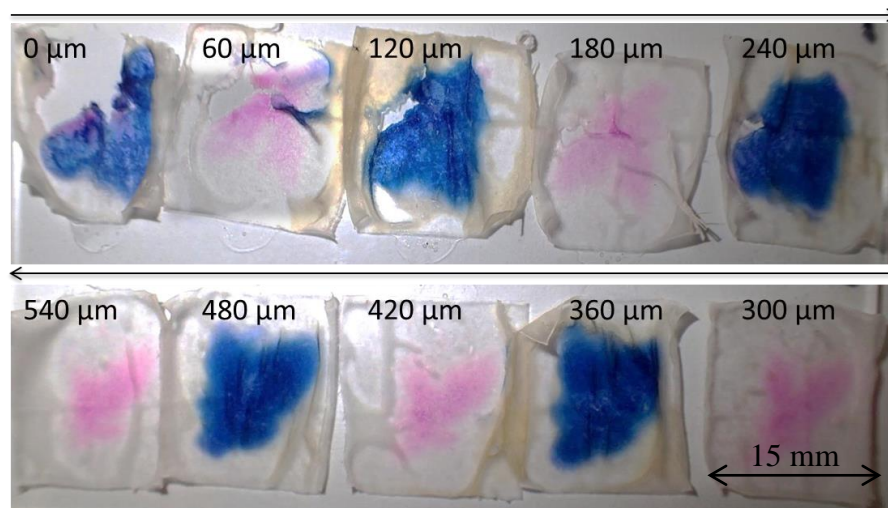
Figure 24. Longitudinal skin slices ordered by increasing depth of 60 µm thickness across the whole injection area.
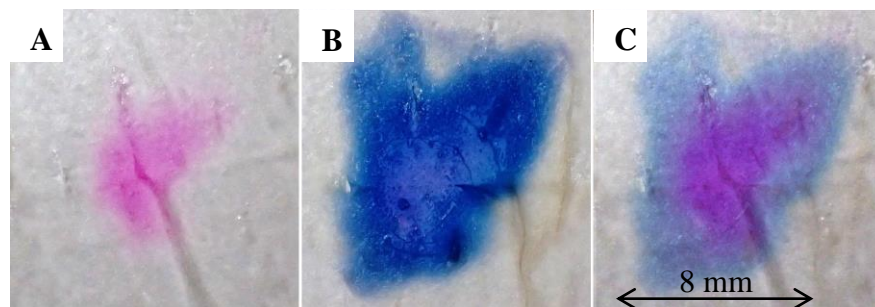
Figure 25. Longitudinal slices of two consecutive slices (A and B) and an overlay (C).
A: Not dyed with Fe (III), B: Dyed with Fe (III), C: Overlay of A and B showing the areas that sulforhodamine (pink) and ferrocyanide (blue) cover.
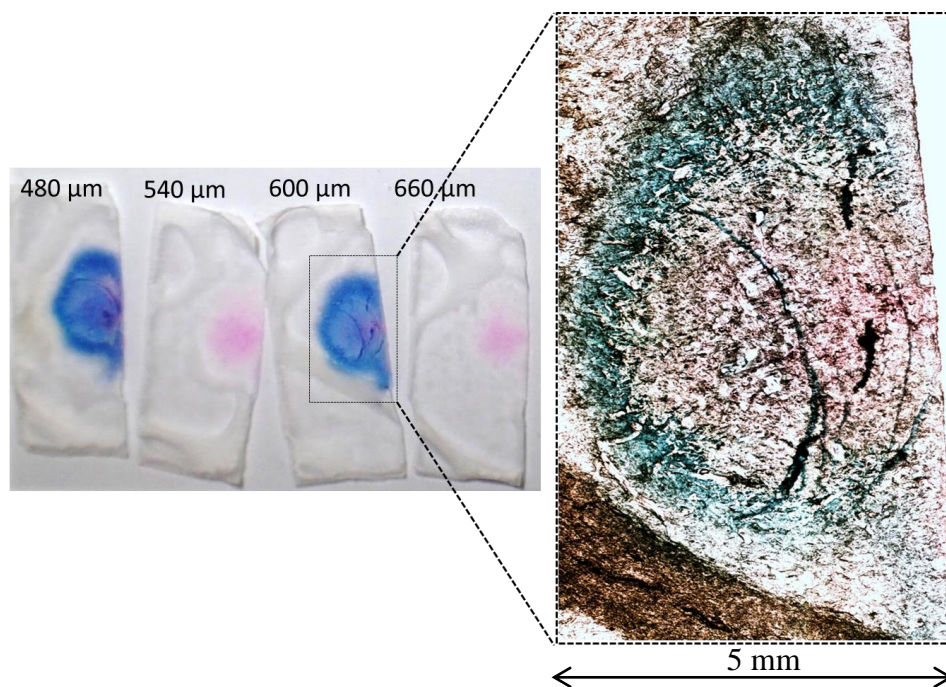
Figure 26. Longitudinal slices of 60 µm thickness of 50 % of the injection area cut in half at the approximate center of injection.
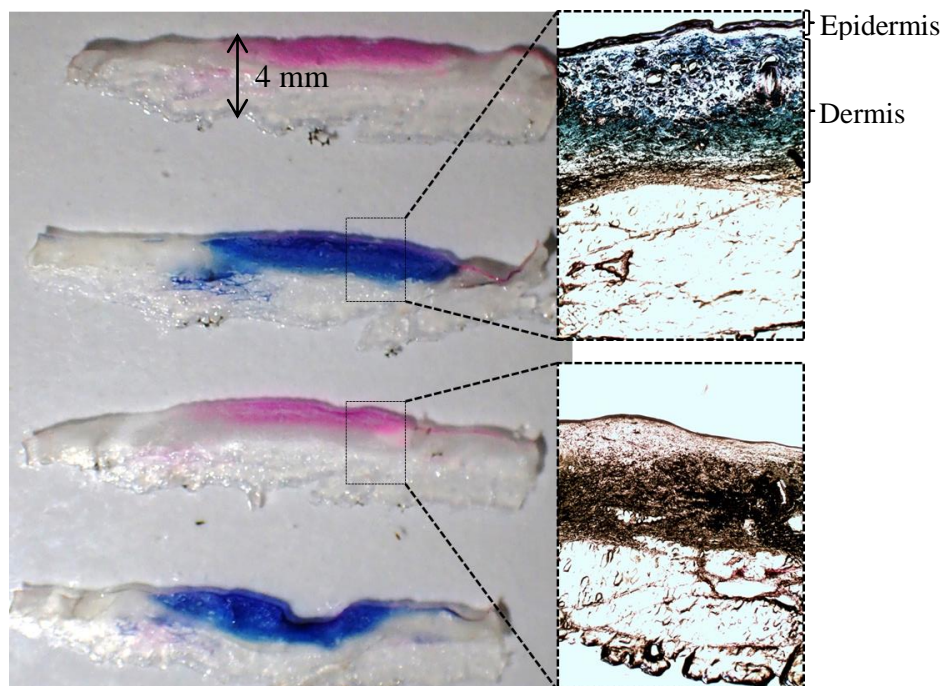
Figure 27. Cross sections of 60 µm thickness through the injection area.
Pink: Sulforhodamine B, blue: Fe (III) applied to sections.

The injection pattern displayed here is partly due to the injection, the interaction of the dye with the tissue and partly due to diffusion.

Under optimal conditions (in solution), diffusion coefficients for ferrocyanide and for sulforhodamine 101, which is structurally very similar to the used sulforhodamine B, have been reported. At room temperature and in aqueous media ferrocyanide diffuses in 1 M KCl at ~$0.67 \cdot 10^{-5}$ cm^2/s [130] and sulforhodamine 101 diffuses in sodium tetraborate buffer 50 mM at ~$0.33 \cdot 10^{-5}$ cm^2/s [131]. The molecular weights of the two dyes are in agreement with the experimentally determined diffusion constants. The molecular weight of the hydrophilic ferrocyanide $\{[Fe(CN)_6]^{4-}\}$ is with M = 251.08 g/mol roughly 50% smaller than sulforhodamine B (M = 580.65 g/mol). Considering the time after injection and subsequent freezing was in the order of 45 min, the diffusion for ferrocyanide could have led to a spreading of roughly 2 mm^2 *vs*. around 1 mm^2 for sulforhodamine B.

Here, the total area covered by dye was ~64 mm^2 and the skin tissue is more complex compared to a solution of a dye. Therefore, diffusion is assumed to have a minimal influence on the observed pattern. The spreading is mostly due to the injection and the interactions of the dye with the tissue and it can be concluded that ferrocyanide colors the interstitial space better and more rapidly than sulforhodamine B.

Ferrocyanide could be a good dye to visualize free liquid in the interstitial space. The injected dye did not disrupt the cell network as seen by intact skin slices and likely distributed along possible liquid channels. If the injection and distribution along these channels is possible, then the extraction of liquid from such channels should also be possible. Due to its good visibility and dark color, ferrocyanide could be used to test different microneedles and how their injection pattern changes based on tip shape, injection volume, injection depth and other variables.

2.4   Discussion and Conclusion

The sampling of ISF is not an easy task. Although its overall volume is as large as 12 L in a human, it is tightly retained in the tissues and is only available in small volumes. Ultrafiltration and microdialysis are currently used to study ISF, but these techniques are invasive and use membrane materials that often prevent larger molecules from passing and being detected. One improvement studied here is the use of microfiltration membranes, which have larger pore sizes and therefore interfere less with free and protein bound drug. Furthermore, we showed that the hydrophilic small molecule ferrocyanide spreads rapidly after intradermal injection and might thus be useful as a general indicator of ISF space, which behaves like a network of small fluid channels. If these channels can be filled with liquid through microneedle injection, the channels can likely be emptied too. Therefore, the extraction of ISF for TDM seems feasible if the extracted liquid can be directly collected and stored in a setup that is delicate and prevents evaporation or will be directly analyzed in the same device.

There is a possibility, however, that there is not enough free liquid available to be extracted. In case free liquid is only available in the skin after the injection of liquid into the skin, it could still be possible to successfully extract ISF. The injected liquid could be taken up through a different access point again. This access point can be either close or further away from the injection site. If it is close, the extracted liquid will resemble the injection liquid if the access point is further away, however, the extracted liquid could be pure ISF that is pushed out through the access point to make space for the injected liquid.

For reliable ISF sampling, more work is needed by researchers and engineers to manufacture devices that can be used to access ISF conveniently and in a pain-free way. Promising results of ISF sampling are shown in a recent publication using a jet injector [132].

Chapter 3: Pharmacokinetics of Drugs in Interstitial Fluid

3.1 Background

The PK of drugs in ISF are usually less well studied and known than in blood. Therapeutic drug monitoring is thus based almost exclusively on drug concentrations in blood with exception of severe cases of infection or when researchers are interested in drug penetration into specific infected or tumor tissue. In such situations, detailed PK knowledge in ISF might be crucial for the treatment outcome [133-135]. The study of PK in blood for TDM is not due to the missing information of tissue data of drugs in general, but methods used to study tissue concentrations are varied and data sets are often difficult to compare. Furthermore, studies of tissue fluid are generally more tedious to perform and quantification methods are not always available, unlike for blood. For these reasons, studies of tissue fluids are often not extensive and specifically focused around a single purpose (e.g., determination of antibiotic concentration in the lung). Nonetheless, many aspects surrounding tissue concentrations have been studied for decades including the possible influence of serum protein binding, diffusion behavior of drugs, transport mechanisms and tissue binding of drugs. If passive diffusion is the only mechanism used by the drug to reach the target site, free concentrations in serum and tissue are the same at a steady-state equilibrium [76]. However, many sites in the body are affected by diffusion barriers (e.g., continuous capillaries in the central nervous system), limited blood perfusion (see Table 2), transport mechanisms (e.g., active transport of drug into the urine) [76], inactivation of drug (e.g., metabolism in the liver, hydrolysis), pH dependent effects (e.g., inflammation, saliva), or contain protein or other binding partners that can reversibly or irreversibly remove acting drug molecules.

One major player that delays or prevents diffusion is protein binding. Protein binding of drugs in serum has been studied extensively and is also known under the name "Free Drug Principle". This principle has been addressed in an expert review [136] and explores the attenuation of drug activity by plasma proteins and its significance for drug discovery. The authors say that if protein and target binding is reversible and the system is at equilibrium, the target occupancy ratio (bound target/free target) can be described as a function of free fraction and total drug concentration according to equation **2**. It is not relevant for the system if the affinity of the drug to the target is much higher than it is to protein (here: protein = albumin). The concentration of target is negligible compared to the protein concentration so the albumin equilibrium will be overarching. Although albumin is the protein that interacts with most drugs, the equation can likely be adjusted for nonspecific binding to other proteins if the unbound fraction for a specific drug is known to be greatly affected by non-albumin binding.

$$\frac{[target \cdot drug]}{[target]_{free}} = \frac{[drug]_{free}}{K_{target}} = \frac{fu \cdot [drug]_{total}}{K_{target}} \qquad (2)$$

With $[]_{free\ or\ total} = free\ or\ total\ concentrations$,

$Free\ fraction\ (fu) = \frac{K_{albumin}}{K_{albumin} + [albumin]_{total}}$,

$K_{target} = \frac{[target]_{free} \cdot [drug]_{free}}{[target \cdot drug]}$ and $K_{albumin} = \frac{[albumin]_{free} \cdot [drug]_{free}}{[albumin \cdot drug]}$;

Usually, the drug molecule has to diffuse through the membrane and across the extravascular space before reaching its target site. Therefore, the drug target is often not near the drug molecule immediately and the considerations get more complicated.

Protein binding in this case will likely influence a drug's passive diffusion speed to other tissues directly after administration. Furthermore, it will also extend a drug's circulation time as protein bound drug is not removed by the kidneys.

70

Other than protein binding, the blood perfusion rate of the drug target tissue can affect how quickly the drug reaches the target tissue and possibly leads to a delay of drug effect.

In summary, target site drug levels are created by a complicated interplay of factors determining diffusion, transport, binding and perfusion. Target site levels can differ substantially from blood levels [137], which seems especially problematic for anti-infective agents that are often required to penetrate into tissues. Infections can occur in variable tissues in the body and drug concentrations measured in one tissue are not necessarily representative of a different tissue. However, extravascular concentrations do have in common that they represent concentrations after crossing the endothelial cells. Measuring and thus knowing the ISF anti-infective drug levels could lead to a much more rational therapy approach not only for anti-infectives, but potentially also for many other TDM drugs.

Currently, clinics use specifically implemented guidelines to adjust drug doses to match target ranges (Table 8) in blood to treat and monitor specific clinical conditions. However, blood sampling is difficult for some patient populations and for many drugs, the blood concentration does not reflect the concentration at the site of action, and therefore also not its pharmacologic effect.

With the current study, we aimed to provide evidence of the importance of the peripheral ISF compartment for TDM and derive useful information for the calculation of drug concentrations in ISF and their correlation to blood levels. Through the knowledge of the extravascular distribution of drugs and their PK, we would like to encourage the development of minimally invasive ISF sampling devices with on board drug analysis for TDM.

Table 8. Therapeutic ranges for the studied drugs after intravenous administration.

Drug	Target Range
Vancomycin	T: 10-20 µg/mL
Gentamicin	T: 0.5-2 µg/mL, P: 3-10 µg/mL
Cyclosporine	T: 100-400 ng/mL
Mycophenolic acid	12 h AUC $\geq$ 40 µg/mL/h
Tacrolimus	T: 5-20 ng/mL
Valproic acid	T: 30-100 µg/mL or 200-700 µmol/L
Phenytoin	T: 10-20 µg/mL or 40-80 µmol/L (total), free: 0.75-1.25 µg/mL or 3-5 µmol/L
Phenobarbital	10-35 µg/mL or 43-150 µmol/L
Methotrexate	0.1 to 1 µmol/L 24 to 72 hours after drug infusion
Digoxin	0.5-0.9 ng/mL
Theophylline	5-15 µg/mL

T: Trough concentration just before next dose is given
P: Peak concentration

3.2 Materials and Methods

3.2.1 Study Design

To study the PK of therapeutically monitored drugs in ISF, we created two data series in New Zealand white rabbits. In one experimental series, groups of rabbits (n = 4-6) were given a single dose of 2 out of 13 drugs, samples were taken from blood and ISF over time (up to 8-72 h) and drug was quantified. In a second experiment, one group of rabbits (n = 5) was given multiple doses of vancomycin. Samples were taken from blood and ISF at steady-state (up to 9 h) and drug concentrations were determined.

Drug levels in blood and ISF were analyzed to explore and compare their time course and steady-state concentrations. The sampling method was ultrafiltration in the single-dose study and microfiltration in the steady-state study. Differences between the two methods are mainly pore size and are covered in detail in chapter 2.1.1.

3.2.2 Studied Drugs

To study the PK in blood and ISF of rabbits, we selected a panel of drugs that is regularly monitored in clinical practice. Vancomycin (vancomycin hydrochloride, United States Pharmacopeia (USP) 500 mg; Hospira, Lake Forest, IL, US), gentamicin (gentamicin injection USP 40 mg/mL; Sandoz, Boucherville, QC, CA), tacrolimus (Prograf® injection 5 mg/mL; Astellas Pharma, Markham, ON, CA), cyclosporine (Sandimmune® injection 50mg/mL; Novartis, Dorval, QC, CA), mycophenolic acid (CellCept® 500 mg; Roche, Mississauga, ON, CA), valproic acid (sodium valproate 50 mg/kg; Sigma, MO, US), phenobarbital (sodium phenobarbital 30 mg/kg; Sigma, MO, US), phenytoin sodium (phenytoin sodium injection USP 50 mg/mL; Sandoz, QC, CA), carboplatin (carboplatin injection 10 mg/mL; Hospira, QC, CA), cisplatin (cisplatin injection 1 mg/mL; Hospira, QC, CA), methotrexate (methotrexate injection 25 mg/mL; Mayne Pharma, Salisbury South, AU), theophylline (theophylline 12 mg/kg; Sigma, ON, CA), and digoxin (digoxin injection 0.25 mg/mL; Sandoz, QC, CA). Tacrolimus, valproic acid, theophylline, and phenobarbital were diluted in sterile NaCl 0.9% and sterile filtered.

3.2.3 Animals

New Zealand White rabbits (1.75–5.5 kg) obtained from Charles River Laboratories (Wilmington, MA, US) were used for the study. This animal species was necessary in order to repeatedly collect blood (1 mL) and ISF samples without reaching the maximum allowance for blood collection during the study (~ 10% of the total blood volume). Rabbits were acclimatized for at least 7 days in group pens in a temperature-controlled room under a 12 h dark/light cycle and fed typical diet and water *ad libitum* before and after testing procedures.

3.2.4 Animal Procedures

3.2.4.1 Implantation of the Ultrafiltration Probe

Rabbits were premedicated with 22.5 mg/kg ketamine (Ketaset®; Wyeth, Guelph, ON, CA) and 2.5 mg/kg xylazine (Rompun®, Bayer, Toronto, ON, CA). Rabbits were maintained on oxygen and isoflurane (AERRANE®, Baxter Corporation, Mississauga, ON, CA) if needed. The implantation site was infiltrated with 0.3 mL bupivacaine (Marcaine® 0.50%; Hospira, QC, CA) subcutaneously. Heart rate, respiration rate, body temperature, and oxygen saturation of hemoglobin (pulse oximetry) were monitored during the procedure. To insert the ultrafiltration (UF) probe, the fur around the implant site was shaved and the skin aseptically prepared. The UF probe reinforced UF-3-12 (Bioanalytical Systems Inc., West Lafayette, IN, US) was 7 cm long and placed subcutaneously between the shoulders with a trocar guide needle. The tubing of the probe was held in place with butterfly tape tabs that were sutured to the rabbit skin. Probe and equipment were ethylene oxide sterilized and an aseptic technique was used. After the procedure, the implant site was covered with sterile Bioclusive® adhesive dressing (Systagenix, Gargrave, North Yorkshire, UK) and rabbits were fitted with a special jacket (Lomir Biomedical Inc., Malone, NY, US) to prevent unintended removal of the probe due to self-scratching. Rabbits were kept in single housing until the next day.

3.2.4.2 Implantation of the Microfiltration Probe

The microfiltration probes had similar dimensions as the ultrafiltration probe and the implantation was similar. The rabbits received 0.03 mL/kg of a mix of 10 mg/mL acepromazine maleate (Bayer Animal Health, ON, CA) and 20 mg/mL butorphanol tartrate (Torbugesic®, Fort Dodge, US) to calm them before the procedure. Their neck was shaved and a maximum of 1 mg/kg bupivacaine hydrochloride (Marcaine®, Hospira, QC, CA) was administered

74

subcutaneously. The operation site was prepared for surgery by scrubbing the skin alternatingly

with isopropanol and chlorhexidine gluconate (Hibitane 4% w/v, Zoetis, NJ, US). A sterile drape

and sterile gloves were used to insert the probe subcutaneously through a 12 G trocar needle. The

location of the probe was slightly left of the spine. The tubing outside of the implantation site

was secured to the skin with Bioclusive® and closed with plasticine™ overnight.

3.2.4.3   Administration of Drugs

3.2.4.3.1   Single-Dose Study

Twenty four hours after the implantation of the UF probe, rabbits' ears were treated with a local

anesthetic before inserting catheters in the ears for administration of drugs or blood sampling.

Rabbits were equipped with an intraarterial catheter in one ear for blood sampling and an

intravenous catheter in the other ear for the administration of a single dose (over 1-2 min) of two

drugs. Each rabbit in a group received a mix of two drugs according to Table 9 to minimize the

use of animals. The two drugs were given in separate syringes, one after the other into the ear

vein. The concomitantly administered drugs of each group were arranged such that no known

drug interactions would occur and interfere with the results of the study.

Table 9. Dose, injection group and sampling times for the single dose study of 13 drugs in rabbits (n = 4-6).

Drugs	Dose Rabbits (mg/kg)	Injection Group (#)	Sampling Times (h)
Vancomycin	20	1	0, 0.25, 0.5, 0.75, 1, 2, 4, 6, 8, 24
Gentamicin	50	3	0, 0.25, 0.5, 0.75, 1, 2, 4, 6, 8, 24
Carboplatin	18.7	6	0, 0.25, 0.5, 0.75, 1, 2, 4, 6, 8, 24
Cisplatin	3	5	0, 0.25, 0.5, 0.75, 1, 2, 4, 6, 8, 24
Methotrexate	15	2	0, 0.25, 0.5, 0.75, 1, 2, 4, 6, 8, 24
Valproic Acid	50	2	0, 0.25, 0.5, 0.75, 1, 2, 4, 6, 8, 24
Phenytoin	10	5	0, 0.25, 0.5, 0.75, 1, 2, 4, 6, 8, 24
Phenobarbital	30	7	0, 0.25, 0.5, 0.75, 1, 2, 4, 6, 8, 24, 72
Cyclosporine	5	6	0, 0.25, 0.5, 0.75, 1, 2, 4, 6, 8, 24
Mycophenolic acid	40	4	0, 0.25, 0.5, 0.75, 1, 2, 4, 6, 8, 24
Tacrolimus	0.1	1	0, 0.25, 0.5, 0.75, 1, 2, 4, 6, 8, 24
Digoxin	0.02	4	0, 0.25, 0.5, 0.75, 1, 2, 4, 6, 8, 24
Theophylline	12	3	0, 0.25, 0.5, 0.75, 1, 2, 4, 6, 8, 24

3.2.4.3.2   Steady-State Study

For the steady-state study, loading dose, maintenance dose and dosing interval were calculated

from the non-compartmental analysis (NCA) from the single-dose study for vancomycin and 5

doses were administered into an intravenous catheter according to Table 10.

Table 10. Doses, sampling and injection times for the steady-state study of vancomycin in rabbits (n = 5).

Drug	Loading Dose (mg/kg)	Maintenance Dose (mg/kg)	Dosing Interval (h)	Sampling Times (h)	Injection Times (h)
Vancomycin	20	15	1.5	Trough samples: 0, 1.5, 3, 4.5, 6; 6.25, 6.5, 7, 7.5, 8, 8.5, 9	0 (D_L), 1.5 (D_M), 3 (D_M), 4.5 (D_M), 6 (D_M)

D_L: Loading dose, D_M: Maintenance dose

3.2.4.4 Blood Sampling

3.2.4.4.1 Single-Dose Study

Blood samples were collected from the opposite non-injection ear through a 24 G 5/8 inch catheter from an intraarterial catheter. EMLA$^®$ analgesic cream was applied to the ear veins prior to venipuncture. At the sampling times, 0.2 mL of blood was removed from the ear and not used for analysis, and then 0.5 mL was collected, the catheter flushed with 0.1 mL heparinized saline, and closed to prevent clotting. Serum, plasma or EDTA whole blood collection tubes were used according to the recommendations for drug quantification (3.2.5). For blood data the exact sampling time-points were recorded. Serum and blood samples were kept at 4°C until the end of the study day and then frozen at -20°C. Sampling times for the single-dose study were: predose, 15, 30, 45, and 60 min; 2, 4, 6, 8, and 24 h (and the additional 72 h time point for phenobarbital).

3.2.4.4.2 Steady-State Study

For the steady-state study, five trough concentrations were taken before the administration of the next dose of vancomycin and seven more samples were taken after the last dose: 15 and 30 minutes, 1, 1.5, 2, 2.5, 3 h. A representative schedule for injection and sampling is given in Table 11.

Table 11. Representative injection and sampling schedule for the steady-state study.

Time	Procedure	Time (completed)	Comment
7.00 am	Application of EMLA$^®$ Cream Placement of *IV* catheter Placement of *IA* catheter		
7.20 am **7.30 am**	Blood Sampling (0.5 mL) ISF Sampling Injection of D$_L$	7.45 am 7.40 am 7.52 am	Blood Baseline ISF Baseline
8.50 am **9.00 am**	Blood Sampling (0.5 mL) ISF Sampling Injection of D$_M$	9.14 am 9.10 am 9.20 am	Blood 1.5 h Sample ISF 1.5 h Sample

Time	Procedure	Time (completed)	Comment
10.20 am 10.30 am	Blood Sampling (0.5 mL) ISF Sampling Injection of D_M	10.40 am 10.35 am 10.45 am	Blood 3 h Sample ISF 3 h Sample
11.50 am 12.00 pm	Blood Sampling (0.5 mL) ISF Sampling Injection of D_M	12.15 am 12.13 am 12.18 am	Blood 4.5 h Sample ISF 4.5 h Sample
1.20 pm 1.30 pm	Blood Sampling (0.5 mL) ISF Sampling Injection of D_M	1.46 pm 1.43 pm 1.50 pm	Blood 6 h Sample ISF 6 h Sample
1.45 pm	Blood Sampling (0.5 mL) ISF Sampling	2.04 pm 2.03 pm	Blood 6 h 15 min Sample ISF 6 h 15 min Sample
2.00 pm	Blood Sampling (0.5 mL) ISF Sampling	2.22 pm 2.20 pm	Blood 6.5 h Sample ISF 6.5 h Sample
2.30 pm	Blood Sampling (0.5 mL) ISF Sampling	2.49 pm 2.47 pm	Blood 7 h Sample ISF 7 h Sample
3.00 pm	Blood Sampling (0.5 mL) ISF Sampling	3.23 pm 3.17 pm	Blood 7.5 h Sample ISF 7.5 h Sample
3.30 pm	Blood Sampling (0.5 mL) ISF Sampling	4.03 pm 4.00 pm	Blood 8 h Sample ISF 8 h Sample
4.00 pm	Blood Sampling (0.5 mL) ISF Sampling	4.36 pm 4.34 pm	Blood 8.5 h Sample ISF 8.5 h Sample
4.30 pm	Blood Sampling (0.5 mL) ISF Sampling	5.15 pm 5.02 pm	Blood 9 h Sample ISF 9 h Sample

D_L: Loading dose, D_M: Maintenance dose

3.2.4.5   ISF Sampling

3.2.4.5.1   Single-Dose Study

ISF was collected (via the UF probe, MWCO 30 kDa) over 10 or 11 time intervals: predose; 0-15, 15-30, 30-45, and 45-60 min; 1-2, 2-4, 4-6, 6-8, and 23-24 h (71-72 h for phenobarbital). ISF data points were adjusted using the calculated mean flow rate for each probe and midpoint adjustment.

The blunt end of a butterfly needle (21G) was inserted into the tubing of the UF probe. A serum collection Vacutainer® was attached to the butterfly needle and held in place by the rabbit jacket.

At the end of each time interval, a fresh collection tube was connected or the needle was removed and the tube of the UF probe sealed with tape. ISF samples were kept at 4°C until the end of the study day, and then frozen at -20°C.

ISF samples contained no protein bound drug as the molecular weight cutoff of 30 kDa excluded larger proteins, especially albumin (60 kDa). To account for drug loss through drug adsorption onto the UF probe material a recovery experiment was implemented. All drugs were diluted in PBS 7.4 and extracted through the UF probe. Three to four extracts were obtained and quantified using the same methodology as for the animal study. The recovery was expressed as

$$\% \, Recovery = \frac{Concentration \; before \; extraction}{Concentration \; after \; extraction} \cdot 100 \; \text{(see chapter 2.2.1.1).}$$

Drug recovery was performed after the animal study has been completed as we had not anticipated drug adsorption to the membrane. The ultrafiltration membrane is a commercially available tool (UF probe reinforced UF-3-12, Bioanalytical Systems Inc., West Lafayette, IN, US) and all drugs used are significantly smaller than the MWCO of 30 kDa.

3.2.4.5.2   Steady-State Study

For the microfiltration sampling (microfiltration device see 2.2.4.1), ISF samples were time-point samples. Just after taking the corresponding blood sample a 27 G ½ inch needle was connected to the microfiltration tubing and suction applied with a 6 mL syringe (plunger pulled to 2 mL and held) for 2×2 minutes. The syringe was removed carefully and the accumulated ISF collected in the needle hub both times with a 10 µL micropipette. The double extraction was necessary to accumulate enough ISF. The animals showed no discomfort during this procedure.

3.2.5   Drug Quantification

3.2.5.1.1   Single-Dose Study

Drug samples were analyzed at Exova (Surrey, BC, CA) and in clinical laboratories at Vancouver General Hospital and Children's & Women's Health Centre of British Columbia (Vancouver, BC, CA) using validated assays. Methotrexate and valproic acid were analyzed in ethylenediaminetetraacetic acid (EDTA)-plasma using fluorescence polarization immunoassays (Abbott Laboratories, Abbott Park, IL, US). Particle-enhanced turbidimetric inhibition immunoassays (Siemens, Deerfield, IL, US) were used to analyze phenytoin, digoxin, phenobarbital, theophylline, vancomycin, and gentamicin in serum. Mycophenolic acid (active metabolite of mycophenolate mofetil), tacrolimus, and cyclosporine were analyzed in EDTA-whole blood using liquid chromatography – tandem mass spectrometry. A platinum trace analysis with inductively coupled atomic emission spectrometry (United States Environmental Protection Agency, 6010 C) for carboplatin and cisplatin in EDTA-whole blood was conducted at Exova. For all analytical assays, ISF samples were used as collected (no sample processing), and all samples were stored at -20 °C until analysis.

3.2.5.1.2   Steady-State Study

The serum and ISF vancomycin samples were quantified using an LCMS method specially developed for microsample amounts (see Chapter 4).

3.2.6   Pharmacokinetic Analysis

While drugs are usually monitored in the blood, little is known about the concentration *vs.* time course in tissues. Using PK software (Phoenix 64, Pharsight) we applied non-compartmental and compartmental approaches to determine the PK of the studied drugs in blood and ISF (Figure 28). Crucial for our compartmental analysis is that we use both data sets from blood and ISF to

build custom models that accommodate each drug separately. This allows plotting the concentration time course for both compartments and the concentration of drug in the compartments can be determined at any time. Conventional compartmental modeling uses only blood concentrations.
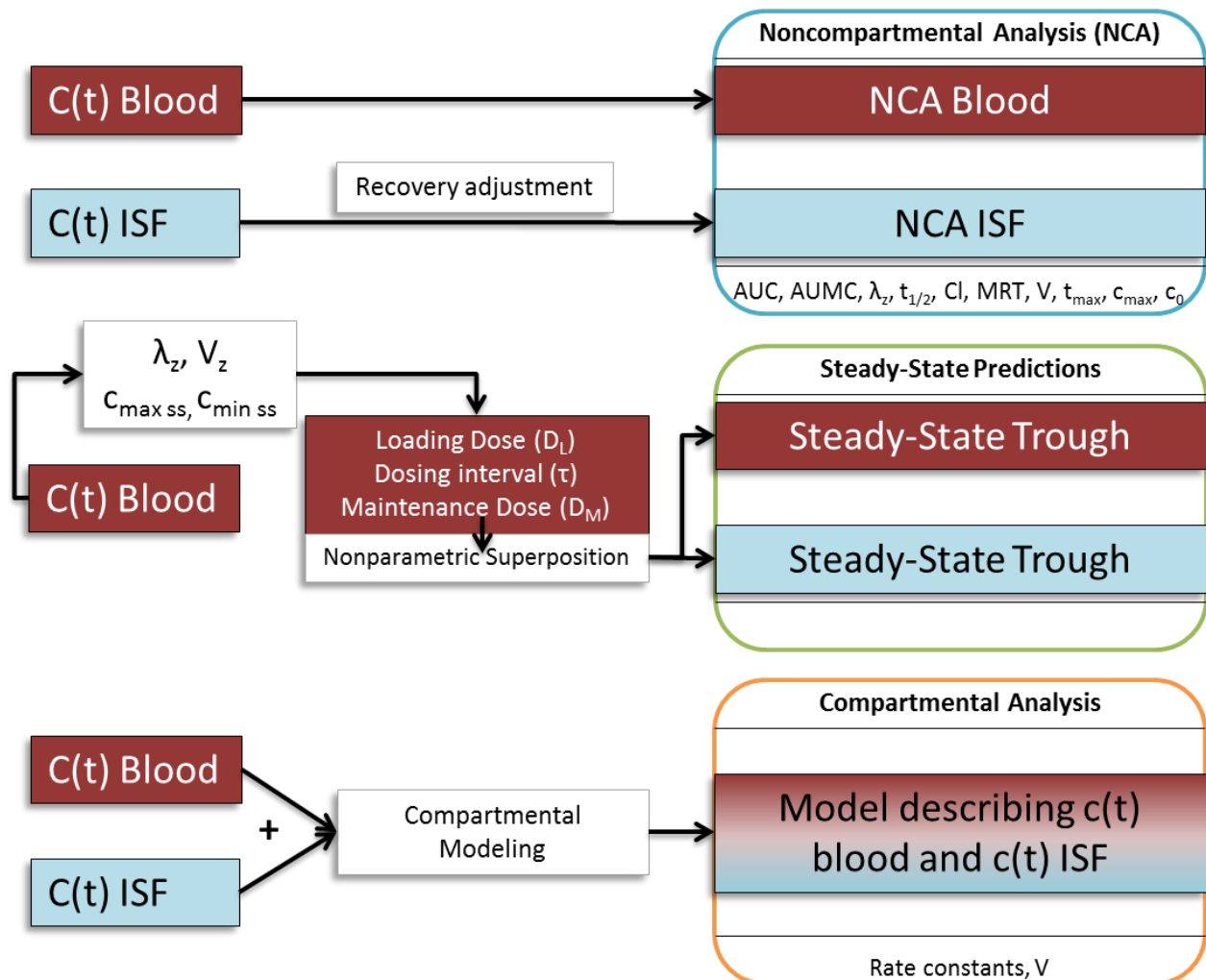
Figure 28. Flowchart for performed PK analyses.

3.2.6.1 Individual Pharmacokinetics: Non-Compartmental Analysis (NCA)

In the first approach PK parameters including the area under the curve or total exposure AUC (**3**), area under the first moment curve AUMC (**4**), elimination rate constant λ_z, terminal half-life $t_{1/2}$ (**6**), clearance CL (**5**), mean residence time MRT (**7**), volume of distribution V_z (**8**), time at maximum concentration t_{max}, maximum exposure C_{max} and concentration at time zero C_0 for each matrix have been derived using NCA for blood and ISF.

AUC and AUMC were calculated using linear trapezoids and linear interpolation and were extrapolated to infinity by adding $\frac{c_{last}}{\lambda_z}$ and $\frac{t_{last} \cdot c_{last}}{\lambda_z} + \frac{c_{last}}{\lambda_z^2}$, respectively, to the areas from time zero to the last sampling point. Further parameters were derived from these areas. The terminal rate constant λ_z was estimated by linear regression of the time versus log-concentration of the terminal part of the curve. The parameters t_{max} and C_{max} are the time of maximum observed concentration and the maximum observed concentration. The initial concentration C_0 is determined through back extrapolation of the log linear transform of the first two sampling points. For ISF data, drug input was set to extravascular and for blood data drug input was intravenous.

$$AUC = AUC_{last} + \frac{c_{last}}{\lambda_z} \tag{3}$$

$$AUMC = AUMC_{last} + \frac{t_{last} \cdot c_{last}}{\lambda_z} + \frac{c_{last}}{\lambda_z^2} \tag{4}$$

$$CL = \frac{Dose}{AUC} \tag{5}$$

$$t_{1/2} = \frac{ln(2)}{\lambda_z} \tag{6}$$

$$MRT = \frac{AUMC}{AUC} \tag{7}$$

$$V_z = \frac{Dose}{\lambda_z \cdot AUC} \qquad (8)$$

3.2.6.2 Steady-State Predictions

Generally, patients take more than just one dose of a drug. After repeated dosing, drug

concentrations in their system reach a so called steady-state, where no accumulation occurs and

drug input and drug elimination are at equilibrium. Therefore, it is desirable to predict the drug

concentration in blood or ISF after multiple doses, based on concentration data from a single

dose. In linear systems, the principle of superposition applies, which states that the total response

after multiple stimuli (here doses) behaves additive. In this special case, where there have been

no model assumptions, non-parametric superposition can be performed. The elimination rate

constant (λ_z) and its intercept (A) with the y-axis are determined by log-linear regression of the

terminal phase and the concentration after n doses can be described by Equation **9**. Finding the

common factor $Ae^{-\lambda_z(t+\tau)}$ and later multiplying and dividing by the common factor $(1 - e^{-\lambda_z t})$

simplifies Equation **9** to Equation **10**. For an infinite amount of doses given ($n \to \infty$) the

concentration at steady-state (C_{ss}) can be calculated using Equation **11** if the loading dose (D_L),

maintenance dose (D_M) and dosing interval (τ) are known or have been calculated.

$$C_n(t) = C_1(t) + Ae^{-\lambda_z(t+\tau)} + Ae^{-\lambda_z(t+2\tau)} + \dots + Ae^{-\lambda_z(t+(n-1)\tau)} \qquad (9)$$

$$C_n(t) = C_1(t) + Ae^{-\lambda_z(t+\tau)} \frac{1 - e^{-\lambda_z(n-1)\tau}}{1 - e^{-\lambda_z\tau}} \qquad (10)$$

$$C_{ss}(t) = C_1(t) + \frac{Ae^{-\lambda_z(t+\tau)}}{1 - e^{-\lambda_z\tau}} \qquad (11)$$

Using the estimated NCA parameters λ_z and V_z and defining specifically desired target ranges

($C_{min\ ss}$ and $C_{max\ ss}$), loading dose D_L (**12**), maintenance dose D_M (**13**) and dosing interval τ (**14**)

can be calculated. Target ranges were defined based on therapeutically desired ranges. For drugs

without concentration time data in ISF (tacrolimus, cyclosporine, phenytoin) no ISF trough

concentrations could be predicted.

$$D_L = c_{max\,ss} \cdot V_z \qquad\qquad (12)$$

$$D_M = D_L \cdot \left(\frac{1}{1 - e^{-\lambda_z \tau}}\right) \qquad\qquad (13)$$

$$\tau = \frac{ln\dfrac{C_{min\,ss}}{C_{max\,ss}}}{\lambda_z} \qquad\qquad (14)$$

V_z is the volume of distribution at pseudo-equilibrium

3.2.6.3   Compartmental Modeling and Nonlinear Regression Analysis

The overall approach for this analysis was to find customized physiologically relevant models

for each drug to produce a set of primary PK parameters (microconstants) that describe the data

well (e.g., rate constants and volume of distribution). Two or three compartment models were

used, depending on the fit of both concentration data from blood and ISF. The simpler two

compartment model was investigated first, then the three compartmental model. The structure of

the models, parameterization and run options are described in more detail in the following

paragraph (adapted from Phoenix®, WinNonlin® 6.3 User Guide).

The PK models used here are compartmental microconstant models. The differential equations

are mass transfer rate constants that describe each compartment. The models are open form and

they use intravenous dosing.

The error model chosen is additive with an Epsilon variable $\in =\ standard\ deviation$ and an

initial standard deviation set to 1. Therefore the observed concentrations in the compartments

(C1 = central compartment, P1 = first peripheral compartment, P2 = second peripheral

compartment) are described with the error added: $C1_{observed} = C1+\in$, $P1_{observed} = P1+\in$

and $P2_{observed} = P2+\in$ respectively.

84

Initial estimates for the fixed effects V_1, k_{10}, k_{12}, k_{21}, k_{23}, k_{31} and V_3 (volumes and rate constants) were determined using an optical interface displaying the plots of the dependent variable (C_{Blood} and C_{ISF}) *vs.* time according to the parameters of the model. The parameters were adjusted to determine the best initial values that fit both data sets simultaneously. The lower bounds for the initial estimates were set to zero or the lower and upper bounds were defined to give a good fit. This means that the model was first run with the initial estimates, then the estimated parameters were compared to the initial estimates and if they were not close or the prediction error was large, the upper and lower bounds were adjusted appropriately to a narrower range. Fixing parameters to the initial estimates or defining narrow bounds can result in a better model fit, but it can suppress error estimation and is usually only recommended if there is evidence that the fixed parameters are valuable estimates.

The modeling engine used was a naïve-pooled engine with 1000 iterations per modeling run. Using the naïve-pooled run engine, all data are pooled into a single individual log likelihood function without random effect parameters. This means that the observations are treated as if they are from a single individual and that inter-individual variations are ignored. Model fit is achieved through a minimization of the exact negative log likelihood of the Gaussian function. The minimization is achieved by iterative passes through a quasi-Newton algorithm until successive runs result in the same log likelihood with a difference of only 0.001.

For the numerical solution of the model, the ordinary differential equations solver method used is the matrix exponent method.

Standard errors for the parameters were estimated using the Hessian method of parameter uncertainty estimation and calculated using central difference of two adjacent points in the likelihood function.

A successful model fit was diagnosed by the engine return code of 1, which means that the reported solution is likely optimal or nearly optimal (Phoenix®, WinNonlin® 6.3 User Guide). Residual plots were used for further assessment of the model fit. Residual plots are often generated to evaluate if the model assumptions are true and give an idea of the model fit and error associated with the model. The random error component epsilon (∈) associated with the modeled y values (concentrations) were computed using an additive error model. This means that the random error is added to each computed observation. Three assumptions are made about the errors: they are normally distributed, have the same variance at every x (homoscedasticity) and are independent of one another. If this is correct, then the observed residuals (ε) should behave very similar and this has to be determined. The observed residuals are computed by subtracting the predicted y value from the measured y value and plotted against the independent variable x (see Appendix). This is done to determine if the residuals are randomly distributed and not too far away from y = 0. If there is no systematic curvature and the variance is similar across the x values, the model assumptions are likely true.

To plot the concentration time course of drug in ISF and blood from the set of primary PK parameters, the differential equations were numerically integrated using the values for the rate constants predicted by the model and plotted.

3.3   Results

The PK of different TDM drugs from Table 8 will be presented in the following pages grouped according to their therapeutic drug class. Specifically, the antibiotics vancomycin and gentamicin will be covered first (3.3.1), then the antineoplastic drugs cisplatin, carboplatin, and methotrexate (3.3.2), the antiepileptics valproic acid, phenytoin and phenobarbital (3.3.3), the immunosuppressants cyclosporine, mycophenolic acid and tacrolimus (3.3.4), the cardiac

86

glycoside digoxin and the smooth muscle relaxant theophylline (3.3.4.3). Although drug
quantification was performed in either blood, serum or plasma for the studied drugs according to
chapter 3.2.5 and Table 12, in this document, the term blood will be used interchangeably with
plasma and/or serum.

Table 12. Definition of "blood sample" for studied drugs

Drug	Blood/Plasma/Serum
Vancomycin	Serum
Gentamicin	Serum
Tacrolimus	EDTA-Blood
Cyclosporine	EDTA-Blood
Mycophenolic acid mofetil	EDTA-Blood
Valproic Acid	EDTA-Plasma
Phenobarbital	Serum
Phenytoin	Serum
Carboplatin	EDTA-Blood
Cisplatin	EDTA-Blood
Methotrexate	Plasma
Theophylline	Serum
Digoxin	Serum

3.3.1 PK Analysis of the Antibiotics Vancomycin and Gentamicin in Blood and ISF

The antibiotics vancomycin and gentamicin are routinely monitored in clinical practice due to
their possibly detrimental effects on ear and kidney. Unlike their names and similar toxicity
spectrum might imply, they are quite different in chemical structure and cover different
antibacterial spectra. Vancomycin is a 1449.3 g/mol large glycopeptide antibiotic, which inhibits
the cell wall synthesis of bacteria and is used for the treatment of life-threatening bacterial
infections by gram positive species like methicillin-resistant *Staphylococcus aureus* and

multiresistant *Staphylococcus epidermidis*. Gentamicin is with 477.6 g/mol a rather small aminoglycoside antibiotic that binds to the ribosomal subunits 30S and 50S, thereby interfering with the bacterial protein synthesis. Gentamicin is more prominently used to treat serious infections by gram negative bacteria including *Pseudomonas, Proteus and Serratia species,* but is also effective against *Staphylococcus species*.

Both molecules are quite hydrophilic, have very low oral bioavailability and are reported to variably distribute into the tissues after intravenous administration [138-141]. However, the tissue distribution of these antibiotics is crucial for positive therapeutic outcomes and concentrations of a minimal level at the site of action (e.g., tissue) are required to visibly inhibit bacterial growth overnight. These minimal inhibitory concentrations (MIC) are very specific for the type of antibiotic and bacterial strain, and most important to prevent the development of resistance. It has been reported that a remarkable accumulation of antibiotic in the tissues can be a predecessor of renal toxicities for gentamicin [141].

3.3.1.1   Concentration Time Profile in Blood and ISF

Both antibiotics were readily detectable in blood and interstitial fluid. Gentamicin ISF data have been adjusted as suggested in the ultrafiltration experiment (2.3.1) to reflect 100% recovery. An adjustment was not necessary for vancomycin. Table 13 summarizes the study facts and a full concentration *vs.* time profile of both antibiotics is given in Figure 29 and 30. Vancomycin distributes rapidly to the peripheral ISF compartment and is eliminated almost identically from both compartments as best seen in the semi-logarithmic plot. Gentamicin, however, accumulates slowly in the peripheral compartment and is eliminated very slowly as indicated by an almost parallel line to the x-axis in the semi-logarithmic plot.

Table 13. Summary study table for the antibiotics vancomycin and gentamicin.

Drug	Study	Study Subjects (#)	Dose (mg/kg)	Recovery Factor R	Drug in ISF	Site of Drug Action
Vancomycin	Single-dose	4	20	1.00	Yes	Periphery
Gentamicin	Single-dose	6	50	8.47	Yes	Periphery
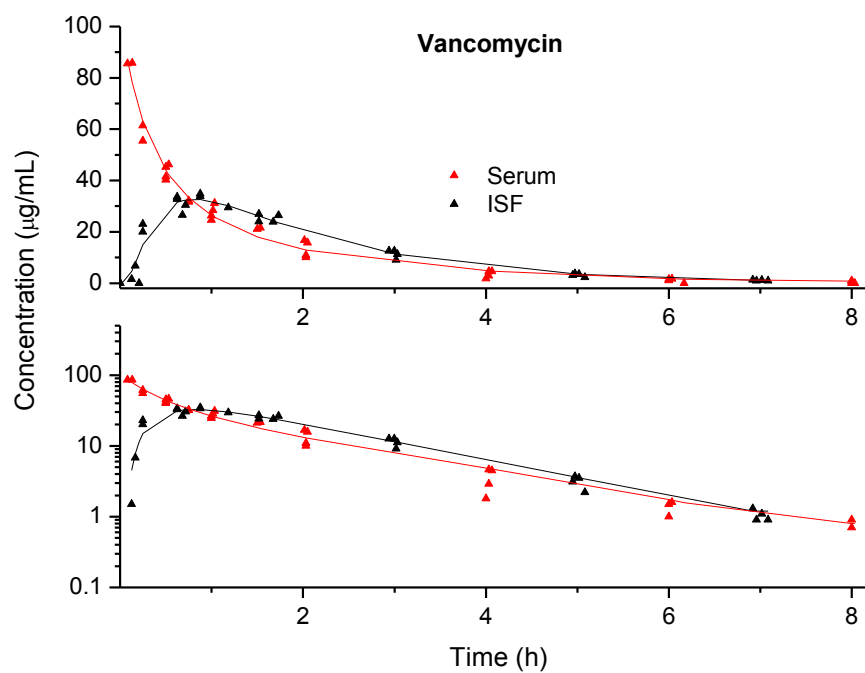
Figure 29. Vancomycin concentration in serum and ISF of rabbits after single dosing, shown both as a linear plot and a logarithmic plot (n = 4). The lines are drawn to serve as visual guides and do not indicate a specific model.
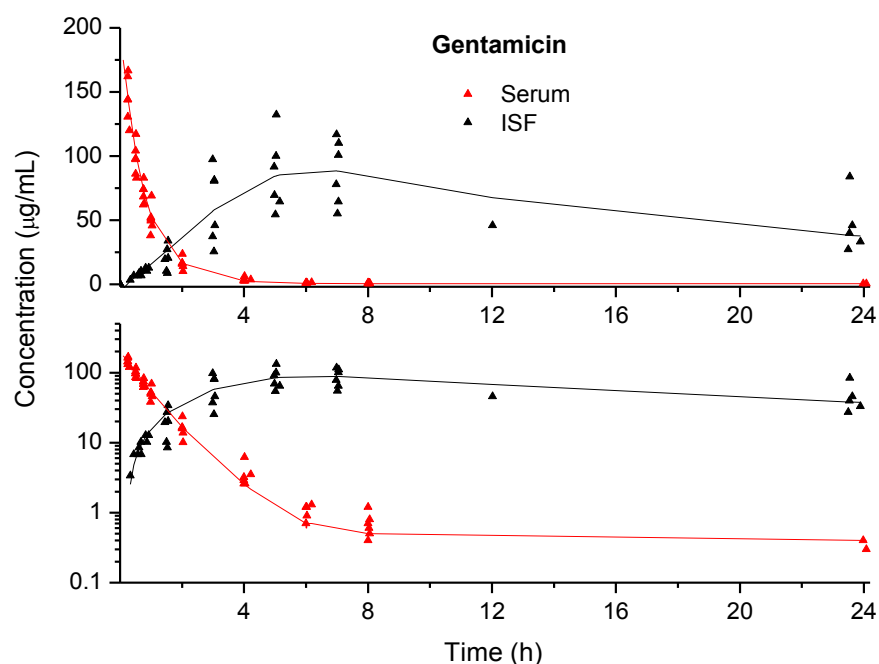
Figure 30. Gentamicin concentration in serum and ISF of rabbits after single dosing, shown both as a linear plot and a logarithmic plot (n = 5). The lines are drawn to serve as visual guides and do not indicate a specific model.

3.3.1.2   Non-Compartmental Pharmacokinetic Analysis (NCA)

Using statistical moment analysis without any model assumptions, basic PK parameters were

calculated for vancomycin (Table 14) and gentamicin (Table 15). ISF concentrations were

adjusted to 100% recovery using ultrafiltration recovery data for gentamicin whereas the

difference in recovery for vancomycin was not significant (Table 6, 2.3.1). Vancomycin shows

very similar PK parameters in blood and ISF and drug elimination and total drug exposure are

comparable. The mean residence time (MRT) of vancomycin in ISF is slightly longer and the

maximum concentration detected in ISF is lower than in blood.

For gentamicin, the PK parameters are very different in blood and ISF. Most notably, the total

drug exposure (AUC) is much higher and the overall drug elimination from the peripheral

compartment is extremely slow as seen by large $t_{1/2}$ and MRT and a very small elimination rate constant.

Table 14. PK parameters (mean ± standard deviation) determined by NCA for vancomycin in serum (n = 4) and ISF (n = 4), dose = 20.000 µg/kg.

Vancomycin	AUC µg·h/mL	AUMC µg·h·h/mL	C_0 µg/mL	CL mL/h/kg	C_{max} (measured) µg/mL
Serum	95.39±16.7	128.28±42.52	93±14.22	214.8±39.17	72.05±15.95
ISF	83.99±4.33	175.53±16.02	0±0	238.57[1]±11.81	32.1±2.61
	$t_{1/2}$ h	λ_z h^{-1}	MRT h	t_{max} h	V_z mL/kg
Serum	1.17±0.27	0.62±0.17	1.32±0.23	0.18±0.08	350.82±37.09
ISF	1.16±0.06	0.6±0.03	2.09±0.16	0.91±0.2	398.61[2]±26.77

[1]for ISF, this value represents CL/F, [2]for ISF, this value represents V_z/F

Table 15. PK parameters (mean ± standard deviation) determined by NCA for gentamicin in serum (n = 6) and ISF (n = 6), dose= 50000 µg/kg.

Gentamicin	AUC µg·h/mL	AUMC µg·h·h/mL	C_0 µg/mL	CL mL/h/kg	C_{max} (measured) µg/mL
Serum	184.71±43.12	262±143.17	218.44±24.01	281.45±56.57	144.5±17.82
ISF	3400.85±3406.47	214.139.2±403.784.0	0±0	22.5[1]±10.5	91.19±30.43
	$t_{1/2}$ h	λ_z h^{-1}	MRT h	t_{max} h	V_z mL/kg
Serum	1.3±0.13	0.54±0.05	1.35±0.46	0.26±0.02	531.34±117.36
ISF	24.15±22.42	0.05±0.03	36.59±32.58	6.37±0.99	538.25[2]±179.26

[1]for ISF, this value represents CL/F, [2]for ISF, this value represents V_z/F

3.3.1.3   Steady-State Concentrations and Non-Parametric Superposition

Steady-state concentrations of antibiotics are more important in clinical practice than single-dose data, as antibiotics are given in multiple dose regimens. To eradicate bacterial infections, the concentrations of antibiotics have to stay above a certain minimal concentration to inhibit bacterial growth significantly and avoid the development of resistant strains.

After calculating the NCA parameters, the dosing regimen for a multiple dose study was derived (Table 16 and 17). Non-parametric superposition was used to estimate concentrations from the single-dose data set at steady state just before giving the next dose (C_{trough}). C_{trough} is a parameter often used in clinics to base dose adjustments on. Comparing the trough concentrations in blood and ISF (Figure 31 and 32) it is apparent that the variability of the blood predictions is larger than the variability in the ISF predictions for vancomycin. An unpaired t-test, with an expected difference between compartments set to zero, revealed that the means are significantly different ($\alpha = 0.05$, two tail). Using the calculated doses and dosing interval to reach a target trough concentration of 20 µg/mL results in C_{trough}(blood) = 16.6 µg/mL and C_{trough}(ISF) = 25.9 µg/mL (Table 16). For gentamicin (Table 17), the predicted trough concentrations are 0.49 µg/mL and 35.88 µg/mL (without the first extremely high data point of 182.71 µg/mL) for blood and ISF respectively with an expected trough concentration of 0.2 µg/mL. It seems likely that C_{trough} of the first rabbit of 182.71 µg/mL is due to a very small terminal elimination rate constant (λ_z) in ISF, which in turn is due to a relatively higher concentration at t_{last} (~8 h). Concentrations at the end of the curve are often close to the detection limit of the quantification method and therefore prone to higher measurement error. An exclusion of this concentration seems appropriate and has been confirmed with Grubb's outlier test for the maximum value. The box and whisker plots (Figure 31 and 32) show a comparison of the predictions in blood and ISF for both drugs. The top and bottom of the box represent the first and third quartile, the band in the box represents the median, and whiskers represent 1 SD from the mean. For gentamicin, the mean trough concentration in ISF is especially high as compared to the mean blood concentration, which is in agreement with a previously reported tissue accumulation of gentamicin [141].

Gentamicin concentrations in citric acid induced saliva, which is a different matrix suggested previously for TDM, have been measured in children and summarized in a recent review [142]. Mean steady-state concentrations in saliva after a dose of 5 mg/kg/day using a dosing interval of 6 h were not higher than in plasma (e.g. two doses/day: plasma: 0.3-1.4 µg/mL and saliva: 0-0.9 µg/mL). The mean steady-state concentrations for gentamicin in serum and ISF were 0.49 and 35.88 µg/mL after a dose of 10 mg/kg/day. The dose administered in the saliva study was about half the dose used for the ISF predictions, but even accounting for this, the difference between saliva and ISF concentrations is large (0-0.9 µg/mL *vs* 17.94 µg/mL). For gentamicin, blood levels are not similar to concentrations measured in saliva or ISF at steady state.

Table 16. The calculation of loading dose (D_L), maintenance dose (D_M) and dosing interval (τ) for vancomycin from λ_z and V_z, $C_{max\ ss}$= 80 µg/mL and $C_{min\ ss}$= 20 µg/mL.

Vancomycin Rabbit #	λ_z (serum) (h^{-1})	V_z (serum) (mL/kg)	D_L (µg/kg)	τ (h)	D_M (µg/kg)	Predicted Trough in Serum (µg/mL)	Predicted Trough in ISF (µg/mL)
1	0.49	377.28	30182.79	2.83	22637.09	20.83	28.24
2	0.53	342.19	27375.42	2.61	20531.56	21.41	26.08
3	0.87	301.94	24154.88	1.59	18116.16	10.70	22.43
4	0.60	381.85	30547.86	2.30	22910.89	13.58	26.85
Mean	**0.62**	**350.82**	**28065.24**	**2.34**	**21048.93**	**16.63**	**25.90**
SD	0.17	37.09	2967.28	0.54	2225.46	5.32	2.48

Table 17. The calculation of loading dose (D_L), maintenance dose (D_M) and dosing interval (τ) for gentamicin from λ_z and V_z, $C_{max\ s}$= 10 µg/mL and $C_{min\ ss}$= 0.2 µg/mL.

Gentamicin Rabbit #	λ_z (serum) (h^{-1})	V_z (serum) (mL/kg)	D_L (µg/kg)	τ (h)	D_M (µg/kg)	Predicted Trough in Serum (µg/mL)	Predicted Trough in ISF (µg/mL)
1	0.53	532.26	5322.62	5.62	5056.48	0.21	182.71*
2	0.52	522.42	5224.15	5.77	4962.94	0.17	40.09
3	0.55	590.18	5901.79	5.46	5606.70	0.13	47.61
4	0.55	641.20	6412.04	5.42	6091.44	0.11	38.59
5	0.61	308.97	3089.71	4.90	2935.22	2.01	24.99
6	0.45	592.99	5929.92	6.66	5633.43	0.30	28.14
Mean	**0.54**	**531.34**	**5313.37**	**5.64**	**5047.70**	**0.49**	**60.36(35.88)**
SD	0.05	117.36	1173.56	0.58	1114.88	0.75	60.51(9.24)

If * excluded, then the mean and SD are as given in brackets
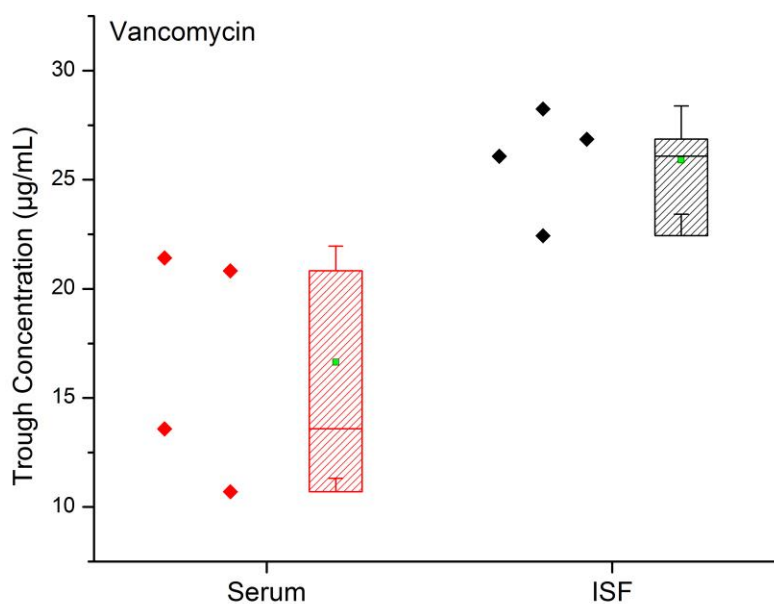
Figure 31. Box and whisker plot of steady-state trough concentrations in serum and ISF for vancomycin:
Top and bottom of box represent the first and third quartile, the band in the box represents the median, whiskers represent 1 SD from the mean (■), the means are significantly different (unpaired t-test, two tail, α = 0.05)
● Serum Concentrations (n = 4)
● ISF Concentrations (n = 4)
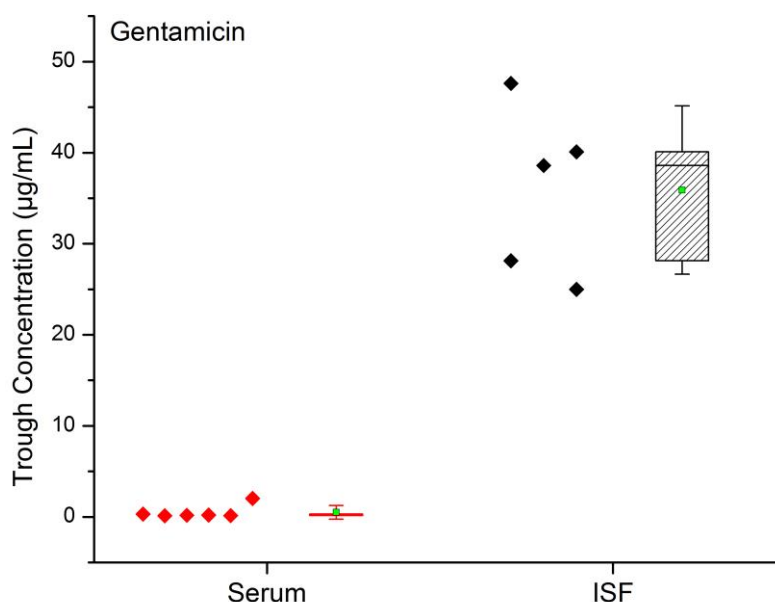
Figure 32. Box and whisker plot of steady-state trough concentrations in serum and ISF for gentamicin: Top and bottom of box represent the first and third quartile, the band in the box represents the median, whiskers represent 1 SD from the mean (■), the means are significantly different if one ISF data point is excluded (182.7 µg/mL) (unpaired t-test, two tail, α = 0.05)

● Serum Concentrations (n=6)

● ISF Concentrations (n=5)

3.3.1.4   Compartmental Analysis

Vancomycin fit a simple two-compartmental model and gentamicin fit a model that has been previously reported for the transport of drug via a lymph-compartment (here called tissue 2) back to the circulation (Figure 33) [143]. The concentration time course in ISF can be represented by Tissue 1 or Tissue 2. For a simple two-compartmental model (A), Tissue 1 generally represents all tissues. For vancomycin, the equilibrium between all possible tissues is rapid and ISF can be used as a representative for all tissues. For gentamicin, the concentration time course in ISF could not be described by a two-compartmental model and Tissue 1 therefore must represent a sum of tissues that are in fast equilibrium with blood and Tissue 2 represents skin ISF, which the drug reaches later, accumulates in and is recirculated via the blood (similar to the flow of lymph).

95
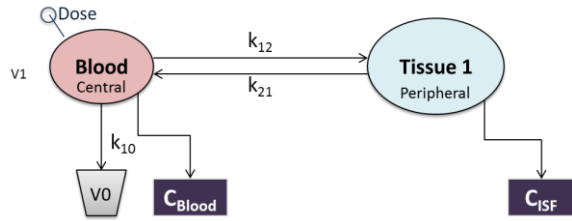
A   Vancomycin

B   Gentamicin
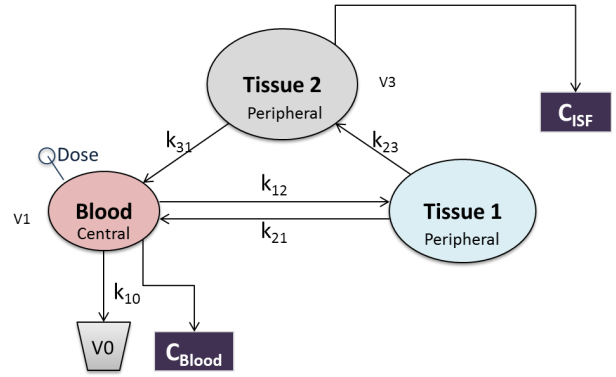
Figure 33. Compartmental models used for the antibiotics vancomycin (A) and gentamicin (B). The central compartment receives the intravenous bolus dose and is connected to the first tissue compartment via the rate constants k_{12} and k_{21}. Drug exchange takes place from the first tissue compartment to the second tissue compartment via k_{23}, and back to the central compartment via k_{31}, while elimination (k_{10}) happens only from the central compartment. Concentration *vs.* time observations are detected from the central compartment (C_{Blood}) and the first tissue compartment (C_{ISF}) for vancomycin and for the second tissue compartment for gentamicin.

For model A, the corresponding rate equations for Compartment Blood (C1) and Compartment

Tissue 1 (P1) can be described by Equations **15** and **16**.

$$\frac{dC1}{dt} = -k_{12}C1 + k_{21}P1 - k_{10}C1 \qquad (15)$$

$$\frac{dP1}{dt} = +k_{12}C1 - k_{21}P1 \qquad (16)$$

For model B, the corresponding rate equations for Compartment Blood (C1), Compartment

Tissue 1 (P1) and 2 (P2) can be described by Equations **17**, **18** and **19**.

$$\frac{dC1}{dt} = -k_{12}C1 + k_{21}P1 - k_{10}C1 + k_{31}P2 \qquad (17)$$

$$\frac{dP1}{dt} = +k_{12}C1 - k_{21}P1 - k_{23}P1 \qquad (18)$$

$$\frac{dP2}{dt} = -k_{31}P2 + k_{23}P1 \qquad (19)$$

96

Table 18. Modeled parameters for vancomycin.

Drug	Vancomycin						
Parameter	**Estimate**	**Unit**	**Standard Error**	**CV (%)**	**Initial Estimate**	**Lower Bound**	**Upper Bound**
V_1	824.56	mL/kg	31.14	3.78	180	0	-
k_{10}	1.02	h^{-1}	0.05	4.99	1.45	0	-
k_{12}	0.75	h^{-1}	0.16	21.22	0.33	0	-
k_{21}	1.14	h^{-1}	0.09	7.85	0.72	0	-

CV% is the coefficient of variation and calculated as $\frac{Standard\ Error}{Estimate} \cdot 100$

Table 19. Modeled parameters for gentamicin.

Drug	Gentamicin						
Parameter	**Estimate**	**Unit**	**Standard Error**	**CV (%)**	**Initial Estimate**	**Lower Bound**	**Upper Bound**
V_1	243.75	mL/kg	9.30	3.82	300	0	-
k_{10}	0.13	h^{-1}	0.02	17.74	0.058	0	-
k_{12}	0.03	h^{-1}	0.02	83.77	0.024	0	-
k_{21}	1.27	h^{-1}	0.07	5.88	0.951	0	-
V_3	3.70	mL/kg	0.00	0.00	3.7	3.5	4.0
k_{23}	0.034	h^{-1}	0.00	0.00	0.034	0.032	0.037
k_{31}	0.33	h^{-1}	0.12	35.99	0.23	0	-

CV% is the coefficient of variation and calculated as $\frac{Standard\ Error}{Estimate} \cdot 100$

Using the values for the microconstants predicted by the model (Table 18 and 19), the

differential equations were numerically solved to plot the concentration time course of drug in

ISF and blood (Figure 34 and 35). The model follows the actually observed drug concentrations

for both drugs quite accurately. Using a two-compartmental model for the distribution between

blood and ISF is accurate for the description of ISF PK for vancomycin for the early time points.

For later time points the model does not fit as well and requires more involved modeling efforts

in the future. For gentamicin, a slightly more complicated model describes gentamicin

concentrations in blood and ISF well. The ISF compartment is here represented by a third

97

compartment that receives flow from the second compartment and is connected to blood via a

one-way flow.
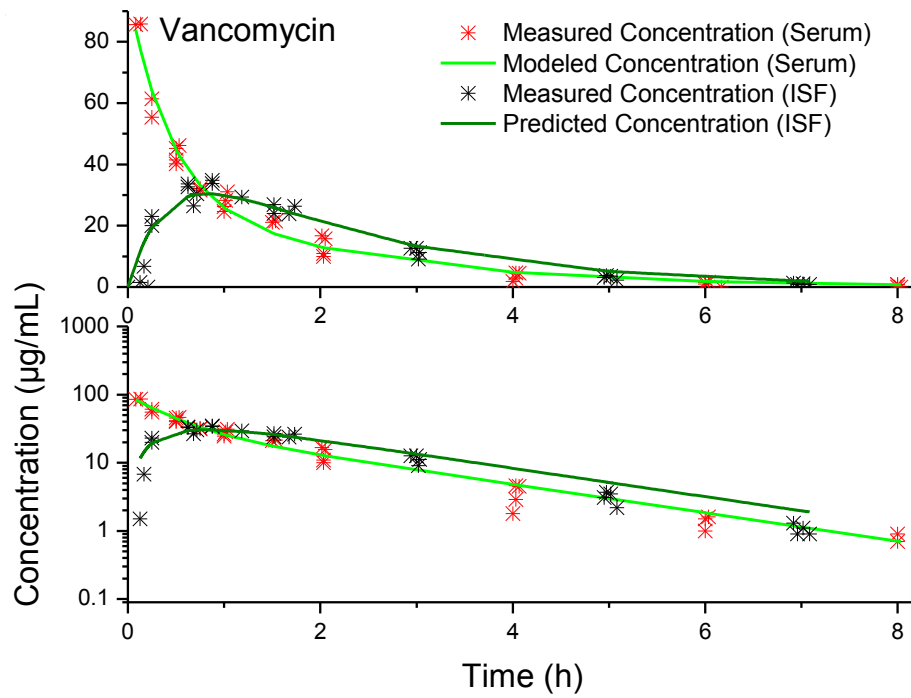
Figure 34. Modeled concentration time course and measured concentrations for vancomycin, upper panel: linear vertical axis, lower panel: logarithmic vertical axis.
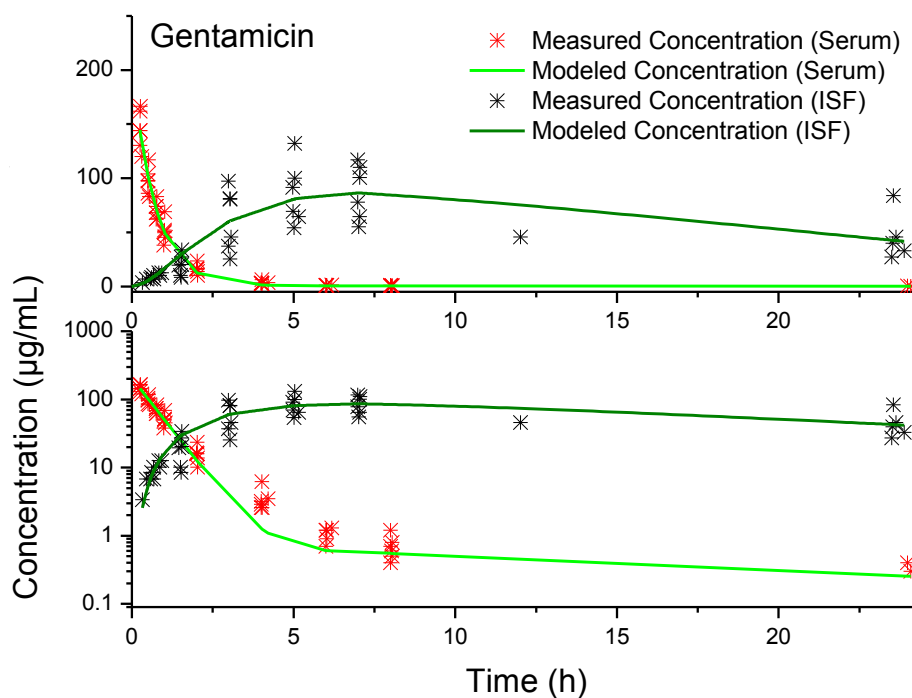
Figure 35. Modeled concentration time course and measured concentrations for gentamicin, upper panel: linear vertical axis, lower panel: logarithmic vertical axis.

3.3.2 PK Analysis of the Antineoplastic Agents Cisplatin, Carboplatin and Methotrexate in Blood and ISF

The platinum Pt (II) coordination complexes cisplatin and carboplatin are used in combination therapy with other antineoplastic agents for the treatment of a wide spectrum of cancers such as ovarian and testicular, head and neck, bladder, esophagus, lung, and colon cancer [144]. Cisplatin and carboplatin are small molecules (371.25 g/mol and 300.01 g/mol) with a mass contribution of the platinum atom of over 50%. They enter cells using the active copper (Cu^{2+}) transporter CTR1 [145] and bind DNA after activation. Activation occurs via aquation, a displacement of the chlorides (cisplatin) and the bidentate dicarboxylate (carboplatin) with water. The positively charged water-complexes can react with electron rich areas on the DNA (e.g.,

sulfhydryls, nitrogen) and create DNA crosslinks that interfere with the correct DNA replication and lead to cell death. The highly reactive species do not only interact with DNA of cancer cells but also with other healthy tissues, which explains side effects including nephrotoxicity, ototoxicity, neuropathy, transient leukopenia and thrombocytopenia. Cisplatin is extremely reactive and undergoes aquation much easier than carboplatin, which explains why the side effects are more pronounced using cisplatin and why cisplatin binds plasma proteins rapidly and covalently to over 90% [144]. Carboplatin protein binding is negligible. Tissue distribution of unbound drug is rapid and cisplatin shows high concentrations in kidney tissue [144].

Due to their high reactivity and hydrophilicity, they have to be administered intravenously or else they would react in the gastro-intestinal tract. Some newer platinum (IV) complexes such as ormaplatin, iproplatin, and satraplatin have entered human clinical trials recently [146]. Satraplatin, [147], a prodrug , is less reactive and more hydrophobic and has been suggested for oral administration, but has not received FDA approval yet.

The third tested antineoplastic agent methotrexate is known as a folic acid analogue that binds to dehydrofolate reductase, partially diminishing tetrahydrofolates and thereby interfering with DNA synthesis. It is used in the management of severe psoriasis, acute lymphoblastic leukemia and in low doses in the treatment of rheumatoid arthritis [144]. Rapidly dividing cells are affected most by antifolates so side effects are most pronounced in healthy rapidly dividing cells of the bone marrow and gastrointestinal tract. With a molecular weight of 454.44 g/mol, it shows good oral bioavailability at low doses but is administered intravenously at higher doses. Methotrexate is reversibly bound to plasma proteins at about 50% and can be easily displaced by other drugs [144].

3.3.2.1 Concentration Time Profile in Blood and ISF

All antineoplastic agents were readily detectable in blood and ISF. Methotrexate ISF data have been adjusted as suggested in the ultrafiltration experiment (2.3.1) to reflect 100% recovery. An adjustment was not necessary for carboplatin and cisplatin.

Table 20 summarizes the study facts and a full concentration *vs.* time profile of the drugs is displayed in Figure 36 - 38. It is apparent that all three drugs distribute rapidly to the peripheral ISF compartment showing very high concentrations within an hour after intravenous application. For cisplatin and carboplatin, the terminal elimination is faster from ISF than it is from blood, with a large amount of cisplatin remaining in the circulation over the study period of 24 h (irreversibly protein-bound drug). Methotrexate is almost identically eliminated from both compartments as best seen in the semi-logarithmic plot.

Table 20. Summary study table for the chemotherapeutics cisplatin, carboplatin and methotrexate.

Drug	Study	Study Subjects (#)	Dose (mg/kg)	Recovery Factor R	Drug in ISF	Site of Drug Action
Cisplatin	Single-dose	5	3	1.00	Yes	Tumor tissue
Carboplatin	Single-dose	4-6	18.7	1.00	Yes	Tumor tissue
Methotrexate	Single-dose	6	33 µmol/kg	1.11	Yes	Tumor tissue
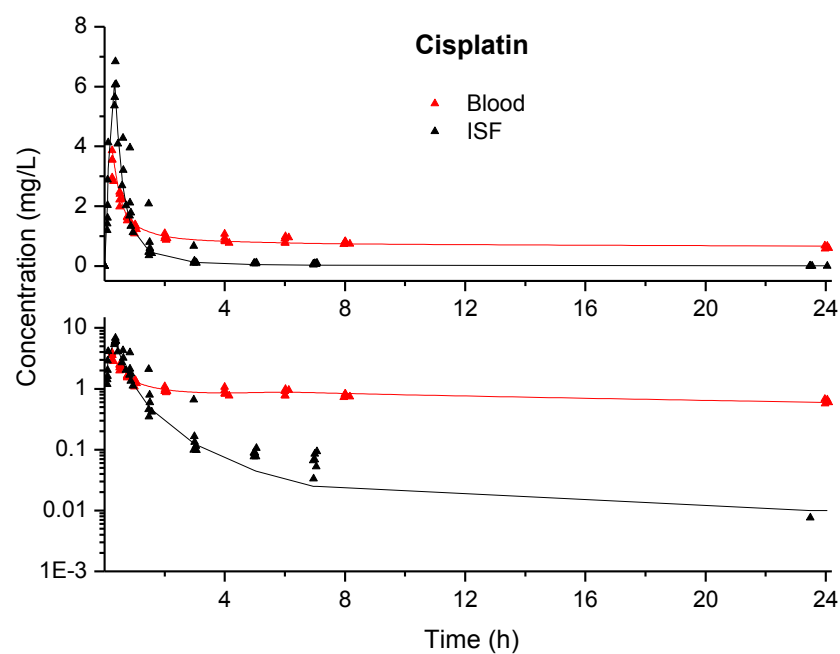
Figure 36. Cisplatin concentration in blood and ISF of rabbits after single dosing, shown both as a linear plot and a logarithmic plot (n = 5). The lines are drawn to serve as visual guides and do not indicate a specific model.
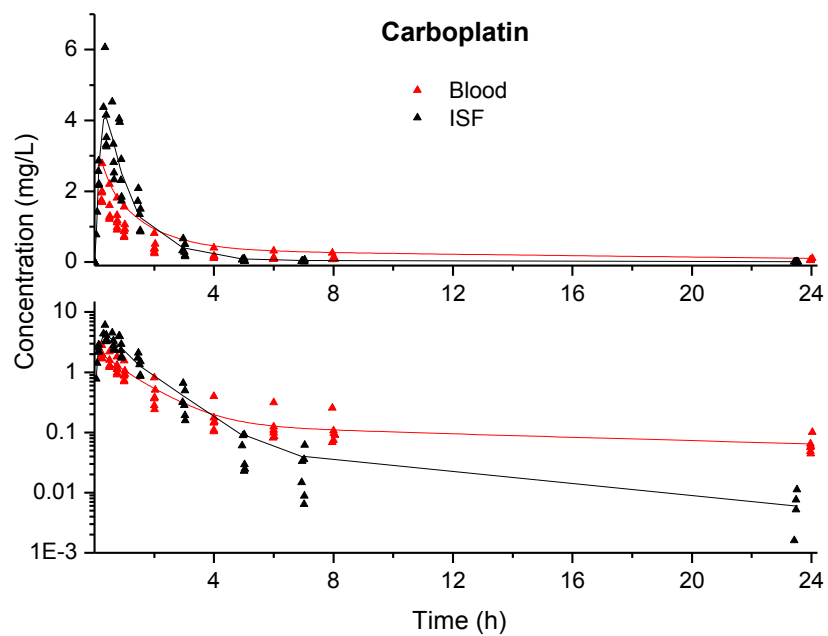
Figure 37. Carboplatin concentration in blood and ISF of rabbits after single dosing, shown both as a linear plot and a logarithmic plot (n = 4-6). The lines are drawn to serve as visual guides and do not indicate a specific model.
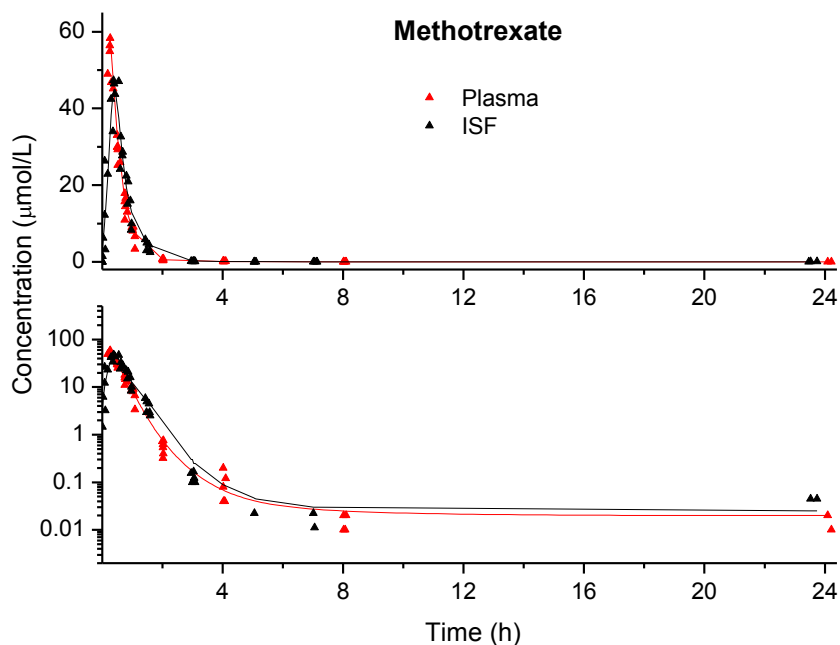
Figure 38. Methotrexate concentration in plasma and ISF of rabbits after single dosing, shown both as a linear plot and a logarithmic plot (n = 6). The lines are drawn to serve as visual guides and do not indicate a specific model.

3.3.2.2   Non-Compartmental Pharmacokinetic Analysis

Using statistical moment analysis without any model assumptions basic PK parameters were

calculated for cisplatin (Table 21), carboplatin (Table 22) and methotrexate (Table 23). ISF

concentrations were adjusted to 100% recovery using ultrafiltration recovery data for

methotrexate whereas the difference in recovery for cisplatin and carboplatin was not significant

(Table 6, 2.3.1). The total drug exposure to carboplatin and methotrexate is almost the same in

both compartments as seen from their almost identical AUCs. For cisplatin, the AUC is much

higher in blood than in ISF, due to the long circulation time of protein bound cisplatin. Terminal

elimination is overall higher from blood as from ISF for the platinum complexes, which results

in a larger mean residence time (MRT). For methotrexate, there is no clear difference between

elimination and MRT in ISF and blood. Interestingly, for both platinum drugs, the maximum

103

concentration detected in ISF at 15 min exceeded the extrapolated concentration at time zero for

blood. This speaks for a rapid distribution of cisplatin and carboplatin into ISF and can only be

explained by ISF acting as a separate tissue compartment.

Table 21. PK parameters (mean ± standard deviation) determined by NCA for cisplatin in blood (n = 5) and ISF (n = 5), dose= 3 mg/kg.

Cisplatin	AUC mg·h /L	AUMC mg·h·h/L	C_0 mg/L	CL L/h/kg	C_{max} (measured) mg/L
Blood	58±19.07	3829.83±3246.98	5.05±1.18	0.06±0.01	3.35±0.44
ISF	4.83±1	13.45±3.51	0±0	0.64^1±0.12	5.6±1.02
	$t_{1/2}$ h	λ_z h^{-1}	MRT h	t_{max} h	V_z L/kg
Blood	42.36±18.76	0.02±0.01	59.14±26.65	0.26±0.02	3.09±0.4
ISF	5.57±0.96	0.13±0.02	2.8±0.6	0.37±0.05	5.16^2±1.32

[1]for ISF, this value represents CL/F, [2]for ISF, this value represents V_z/F

Table 22. PK parameters (mean ± standard deviation) determined by NCA for carboplatin in blood (n = 6) and ISF (n = 4), dose= 18.7 mg/kg.

Carboplatin	AUC mg·h /L	AUMC mg·h·h/L	C_0 mg/L	CL L/h/kg	C_{max} (measured) mg/L
Blood	6.63±2.04	116.36±14.11	2.56±0.49	3±0.73	1.98±0.42
ISF	6.93±1.26	13.39±3.61	0±0	2.76^1±0.48	4.11±1.06
Carboplatin	$t_{1/2}$ h	λ_z h^{-1}	MRT h	t_{max} h	V_z L/kg
Blood	20.17±4.67	0.04±0.01	18.52±4.23	0.25±0.01	90.93±35.25
ISF	5.9±1.35	0.12±0.03	1.95±0.49	0.37±0.04	23.62^2±7.38

[1]for ISF, this value represents CL/F, [2]for ISF, this value represents V_z/F

Table 23. PK parameters (mean ± standard deviation) determined by NCA for methotrexate in plasma (n = 6) and ISF (n = 6), dose= 33 μmol//kg.

Methotrexate	AUC μmol·h/L	AUMC μmol·h·h/L	C_0 μmol/L	CL L/h/kg	C_{max} (measured) μmol/L
Plasma	43.89±3.83	19.42±3.63	98.61±19.08	0.76±0.07	51.75±5.49
ISF	40.56±28.83	93.7±169.36	0±0	1.12[1]±0.65	38.07±14.64
	$t_{1/2}$ h	λ_z h^{-1}	MRT h	t_{max} h	V_z L/kg
Plasma	0.46±0.17	1.64±0.51	0.44±0.07	0.27±0.06	0.5±0.16
ISF	0.31±0.02	2.24±0.12	1.52±1.53	0.51±0.24	0.51[2]±0.31

[1]for ISF, this value represents CL/F, [2]for ISF, this value represents V_z/F

3.3.2.3 Steady-State Concentrations and Non-Parametric Superposition

Chemotherapeutics are highly reactive and toxic drugs. Reaching a steady-state concentration is not feasible due to the serious toxic effects. Chemotherapeutic drugs are given with long dosing intervals of 3-4 weeks as a long infusion (1-6 h depending on the agent), so that the drug at target site is kept high for a couple of hours, but will then decline and be cleared before the next dose is given weeks later. Instead of steady-state predictions, it is more interesting to determine AUC ratios of blood and ISF and tissue accumulation for the chemotherapeutics.

Carboplatin and methotrexate both have very similar values of AUCs in blood and ISF (Table 22 and 23), whereas cisplatin seems to have a much larger exposure in blood than ISF (Table 21), which is understandable when comparing the profiles 2 h after administration (Figure 36-38). Cisplatin stays in the blood at a concentration of ~1 mg/L over 24 h, whereas unbound cisplatin is cleared from the tissue and almost undetectable after 2.5 h. Comparing the AUC ratios points to cisplatin binding irreversibly to proteins in the blood. Unbound, as measured in ISF, cisplatin exposure is very similar to carboplatin in blood or ISF. Methotrexate and carboplatin are both equally distributed in blood and ISF (Table 24), which points to minimal influence from protein

binding. In the literature, low and reversible protein binding has been reported for carboplatin

and for methotrexate 50% is reversibly bound to proteins [144].

Table 24. Drug exposures for the tested chemotherapeutic drugs between blood and ISF.

	Cisplatin	Carboplatin	Methotrexate
$\dfrac{AUC_{Blood}}{AUC_{ISF}}$	12.01	0.96	1.08

3.3.2.4   Compartmental Analysis

Methotrexate fit the compartmental model used for gentamicin but the observation compartment

for ISF was switched to the Tissue 1 compartment, due to the rapid high concentrations

measured in ISF (Figure 39).

Carboplatin and cisplatin did not fit the compartmental models used for methotrexate or the

antibiotics and it was impossible to find a reasonable fit using two to three compartments with

any combination of one or two way rate constants. The concentrations measured in ISF were too

high and significantly underestimated by all tested models.
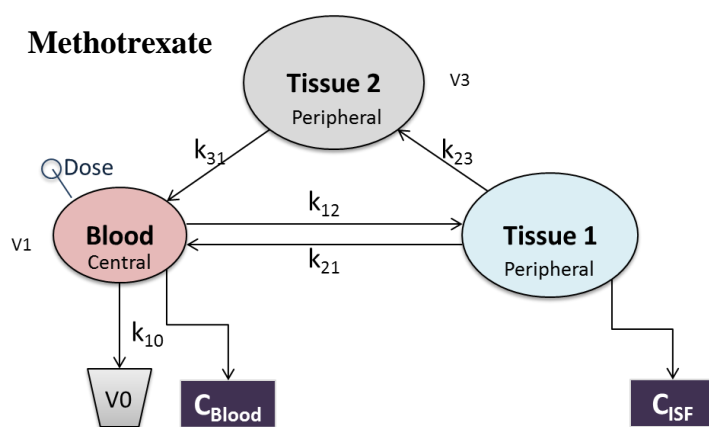
Figure 39. Compartmental model used for methotrexate. The central compartment receives the intravenous bolus dose and is connected to the first tissue compartment via the rate constants k_{12} and k_{21}. Drug exchange takes place from the first tissue compartment to the second tissue compartment via k_{23}, and back to the central compartment via k_{31}, while elimination (k_{10}) happens only from the central compartment. Concentration *vs.* time observations are detected from the central compartment (C_{Blood}) and the first tissue compartment (C_{ISF}).

The corresponding rate equations for Compartment Blood (C1), Compartment Tissue 1 (P1) and 2 (P2) are Equation **17**, **18** and **19** as given in Chapter 3.3.1.4 .

Table 25. Modeled parameters for methotrexate.

Drug	Methotrexate						
Parameter	Estimate	Unit	Standard Error	CV (%)	Initial Estimate	Lower Bound	Upper Bound
V_1	0.35	L/kg	0.01	4.09	0.22	0	-
k_{10}	2.22	h^{-1}	0.10	4.44	2.50	0	-
k_{12}	0.10	h^{-1}	0.00	0.00	0.095	Fixed	
k_{21}	4.61	h^{-1}	0.93	20.14	33.00	0	-
k_{23}	2.64	h^{-1}	0.76	28.83	3.70	2.60	4.00
k_{31}	0.03	h^{-1}	0.00	0.00	0.033	Fixed	

CV% is the coefficient of variation and calculated as $\frac{Standard\ Error}{Estimate} \cdot 100$

Using the values for the microconstants predicted by the model (Table 25), the differential equations were numerically solved to plot the concentration time course of drug in ISF and blood (Figure 40). The model follows the actually observed drug concentrations accurately.
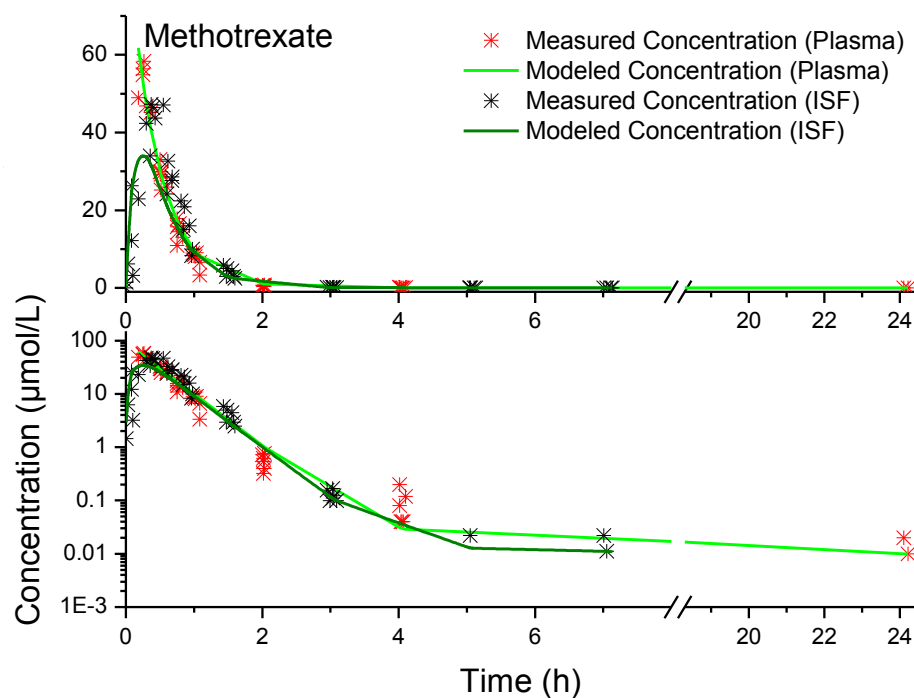
Figure 40. Modeled concentration time course and measured concentrations for methotrexate, upper panel: linear vertical axis, lower panel: logarithmic vertical axis.

3.3.3 PK Analysis of the Antiepileptics Valproic Acid, Phenobarbital and Phenytoin in Blood and ISF

Valproic acid, phenytoin and phenobarbital are anti-seizure drugs used to control a recurrent firing of clusters of brain neurons in epileptic patients. Valproic acid acts by prolonging the recovery of voltage activated sodium channels from inactivation [148] similar to phenytoin that binds to the inactive state of the sodium channels in the motor cortex, and inhibits the repetitive formation of action potentials. Phenobarbital is likely to act similar to the inhibitory neurotransmitter γ-aminobutyric acid (GABA) on GABA receptors of the subtype A and thereby minimizes the frequency of seizures.

All three candidates are small molecules with molecular weights between 144.2 g/mol (valproic acid) and 252.27 g/mol (phenytoin). They are readily absorbed after oral administration, although the absorption of phenobarbital has been reported to be slow [148]. Monitoring of steady-state drug concentrations is often warranted in epileptic patients to ensure adequate seizure control. It has been reported that plasma concentrations for valproic acid correlate only poorly with clinical efficacy [148] which could be due to inadequate target site concentrations. Valproic acid, phenytoin and phenobarbital all have to leave the blood circulation and reach the brain neurons in the central nervous system (CNS) to be active. Measured extravascular concentrations might therefore be more meaningful than blood concentrations, although the endothelial cells of the CNS differ from the normal capillaries in the periphery (Chapter 1.1.5). Endothelial cells in the CNS also express active influx and efflux pumps (transporters) which can lead to difficulties in predicting drug distribution reliably [149]. Extravascular concentrations are further affected by plasma protein binding, which is reported to be reversible for all drugs and is 40-60% for phenobarbital, and ~ 90 % for phenytoin and valproic acid. For valproic acid, protein saturation occurs at therapeutic concentrations of 200-300 µmol/L [148]. Furthermore, phenytoin's PK are reported to be unusual and non-linear, which can make dose adjustments difficult as the plasma concentrations change disproportionally.

3.3.3.1   Concentration Time Profile in Blood and ISF

Valproic acid and phenobarbital were readily detectable in blood and ISF, whereas phenytoin was not detected in ISF. Phenobarbital ISF data has been adjusted as suggested in the ultrafiltration experiment (2.3.1) to reflect 100% recovery. An adjustment was not necessary for valproic acid.

Table 26 summarizes the study facts and a full concentration *vs.* time profile of the drugs is displayed in Figure 41- 43. Valproic acid and phenobarbital distribute quickly into the ISF compartment but stay overall well below blood concentrations. The curves in both compartments follow similar progressions, except for a short and slight appearance of valproic acid after five hours, as seen by a positive slope between 5 and 24 hours in the semi-logarithmic plot. Phenytoin concentrations were undetectable in ISF which could indicate tight tissue binding of the drug or very low ISF penetration.

Table 26. Summary study table for the anti-seizure therapeutics valproic acid, phenobarbital and phenytoin.

Drug	Study	Study Subjects (#)	Dose (µmol/kg)	Recovery Factor R	Drug in ISF	Site of Drug Action
Valproic Acid	Single-dose	6	346.7	1.00	Yes	Extravascular, CNS
Phenobarbital	Single-dose	6	129.2	1.16	Yes	Extravascular, CNS
Phenytoin	Single-dose	5	39.6	1.41	No	Extravascular, CNS
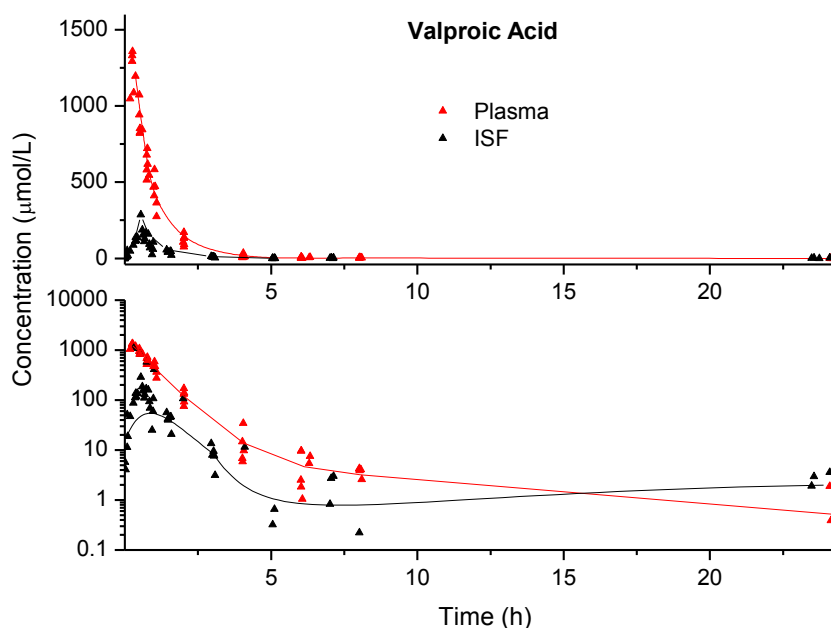
Figure 41. Valproic acid concentration in plasma and ISF of rabbits after single dosing, shown both as a linear plot and a logarithmic plot (n = 6). The lines are drawn to serve as visual guides and do not indicate a specific model.
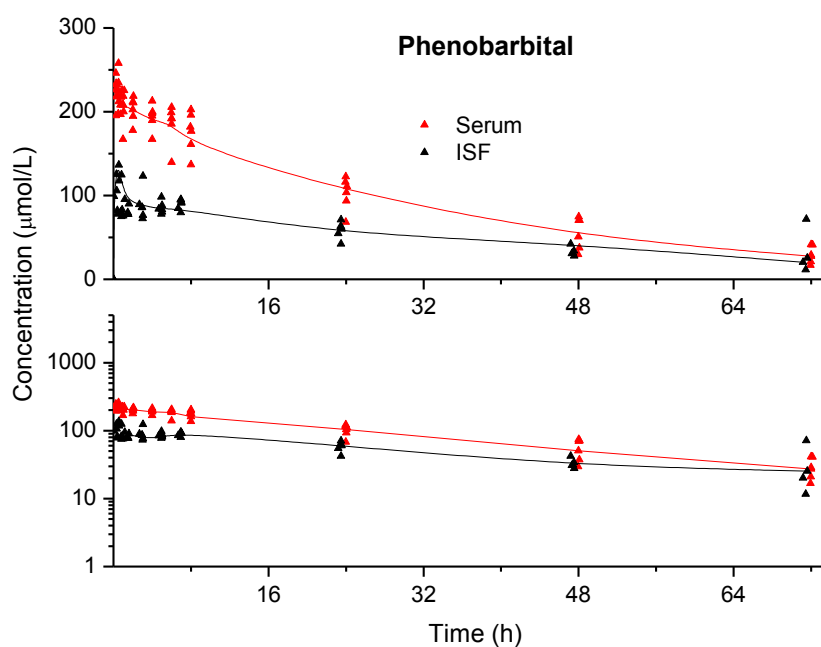
Figure 42. Phenobarbital concentration in serum and ISF of rabbits after single dosing, shown both as a linear plot and a logarithmic plot (n = 6). The lines are drawn to serve as visual guides and do not indicate a specific model.
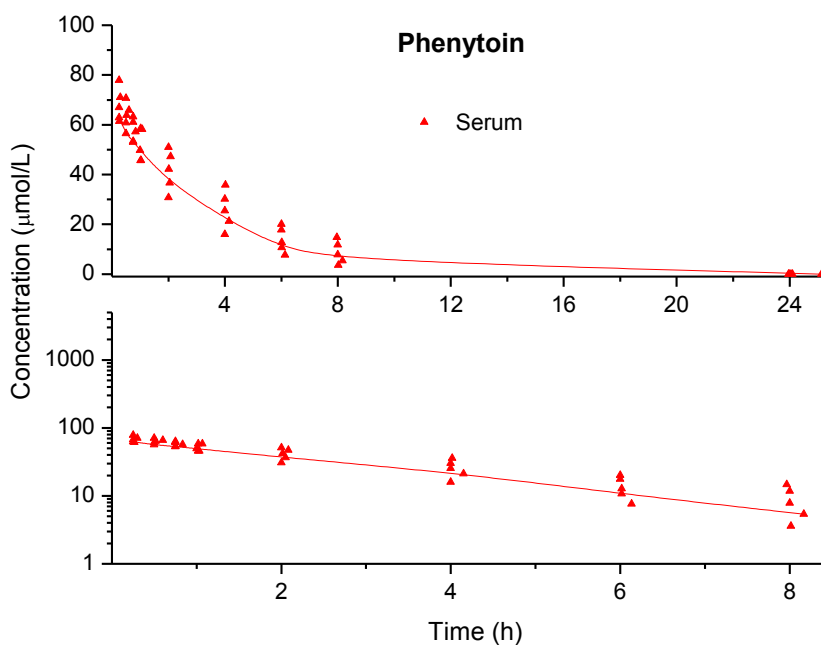
Figure 43. Phenytoin concentration in serum of rabbits after single dosing, shown both as a linear plot and a logarithmic plot (n = 5). The lines are drawn to serve as visual guides and do not indicate a specific model.

3.3.3.2   Non-Compartmental Pharmacokinetic Analysis

Basic PK parameters were calculated for valproic acid (Table 27), phenobarbital (Table 28) and

phenytoin (Table 29) using statistical moment analysis without any model assumptions. ISF

concentrations were adjusted to 100% recovery using ultrafiltration recovery data for

phenobarbital whereas the difference in recovery for valproic acid was not significant (Table 6,

2.3.1) and no phenytoin was detected in ISF. Drug exposure to valproic acid and phenobarbital

was overall lower in ISF than in blood as seen from their AUCs. The terminal elimination rate

constants were very similar in blood and ISF for both compartments. For valproic acid, the mean

residence time (MRT) was increased in ISF compared to blood which could be explained by the

second appearance of valproic acid in ISF. After reaching almost zero at 5 h, concentrations

increased again to 0.4-1.9 µmol/L at 24 h.

Table 27. PK parameters (mean ± standard deviation) determined by NCA for valproic acid in plasma (n =6) and ISF (n = 5), dose= 346.7 µmol/kg.

Valproic Acid	AUC µmol·h/L	AUMC µmol·h·h/L	C_0 µmol/L	CL L/h/kg	C_{max} (measured) µmol/L
Plasma	1443.6±188.63	1372.62±499.62	1740.97±319.32	0.24±0.03	1219.08±130.12
ISF	207.38±30.37	684.08±384.58	0±0	1.7^1±0.25	180.68±54.47
	$t_{1/2}$ h	λ_z h^{-1}	MRT h	t_{max} h	V_z L/kg
Plasma	0.86±0.27	0.86±0.21	0.93±0.22	0.27±0.06	0.29±0.07
ISF	1.01±0.44	0.79±0.32	3.46±2.14	1.66±2.64	2.46^2±1

[1]for ISF, this value represents CL/F, [2]for ISF, this value represents V_z/F

Table 28. PK parameters (mean ± standard deviation) determined by NCA for phenobarbital in serum (n = 6) and ISF (n = 5), dose= 129.2 µmol/kg.

Phenobarbital	AUC µmol·h/L	AUMC µmol·h·h/L	C_0 µmol/L	CL L/h/kg	C_{max} (measured) µmol/L
Serum	7866.93±1710.15	286660.18±107866.29	232±26.88	0.02±0	230.02±21.35
ISF	4331.58±528.65	185362.22±47361.25	0±0	0.03[1]±0	110.93±19.47
	$t_{1/2}$ h	λ_z h^{-1}	MRT h	t_{max} h	V_z L/kg
Serum	26.38±4.04	0.03±0	35.42±6.28	0.39±0.14	0.64±0.1
ISF	30.07±3.43	0.02±0	42.21±6.28	3.9±2.89	1.3[2]±0.07

[1]for ISF, this value represents CL/F, [2]for ISF, this value represents V_z/F

Table 29. PK parameters (mean ± standard deviation) determined by NCA for phenytoin in serum (n = 5), dose = 39.6 µmol/kg.

Phenytoin	AUC µmol·h/L	AUMC µmol·h·h/L	C_0 µmol/L	CL L/h/kg	C_{max} (measured) µmol/L
Serum	274.49±72.68	1038.3±488.81	73.47±8.94	non-linear	68.5±6.14
ISF	0±0	0±0	0±0	0±0	0±0
	$t_{1/2}$ h	λ_z h^{-1}	MRT h	t_{max} h	V_z L/kg
Serum	2.53±0.52	0.28±0.06	3.62±0.79	0.31±0.12	0.53±0.03
ISF	0±0	0±0	0±0	0±0	0±0

3.3.3.3 Steady-State Concentrations and Non-Parametric Superposition

Steady-state concentrations of anti-seizure drugs are more important in clinical practice than single-dose data, as antiepileptics are given in multiple dose regimens usually life-long. To successfully control seizure activity of neurons, the concentrations of antiepileptics have to stay above a certain concentration that might be patient specific and depend on the exact manifestation of symptoms.

After calculating the NCA parameters, the dosing regimen for a multiple dose study was derived (Table 30 and 31). Non-parametric superposition was used to estimate concentrations from the single-dose data set at steady state just before giving the next dose (C_{trough}). C_{trough} is the parameter most often used in clinics to base dose adjustments on. Comparing the trough concentrations in blood and ISF (Figure 44 and 45), it is apparent that the variability of the blood predictions is larger than the variability in the ISF predictions. Unpaired t-tests, with an expected difference between compartments set to zero, revealed that the means are significantly different ($\alpha = 0.05$, two tail) for valproic acid but not for phenobarbital. Using the calculated doses and dosing interval to reach a target trough concentration of 200 µmol/L (valproic acid) and 43 µmol/L (phenobarbital) results in C_{trough}(blood) = 148.96 µmol/L and C_{trough}(ISF) = 31.35 µmol/L (Table 30) for valproic acid. For phenobarbital (Table 31), the predicted trough concentrations are 42.22 µmol/mL and 27.75 µmol/L for blood and ISF, respectively. One extremely high data point of 291.22 µmol/L was determined to be an outlier and removed from this data set due to previously discussed reasons (Chapter 3.3.1.3). The box and whisker plots (Figure 44 and 45) show a comparison of the predictions in blood and ISF for both drugs.

Table 30. The calculation of loading dose (D_L), maintenance dose (D_M) and dosing interval (τ) for valproic acid from λ_z and V_z, $C_{max\ ss}$= 690 µmol/L and $C_{min\ ss}$= 200 µmol/L.

Valproic Acid Rabbit #	λ_z (plasma) (h⁻¹)	V_z (plasma) (L/kg)	D_L (µmol/kg)	τ (h)	D_M (µmol/kg)	Predicted Trough in Blood (µmol/L)	Predicted Trough in ISF (µmol/L)
1	0.98	0.25	169.23	1.26	120.18	120.65	29.82
2	0.69	0.28	194.86	1.80	138.38	215.05	29.04
3	1.05	0.26	178.46	1.17	126.73	95.40	25.94
4	0.52	0.44	304.66	2.38	216.35	160.02	40.60
5	0.94	0.28	192.91	1.32	136.99	138.28	-*
6	1.01	0.26	178.55	1.23	126.80	164.37	-*
Mean	**0.86**	**0.29**	**203.11**	**1.53**	**144.24**	**148.96**	**31.35**
SD	0.21	0.07	50.68	0.47	35.99	41.26	6.39

-*No predictions are possible if the elimination is too fast to accumulate for the chosen dosing interval τ or if the terminal slope cannot be determined for sparse data sets.

Table 31. The calculation of loading dose (D_L), maintenance dose (D_M) and dosing interval (τ) for phenobarbital from λ_z and V_z, $C_{max\ ss}$= 150 µmol/L and $C_{min\ ss}$= 43 µmol/L.

Phenobarbital Rabbit #	λ_z (serum) (h⁻¹)	V_z (serum) (L/kg)	D_L (µmol/kg)	τ (h)	D_M (µmol/kg)	Predicted Trough in Blood (µmol/L)	Predicted Trough in ISF (µmol/L)
1	0.023	0.58	87.23	54.94	62.22	56.88	30.50
2	0.028	0.55	82.49	44.44	58.84	51.56	-*
3	0.031	0.60	89.83	39.98	64.08	26.99	18.60
4	0.028	0.63	94.01	45.08	67.06	37.58	33.30
5	0.021	0.63	94.95	58.22	67.73	58.58	291.22*
6	0.029	0.84	126.44	42.64	90.20	21.74	28.61
Mean	**0.027**	**0.64**	**95.83**	**47.55**	**68.36**	**42.22**	**80.45(27.75)**
SD	0.004	0.10	15.68	7.29	11.18	15.77	117.96(6.40)

-*No predictions are possible if the elimination is too fast to accumulate for the chosen dosing interval τ or if the terminal slope cannot be determined for sparse data sets.
If * excluded, then the mean and SD are as given in brackets

115
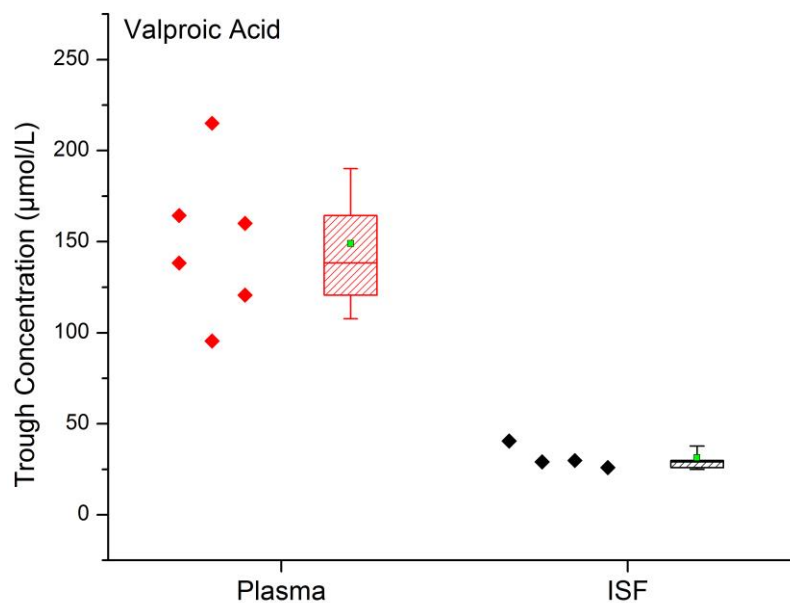
Figure 44. Box and whisker plot of steady-state trough concentrations in plasma and ISF for valproic acid: Top and bottom of box represent the first and third quartile, the band in the box represents the median, whiskers represent 1 SD from the mean (■), the means are significantly different (unpaired t-test, two tail, α = 0.05).
● Plasma Concentrations (n = 6)
● ISF Concentrations (n = 4)
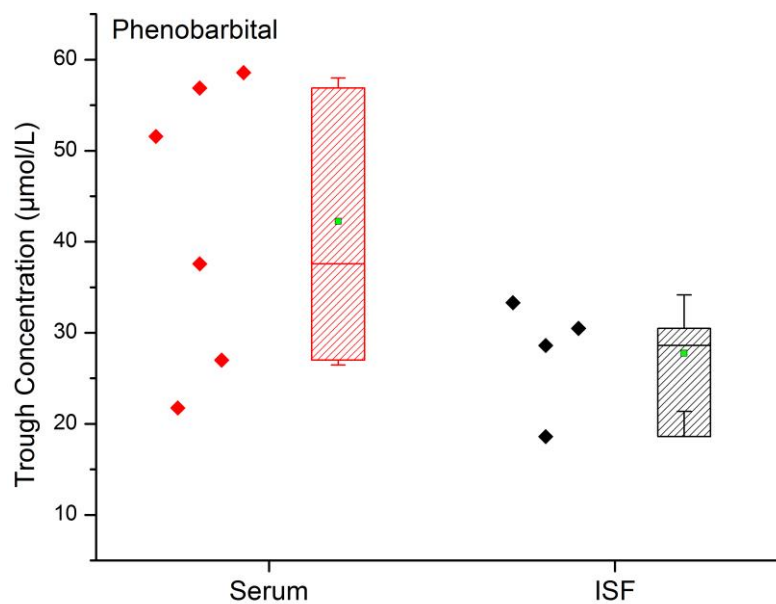
Figure 45. Box and whisker plot of steady-state trough concentrations in serum and ISF for phenobarbital: Top and bottom of box represent the first and third quartile, the band in the box represents the median, whiskers represent 1 SD from the mean (■), the means are not significantly different (unpaired t-test, two tail, α = 0.05)
● Serum Concentrations (n = 6)
● ISF Concentrations (n = 4)

3.3.3.4   Compartmental Analysis

Phenobarbital concentrations could be described by the same model as theophylline and methotrexate. Valproic acid was modeled using three compartments, but instead of the flow going from the second tissue compartment back to blood, it was connected to the first tissue compartment (Figure 46). Using this model, valproic acid concentrations in ISF stayed higher than in blood in the terminal phase, precisely as it has been measured experimentally.
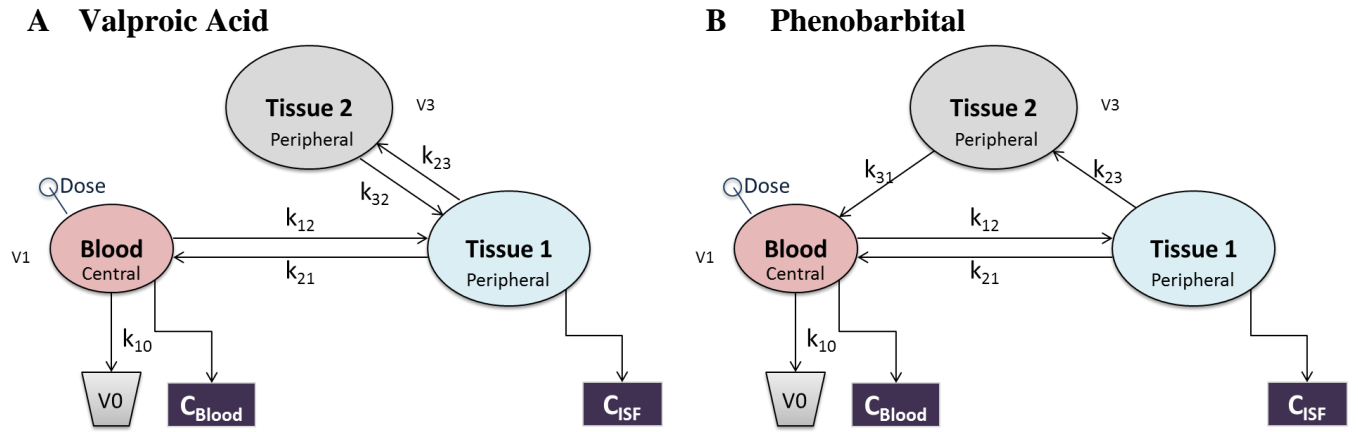
Figure 46. Compartmental models used for valproic acid (A) and phenobarbital (B). The central compartment receives the intravenous bolus dose and is connected to the first tissue compartment via the rate constants k_{12} and k_{21}. Drug exchange takes place from the first tissue compartment to the second tissue compartment via k_{23}, and back to the central compartment via k_{31} (phenobarbital) and back to the first tissue via k_{32} (valproic acid), while elimination (k_{10}) happens only from the central compartment. Concentration *vs.* time observations are detected from the central compartment (C_{Blood}) and the first tissue compartment (C_{ISF}).

For model A, the corresponding rate equations for Compartment Blood (C1), Compartment Tissue 1 (P1) and 2 (P2) are Equation **20**, **21**, and **22** The corresponding rate equations for model B are Equation **17**, **18** and **19** as given in Chapter 3.3.1.4.

$$\frac{dC1}{dt} = -k_{12}C1 + k_{21}P1 - k_{10}C1 \qquad (\ 20\ )$$

$$\frac{dP1}{dt} = +k_{12}C1 - k_{21}P1 - k_{23}P1 + k_{32}P1 \qquad (\ 21\ )$$

$$\frac{dP2}{dt} = -k_{32}P2 + k_{23}P1 \qquad (\ 22\ )$$

Table 32. Modeled parameters for valproic acid.

Drug	Valproic Acid						
Parameter	Estimate	Unit	Standard Error	CV (%)	Initial Estimate	Lower Bound	Upper Bound
V_1	0.20	L/kg	0.00	0.48	0.22	0	-
k_{10}	1.23	h^{-1}	0.01	0.73	2.5	0	-
k_{12}	0.10	h^{-1}	0.00	0.00	0.095	Fixed	
k_{21}	0.38	h^{-1}	0.07	19.27	33	0	-
k_{23}	2.20	h^{-1}	0.59	26.85	3.7	2.6	-
k_{32}	0.02	h^{-1}	0.05	240.79	0.033	0	0.021

CV% is the coefficient of variation and calculated as $\frac{Standard\ Error}{Estimate} \cdot 100$

Table 33. Modeled parameters for phenobarbital.

Drug	Phenobarbital						
Parameter	Estimate	Unit	Standard Error	CV (%)	Initial Estimate	Lower Bound	Upper Bound
V_1	0.55	L/kg	0.02	3.96	0.22	0	-
k_{10}	0.03	h^{-1}	0.00	5.22	2.5	0	-
k_{12}	0.17	h^{-1}	0.14	82.75	0.095	0	-
k_{21}	3.62	h^{-1}	1.43	39.33	33	0	-
k_{23}	4.16	h^{-1}	1.71	41.13	3.7	2.6	-
k_{31}	1.15	h^{-1}	0.74	64.71	0.033	0	1.15

CV% is the coefficient of variation and calculated as $\frac{Standard\ Error}{Estimate} \cdot 100$

Using the values for the microconstants (Table 32 and 33), the differential equations were numerically solved to plot the concentration time course of drug in ISF and blood (Figure 47 and Figure 48). For valproic acid, the model prediction in the logarithmic plot seems lower at 24 h than the real data points. The reason is that some of the subjects had already eliminated all drug and the concentration at 24 h was zero.

118
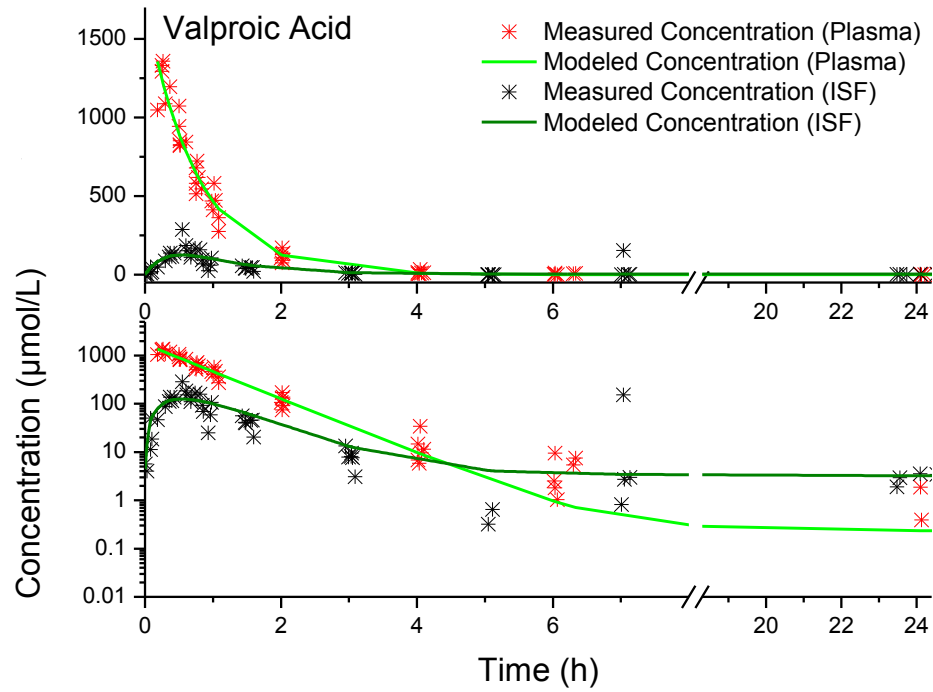
Figure 47. Modeled concentration time course and measured concentrations for valproic acid, upper panel: linear vertical axis, lower panel: logarithmic vertical axis.
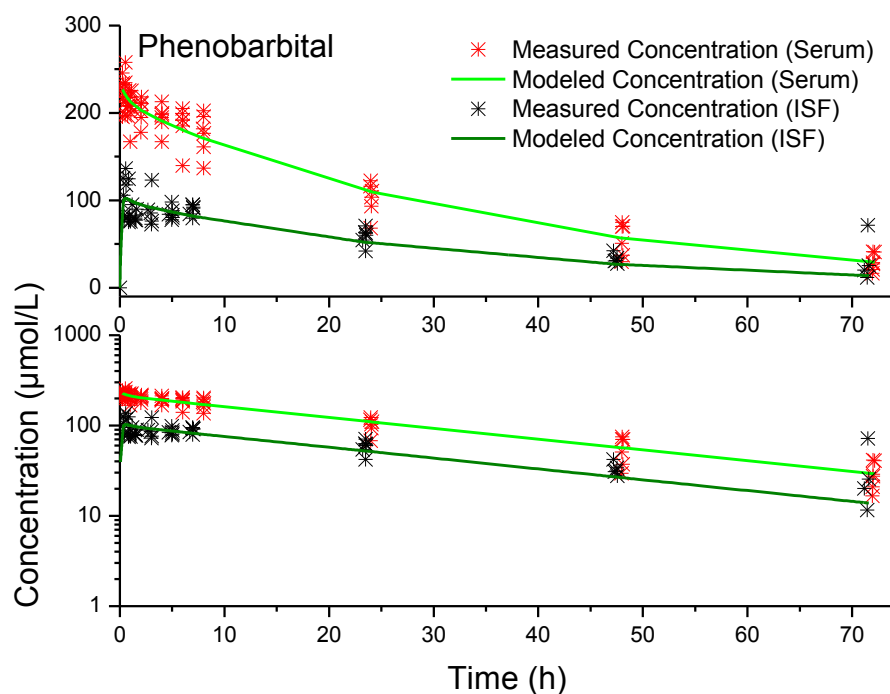
Figure 48. Modeled concentration time course and measured concentrations for phenobarbital, upper panel: linear vertical axis, lower panel: logarithmic vertical axis.

3.3.4 PK Analysis of the Immunosuppressive Agents Cyclosporine, Tacrolimus and Mycophenolic Acid in Blood and ISF

Immunosuppressive drugs are used to control and reduce immune response in organ transplantation and auto immune diseases. The calcineurin inhibitors cyclosporine and tacrolimus are most often used in solid-organ allograft rejection, whereas mycophenolic acid (or its prodrug mycophenolate mofetil) is indicated for the prophylaxis of transplant rejection [150]. All three immunosuppressives inhibit the activation or proliferation of T- and/or B- lymphocytes, the most important mediators of the adaptive targeted immune response. Cyclosporine and tacrolimus bind to intracellular immunophilin proteins called cyclophilin and FK506 binding protein-12, which in complex with calmodulin, calcium and calcineurin prevent the translocation of NFAT (nuclear factor of activated T-cells) into the nucleus (inhibition of calcineurin

120

phosphatase activity). Mycophenolic acid inhibits an enzyme called inosine monophosphate dehydrogenase (IMPDH) noncompetitively and reversibly. Without the enzyme, the synthesis of guanine nucleotides is hindered and B- and T- lymphocytes seize to proliferate.

Mycophenolic acid is a small and reasonably hydrophobic molecule (320.34 g/mol) that is readily absorbed orally using the sodium or mofetil salt forms. Tacrolimus, a macrolide lactone, and cyclosporine, a cyclic polypeptide, are large, water insoluble and hydrophobic with molecular weights of 804.02 and 1202.61 g/mol, respectively. Intravenous solutions use ethanol and castor oil as solvents and have to be diluted before administration. Oral absorption is slow and incomplete (20-50%) [150] and variable between patients, although a cyclosporine microemulsion (NEORAL$^{®}$) has shown improvements.

Cyclosporine is distributed widely outside the vascular compartment [150] and mycophenolic acid distribution to the interstitial space has been reported to be rapid. Equilibrium is so fast that vasculature and ISF act together as a single compartment [151].

All three immunosuppressants show high protein binding of often > 90% and tacrolimus binds red blood cells reversibly [152], which is why whole blood is used for therapeutic drug monitoring. Monitoring is required for immunosuppressants to ensure adequate control of the immune response after transplantation and to minimize the risk of kidney damage.

Nephrotoxicity is the limiting factor for cyclosporine [150] therapy. In certain transplant populations cyclosporine monitoring is done two hours after dose (C_2). More commonly, cyclosporine concentrations are monitored before giving the next dose (C_{trough} or C_0) or LSS have been established. Similarly, tacrolimus and mycophenolic acid are often monitored before the next dose is given (C_{trough}), although other monitoring schemes have been proposed [6].

3.3.4.1   Concentration Time Profiles in Blood and ISF

Of the immunosuppressants, only mycophenolic acid was detectable ISF, whereas tacrolimus and cyclosporine were not detected. Interestingly, neither undetectable drug was recovered in an *in vitro* membrane permeability experiment. For further investigation, tacrolimus membrane permeability was studied in Chapter 5. Mycophenolic acid concentrations in ISF were slightly reduced using the ultrafiltration membrane and therefore adjusted to reflect 100% recovery (2.3.1).

Table 34 summarizes the study facts and a full concentration *vs.* time profile of the drugs is displayed in Figure 49 - 51. Mycophenolic acid distributes into the ISF compartment slowly, but after one hour the decline in concentration is identical in blood and ISF, which could indicate similar steady-state concentrations and accumulation if given as multiple doses (3.3.4.3). Cyclosporine and tacrolimus concentrations were undetectable in ISF which could be correlated to their low solubility and high protein binding. However, mycophenolic acid shows high protein binding as well but was still detectable, so the main factor must be the solubility and possible interactions with the filtration device as shown in extremely low recovery rates *in vitro* (Table 34). Tacrolimus and cyclosporine are likely present in ISF as they have been recorded to distribute readily into the extravascular space [150].

Table 34. Summary study table for the immunosuppressants cyclosporine, tacrolimus and mycophenolic acid.

Drug	Study	Study Subjects (#)	Dose (µg/kg)	Recovery Factor R	Drug in ISF	Site of Drug Action
Cyclosporine	Single-dose	6	5000	8.47	No	Intracellular
Tacrolimus	Single-dose	4	100	29.4	No	Intracellular
Mycophenolic Acid	Single-dose	6	40000	1.79	Yes	Intracellular
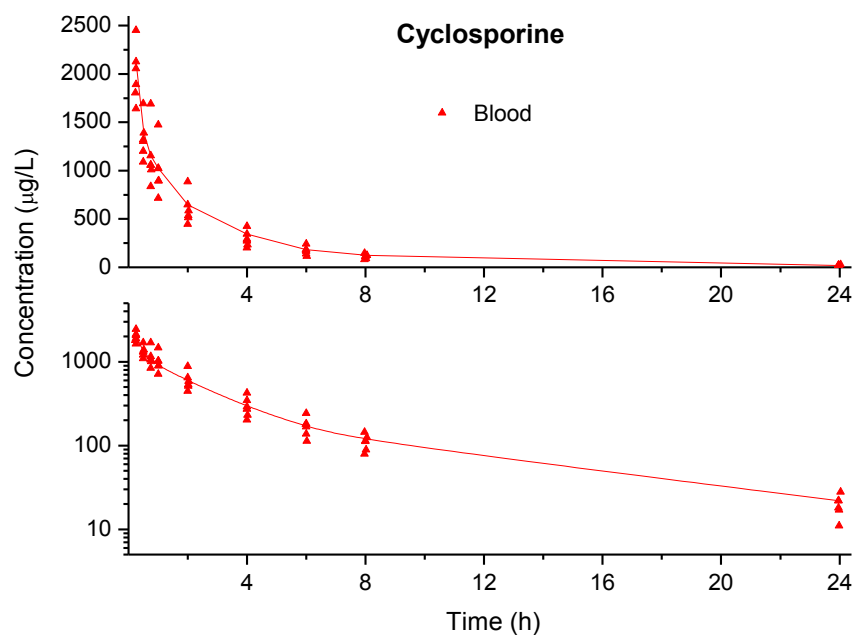
Figure 49. Cyclosporine concentration in blood of rabbits after single dosing, shown both as a linear plot and a logarithmic plot (n = 6). The lines are drawn to serve as visual guides and do not indicate a specific model.
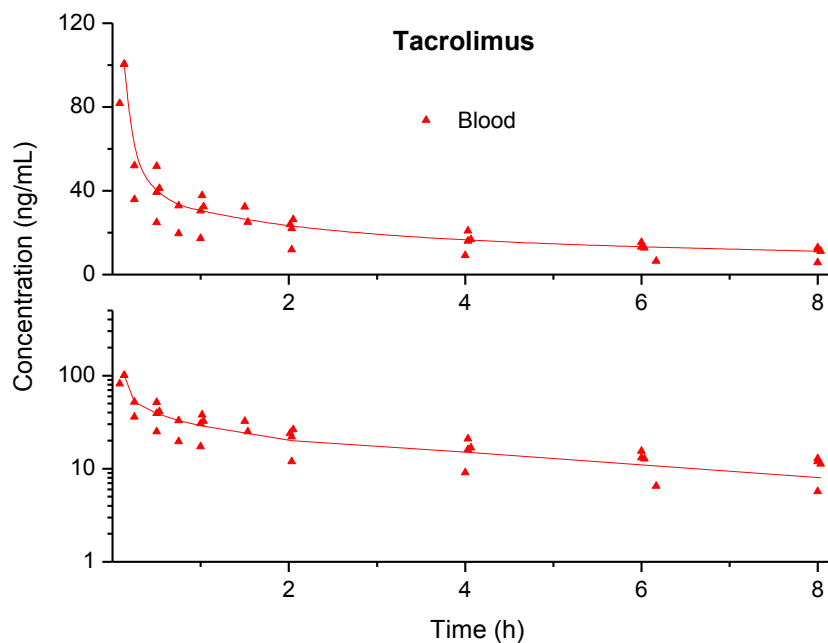
Figure 50. Tacrolimus concentration in blood of rabbits after single dosing, shown both as a linear plot and a logarithmic plot (n = 4). The lines are drawn to serve as visual guides and do not indicate a specific model.
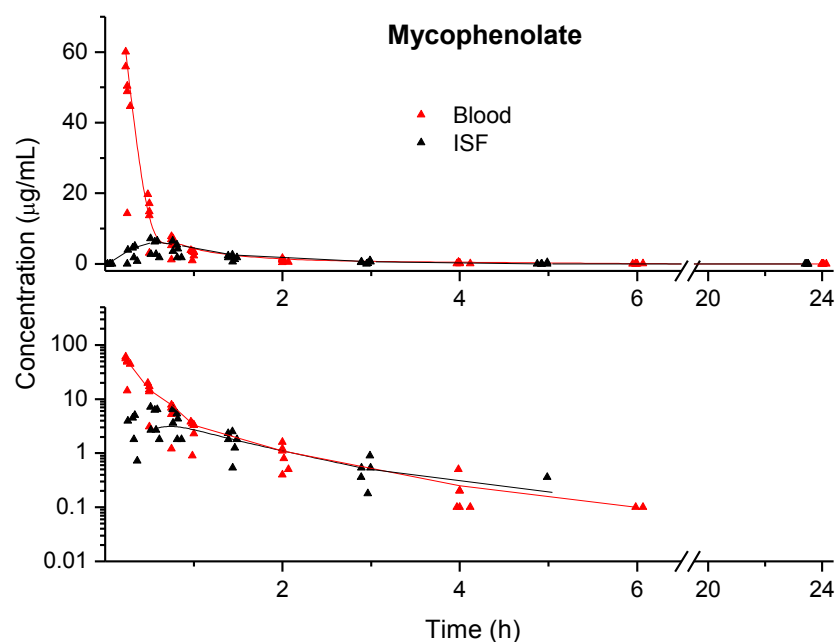
Figure 51. Mycophenolic acid concentration in blood and ISF of rabbits after single dosing, shown both as a linear plot and a logarithmic plot (n = 6). The lines are drawn to serve as visual guides and do not indicate a specific model.

3.3.4.2 Non-Compartmental Pharmacokinetic Analysis

Basic PK parameters were calculated for cyclosporine (Table 35), tacrolimus (Table 36) and mycophenolic acid (Table 37) using statistical moment analysis without any model assumptions. ISF concentrations were adjusted to 100% recovery using ultrafiltration recovery data (e.g., multiplication by factor 1.79) for mycophenolic acid whereas the other two immunosuppressants were not detected in ISF. Drug exposure to mycophenolic acid was much lower in ISF than in blood but the terminal elimination was almost identical. The maximum detected concentration in ISF was about 10 times lower than the maximum detected concentration in blood (4.7 *vs.* 45.7 μg/mL).

124

Table 35. PK parameters (mean ± standard deviation) determined by NCA for cyclosporine in blood (n = 6), dose = 5.000 µg/kg.

Cyclosporine	AUC µg·h/L	AUMC µg·h·h/L	C_0 µg/L	CL L/h/kg	C_{max} (measured) µg/L
Blood	5272.35±1154.42	24681.81±6253.21	2961.98±461.15	0.99±0.21	1994.67±284.23
ISF	0±0	0±0	0±0	0±0	0±0
	$t_{1/2}$ h	λ_z h^{-1}	MRT h	t_{max} h	V_z L/kg
Blood	5.98±0.4	0.12±0.01	4.65±0.37	0.25±0.01	8.46±1.6
ISF	0±0	0±0	0±0	0±0	0±0

Table 36. PK parameters (mean ± standard deviation) determined by NCA for tacrolimus in blood (n = 4), dose = 100.000 ng/kg.

Tacrolimus	AUC ng·h/mL	AUMC ng·h·h/mL	C_0 ng /mL	CL mL/h/kg	C_{max} (measured) ng/mL
Blood	247.44±74.29	1895.65±566.81	85.29±32.96	444.06±179.3	67.5±29
ISF	0±0	0±0	0±0	0±0	0±0
	$t_{1/2}$ h	λ_z h^{-1}	MRT h	t_{max} h	V_z mL/kg
Blood	5.86±0.27	0.12±0.01	7.66±0.52	0.18±0.08	3763.99±1539.27
ISF	0±0	0±0	0±0	0±0	0±0

Table 37. PK parameters (mean ± standard deviation) determined by NCA for mycophenolic acid in blood (n = 6) and ISF (n = 6), dose = 40.000 µg/kg.

Mycophenolic acid	AUC µg·h/mL	AUMC µg·h·h/mL	C_0 µg/mL	CL mL/h/kg	C_{max} (measured) µg/mL
Blood	40.01±12.77	12.51±4.8	160.04±49.29	1206.19±781.39	45.68±16.31
ISF	6.23±2.39	8.38±4.66	0±0	7802.8[1]±4667.78	4.65±2.25
	$t_{1/2}$ h	λ_z h^{-1}	MRT h	t_{max} h	V_z mL/kg
Blood	0.84±0.2	0.87±0.23	0.31±0.06	0.25±0.02	1519.99±1178.7
ISF	0.72±0.41	1.17±0.49	1.34±0.68	0.6±0.09	7414.95[2]±4209.32

[1]for ISF, this value represents CL/F, [2]for ISF, this value represents V_z/F

3.3.4.3 Steady-State Concentrations and Non-parametric Superposition

Immunosuppressants have to be given long term to prevent organ rejection. Multiple dose regimens are required to keep a fairly constant concentration in the patient's circulation life-long. Doses and target ranges vary depending on the situation. Slightly higher target ranges are required prophylactically before surgery and until three months after surgery while the maintenance range is 10-15 ng/mL [150].

After calculating the NCA parameters, a dosing regimen for a multiple dose study was derived for mycophenolic acid (Table 41). Non-parametric superposition was used to estimate concentrations from the single dose data set at steady-state just before giving the next dose (C_{trough}) for mycophenolic acid. Drug monitoring for mycophenolic acid is less frequently done using specific time-point concentrations. The parameter most interesting is the AUC from time zero to 12 hours, which should be > 40 h·µg/mL. There is a controversy about which concentrations to use for the best AUC estimation and it is often mentioned that as many as three levels are necessary in order to get a good correlation [153]. For this study, a sampling strategy using only C_{trough} was used to determine the total drug exposure (AUC_{0-12h}): $AUC = 6.74 \cdot c_{trough} + 34.8$ [154]. Using this equations a C_{trough} of 0.77 µg/mL is required to keep the AUC > 40 h·µg/mL. Comparing the predicted AUCs in blood and ISF (Figure 52), it is apparent that there is no difference between the predictions in blood and ISF as expected from the very similar concentrations and elimination profile after 1 h (compare to Figure 51). The drug exposure is equal in both compartments at a steady state using the predicted trough concentrations through non-parametric superposition. An unpaired t-test, with an expected difference between compartments set to zero, confirmed that the means are not significantly different (α = 0.05, two tail). The mean predicted trough concentrations are 0.15 µg/mL and 0.19 µg/mL and the

126

corresponding AUCs are 35.84 and 36.09 h·µg/mL for blood and ISF, respectively (Table 38).

The box and whisker plots (Figure 52) compare the predictions in blood and ISF for both

compartments.

Table 38. The calculation of loading dose (D_L), maintenance dose (D_M) and dosing interval (τ) for mycophenolic acid from λ_z and V_z, $C_{max\ ss}$= 5 µg/mL and $C_{min\ ss}$= 0.77 µg/mL.

Mycophenolic Acid Rabbit #	λ_z (blood) (h^{-1})	V_z (blood) (mL/kg)	D_L (µg/kg)	τ (h)	D_M (µg/kg)	Predicted AUC in Blood (µg·h/mL)	Predicted AUC in ISF (µg·h/mL)
1	0.83	1110.05	5550.25	2.38	4773.22	36.03	36.62
2	1.17	699.47	3497.33	1.68	3007.71	35.35	35.54
3	0.64	1357.24	6786.18	3.07	5836.12	36.03	-*
4	0.72	1268.84	6344.19	2.72	5456.00	36.48	35.93
5	1.12	815.11	4075.55	1.75	3504.97	35.88	36.28
6	0.72	3869.22	19346.11	2.72	16637.65	35.24	-*
Mean	**0.87**	**1519.99**	**7599.94**	**2.39**	**6535.95**	35.84	36.09
SD	0.23	1178.70	5893.48	0.57	5068.39	0.47	0.46

-*No predictions are possible if the elimination is too fast to accumulate for the chosen dosing interval τ or if the terminal slope cannot be determined for sparse data sets.
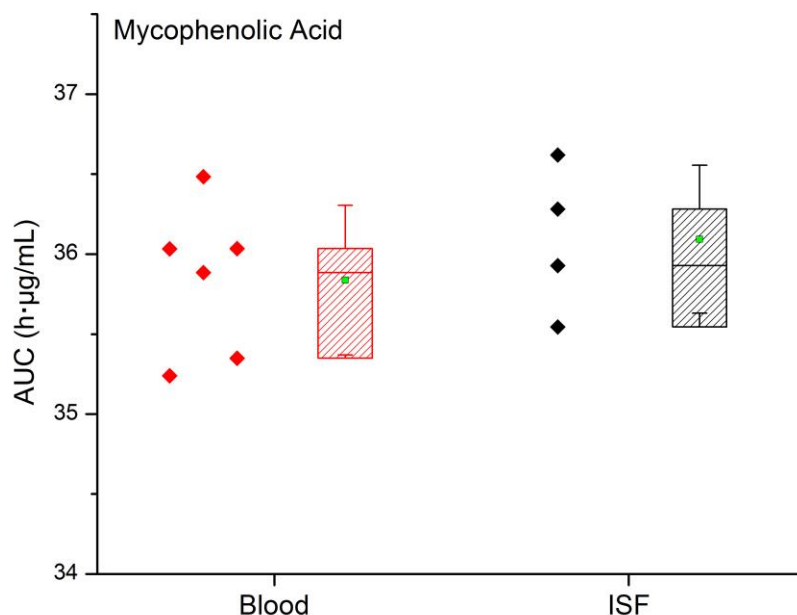
Figure 52. Box and whisker plot of AUC predictions $6.74 \cdot C_{trough} + 34.8$ [154]in blood and ISF for mycophenolic acid. Top and bottom of box represent the first and third quartile, the band in the box represents the median, whiskers represent 1 SD from the mean (■), the means are not significantly different (unpaired t-test, two tail, $\alpha = 0.05$).
● AUC in Blood (n = 6)
● AUC in ISF (n = 4)

3.3.4.4 Compartmental Analysis

Mycophenolic acid fit the same lymph-model suggested for gentamicin (Figure 39).
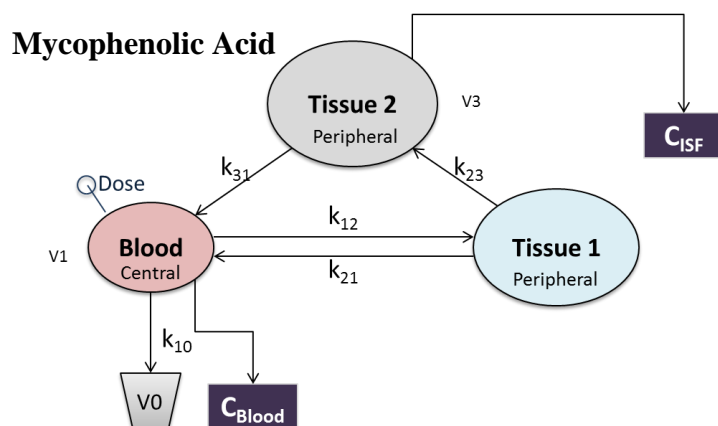
Figure 53. Compartmental model used for mycophenolic acid. The central compartment receives the intravenous bolus dose and is connected to the first tissue compartment via the rate constants k_{12} and k_{21}. Drug exchange takes place from the first tissue compartment to the second tissue compartment via k_{23}, and back to the central compartment via k_{31}, while elimination (k_{10}) happens only from the central compartment. Concentration *vs.* time observations are detected from the central compartment (C_{Blood}) and the second tissue compartment (C_{ISF}).

128

The corresponding rate equations for Compartment Blood (C1), Compartment Tissue 1 (P1) and 2 (P2) are Equation **17**, **18** and **19** as given in Chapter 3.3.1.4 .

Table 39. Modeled parameters for mycophenolic acid.

Drug	Mycophenolic Acid						
Parameter	Estimate	Unit	Standard Error	CV (%)	Initial Estimate	Lower Bound	Upper Bound
V_1	160.00	mL/kg	40.32	25.20	160.00	104.00	220.00
k_{10}	6.80	h^{-1}	1.02	14.99	6.80	0	-
k_{12}	1.00	h^{-1}	0.47	46.89	1.00	0.90	1.20
k_{21}	2.40	h^{-1}	1.49	62.20	2.40	2.10	2.50
V_3	480.00		500.85	104.34	480.00	400.00	500.00
k_{23}	1.25	h^{-1}	1.34	106.98	1.25	0	-
k_{31}	0.74	h^{-1}	0.31	42.10	0.74	0.74	-

CV% is the coefficient of variation and calculated as $\frac{Standard\ Error}{Estimate} \cdot 100$

Using the values for the microconstants (Table 39), the differential equations were numerically solved to plot the concentration time course of drug in ISF and blood (Figure 54).
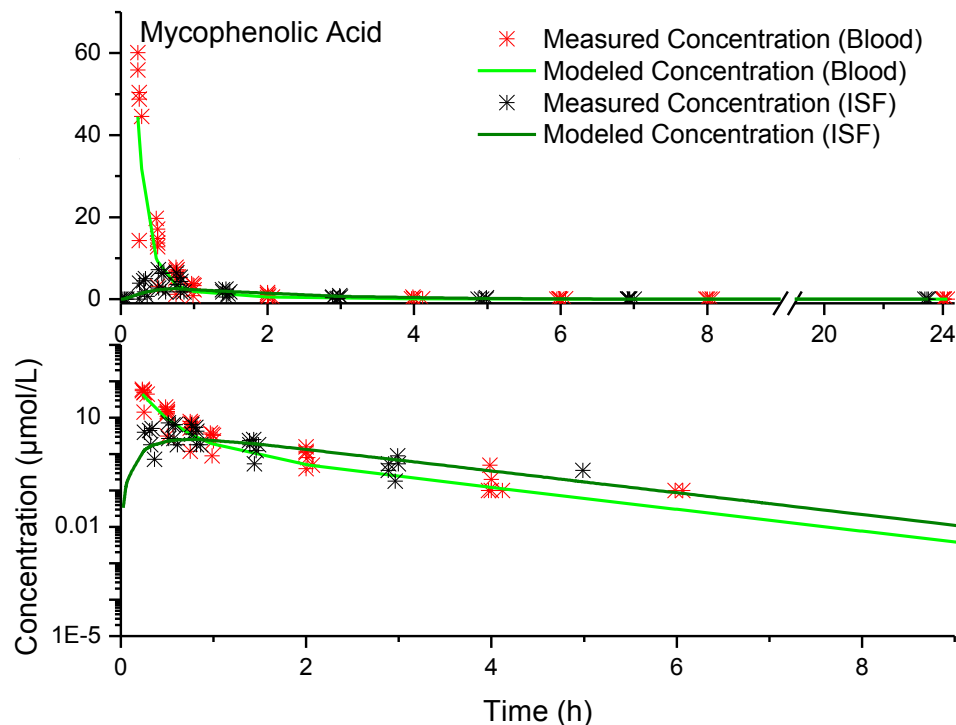
Figure 54. Modeled concentration time course and measured concentrations for mycophenolic acid, upper panel: linear vertical axis, lower panel: logarithmic vertical axis.

3.3.5   PK Analysis of Digoxin and Theophylline in Blood and ISF

Digoxin is used clinically as an antiarrhythmic to increase cardiac output in congestive heart failure and to control ventricular function in several heart conditions including atrial fibrillation and atrial flutter [155]. Digoxin is a cardiac glycoside that contains a hydrophilic sugar unit and a rather lipophilic steroid moiety with a molecular weight of 780.94 g/mol. Digoxin inhibits the Na/K ATPase pump in cardiomyocytes, which leads to an accumulation of sodium inside the cells and a directly related increase of calcium influx. As a result, three effects occur in the heart: increased contractility (positive inotropic effect), slowing of the heart rate (negative chronotropic effect) and slowing of the rate of electrical impulses (negative dromotropic effect) [155]. Cardiac glycosides are extremely potent drugs that can be given orally and intravenously. Oral

130

bioavailability is between 70-90 % depending on the formulation [155]. Protein binding is ~ 25% rather low and the distribution space of digoxin is reported to be large with an apparent volume of distribution of 5.6-7.3 L/kg [155, 156].

Theophylline is a plant derived small alkaloid with a molecular weight of 180.16 g/mol. It blocks a phosphodiesterase which leads to increased tissue cyclic adenine monophosphate (cAMP) with a broad range of effects including bronchodilation, diuresis, central nervous system and cardiac stimulation. It is used for asthma and chronic obstructive pulmonary disease, but its narrow therapeutic window and its non-linear PK have led to a decline in use [157]. Administered orally as in its salt form aminophylline, it is absorbed completely, distributes rapidly into the CNS and exhibits Michaelis-Menten kinetics. At higher concentrations the decline of concentration is zero order.

3.3.5.1 Concentration Time Profiles in Blood and ISF

Digoxin was readily detectable in ISF and the concentrations were corrected to account for 100% recovery (2.3.1). Digoxin reaches higher concentrations than in blood at 1 h after administration and is subsequently more rapidly eliminated than in blood with concentrations falling below drug levels in blood at 2.5 h and to zero at 7 h. Digoxin stays in blood over 24 h.

Theophylline concentrations are similar in blood and ISF with generally much lower concentrations in ISF but parallel elimination profiles.

Table 40 summarizes the study facts. A full concentration *vs.* time profile of the drugs is displayed in Figure 55 and 56.

Table 40. Summary study table for digoxin and theophylline.

Drug	Study	Study Subjects (#)	Dose (µgl/kg)	Recovery Factor R	Drug in ISF	Site of Drug Action
Digoxin	Single-dose	6	25.6 nmol/kg	1.19	Yes	Intracellular
Theophylline	Single-dose	6	66.6 µmol/kg	1.00	Yes	Intracellular
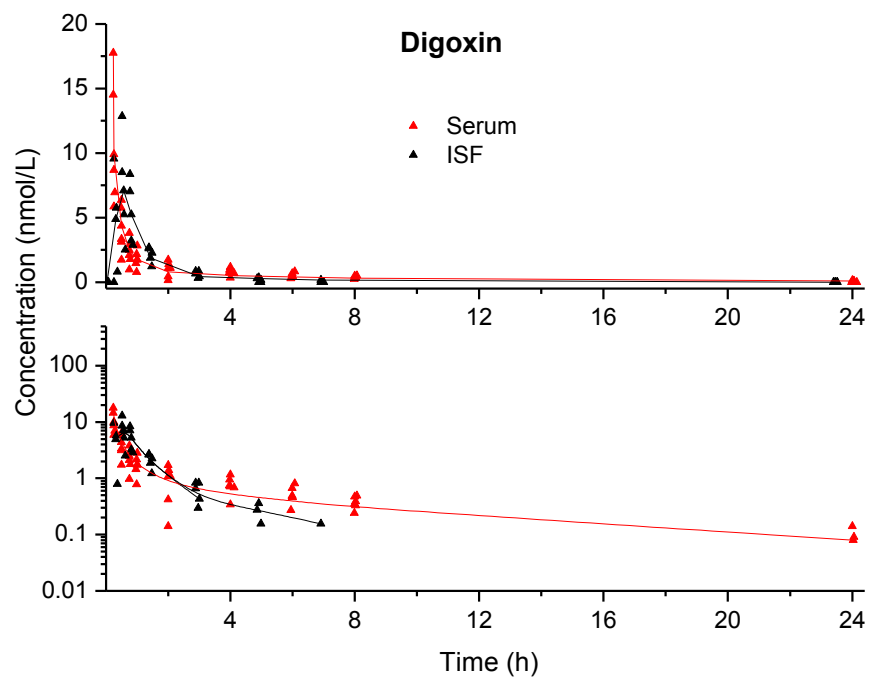
Figure 55. Digoxin concentration in serum and ISF of rabbits after single dosing, shown both as a linear plot and a logarithmic plot (n = 6). The lines are drawn to serve as visual guides and do not indicate a specific model.
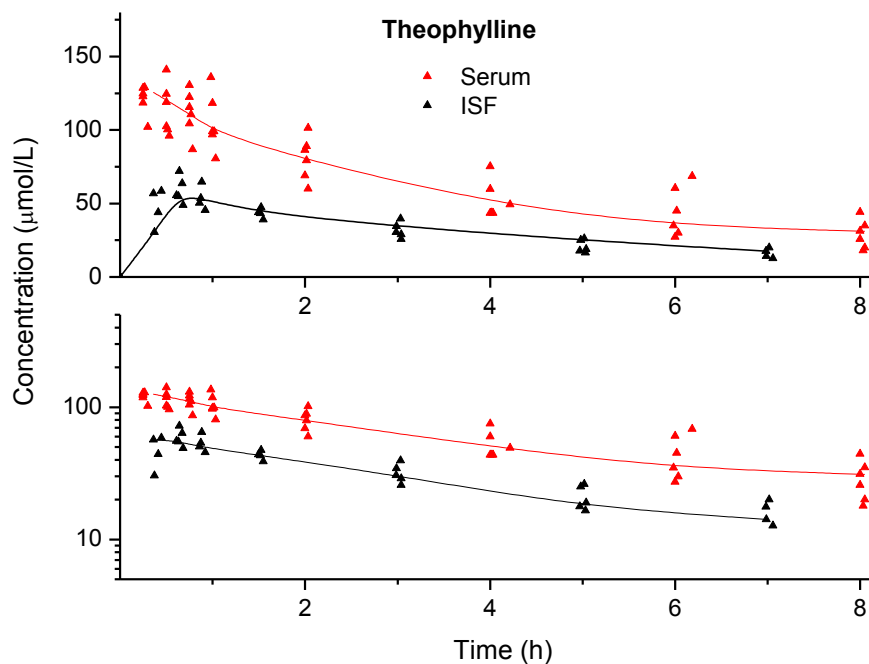
Figure 56. Theophylline concentration in serum and ISF of rabbits after single dosing, shown both as a linear plot and a logarithmic plot (n = 6). The lines are drawn to serve as visual guides and do not indicate a specific model.

3.3.5.2   Non-Compartmental Pharmacokinetic Analysis

Basic PK parameters were calculated for digoxin (Table 41) and theophylline (Table 42) using statistical moment analysis without any model assumptions. ISF concentrations of digoxin were adjusted to 100% recovery using ultrafiltration recovery data (e.g., multiplication by factor 1.19). Drug exposure to digoxin and theophylline in ISF was lower than in blood but the terminal elimination was almost identical for theophylline, whereas digoxin was faster eliminated from ISF than from blood.

Table 41. PK parameters (mean ± standard deviation) determined by NCA for digoxin in serum (n = 6) and ISF (n = 5), dose = 25.6 nmol/kg.

Digoxin	AUC nmol·h/L	AUMC nmol·h·h/L	C_0 nmol/L	CL L/h/kg	C_{max} (measured) nmol/L
Serum	16.92±6.14	81.75±33.13	27.14±9.73	1.68±0.59	10.6±4.62
ISF	9.02±3.62	12.32±5.82	0±0	3.17^1±1.05	7.02±3.44
	$t_{1/2}$ h	λ_z h^{-1}	MRT h	t_{max} h	V_z L/kg
Serum	6.21±1.78	0.12±0.04	4.89±1.17	0.25±0.02	15.14±7.54
ISF	0.95±0.42	0.83±0.28	1.36±0.33	0.56±0.17	3.93^2±0.92

[1]for ISF, this value represents CL/F, [2]for ISF, this value represents V_z/F

Table 42. PK parameters (mean ± standard deviation) determined by NCA for theophylline in serum (n = 6) and ISF (n = 6), dose = 66.6 µmol/kg.

Theophylline	AUC µmol·h/L	AUMC µmol·h·h/L	C_0 µmol/L	CL L/h/kg	C_{max} (measured) µmol/L
Serum	700.07±184.26	4241.76±1864.02	133.06±19.72	0.1±0.03	123.33±12.87
ISF	293.38±51.74	1571.75±552.71	0±0	0.23^1±0.04	62.57±7.05
	$t_{1/2}$ h	λ_z h^{-1}	MRT h	t_{max} h	V_z L/kg
Serum	4.21±0.84	0.17±0.04	5.84±1.22	0.34±0.12	0.59±0.08
ISF	3.57±0.75	0.2±0.06	5.23±1.07	0.56±0.12	1.17^2±0.17

[1]for ISF, this value represents CL/F, [2]for ISF, this value represents V_z/F

3.3.5.3   Steady-State Concentrations and Non-parametric Superposition

Digoxin and theophylline are usually used for chronic conditions and therefore used long-term so steady-state concentrations are reached in the patient.

After calculating the NCA parameters, a dosing regimen for a multiple dose study was derived for digoxin (Table 43) and theophylline (Table 44). Non-parametric superposition was used to estimate concentrations from the single dose data set at steady-state just before giving the next dose (C_{trough}). For digoxin, the concentrations in ISF were not high enough to actually reach a

134

steady-state due to its slow and incomplete ISF penetration but quick elimination compared to

blood. The drug was eliminated from ISF at the end of the dosing interval.

Theophylline is known to follow Michaelis-Menten PK in a minority of patients, so the steady-

state predictions here are hypothetical, because they assume linear kinetics. According to [158],

theophylline levels are sometimes even taken 30 min after giving a dose, but the predicted

concentrations here are trough concentrations. The predictions for theophylline in ISF are very

similar to blood with overall lower but similar accumulation.

The box and whisker plots (Figure 57) compare the predictions in blood and ISF for both

compartments.

Table 43. The calculation of loading dose (D_L), maintenance dose (D_M) and dosing interval (τ) for digoxin from λ_z and V_z, $C_{max\ ss}$= 2.6 nmol/L and $C_{min\ ss}$= 1.15 nmol/L.

Digoxin Rabbit #	λ_z (serum) (h^{-1})	V_z (serum) (L/kg)	D_L (nmol/kg)	τ (h)	D_M (nmol/kg)	Predicted Trough in Blood (nmol/L)	Predicted Trough in ISF (nmol/L)
1	0.09	20.04	52.09	9.39	29.05	0.73	0
2	0.19	10.30	26.77	4.23	14.93	0.57	0
3	0.16	8.02	20.84	5.12	11.62	0.81	0
4	0.10	9.58	24.90	8.29	13.89	1.09	0.26
5	0.10	15.30	39.79	8.29	22.19	0.77	0
6	0.10	27.60	71.75	8.51	40.02	0.41	0
Mean	**0.12**	**15.14**	**39.36**	**7.30**	**21.95**	**0.73**	**0.26**
SD	0.04	7.54	19.61	2.10	10.93	0.57	0

Table 44. The calculation of loading dose (D_L), maintenance dose (D_M) and dosing interval (τ) for theophylline from λ_z and V_z, $C_{max\ ss}$= 110 µmol/L and $C_{min\ ss}$= 27.8 µmol/L.

Theophylline Rabbit #	λ_z (serum) (h^{-1})	V_z (serum) (L/kg)	D_L (µmol/kg)	τ (h)	D_M (µmol/kg)	Predicted Trough in Blood (µmol/L)	Predicted Trough in ISF (µmol/L)
1	0.23	0.59	64.80	0.45	48.43	13.93	-*
2	0.17	0.54	58.96	0.34	44.06	27.85	13.55
3	0.19	0.69	75.59	0.39	56.49	16.96	9.59
4	0.14	0.49	54.19	0.27	40.50	45.20	15.34
5	0.13	0.67	73.86	0.26	55.19	31.22	8.14
6	0.16	0.56	61.08	0.32	45.64	29.65	10.09
Mean	**0.17**	**0.59**	**64.75**	**0.34**	**48.38**	**27.47**	**11.34**
SD	0.04	0.08	8.47	0.07	6.33	11.20	2.99

-*No predictions are possible if the elimination is too fast to accumulate for the chosen dosing interval τ or if the terminal slope cannot be determined for sparse data sets.
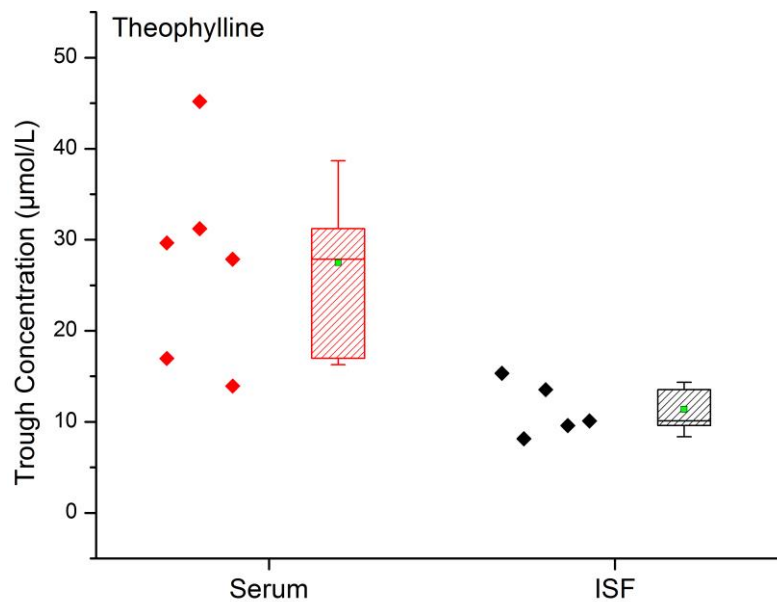
Figure 57. Box and whisker plot of predicted trough concentrations in serum and ISF for theophylline: Top and bottom of box represent the first and third quartile, the band in the box represents the median, whiskers represent 1 SD from the mean (■), the means are significantly different (unpaired t-test, two tail, $\alpha = 0.05$)
● Serum Concentrations (n = 6)
● ISF Concentrations (n = 5)

3.3.5.4 Compartmental Analysis

Theophylline and digoxin fit the model that has been previously reported for the transport of

drug via a lymph-compartment (here called tissue 2) back to the circulation (Figure 58) [143].

Digoxin and Theophylline
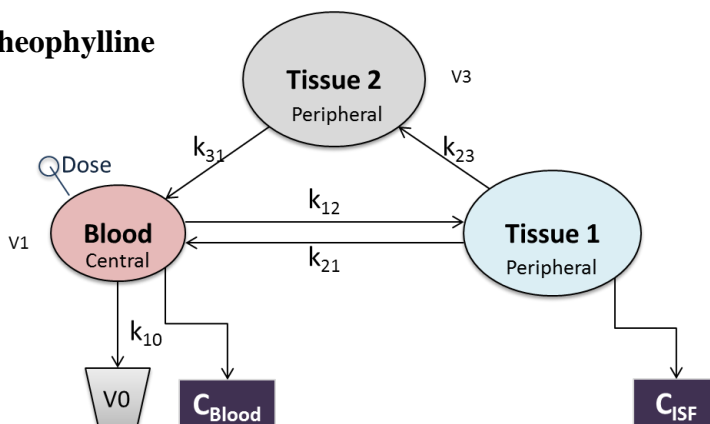
Figure 58. Compartmental model used for theophylline and digoxin. The central compartment receives the intravenous bolus dose and is connected to the first tissue compartment via the rate constants k_{12} and k_{21}. Drug exchange takes place from the first tissue compartment to the second tissue compartment via k_{23}, and back to the central compartment via k_{31}, while elimination (k_{10}) happens only from the central compartment. Concentration *vs.* time observations are detected from the central compartment (C_{Blood}) and the first tissue compartment (C_{ISF}).

The corresponding rate equations for Compartment Blood (C1), Compartment Tissue 1 (P1) and

2 (P2) can be described by Equations **17**, **18** and **19** (see Chapter 3.3.1.4).

Table 45. Modeled parameters for digoxin.

Drug	Digoxin						
Parameter	Estimate	Unit	Standard Error	CV (%)	Initial Estimate	Lower Bound	Upper Bound
V_1	0.71	L/kg	0.26	36.57	0.78	0	-
k_{10}	1.99	h^{-1}	0.97	48.71	1.95	0	1.99
k_{12}	3.84	h^{-1}	2.31	60.07	4.60	3	5.00
k_{21}	1.62	h^{-1}	0.63	38.90	2.40	0	-
k_{23}	1.80	h^{-1}	0.85	47.01	1.95	1.80	-
k_{31}	0.25	h^{-1}	0.35	140.21	0.30	0.25	0.35

CV% is the coefficient of variation and calculated as $\frac{Standard\ Error}{Estimate} \cdot 100$

137

Table 46. Modeled parameters for theophylline.

Drug	Theophylline						
Parameter	Estimate	Unit	Standard Error	CV (%)	Initial Estimate	Lower Bound	Upper Bound
V_1	0.48	L/kg	0.04	7.94	0.21	0	-
k_{10}	0.21	h^{-1}	0.02	10.78	0.56	0	-
k_{12}	0.25	h^{-1}	0.26	104.70	1.5	0	-
k_{21}	2.40	h^{-1}	0.49	20.52	1.15	0	-
k_{23}	2.56	h^{-1}	0.61	23.61	1.15	0	-
k_{31}	1.40	h^{-1}	1.83	1.4	0.23	0.10	1.40

CV% is the coefficient of variation and calculated as $\frac{Standard\ Error}{Estimate} \cdot 100$

Using the values for the microconstants (Table 45 and Table 46), the differential equations were

numerically integrated to plot the concentration time course of drug in ISF and blood (Figure 59

and 60).
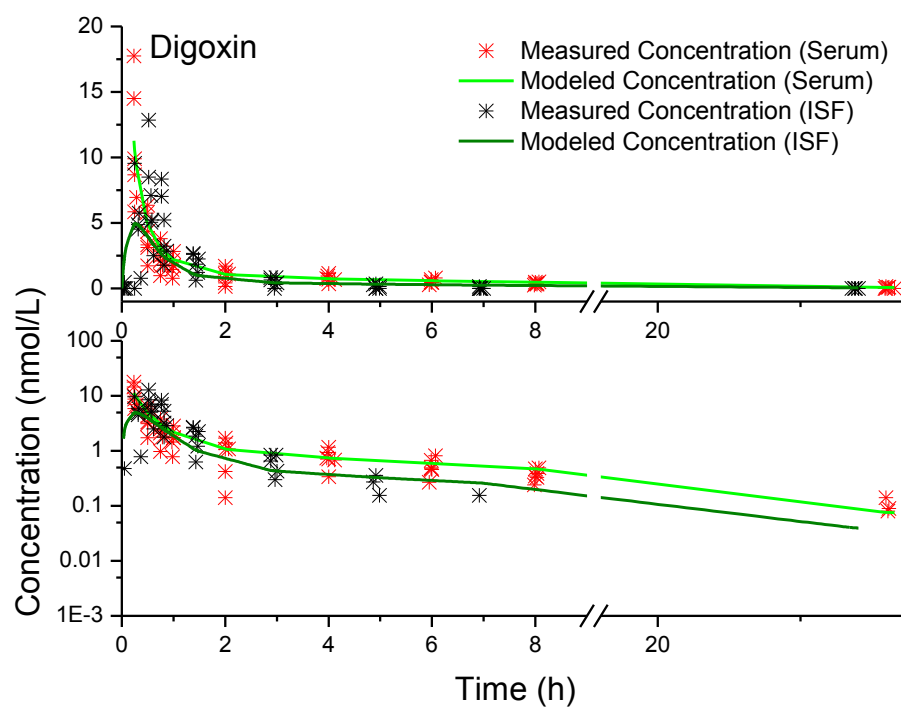
Figure 59. Modeled concentration time course and measured concentrations for digoxin, upper panel: linear vertical axis, lower panel: logarithmic vertical axis.
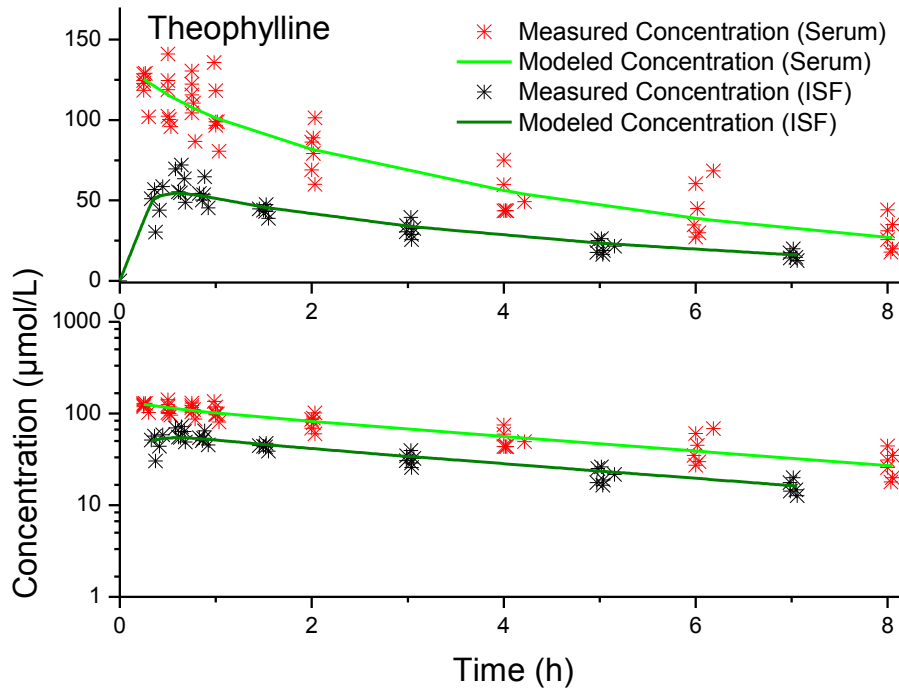
Figure 60. Modeled concentration time course and measured concentrations for theophylline, upper panel: linear vertical axis, lower panel: logarithmic vertical axis.

3.3.6 Steady-State Study of Vancomycin *In Vivo*

Measured trough concentrations from the steady-state study are shown in blood and ISF in

Figure 61. ISF concentrations exceed blood concentrations after 1.5 h and stay high in a steady

state. ISF steady state is slightly delayed and reached after the second dose, whereas blood

concentrations are obviously high after the first dose.
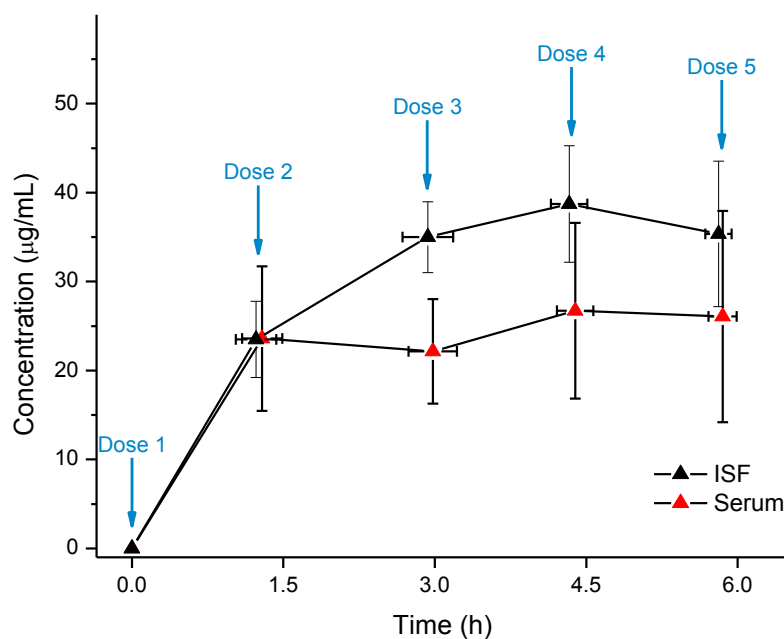
Figure 61. Trough concentrations of vancomycin in serum and ISF after 5 doses of vancomycin and a dosing interval of 1.5 h.

The measured steady-state trough concentrations were compared to the previously predicted concentrations trough superposition (see 3.3.1.3). Figure 62 shows that both times, ISF concentrations are higher than blood concentrations. For both sets (measured *vs.* predicted), blood steady state is significantly lower than ISF steady-state concentrations. Assay procedures were different for the data used for predictions (clinical immunoassay) and the experimental determinations (LCMS), so it might not be possible to compare the total concentrations. The variability of the data points is larger in blood than in ISF for both data sets.
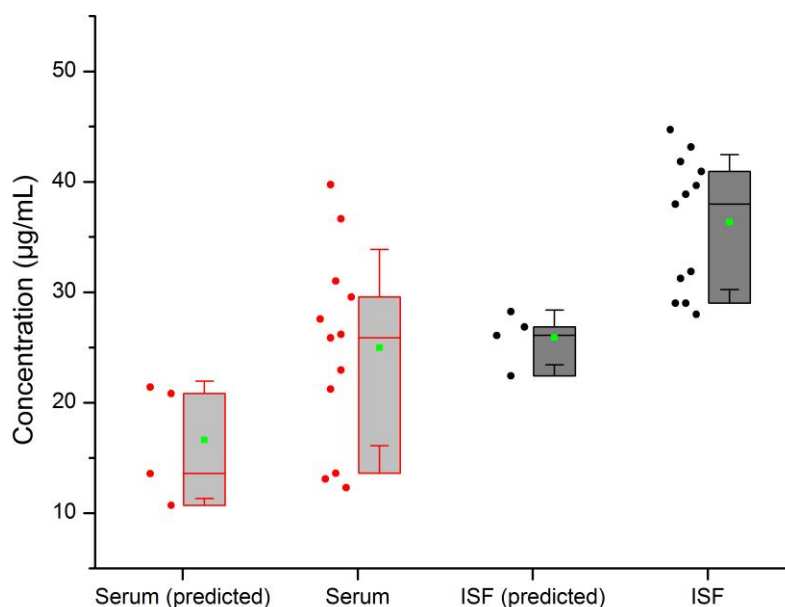
Figure 62. Boxplot displaying experimentally measured (3, 4.5, and 6 h measurements) and predicted steady-state trough concentrations of vancomycin.

3.4   Discussion and Conclusion

In the current study, we obtained detailed *in vivo* data of 13 drugs. Full concentration time courses in blood and ISF were described, important PK parameters were calculated using non-compartmental analysis and compartmental approaches related ISF concentrations to measured blood concentrations. Compartmental modeling can predict free drug concentrations in ISF tissue. Furthermore, we predicted through non-parametric superposition that ISF concentrations in a steady state can be even higher, less fluctuating and more stable than in blood. For vancomycin, this finding was confirmed experimentally.

This study is novel and superior compared to current data presented in the literature. The first reason is that we used a comprehensive panel of drugs and the same ISF extraction method for all drugs. The different drugs can therefore be compared. The second reason is that we used the compartmental approach and fit both blood and ISF data simultaneously to one model. The

advantage is that each model is based on twice as many data points and the blood and ISF concentrations are directly related. Usually, only one data set is fit at a time.

All these presented results are essential to determine if ISF should be used in the future for TDM. Furthermore, physicochemical properties of a drug can also help to determine if TDM in ISF is feasible. In the following paragraphs, the data are discussed in the light of the drugs' physicochemical properties. This can help to understand ISF penetration of drugs and the observed concentration time courses.

Selected properties of the drugs are summarized in Table 47 and 48. A color coding is applied to make the interpretation easier. For the molecular weight, the smaller the molecule the easier it can diffuse into ISF. Drugs that are larger than 500 g/mol are marked as red. Low protein binding makes the initial diffusion into ISF faster than if the drug is immobilized and circulates with the proteins. Maximum detected concentrations in blood and ISF are marked in red if 10% or less is detected in ISF. If the AUC ratio (AUC_{ISF}/AUC_{Blood}) is close to 1, drug exposure in blood and ISF are very similar. If the AUC ratio is > 1, the drug exposure is higher in ISF, which can point to toxicities that might be undetectable in blood. If the AUC ratio is << 1, drug exposure in ISF is limited and the drug is mostly in blood or tissue bound. High protein binding seems to correlate with a low AUC. Drugs that score at maximum 1 time in the red category are marked in the following Table 47 as green. Table 48 reports several properties that make a molecule more likely to cross biological membranes and two rules that are a combination of such properties:

- Log D is a measure of the drug's hydrophobicity and calculated as the distribution of drug between octanol and water ($log\ D_{octanol/water} = \log(\frac{[drug]_{octanol}^{ionized}+[drug]_{octanol}^{un-ionized}}{[drug]_{water}^{ionized}+[drug]_{water}^{un-ionized}})$).

- H-Bond donors and acceptors indicate a molecules possibility to form hydrogen bonds.

- The topological polar surface area (TPSA) is a predictor of the sum of surfaces of polar atoms in a molecule [26].

- <u>Rule 1:</u> A rule for the determination of bioavailability: Molecular weight ≤ 500 g/mol AND the octanol/water partition coefficient logP ≤ 5 AND H-donor count ≤ 5 AND H-acceptor count ≤ 10) AND rotable bond count ≤ 10 AND polar surface area ≤ 200 Å^2 AND fused aromatic ring count ≤ 5 or ≥ 6

- <u>Rule 2:</u> Lipinski's Ro5: Molecular weight ≤ 500 g/mol AND the octanol/water partition coefficient logP ≤ 5 AND H-donor count ≤ 5 AND H-acceptor count ≤ 10)

It is apparent from the table that some drugs (vancomycin, gentamicin, methotrexate) were measured in ISF, although they did not fulfill the two mentioned rules indicating a higher likelihood of crossing biological membranes (Table 48). Other drugs (valproic acid, phenytoin, mycophenolic acid) fulfill all criteria but were only detectable in small concentrations or undetectable in ISF. It is likely that the limitation of the extraction procedure, namely the exclusion of all protein bound drug from ISF and a possible drug adsorption to the membrane, has to be taken into account. Drug in ISF is likely also protein bound and maybe even immobilized otherwise on extracellular matrix. Some drugs that are highly protein bound in blood were still detected in ISF (cisplatin, valproic acid, mycophenolic acid), but the exposure was generally lower. Most drug protein binding is reversible so whenever drug moves to the tissues (or leaves the circulation otherwise), a new equilibrium will be reached and some protein-bound drug will dissociate and replenish the free fraction in case the plasma proteins are not saturated. If the exposure to drug is extended (steady state) or a saturation of plasma protein occurs, plasma protein binding might become less important.

144

For the drugs not detected in ISF phenytoin, tacrolimus and cyclosporine, protein binding could have been a major player. The drug can either be immobilized in the tissue or in the blood. In the first case, the drug would not be extracted using ultrafiltration with a molecular weight cutoff that excludes the protein albumin, the major binding partner found in biological fluids. In the second case, the drug would not diffuse quickly into the interstitial space as "free drug" (see Chapter 3.1). Furthermore the ultrafiltration probe material was not ideal at least for tacrolimus and cyclosporine and interacted with the drug as seen in the low *in vitro* recovery.

Overall, no specific conclusions or rules for ISF penetration can be derived without including or measuring protein bound drug in ISF. The presented tables serve as a starting point for further studies of ISF penetration of drugs depending on their physicochemical properties. Only three drugs namely carboplatin, theophylline and phenobarbital fulfilled one or two of the presented rules and at the same time showed high concentrations in ISF (green or orange coding for C_{max} and AUC Ratio as depicted in Table 47) as indicated in green in Table 48. Vancomycin, gentamicin and methotrexate in contrast did not fulfill either of the rules but showed high concentrations in ISF (orange or green coding for C_{max} and AUC Ratio in Table 47).

Further studies are required to determine the most important properties for ISF penetration and a possible model could be developed to describe concentrations in ISF in this light. Such a model can be an improvement to the presented compartmental models.

Table 47. Part 1. Drug summary table for relevant PK parameters and physicochemical properties.
Color coding: Drug properties that are likely advantageous for a fast distribution into ISF (green), mediocre (orange) and not-advantageous (red).

Drug	Molecular Weight (g/mol)	Plasma Protein Binding (%)	C_{max} in Blood, Plamsa or Serum	C_{max} in ISF	AUC Ratio (AUC_{ISF}/AUC_{Blood})
Vancomycin	1449.25	55	72.05 µg/mL	32.10 µg/mL	0.88
Gentamicin	477.6	0-30	144.50 µg/mL	91.19 µg/mL	18.41
Cisplatin	300.05	> 90	3.35 mg/L	5.60 mg/L	0.08
Carboplatin	371.25	very low	1.98 mg/L	4.11 mg/L	1.05
Methotrexate	454.44	50	51.75 µmol/L	38.07 µmol/L	0.92
Valproic Acid	144.21	80-90*	1219.08 µmol/L	180.68 µmol/L	0.14
Phenobarbital	232.24	40-60	230.02 µmol/L	110.93 µmol/L	0.55
Phenytoin	252.27	90	68.5 µmol/L	-	-
Cyclosporine	1202.61	90	1994.67 µg/L	-	-
Tacrolimus	804.02	75-99	67.50 ng/mL	-	-
Mycophenolic acid	433.49	98	45.68 µg/mL	4.65 µg/mL	0.16
Digoxin	780.94	25	10.60 nmol/L	7.02 nmol/L	0.53
Theophylline	180.16	40	123.33 µmol/L	62.57 µmol/L	0.37

*saturable at 200-350 µmol/L

Table 48. Part 2. Drug summary table for relevant molecular properties and bioavailability rules.
Color coding: Drug names appear in green if they scored ≤ 1 time in the red category in Table 47. Rule 1 and 2 are marked in green if fulfilled and in red if not fulfilled.

Drug	LogD at pH 7.4	Number of H Bond Acceptors	Number of H Bond Donors	TPSA (Å²)	Bioavailability (Rule 1)	Lipinski Rule (Rule 2)
Vancomycin	-4.86	24	19	530.49	FALSE	FALSE
Gentamicin	-11.79	12	8	199.73	FALSE	FALSE
Cisplatin	0.03	0	0	0	TRUE	TRUE
Carboplatin	1.06	2	0	52.6	TRUE	TRUE
Methotrexate	-6.56	12	5	210.54	FALSE	FALSE
Valproic Acid	0.56	2	1	37.3	TRUE	TRUE
Phenobarbital	1.33	3	2	75.27	TRUE	TRUE
Phenytoin	2.14	2	2	58.2	TRUE	TRUE
Cyclosporine	3.64	12	5	278.8	FALSE	FALSE
Tacrolimus	5.59	11	3	178.36	FALSE	FALSE
Mycophenolic acid	3.45	6	1	94.53	TRUE	TRUE
Digoxin	1.92	13	6	203.06	FALSE	FALSE
Theophylline	-0.89	3	1	69.3	TRUE	TRUE

log D (7.4) is the water-octanol distribution coefficient at physiological pH, a measure for molecule hydrophobicity, the smaller the more hydrophilic a drug, TPSA topological polar surface area, plasma protein binding values from [144, 148, 150, 155, 157, 159], log D, TPSA, bioavailability and Lipinski rule estimated using MarvinSketch (ChemAxon LLC, Cambridge, MA).

The compartmental modeling of this chapter is one way of analyzing tissue fluid data sets. There are many other possibilities to handle such data sets. A different approach could be to fit the blood data to a compartmental model and handle the tissue concentrations as a "biophase" compartment. The concentration time course in this biophase could be described by concentrations in the central compartment but adjusted using observed ISF concentrations and a constant that represents physicochemical properties of the drug. Furthermore, the fraction of unbound drug or protein binding could be included into the model.

Chapter 4: Quantification of Vancomycin in Microvolumes of Serum

4.1 Background

Many sensitive liquid chromatography assays need sample volumes in the order of hundred(s) of microliters [160-163]. The main reason for this requirement is that the error associated with the procedure (e.g., sample evaporation, pipetting errors) is relatively smaller with larger volumes and the assay procedure is therefore more robust. Another reason is that a minimum fill volume is often required for the assays that are run on the automated clinical chemistry analyzers at hospitals and specialized medical laboratories.

However, large sample volumes are sometimes difficult to obtain, especially for researchers that study drugs or biomarkers in small animals or in less voluminous biological matrices than blood, such as tissue fluid (interstitial fluid) or cerebrospinal fluid. To obtain the appropriate sample volume for the clinical assay procedure, the biological sample often has to be diluted. If diluted further to reach the minimum volume necessary for an assay, the drug concentration can easily drop below the lower limit of quantitation (LLOQ). An example for this problem is the analysis of vancomycin.

Vancomycin is monitored in a patient's serum using most often a particle enhanced turbidimetric immunoassay (PETINIA). Even if the sample volume that is delivered to the reaction cuvette by the machine is low (1 µL), the required sample volume to fill the cuvette is 50 µL. If a biological matrix other than serum is used, a volume of 50 µL can be challenging to obtain. For example if an ISF sample containing vancomycin has a volume of only 2 µL and a concentration between 10-20 µg/mL, a dilution to 50 µL will mean that the concentration is at or below the LLOQ of the assay (0.8-50 µg/mL).

148

Vancomycin is a glycopeptide antibiotic used only for severe cases of bacterial infections in hospitalized patients and has been associated with nephro- and oto- toxicity. Monitoring vancomycin concentrations and thereby minimizing the risk of over- and under-dosing is clinically warranted. While standard monitoring in the patient's serum is both painful and inconvenient, no other biological matrix has been implemented successfully yet to replace serum monitoring for vancomycin. But as discussed in chapter 3.3.1, monitoring vancomycin in ISF could be especially advantageous, as anti-infective agents usually need to penetrate into the tissues in order to fight a bacterial infection. Tissue fluid concentrations could therefore be a great addition to clinical monitoring. To study the distribution of drugs like vancomycin in interstitial fluid (ISF), where barely more than a couple of microliters can be extracted, a sensitive assay for very small sample volumes is needed.

Therefore, the objective of this study was to develop and validate a sensitive and selective ultra-high performance liquid chromatography tandem mass spectrometry (UHPLC-MS/MS) method for the quantification of trace levels of vancomycin in rabbit serum requiring only 2 µL of sample.

4.2 Materials and Methods

4.2.1 Materials

Vancomycin hydrochloride (> 80%), teicoplanin (purity ≥ 80%), methanol (HPLC grade) were from Sigma-Aldrich (St. Louis, MO, US). Formic acid (purity 98%) was purchased from Acros Organics (Geel, Belgium), ammonium acetate (purity 97%) was from Caledon Laboratories (Georgetown, ON, CA). Blank rabbit serum was pooled drug-free rabbit serum from female New

Zealand white rabbits that had a protein content, normalized to BSA, of 63.0 ± 0.3 mg/mL (Centre For Comparative Medicine, Vancouver, BC, CA), and ultra-pure water was prepared in our laboratory using a Milli-Q Synthesis system (Millipore, Billerica, MA, US).

4.2.2   Preparation of Standards

A stock solution of 1 mg/mL vancomycin (V0) was prepared in 50% methanol/water (v/v) then further diluted to form a second stock solution of (V1) 40 µg/mL in rabbit serum. Ten calibration standards (C0-C9) were prepared from V1 with the concentrations of 0, 0.1, 0.25, 0.5, 1, 5, 10, 20, 30 and 40 µg/mL and stored at 4°C. Quality control (QC) of 0.1 µg/mL (at the LLOQ), 0.3 µg/mL (QL), 12 µg/mL (QM) and 32 µg/mL (QH) were prepared for accuracy and precision measurements and stored at 4°C.

A stock solution of 1 mg/mL of the teicoplanin (internal standard) (T0) was prepared in 50% methanol/water (v/v) then further diluted to 600 ng/mL in pure methanol (T1). This solution was stored at -20°C and used as the precipitation reagent resulting in a final IS concentration of 250 ng/mL.

4.2.3   Preparation of Samples

Ten µL of ice-cold precipitation reagent (T1) was pipetted into cooled 0.5 mL tubes (Eppendorf, lowBind, Mississauga, ON, CA). After adding exactly 2 µL of calibrator (C0-C9) without aspirating to flush the pipette tip, the tubes were vortexed (1 s, ~3000 rpm), sonicated for 5 min, again vortexed (1 s, ~3000 rpm) and subsequently spun for 2 min at 9000 rpm or ~8000 g (Eppendorf centrifuge, Mississauga, ON, CA) using 2 mL Eppendorf tubes as inserts. On ice, 9.7 µL of the supernatant was transferred to 384 well plates already containing 10 µL of Milli-Q water in each well and mixed by repeated aspiration. A short sonication was applied and the

150

plate was closed with a silicone mat to prevent sample evaporation. Up to 31 samples were prepared in one batch and analyzed immediately at a tray temperature of 10°C.

A full calibration set consisting of a zero sample (containing no IS), C0-C9, five QL, QM and QH samples was prepared on 3 consecutive days, whereas 5 LLOQ samples were measured on one single day. The LLOQ, range, accuracy and precision of the assay was determined from these measurements.

4.2.4   Instrumentation and Chromatographic Conditions

The instrument and chromatographic conditions are summarized in Table 53. The UHPLC-MS/MS consisted of an Agilent 1290 Infinity UHPLC connected to an AB Sciex QTrap® 5500 hybrid linear ion-trap triple quadrupole mass spectrometer equipped with a Turbo Spray source, and operated in positive ionization mode. Chromatographic separation was achieved using a Waters Acquity UPLC BEH C_{18} (1.7 μm, 2.1 x 100 mm) column, which was protected by a Waters Acquity UPLC BEH C_{18} VanGuard (1.7 μm, 2.1 x 5 mm) guard column.

After loading the 384 well-plate on the sample tray kept at 10 °C, 5 µL of sample was injected onto the column. The mobile phase consisted of water and methanol both containing 5 mM ammonium acetate and 0.1% formic acid. To minimize carry-over between samples, and the needle was rinsed with a wash solvent of 50% methanol/water (v/v). The first 2 minutes of the chromatographic run were diverted to waste to prevent water soluble biological matrix components to enter the mass spectrometer, and data collection started at 2 to 6 min.

Vancomycin was quantitated with multiple reaction monitoring (MRM) using the MRM transition at 725.5/144.2 (m/z), and teicoplanin (internal standard) at 940.6/316.4 (m/z). Vancomycin and teicoplanin eluted at 2.27 and 2.68 min, respectively (Figure 64). Teicoplanin was chosen as the internal standard because it has been used successfully before [164] due to its

structural similarity to vancomycin. The two molecules (Figure 63) share the same glycopeptide core, but have different hydrophobic side chains. Teicoplanin has more hydrophobic side groups and therefore elutes on a C-18 column 25 seconds later. If mass spectrometry is used as a detection method, ideally an internal standard should co-elute with the differences between analyte and internal standard being so minor that separation is impossible. Therefore, stable isotope labels have been recommended for internal standardization [165]. As they were not accessible for vancomycin, teicoplanin was used.
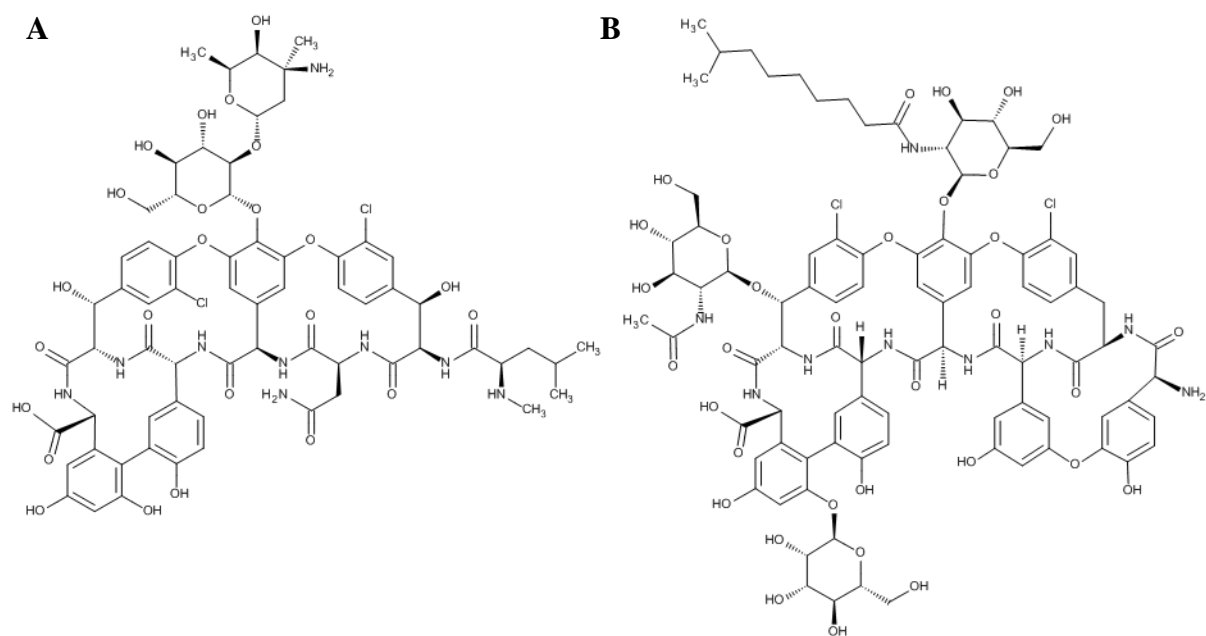
Figure 63. The molecular structure of (A) the analyte vancomycin (M=1449.25 g/mol) and (B) the internal standard teicoplanin A2-2 (M=1879.66 g/mol).

Table 49 Instrumentation and chromatographic conditions of the assay.

Parameter	Description
Mobile Phase	A: Water, 5 mM ammonium acetate, 0.1% formic acid B: Methanol, 5 mM ammonium acetate, 0.1% formic acid
	Step **Total Time (min)** **Flow Rate (μL/min)** **A (%)** **B (%)** 0 0.00 200 95.0 5.0 1 0.80 200 5.0 95.0 2 4.00 200 5.0 95.0 3 4.10 200 95.0 5.0 4 6.00 200 95.0 5.0
UHPLC	Agilent 1290 Infinity Binary Pump, 1290 Infinity Sampler, 1290 Infinity Thermostat, 1290 Infinity Thermostated Column Compartment (Agilent, Mississauga, Ontario, Canada)
Column	Waters Acquity UPLC, BEH C-18, 1.7 μm, 2.1 x 100 mm (Waters Corp., Milford, MA, US)
Guard Column	Waters Acquity UPLC, BEH C-18 VanGuard, 1.7 μm, 2.1 x 5 mm (Waters Corp., Milford, MA, US)
Column Temperature	35 °C
Autosampler tray temperature	10 °C
Injection volume	5 μL
Needle flush port	8 s
Mass Spectrometer	AB Sciex QTrap® 5500 hybrid linear ion-trap triple quadrupole mass spectrometer equipped with a Turbo Spray source (AB Sciex, Concord, Ontario, Canada)
Source Type and Temperature	Turbo Spray, 450 °C
Ionization Mode	Positive Ionization
	Compound **Comment** **MRM transition** **DP (V)** **CE (V)** **CXE (V)** vancomycin analyte 725.5/144.2 146 21 24 teicoplanin internal standard 940.6/316.4 176 21 6
Diverter valve	0-2 min to waste, 2-6 min to mass spectrometer.

MRM: Multiple Reaction Monitoring, DP: Declustering Potential, CE: Collision Energy, CXE: Collision Cell Exit Potential.

4.2.5   Data Analysis

Total peak area counts and peak area ratios (peak area counts$_{Vancomycin}$ /peak area counts$_{IS}$) were

determined using the Analyst software version 1.5.2, and automatic integration mode, no

smoothing, no bunching and linear weighted least squares analysis (weighting factor of $1/x^2$)

through zero were performed. The signal to noise ratio (S/N) was determined for the LLOQ by

the software after defining the limits for S/N that should be included in the calculations. Accuracy was determined by replicate (n = 5) measurement of samples containing known amounts of the analyte at the LLOQ QL, QM, and QH. Accuracy was acceptable within ± 15% of the actual value and within ± 20% for the LLOQ and was calculated as the deviation of the mean from the true value. Precision was determined using the same QC samples that have been used for accuracy measurements (LLOQ, QL, QM, QH). Precision was acceptable if the RSD was less than 15% at all concentrations except for the LLOQ where the RSD was less than 20%. Precision and accuracy is reported as intra-day (n = 5) and inter-day (n = 15) precision and accuracy.

4.3   Results and Discussion

For assay validation, the lower limit of quantification (LLOQ) and upper limit of quantification (ULOQ) were determined, and the range of the assay was established as 0.1 to 40 µg/mL vancomycin. Vancomycin and teicoplanin eluted at 2.27 and 2.68 min, respectively (Figure 46). Accuracy and precision for the LLOQ was ≤ 20% relative standard deviation (RSD). Intra- and inter- day accuracy and precision at three different levels were determined over 3 days and were ≤ 15% RSD (Table 50). These accuracy and precision limits have been suggested for the validation of bioanalytical methods [166]. The S/N for the LLOQ at 0.1 µg/mL was determined by the analyst software to be > 5 using the signal between 2.18 and 2.45 minutes as vancomycin signal and from 2.5 to 3.1 minutes as noise (Figure 65). The range for noise in the chromatogram was selected in direct proximity of the signal where the chromatogram showed the highest noise. An average noise level was calculated by the software over the given range.

To determine accuracy and precision, calculations have been performed using two methods. The first set of calculations use the peak area counts of vancomycin (CPS) only and the second set of

154

calculations include the internal standard as peak area ratios (peak are ratio). Precision and accuracy were ≤15% RSD for all quality control samples (QL,QM,QH) and ≤ 20% RSD for the LLOQ regardless of including or excluding the internal standard (Table 50). However, RSDs for precision of all samples and the RSD for accuracy at the LLOQ are smaller when using the peak area counts of the analyte vancomycin alone (CPS), suggesting that teicoplanin adds variation to the assay. We chose teicoplanin as internal standard as it has been used successfully before [164] but we think that it is not the ideal compound and the assay could be improved with a different internal standard. To determine teicoplanin performance, the total peak area counts were observed using the same teicoplanin injection solution in different sample wells over time. After ~ 3 hours approximately at the 29th injection, the peak area counts for teicoplanin significantly decreased from an average of 475436.68 ± 18.98% (n = 28) to an average of 223497.9 ± 26.70% (n = 15) and the chromatogram showed several peaks after the main peak at 2.68 min. Teicoplanin is thus suboptimal for sample runs that are longer than 3 hours. Currently, the most closely related compound that has been used for vancomycin LCMS is vancomycin glycine, but it is not commercially available [165].

Table 50. Accuracy and precision of the vancomycin assay.
Calculation method 1 (CPS): Total peak area counts for vancomycin; Calculation method 2 (Ratio): Peak area ratio of analyte to internal standard.

	Calculated Concentration (µg/mL)			Accuracy (%)			Precision (%)		
Calculation Method	**Method 1 (CPS)**			**Method 1 (CPS)**			**Method 1 (CPS)**		
LLOQ Qualification 0.1 µg/mL (n=5)	0.1			3.88			5.99		
Sample Concentration	QL 0.3 µg/mL	QM 12 µg/mL	QH 32 µg/mL	QL	QM	QH	QL	QM	QH
Intra Day 1 (n=5)	0.27	12.06	28.63	9.88	7.05	10.53	6.05	8.38	5.55
Intra Day 2 (n=5)	0.33	12.76	30.81	8.52	6.34	4.68	5.00	2.87	4.57
Intra Day 3 (n=5)	0.30	12.45	33.37	5.07	3.73	4.28	7.40	1.13	2.50
Inter 3-Day (n=15)	0.30	12.42	30.94	7.82	5.71	6.50	6.15	4.12	4.21
Calculation Method	**Method 2 (Ratio)**			**Method 2 (Ratio)**			**Method 2 (Ratio)**		
LLOQ Qualification 0.1 µg/mL (n=5)	0.08			20.21			8.39		
Sample Concentration	QL 0.3 µg/mL	QM 12 µg/mL	QH 32 µg/mL	QL	QM	QH	QL	QM	QH
Intra Day 1 (n=5)	0.27	12.32	32.20	9.08	7.98	8.36	9.44	9.27	10.59
Intra Day 2 (n=5)	0.30	11.86	28.82	6.45	5.12	9.93	8.51	7.60	6.14
Intra Day 3 (n=5)	0.29	12.11	32.44	6.79	2.11	2.51	8.87	2.51	3.64
Inter 3-Day (n=15)	0.29	12.10	31.16	7.44	5.07	6.93	8.94	6.46	6.79
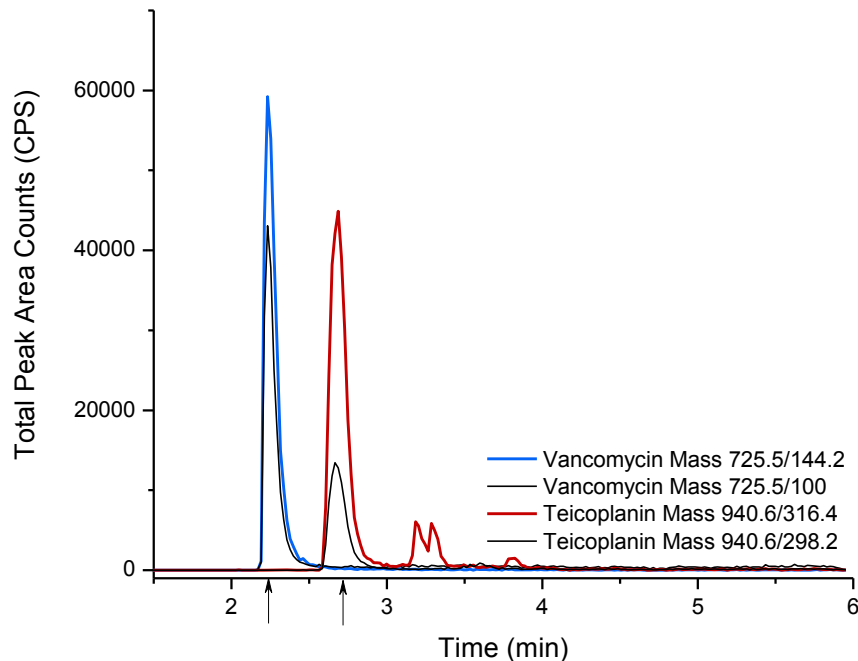
Figure 64. Chromatogram of vancomycin and teicoplanin.
Elution profile and retention times for vancomycin (5 µg/mL) and the internal standard teicoplanin (0.25 µg/mL).
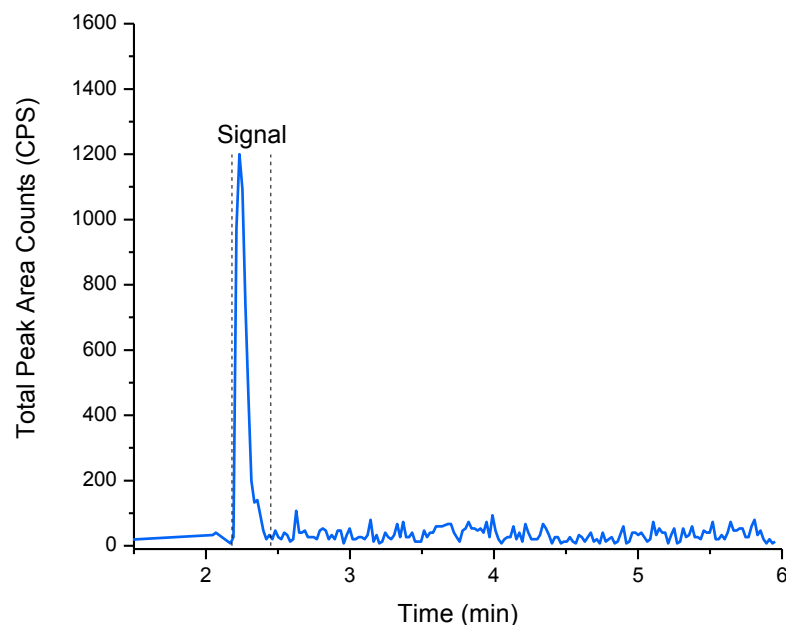
Figure 65. Signal and noise in a vancomycin chromatogram (Vancomycin Mass 725.5/144.2) at the lower limit of quantitation (LLOQ = 0.1 μg/mL).

Our assay was sensitive enough to quantify our *in vivo* data set of the steady-state study (Chapter 3.3.6) and was one of the most sensitive ones when compared to other published methods (Table 51). To compare assay performance with other published methods further, multiple criteria were chosen and a quality score (Q-Score) calculated. Sample volume, linear range, dilution steps, LLOQ and injection volume were selected as most appropriate criteria for the calculation of the quality-score (Q-Score) (**23**). The selected assays were similar to our assay and aimed to quantify at least vancomycin in serum or plasma and have been qualified or validated regarding accuracy and precision measurements over multiple days.

$$Q - Score = LLOQ_{measurement\ range}\ [ng/\mu L] \cdot sample\ volume\ [\mu L] \cdot injected\ volume\ [\mu L] \qquad (\ 23\ )$$

Table 51. Characteristics of selected liquid chromatography assays for the quantification of vancomycin in biological matrix (serum/plasma) using protein precipitation techniques.
Measurement ranges are concentrations after taking into account the dilution factor.

Reference	Method	Sample Vol. (µL)	Linear Range (µg/mL)	Dilution Factor	Measurement Range (ng/mL)	Injection Volume (µL)	Q-Score (µg·µL)
Zhang *et al.,* 2014 [167]	HPLC-MS/MS	50	0.05-50	66	0.76-757.58	10	**380**
Cao *et al.,* 2014 [161]	UHPLC-UV	200	1-100	1	1000-100000	5	**1000000**
Tsai *et al.,* 2013 [162]	UHPLC-MS/MS	100	0.5-100	26	19.23-3846.15	10	**19230**
Hagihara *et al.,* 2013 [163]	HPLC-UV	200	1-80	1	1000-80000	10-20*	**2000000**
Li *et al.,* 2014 [160]	2D-LC-UV	200	0.195–49.92	4	48.75-12480	200	**1950000**
Cheng *et al.,* 2010 [168]	HPLC-MS/MS	50	0.001-5	5	0.2-1000	10	**100**
König *et al.,* 2013 [165]	HPLC-MS/MS	75	1.06-84.4	6	176.6-14066.67	20	**264900**
Cazorla-Reyes *et al.,* 2014 [169]	UHPLC-MS/MS	1000	0.4-5	8	50-625	5	**250000**
Our assay	UHPLC-MS/MS	2	0.1-40	12.2	8.2-3281.38	5	**82**

*estimated

The Q-Score of our assay is the lowest and therefore correlates with a superior method based on an equal weight of the three criteria sample and injection volume and lower limit of the measurement range. This makes our assay highly useful in a research setting where only small volumes of biological samples can be obtained repeatedly. It also reduces the impact on experimental animals and the environment, and minimizes the overall direct cost (e.g., solvents) and the indirect cost (e.g., column life).

4.4   Conclusion

Our sensitive and selective UHPLC-MS/MS assay is novel, because it uses only 2 µL of rabbit serum sample, which is $25 \times$ less than the lowest sample volume reported in the literature. Despite these minimal sample volumes, our method was validated for vancomycin concentrations between 0.1 and 40 µg/mL which are clinically relevant.

Sample workup was simple and employed a single protein precipitation step with methanol that also contained the internal standard teicoplanin. Although accuracy and precision results are acceptable using teicoplanin, some variability and stability issues were observed and a different internal standard might be beneficial and recommended.

The total assay volume is $\sim$ 20 µL and uses an injection volume of 5 µL onto the column. The mobile phase is water and methanol [165, 169, 170] both containing 5 mM ammonium acetate and 0.1% formic acid. Most published LC methods use the more expensive acetonitrile [160-164, 168, 171-173] as mobile phase, probably due to its generally superior performance when using UV detection below 250 nm, lower column pressure and higher elution strength. However, in our case methanol was used as it provided better chromatographic performance and increased sensitivity.

Our technique shows that quantification of drugs is possible with good accuracy and precision for small biological samples of 2 µL. This is especially useful in preclinical research using small animals or for the discovery of novel minimally invasive extraction methods (e.g., microneedles, microfluidic devices) and other cases where the available biological sample size is limited.

Chapter 5: Tacrolimus Adsorption to Polymeric Membranes

Tacrolimus was not detected in ISF during our single dose study and it was not possible to determine whether the drug was truly not present in ISF or if it was merely retained by the membrane material that was used for extraction (polyacrylonitrile (PAN), 30 kDa). It has been reported previously in this work (Table 6) that only 3.4% of tacrolimus permeated the PAN membrane under the chosen *in vitro* experimental conditions (e.g., tacrolimus dissolved in PBS 7.4). Due to the drug's important role in the clinic as an immunosuppressant for liver, kidney and heart transplant patients and its warranted life-long administration, it appeared relevant to study tacrolimus solubility and possible membrane adsorption further in this chapter.

5.1   Background: Tacrolimus Solubility and Adsorption

Drugs that show low solubility in aqueous solutions are always problematic in pharmaceutical research, because a drug has to be dissolved to interact with its target.

Tacrolimus is a class II drug in the biopharmaceutical classification system, which means it shows low solubility but a high permeability of biological membranes [174]. Patients that receive the same dose of tacrolimus, can achieve very different concentrations in blood partly due to solubility issues and partly due to genetically determined inter-patient variability. The commercially available tacrolimus solution of 5 mg/mL in ethanol and castor oil (Prograf®) has to be diluted to 2-50 µg/mL in sodium chloride or dextrose solution prior to intravenous administration as recommended in its package insert. However, due to the poor solubility of tacrolimus in water (4-12 µg/mL [174]) precipitation may occur. Not only precipitation can introduce error in dosing but also the adsorption of tacrolimus to infusion bags, tubing or storage containers.

Drug adsorption is generally a problem and many studies therefore aim to determine adsorption and stability after a drug formulation is prepared [175, 176]. Adsorption of a drug molecule to a filter, container or tubing material will occur likely through intermolecular forces, most notably dipole-dipole interactions and van der Waals forces and the solvent and therefore type of dispersion that is tested (suspension, colloid or solution) plays a very important role. If the interaction of solvent molecules with tacrolimus is high, a smaller number will interact with the surface of storage container or membrane. If the solvent interacts less with tacrolimus, the drug can preferably adsorb to surfaces or precipitate. It has been reported that tacrolimus can adsorb to polyvinylchloride [177] which is the standard polymer for intravenous tubing in the hospital. Tacrolimus thus has to be administered via non-PVC tubing or orally. In a different study, tacrolimus was not found to adsorb to storage containers of polyvinylchloride, glass, or polyolefines [178] in significant quantities. However, results can vary depending on the tacrolimus concentration, solvent and volumes used in the study. Studies on tacrolimus adsorption are often performed at high concentrations, where involved adsorption surfaces can be possibly saturated by the drug and a total decrease in concentration appears negligible. In therapeutically relevant concentrations in the low ng/mL range, surface saturation could result in a significant decrease in concentration and will be much more noticeable and therapeutically unsafe. It is further known that tacrolimus readily binds to red blood cells and serum proteins. Once administered intravenously, it circulates bound to proteins and erythrocytes so the standard matrix to quantify tacrolimus is EDTA whole blood. It is a crucial step to treat EDTA blood samples with a methanol/zinc sulfate mixture to release the bound tacrolimus and dissolve it in methanol before quantification.

161

The aim of this chapter is to test how the matrix and solvent affects adsorption or solubility of tacrolimus in therapeutic concentrations. We therefore tested three different solvents/matrices: methanol, water, and an aqueous protein solution (serum) and quantified tacrolimus before and after passing through different filter membranes (Table 52) including the previously used PAN (see chapter 2.3.1). PAN is used for many ultrafiltration devices and resembles PVC (Figure 66), to which drug adsorption has been reported for tacrolimus (see above). While PVC contains a halogen ion (chloride), PAN contains a pseudo-halogenide (cyanide) so choosing structurally very different polymers can change drug adsorption and will be studied here.
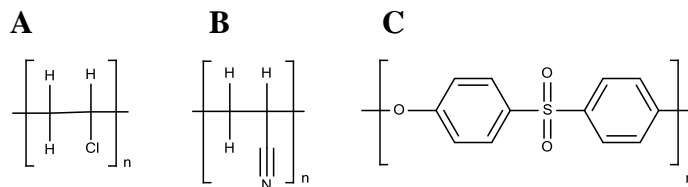
Figure 66. A: Polyvinylchloride (PVC), B: polyacrylonitrile (PAN), C: polyethersulfone (PES).

5.2 Materials and Methods

5.2.1 Tacrolimus Solutions for Membrane Filtration

A commercially available tacrolimus solution of 5 mg/mL (Prograf®) was diluted to 0.1 mg/mL to 0.01 mg/mL and to 1 µg/mL (Stock T) in a water/methanol mixture (50% V/V). There are two reasons for the use of methanol in this *in vitro* experiment: first, it is a very good solvent for tacrolimus (like ethanol which is used in Prograf®) and therefore guaranteed that tacrolimus was in solution. Second, methanol is also used as a mobile phase for later LCMS quantification and the chromatographic separation and peak shape are best if the sample is dissolved in the mobile phase.

The prepared Stock T solution was further diluted to 4 ng/mL using three different matrices:

a) 25 mL of 50% V/V water/methanol (WM): 100 μL of Stock T in 25 mL WM (T_{WM})

b) 25 mL of deionized water (W): 100 μL of Stock T in 25mL W (T_W)

c) 12.5 mL drug-free rabbit serum (S): 50 μL of Stock T in 12.50 mL S (T_S)

The concentration of the drug solutions was determined before extraction (T_{W0}, T_{WM0}, T_{S0}).

The three tacrolimus solutions were used to perform the extraction experiments on 12 commercially available syringe filters and capillary filter membranes (Table 52). All tacrolimus solutions (T_W, T_{WM}, T_S) were tested on separate syringe filters, whereas capillary filter membranes were reused after washing with copious amounts of water, drying and rehydrating. Filter capillaries were closed on one side with a drop of epoxy glue and mounted on hypodermic needles for testing. Three extractions of 100 μL were performed for each filter, and each tacrolimus solution was analyzed for tacrolimus content (T_{W1}, T_{WM1}, T_{S1}) and compared to the tacrolimus content before extraction (T_{W0}, T_{WM0}, T_{S0}). The percent of tacrolimus that passed the membrane was calculated for each membrane and solvent using Equation **24**.

$$\%Pass = \frac{T_1}{T_0} \cdot 100 \qquad\qquad (\ 24\ )$$

Table 52. Commercially available filter membranes tested in the tacrolimus permeability study.

Filter Material	Manufacturer	Filter Type	Pore Size	Exposure to Methanol	Chemical Structure
Polyvinylidene fluoride (PVDF)	Millipore	Syringe filter	0.45 μm	Recommended	
	Pall	Syringe filter	0.2 μm		
Polytetrafluorethylene (PTFE)	Pall	Syringe filter	0.2 μm	Recommended	
	Cronus	Syringe filter	0.45 μm		
Polyacrylonitrile (PAN)	BASi	Capillary membrane	30 kDa	Limited exposure	
Polyethersulfone (PES) modified	Millipore	Syringe filter	0.22 μm	Recommended	
	Pall	Syringe filter	0.2 μm	Recommended	
	Spectrum Labs	Capillary membrane	0.2 μm	Limited exposure	
	Spectrum Labs	Capillary membrane	30 kDa	Limited exposure	
Polypropylene, hydrophilic (GHP)	Pall	Syringe filter	0.2 μm	Recommended	
Nylon	Pall	Syringe filter	0.2 μm	Recommended	
Mixed cellulose esters (ME)	Spectrum Labs	Capillary membrane	0.2 μm	Limited exposure	Cellulose

5.2.2   Tacrolimus Quantification

Tacrolimus was quantified using liquid chromatography mass spectrometry. The system

parameters and mobile phase were the same as used previously for vancomycin analysis. The

assay procedure can be used for the quantification of vancomycin and tacrolimus simultaneously.

Ascomycin was used as the internal standard. Eight tacrolimus calibration standards between 0

and 50 ng/mL were run together with the sample batches (Table 55 and 56). Peak area ratios

(peak area counts$_{Tacrolimus}$ /peak area counts$_{Ascomycin}$) for the calibrators and the samples were

determined using the Analyst software version 1.5.2 with automatic integration mode, no

smoothing, and no bunching. Linear weighted least squares analysis (weighting factor of $1/x^2$)

with slope and intercept was performed to calculate the concentrations in the samples.

5.2.2.1 Chromatographic Conditions

The instrument and chromatographic conditions are summarized in Table 53 and Table 54.

The sample tray was maintained at 10 °C and 7 µL of sample was injected onto the column. To

minimize carry-over between samples, the needle was rinsed with a wash solvent of 50%

methanol/water (v/v) between injections. The first 2 minutes of the chromatographic run were

diverted to waste to prevent water soluble biological matrix components to enter the mass

spectrometer, and data collection started at 2 to 6 min. Tacrolimus and ascomycin co-eluted at

3.29 min (Figure 67 and 68) due to their almost identical structure (Figure 69).

Table 53. Instrumentation and chromatographic conditions for the tacrolimus analysis.

Parameter	Description
Mobile Phase	A: Water, 5 mM ammonium acetate, 0.1% formic acid B: Methanol, 5 mM ammonium acetate, 0.1% formic acid
	<table><tr><td>Step</td><td>Total Time (min)</td><td>Flow Rate (µL/min)</td><td>A (%)</td><td>B (%)</td></tr><tr><td>0</td><td>0.00</td><td>200</td><td>95.0</td><td>5.0</td></tr><tr><td>1</td><td>0.80</td><td>200</td><td>5.0</td><td>95.0</td></tr><tr><td>2</td><td>4.00</td><td>200</td><td>5.0</td><td>95.0</td></tr><tr><td>3</td><td>4.10</td><td>200</td><td>95.0</td><td>5.0</td></tr><tr><td>4</td><td>6.00</td><td>200</td><td>95.0</td><td>5.0</td></tr></table>
UHPLC	Agilent 1290 Infinity Binary Pump, 1290 Infinity Sampler, 1290 Infinity Thermostat, 1290 Infinity Thermostatted Column Compartment (Agilent, Mississauga, Ontario, Canada)
Column	Waters Acquity UPLC, BEH C-18, 1.7 µm, 2.1 x 100 mm (Waters Corp., Milford, MA, US)
Guard Column	Waters Acquity UPLC, BEH C-18 VanGuard, 1.7 µm, 2.1 x 5 mm (Waters Corp., Milford, MA, US)
Column Temperature	35 °C
Autosampler tray temperature	10 °C
Injection volume	7 µL
Needle flush port	8 s
Mass Spectrometer	AB Sciex QTrap® 5500 hybrid linear ion-trap triple quadrupole mass spectrometer equipped with a Turbo Spray source (AB Sciex, Concord, Ontario, Canada)

Parameter	Description
Source Type and Temperature	Turbo Spray, 450 °C
Ionization Mode	Positive Ionization
Diverter valve	0-2 min to waste, 2-6 min to mass spectrometer

Table 54. Mass and assay range for tacrolimus and its internal standard ascomycin**.**

Compound	Comment	Concentration Range Tested	Q1 Mass (Da)	Q3 Mass (Da)	DP (V)	CE (V)	CXE (V)
Tacrolimus	Analyte	0.1- 20 ng/mL for T_W and T_{WM} 0.5- 50 ng/mL for T_S	821.5	768.7	46	29	4
Ascomycin	Internal Standard	250 ng/mL for T_W and T_{WM} 1.5 ng/mL for T_S	809.5	756.5	106	29	10

MRM: Multiple Reaction Monitoring, DP: Declustering Potential, CE: Collision Energy, CXE: Collision Cell Exit Potential.
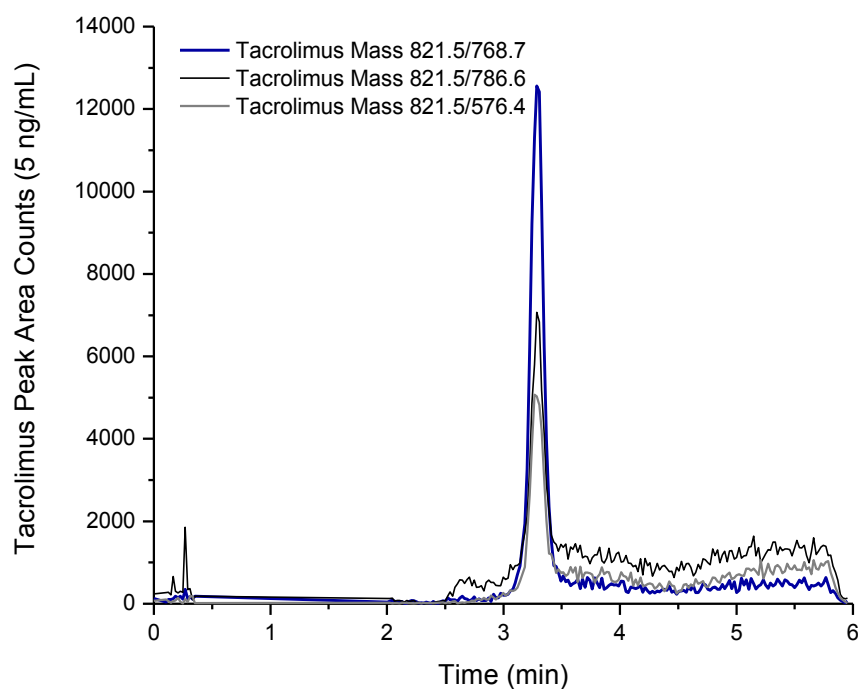
Figure 67. Sample chromatogram for tacrolimus at 5 ng/mL in a 50% water/methanol mixture; blue: mass used for quantification, black and grey: additional mass fragments not used for quantification;

166
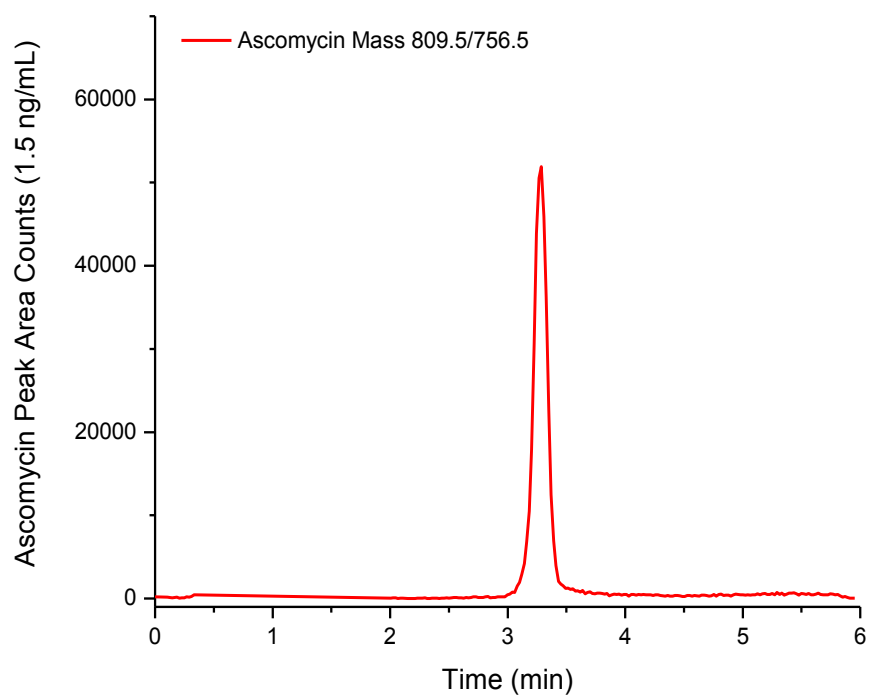
Figure 68. Sample chromatogram for the internal standard ascomycin at a concentration of 1.5 ng/mL in a 50% water/methanol mixture.

A   B
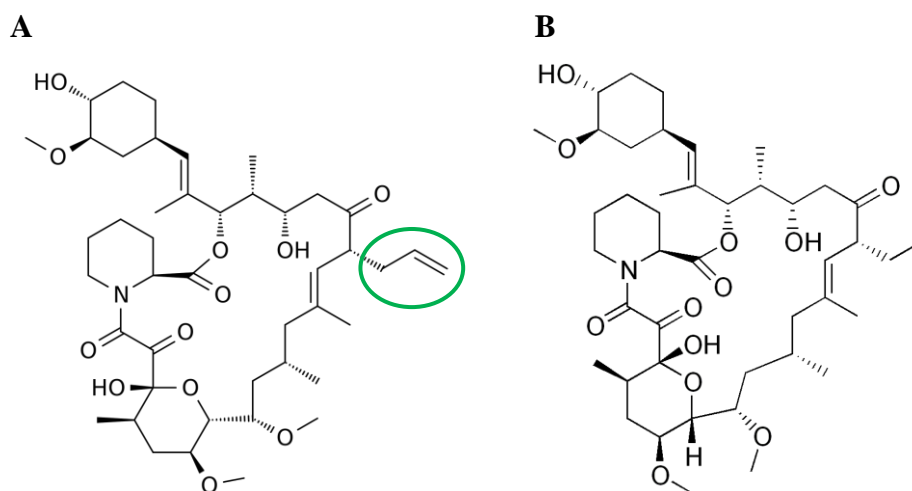
Figure 69. The molecular structure of (A) the analyte tacrolimus (M=804.02 g/mol) and
(B) the internal standard ascomycin (M=792.01 g/mol).
Marked in green is the alkene moiety that is the only difference between the molecules.

5.2.2.2   Preparation of the Calibrators

Stock T (Tacrolimus 1 µg/mL) was diluted to 100 ng/mL (Stock T2) in WM. Two calibration

curves were prepared: one for T_W and T_{WM} samples and one for T_S samples (Figure 70 and 71).

Calibration standards for T_W and T_{WM} samples were prepared with Stock T2 in WM according to

Table 55. Serum calibrators for T_S samples were prepared using drug-free rabbit serum spiked

with Stock T or Stock T2 according to Table 56.

Table 55. Preparation of calibration standards for tacrolimus samples in water (T_w) and tacrolimus samples in water/methanol (T_{WM}).

Concentration (ng/mL)	0	0.1	0.2	0.5	1	5	10	20
Stock T2 (µL)	0	1	2	5	10	50	100	200
WM (µL)	1000	999	998	995	990	950	900	800

Table 56. Preparation of calibration standards for tacrolimus samples in serum (T_S).

Concentration (ng/mL)	0	0.5	1	2.5	5	10	25	50
Stock T (µL)	0	0	0	0	5	10	25	50
Stock T2 (µL)	0	5	10	25	0	0	0	0
WM (µL)	1000	995	990	975	995	990	975	950

5.2.2.3   Preparation of the Internal Standard

Ascomycin (95%, Alfa Aesar, Ward Hill, MA, US) was used as the internal standard. The

concentration of the internal standard should be chosen so that the peak area ratios of

analyte/internal standard are between 0.01 and 10 between the lowest and highest calibration

standard. A stock solution of 0.102 mg/mL was prepared and further diluted to 0.5 µg/mL

(internal standard Stock A) in WM (75 µL Stock A in 15 mL WM). For T_W and T_{WM} samples

Stock A was used directly and for T_S Samples, internal standard Stock A was diluted to 1.8

ng/mL (internal standard Stock A2) in methanol (M) (36 µL in 10 mL M). Using the Stock A

directly for T_W and T_{WM} samples resulted in an internal standard concentration of 250 ng/mL in the injected sample. For the T_S samples, the internal standard concentration resulted in a concentration of 1.5 ng/mL in the injected sample.

5.2.2.4   Preparation of Samples for LCMS Injection

Calibration standard samples and extraction samples were prepared according to Table 57. The same calibration curve was used for T_W and T_{WM} and a different calibration curve was prepared for T_S samples due to the different matrix serum. T_W samples involve an extra dilution step and will result in 50% lower concentration (2 ng/mL) compared to the T_{WM} samples of 4 ng/mL. This is due to the extraction sample being originally in water, but in a water/methanol mixture when measured in the LCMS. T_S samples use a precipitation procedure and only the supernatants will be injected into the LCMS (see Table 57).

Table 57. Sample preparation for LCMS injection.
Extraction sample and calibrator preparation in water/methanol, water and serum.

Sample Type	Extraction Sample			Calibrator Standard		
	T_{WM}	T_W	T_S	T_{WM}	T_W	T_S
Extraction sample/Calibrator (μL)	100	50	10	100		10
Methanol (μL)	-	50	-	-		-
Internal standard - Stock A (μL)	100	100	-	100		-
Internal standard - Stock A2 (μL)	-	-	50	-		50

5.2.3   Protein Measurement

The protein content of T_S samples before and after extraction were measured to determine if a decrease in tacrolimus concentration correlates with a decrease in protein concentration after passing a membrane. The protein content of serum was measured at 280 nm using a small volume spectrophotometer (NanoDrop 2000). The measurement range for protein measurements at 280 nm is 0.1- 400 mg/mL with a typical reproducibility of 2% CV. The absorbance of a 1%

solution of bovine serum albumin ($A_{280\,nm}^{1\%}(BSA) = 6.7\ \frac{1}{\frac{g}{100\,mL}\cdot cm}$) was used as a reference to

determine protein concentration in mg/mL. This method can only determine a total decrease in

protein content and not distinguish between different proteins as it only measures absorbance at

280 nm, a wavelength at which all proteins that contain tyrosine or tryptophan residues or

cysteine disulfide bonds absorb ultraviolet light.

5.3   Results and Discussion

5.3.1   Calibration Curves

To quantify the concentration of tacrolimus in the membrane extracts, 8 calibrators were

submitted with the sample batch for the matrix methanol/water and water (Figure 70) and 8

calibrators were submitted together with the sample batch that used serum as a matrix (Figure

71). The range for the calibration curves was 0.1-20 ng/mL in 50% water/methanol and

0.5-50 ng/mL in serum. Error bars for the calibration curve are expected relative errors in % and

are based on a previously validated assay for vancomycin that uses the same chromatographic

conditions (Chapter 4.3) and the variability limits for bioanalytical method validation [166]. For

the lowest concentration 20% CV was plotted and for all other concentrations 15% CV.
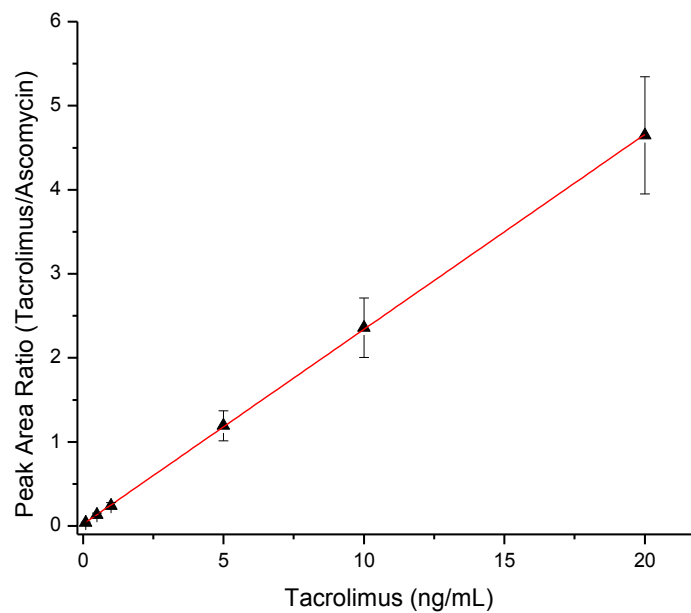
Figure 70. Calibration curve of tacrolimus in 50% water/methanol, error bars are expected relative errors in %, the peak area ratio was multiplied by 166 to account for the different concentrations of internal standard used (1.5 ng/mL for serum calibration, 250 ng/mL for water/methanol calibration).
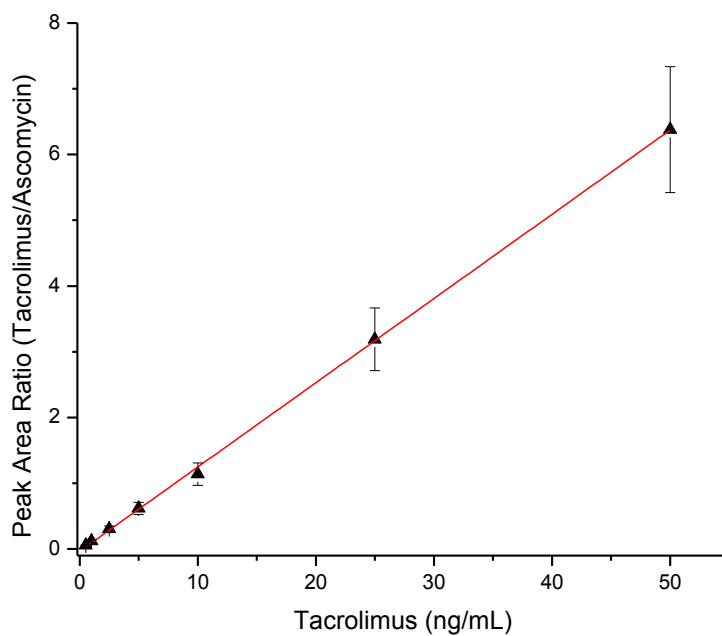
Figure 71. Calibration curve for tacrolimus in serum, error bars are expected relative errors in %.

5.3.2 Tacrolimus Concentrations Before and After Membrane Filtration

The goal of this study is to assess the adsorption of tacrolimus to different polymeric membranes in aqueous media, an organic/aqueous solvent mixture and serum.

Tacrolimus concentration of T_{WM0}, T_{W0}, and T_{S0} before extraction were 4.05 ng/mL, 0.484 ng/mL and 4.25 ng/mL, respectively and T_{WM1} and T_{S1} after extraction are shown in Figure 72 and 73. All membrane materials show high recovery rates (% Pass) and no adsorption of tacrolimus when using 50% water/methanol (T_{WM1}) except for PAN 30 kDa, which shows less than 50% pass (Figure 72). In contrast, all membrane materials showed a decrease in tacrolimus concentration (% Pass) when dissolved in serum (T_{S1}) (Figure 73). When using serum as the matrix, a 30 kDa and a 100 kDa centrifugal filter was used as control. These two filters are protein restricting and should show a large decrease in protein and tacrolimus, if tacrolimus is bound to them. This was indeed detected and no tacrolimus or very low concentrations of tacrolimus were present when all protein or most protein was removed (30 kDa *vs.* 100 kDa). Using water as matrix, there was no clear peak for tacrolimus in the chromatogram and the calculated concentration was lower than the lowest calibration standard (< 0.1 ng/mL). These data are therefore considered unusable and not shown.
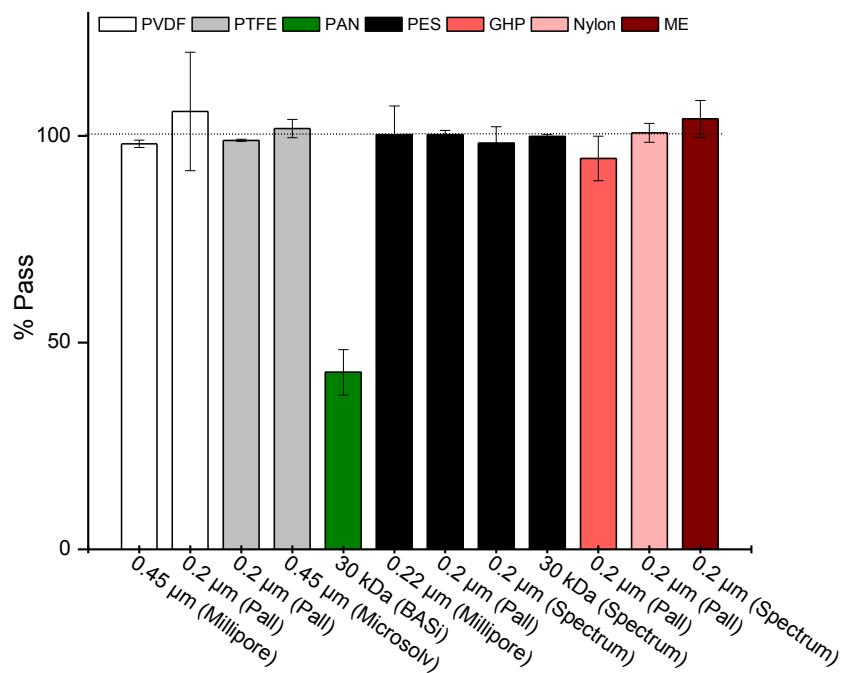
Figure 72. Tacrolimus recovery rates (% Pass) for all tested membranes using water/methanol as the matrix (T_{WM1}).
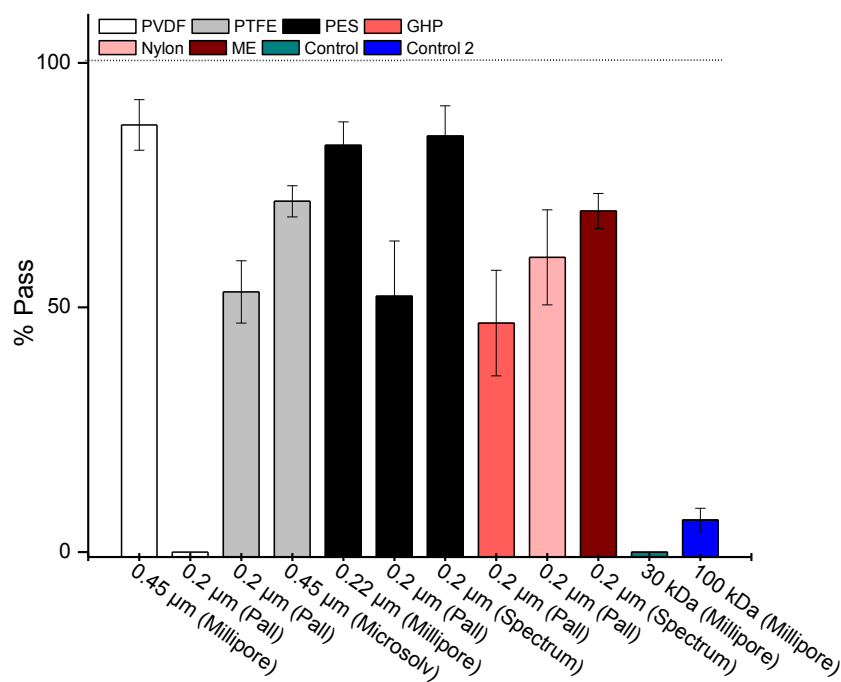
Figure 73. Tacrolimus recovery rates (% Pass) for all tested membranes using serum as the matrix (T_{S1}).

173

5.3.3   Protein Recovery

Serum protein concentration of all samples before and after passing the membrane material were unchanged (% Pass = 100%) except for the 30 kDa and 100 kDa centrifugal filters, that showed a large decrease (Figure 74). It was expected that a 30 kDa filter removes all proteins and a 100 kDa filter removes most proteins as the most abundant protein found in serum is albumin with a molecular weight of ~ 60 kDa. Tacrolimus adsorption is therefore not strictly due to a removal of protein but is a mix of real adsorption to membrane material and protein bound tacrolimus removal. It could also be possible that the minimal change of protein content (removed protein that had tacrolimus bound) was not detectable with the chosen protein assay, whereas the tacrolimus assay is more sensitive and can easily detect changes of tacrolimus. This supposition is confirmed by comparing the 30 kDa and 100 kDa centrifugal filter results. Both the tacrolimus pass and the serum protein pass are the same.

Using protein restricting filters (here: the control filters of 30 and 100 kDa), the results are clear and a reduction of tacrolimus correlates very well with a reduction in protein (Table 58).
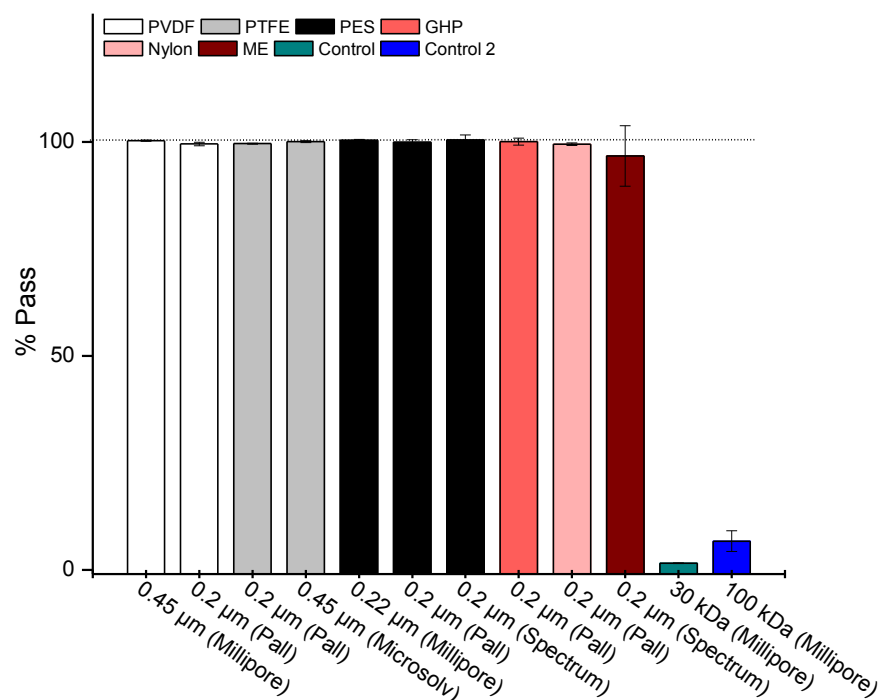
Figure 74. Protein recovery rates (% Pass) for all tested membranes using serum as the matrix (T_{S1}).

Table 58. Comparison of % Pass Protein and % Pass Drug for two selected filters (protein restricting)

Pore Size (Millipore centrifugal filter)	% Pass Protein	% Pass Tacrolimus
30 kDa	1.54± 0.07	0
100 kDa	6.68± 2.42	6.56±2.40

5.4 Conclusion

Tacrolimus is well dissolved in water/methanol mixtures but did not dissolve in water at the

tested concentrations of 4 ng/mL. However, tacrolimus solubility is reported in the literature to

be 4-12 µg/mL [174] in water and intravenously administered tacrolimus solutions are

recommended to be diluted to 4-100 µg/mL in sodium chloride or dextrose solution.

In the experiment performed here, tacrolimus was undetectable when dissolved in aqueous

solution. This could mean when used for intravenous infusion, the concentration of tacrolimus

175

reaching the patient could be lower than expected if some of the tacrolimus precipitated.

Interestingly, when serum was used as a "solvent" for tacrolimus, the protein (albumin) served as a carrier for tacrolimus, and tacrolimus concentrations detected in T_{S0} were as high as T_{WM0}. Although protein concentration did not decrease after passing the different membrane materials, the total detected tacrolimus (% Pass) for the T_{S1} samples was significantly decreased. It was expected that if protein serves as a carrier that the concentrations of tacrolimus are not significantly decreased. However, this decrease may be explained by the difference in sensitivities of the tacrolimus and protein assays. The tacrolimus assay used is a highly sensitive LCMS method and slight differences in drug concentrations can be measured, whereas the spectrophotometric protein assay is inherently less sensitive and slight changes in protein might be undetected. This supposition was confirmed by using a higher molecular weight protein restricting filter (30 kDa and 100 kDa centrifugal filters) where the decrease of drug correlated well with a decrease in protein.

To summarize, tacrolimus needs a carrier in the form of a good solvent or protein to pass membranes materials *in vitro*. In the absence of carriers such as protein, RBC or organic solvent, tacrolimus can possibly form small precipitates leading to lower tacrolimus concentrations in solution.

Relating these findings back to our ISF study, we believe that tacrolimus was not detected in ISF due to several reasons. The ultrafiltration filter membrane (PAN) does definitely retain tacrolimus even if tacrolimus is dissolved in a good solvent (water/methanol) as seen in Figure 72. Tacrolimus is available in ISF but bound to carrier proteins. Unfortunately, the used 30 kDa ultrafiltration probe excluded proteins. We believe that tacrolimus can likely be extracted from

ISF but larger pore sizes of the filtration membrane are required (0.2 to 0.45 µm). The best

materials for tacrolimus extraction are PVDF and PES (seen in Figure 73).

Chapter 6: Conclusion

Our current studies aimed to support the continuing research of the peripheral interstitial fluid (ISF) compartment for therapeutic drug monitoring (TDM). Through the knowledge of the extravascular distribution of drugs and their PK, we can encourage the development of minimally invasive ISF sampling devices with on board drug analysis for TDM. Currently, ISF is neglected by researchers for TDM and its PK parameters are understudied. The only application that has been thoroughly investigated for many years is the determination of glucose concentrations in ISF [179]. Our research focuses on the potential advantages of ISF for drug quantification and TDM.

6.1 Hypotheses and Objectives of the Thesis, Overall Significance and Contribution of the Thesis Research

The hypothesis of this work was that ISF is a valuable sampling matrix for TDM. Based on our data, we can fully support this hypothesis based on research results obtained through investigating three objectives.

The first objective was to determine a method of accessing interstitial fluid reliably to study ISF concentrations. For our studies, we have used ultrafiltration to achieve the objective but furthermore we have also explored newer directions. We encountered some difficulties to achieve a reliable and minimally invasive technique for the sampling of ISF but the knowledge gained on mechanical skin properties and liquid distribution in skin is valuable and encouraging for the future development of minimally invasive ISF sampling tools. Through our studies of ISF sampling tools we have also explored new membrane materials for future drug extraction using

microfiltration and found that drug adsorption of tacrolimus to these membrane materials depend on the solvent used.

The second objective was to determine the PK of therapeutically monitored drugs in ISF and to compare them to blood levels. This has been achieved through collecting a rigorous data set in a rabbit model, non-compartmental analysis and compartmental modeling. Compartmental modeling can predict free drug concentrations in ISF tissue. Monitoring of drug levels in ISF is possible and has advantages over blood sampling, at least for some of the studied drugs. The drug target is often at least one compartment away from the blood circulation and blood concentrations are therefore not sufficient to describe what is happening in the body. Furthermore, ISF contains less protein and cellular matter than blood and therefore requires less sample preparation.

The third objective aimed to develop a quantification method for the sample drug vancomycin in microvolumes of biological sample. Considering that most clinical assays use hundreds of microliters, this objective has successfully been completed using only 2 μL of biological sample.

6.2   Strengths and Limitations of the Thesis Research

The quantification of drug in ISF for such a large panel of drugs is new. The concentrations of drugs in ISF are largely unknown and our study can serve as a starting point for further efforts to improve TDM.

Our ISF studies employed reasonably large data sets and covered a wide variety of drugs. The more than 64 data points taken for each drug are adequate to do compartmental modeling and describe the concentration time course both in blood and ISF. The strength of our compartmental modeling is based on two data sets taken simultaneously from two different compartments. The intention here was not to derive any dosing or sampling schedules for future TDM but to connect

179

drug concentrations measured in blood and ISF compartments. The employed compartmental models were able to relate ISF and blood and strongly support future TDM in ISF.

The applied compartmental analysis, however, was rather basic and more advanced modeling might be advantageous. For example, random effects could be included in the model and might improve its predictive value. This would be especially useful in future clinical human studies, but requires larger data sets. Our study subjects here were rabbits not humans. Studies in humans would necessitate the need for a non-invasive and reliable ISF sampling technique. Painless and bleeding-free microneedles, and arrays thereof, are such sampling techniques currently under development [87, 89, 92, 180]. Since the liquid-trapping volumes of a microneedle are minimal, it would then also require a quantification method that is possible in minimal volumes. Current clinical assays are meant for blood, and would have to be adjusted not only for the different matrix, but also for the potentially different target concentrations of the drugs. Under those conditions, potentially new, convenient, rapid and significant point of care devices for TDM assays might be developed.

6.3 Potential Applications of the Research Findings

Potential applications of our research findings are clearly related to TDM, drug resistance and drug toxicities.

Regarding TDM, all drugs that have a therapeutic target outside of the blood vessels could be monitored in ISF as long as their concentration is high enough for detection. The first drugs that come in mind are anti-infective drugs, which have been discussed in a recent review [181] and anti-cancer drugs. However, there are possibly many more applications that could profit from ISF monitoring such as diseases that are treated with antivirals, biologics and cytokines.

Furthermore, the use of ISF could improve knowledge in the field of drug toxicity and resistance. In these regards, ISF drug concentrations are much less researched than blood concentrations even though valuable information could be drawn from them. For example, drug accumulation in the ISF might point to increased toxicities, even if the drug concentration in blood is low or cleared. Drug accumulation in the ISF might also point to possible resistance, as drug likely accumulates in the tissue if resistance mechanisms prevent the drug from accumulating inside the target cells.

One still to be proven hypothesis thus might be that the therapeutic outcome and the prevention of resistance are better monitored in ISF than in blood.

6.4   Future Research Directions

Future research should focus on the development of point of care devices for sampling and analyzing ISF. If drug concentrations are detected with an ISF-based point of care device then currently used clinical assays for drug quantification that are often expensive might not be needed anymore. This would make therapeutic drug monitoring incredibly easy and affordable. Our studies support ISF-based sampling and PK modeling and are a first step towards its potential implication in health care.

References

[1] Animal resources centre: Guide to the care and use of experimental animals, Canadian Council on Animal Care, University of Saskatchewan, 1993, pp. 1-298.

[2] D.W. Duhme, D.J. Greenblatt, J.A.N. Koch-Weser, Reduction of digoxin toxicity associated with measurement of serum levels: A report from the boston collaborative drug surveillance program, Ann. Intern. Med. 80 (1974) 516-519.

[3] A.L. Robles-Piedras, Therapeutic drug monitoring of vancomycin, Proc. West. Pharmacol. Soc. 52 (2009) 21-33.

[4] Z.-K. Ye, H.-L. Tang, S.-D. Zhai, Benefits of therapeutic drug monitoring of vancomycin: A systematic review and meta-analysis, PLoS ONE 8 (2013) e77169.

[5] B.D. Kahan, P. Keown, G.A. Levy, A. Johnston, Therapeutic drug monitoring of immunosuppressant drugs in clinical practice, Clin. Ther. 24 (2002) 330-350.

[6] P. Langers, Monitoring immunosuppression after liver transplantation; development of individualized bayesian limited sampling monitoring (Doctoral Thesis), Leiden University (2012).

[7] L.S. Ting, E. Villeneuve, M.H. Ensom, Beyond cyclosporine: A systematic review of limited sampling strategies for other immunosuppressants, Ther. Drug. Monit. 28 (2006) 419-430.

[8] J. Haymond, M.H. Ensom, Does valproic acid warrant therapeutic drug monitoring in bipolar affective disorder?, Ther. Drug. Monit. 32 (2010) 19-29.

[9] K.J. DeVore, R.A. Hobbs, Plasma digoxin concentration fluctuations associated with timing of plasma sampling and amiodarone administration, Pharmacother. 27 (2007) 472-475.

[10] N.C. Touw D. J., Thomson A. H., Vinks A. A., Cost-effectiveness of therapeutic drug monitoring a systematic review, Ther. Drug. Monit. 27 (2005) 10-17.

[11] P.A. Stewart, J.A. Kellum, P.W. Elbers, Body fluids, Stewart's textbook of acid-base, AcidBase.org Amsterdam, The Netherlands, 2009, pp. 501.

[12] D.G. Levitt, The pharmacikinetics of the interstitial space in humans, BMC Clin. Pharmacol. 3 (2003) 29.

[13] G. Hall John E., Arthur C. , Textbook of medical physiology, 11 ed., Elsevier Inc., Philadelphia, Pennsylvania, 2006.

[14] L.G. Gomella, S.A. Haist, Chapter 9: Fluids and electrolytes, Clinician's pocket reference, The McGraw-Hill Companies, New York, NY, 2007.

[15] K. Aukland, G. Nicolaysen, Interstitial fluid volume: Local regulatory mechanisms, Physiol. Rev. 61 (1981) 556-643.

[16] Thermo Fisher Scientific, Plasma and serum preparation, https://www.lifetechnologies.com/ca/en/home/references/protocols/cell-and-tissue-analysis/elisa-protocol/elisa-sample-preparation-protocols/plasma-and-serum-preparation.html, (accessed 15/10/5).

[17] K. Aukland, R.K. Reed, Interstitial-lymphatic mechanisms in the control of extracellular fluid volume, Physiol. Rev. 73 (1993) 1-78.

[18] J.R. Levick, C.C. Michel, Microvascular fluid exchange and the revised starling principle, Cardiovasc. Res. 87 (2010) 198-210.

[19] N. Fogh-Andersen, B.M. Altura, B.T. Altura, O. Siggaard-Andersen, Composition of interstitial fluid, Clin. Chem. 41 (1995) 1522-1525.

[20] T.E. Woodcock, T.M. Woodcock, Revised starling equation and the glycocalyx model of transvascular fluid exchange: An improved paradigm for prescribing intravenous fluid therapy, Br. J. Anaesth. 108 (2012) 384-394.

[21] J.R. Levick, Revision of the starling principle: New views of tissue fluid balance, J. Physiol. 557 (2004) 704.

[22] C.C. Michel, M.E. Phillips, Steady-state fluid filtration at different capillary pressures in perfused frog mesenteric capillaries, J. Physiol. 388 (1987) 421-435.

[23] T. Tammela, K. Alitalo, Lymphangiogenesis: Molecular mechanisms and future promise, Cell 140 (2010) 460-476.

[24] J. Titze, Interstitial fluid homeostasis and pressure: News from the black box, Kidney Int. 84 (2013) 869-871.

[25] L.M. Ebah, H. Wiig, I. Dawidowska, C. O'Toole, A. Summers, M. Nikam, A. Jayanti, B. Coupes, P. Brenchley, S. Mitra, Subcutaneous interstitial pressure and volume characteristics in renal impairment associated with edema, Kidney Int. 84 (2013) 980-988.

[26] R.K. Reed, K. Rubin, H. Wiig, S.A. Rodt, Blockade of beta 1-integrins in skin causes edema through lowering of interstitial fluid pressure, Circ. Res. 71 (1992) 978-983.

[27] A. Machnik, W. Neuhofer, J. Jantsch, A. Dahlmann, T. Tammela, K. Machura, J.-K. Park, F.-X. Beck, D.N. Muller, W. Derer, J. Goss, A. Ziomber, P. Dietsch, H. Wagner, N. van Rooijen, A. Kurtz, K.F. Hilgers, K. Alitalo, K.-U. Eckardt, F.C. Luft, D. Kerjaschki, J. Titze, Macrophages regulate salt-dependent volume and blood pressure by a vascular endothelial growth factor-c-dependent buffering mechanism, Nat. Med. 15 (2009) 545-552.

[28] R.R.R. Yuan S Y., Chapter 4: The endothelial barrier, Regulation of endothelial barrier function, Morgan&Claypool Life Sciences, San Rafael, CA, 2010.

[29] Y. Komarova, A.B. Malik, Regulation of endothelial permeability via paracellular and transcellular transport pathways, Annu. Rev. Physiol. 72 (2010) 463-493.

[30] S.-T. Hwang, Fundamentals of membrane transport, Korean J. Chem. Eng. 28 (2010) 1-15.

[31] D. Mehta, R.D. Minshall, A.B. Malik, Regulation of endothelial barrier function, in: J. Bhattacharya (Ed.) Cell signaling in vascular inflammation, Humana Press 2005, pp. 73-90.

[32] F.-R.E. Curry, Microvascular solute and water transport, Microcirculation 12 (2005) 17-31.

[33] G.J.G.N. Stevens Troy, Shasby D. Michael, Bhattacharya Jahar, Malik Asrar B. , Mechanisms regulating endothelial cell barrier function, Am. J. Physiol. Lung Cell. Mol. Physiol. 279 (2000) 419-422.

[34] M. Palmer, Chan Alice, Dieckmann Thorsten, J. Honek, Wiley, Notes to biochemical pharmacology, http://watcut.uwaterloo.ca/webnotes/Pharmacology/index.html#sec58, (accessed 15/10/06).

[35] A.C. Guyton, J.E. Hall, Textbook of medical physiology, Elsevier Saunders 2006.

[36] C.A. Lipinski, F. Lombardo, B.W. Dominy, P.J. Feeney, Experimental and computational approaches to estimate solubility and permeability in drug discovery and development settings, Adv. Drug Del. Rev. 46 (2001) 3-26.

[37] A.L. Kierszenbaum, L. Tres, Histology and cell biology: An introduction to pathology, 3 ed., Elsevier Health Sciences 2011.

[38] M. Paulsson, Basement membrane proteins: Structure, assembly, and cellular interactions, Crit. Rev. Biochem. Mol. Biol. 27 (1992) 93-127.

[39] F.H. Dost, Der blutspiegel: Kinetik der konzentrationsabläufe in der kreislaufflüssigkeit, Georg Thieme 1953.

[40] J.G. Wagner, History of pharmacokinetics, Pharmacol. Ther. 12 (1981) 537-562.

[41] M. Gibaldi, G. Levy, Pharmacokinetics in clinical practice, J. Am. Med. Assoc. 235 (1976) 1864-1867.

[42] M. Gibaldi, D. Perrier, Pharmacokinetics, Drugs and the Pharmaceutical Sciences, Marcel Dekker Inc., New York, NY, USA 15 (1982).

[43] P.-L. Toutain, A. BOUSQUET-MÉLOU, Volumes of distribution, J. Vet. Pharmacol. Ther. 27 (2004) 441-453.

[44] R.E. Aarnoutse, J.M. Schapiro, C.A.B. Boucher, Y.A. Hekster, D.M. Burger, Therapeutic drug monitoring, Drugs 63 (2003) 741-753.

[45] C.L. Gordon, C. Thompson, J.R. Carapetis, J. Turnidge, C. Kilburn, B.J. Currie, Trough concentrations of vancomycin: Adult therapeutic targets are not appropriate for children, Pediatr. Infect. Dis. J. 31 (2012) 1269-1271.

[46] S. Pichini, I. Altieri, P. Zuccaro, R. Pacifici, Drug monitoring in nonconventional biological fluids and matrices, Clin. Pharmacokinet. 30 (1996) 211-228.

[47] S. Moncada, A. Higgs, The vascular endothelium 1, 2004.

[48] S. Sarem, F. Nekka, I.S. Ahmed, C. Litalien, J. Li, Impact of sampling time deviations on the prediction of the area under the curve using regression limited sampling strategies, Biopharm. Drug Disposition DOI 10.1002/bdd.1951(2015).

[49] A. Jorga, D.W. Holt, A. Johnston, Therapeutic drug monitoring of cyclosporine, Transplant. Proc. 36 (2004) 396-403.

[50] O. David, A. Johnston, Limited sampling strategies, Clin. Pharmacokinet. 39 (2000) 311-311.

[51] W. Sallas, Development of limited sampling strategies for characteristics of a pharmacokinetic profile, J. Pharmacokinet. Biopharm. 23 (1995) 515-529.

[52] W. Jawien, Searching for an optimal auc estimation method: A never-ending task?, Journal of Pharmacokinetics and Pharmacodynamics 41 (2014) 655-673.

[53] S. Schmidt, R. Banks, V. Kumar, K.H. Rand, H. Derendorf, Clinical microdialysis in skin and soft tissues: An update, J. Clin. Pharmacol. 48 (2008) 351-364.

[54] C. Joukhadar, M. Muller, Microdialysis: Current applications in clinical pharmacokinetic studies and its potential role in the future, Clin. Pharmacokinet. 44 (2005) 895-913.

[55] F.J. Azeredo, T. Dalla Costa, H. Derendorf, Role of microdialysis in pharmacokinetics and pharmacodynamics: Current status and future directions, Clin. Pharmacokinet. 53 (2014) 205-212.

[56] M. Brunner, H. Derendorf, M. Muller, Microdialysis for in vivo pharmacokinetic/pharmacodynamic characterization of anti-infective drugs, Current opion in pharmacology 5 (2005) 495-499.

[57] T.L. Bidgood, M.G. Papich, Plasma and interstitial fluid pharmacokinetics of enrofloxacin, its metabolite ciprofloxacin, and marbofloxacin after oral administration and a constant rate intravenous infusion in dogs, J. Vet. Pharmacol. Ther. 28 (2005) 329-341.

[58] G. Leegsma-Vogt, E. Janle, S.R. Ash, K. Venema, J. Korf, Utilization of in vivo ultrafiltration in biomedical research and clinical applications, Life Sci. 73 (2003) 2005-2018.

[59] G. Hauschild, K. Rohn, E. Engelhardt, M. Sager, J. Hardes, G. Gosheger, Pharmacokinetic study on pradofloxacin in the dog - comparison of serum analysis, ultrafiltration and tissue sampling after oral administration, BMC Vet. Res. 9 (2013) 32.

[60] D.M. Foster, M.E. Jacob, C.D. Warren, M.G. Papich, Pharmacokinetics of enrofloxacin and ceftiofur in plasma, interstitial fluid, and gastrointestinal tract of calves after subcutaneous injection, and bactericidal impacts on representative enteric bacteria, J. Vet. Pharmacol. Ther. DOI 10.1111/jvp.12236(2015).

[61] BASi, Bioanalytical Systems, Inc., Microdialysis & in vitro ultrafiltration, https://www.basinc.com/products/iv/MD.html, (accessed 15/10/7).

[62] CMA Microdialysis, Cma microdialysis products, http://www.microdialysis.se/us/products/products, (accessed 15/10/9).

[63] Eicom, Eicom Microdialysis, Microdialysis, http://www.eicom-usa.com/microdialysis-probes, (accessed 15/10/7).

[64] Spectrum Labs, Pore size chart, http://www.spectrumlabs.com/filtration/PoreSize.html, (accessed 15/10/7).

[65] C. Chaurasia, M. Müller, E. Bashaw, E. Benfeldt, J. Bolinder, R. Bullock, P. Bungay, E.M. DeLange, H. Derendorf, W. Elmquist, M. Hammarlund-Udenaes, C. Joukhadar, D. Kellogg, Jr., C. Lunte, C. Nordstrom, H. Rollema, R. Sawchuk, B.Y. Cheung, V. Shah, L. Stahle, U. Ungerstedt, D. Welty, H. Yeo, Aaps-fda workshop white paper: Microdialysis principles, application and regulatory perspectives, Pharm. Res. 24 (2007) 1014-1025.

[66] M. Ellmerer, L. Schaupp, G. Sendlhofer, A. Wutte, G.A. Brunner, Z. Trajanoski, F. Skrabal, P. Wach, T.R. Pieber, Lactate metabolism of subcutaneous adipose tissue studied by open flow microperfusion, J. Clin. Endocrinol. Metab. 83 (1998) 4394-4401.

[67] E. Benfeldt, J. Serup, T. Menné, Microdialysis vs. Suction blister technique for in vivo sampling of pharmacokinetics in the human dermis, Acta Derm. Venereol. 79 (1999) 338-342.

[68] U. Kiistala, Suction blister device for separation of viable epidermis from dermis1, J. Invest. Dermatol. 50 (1968) 129-137.

[69] C. Svedman, J.S. Samara, M.L. Clark, J.C. Levy, K.N. Frayn, Skin mini-erosion technique for monitoring metabolites in interstitial fluid: Its feasability demonstrated by ogtt results in diabetic and non-diabetic subjects, Scand. J. Clin. Lab. Invest. 59 (1999) 115-124.

[70] H.O. Fadnes, R.K. Reed, K. Aukland, Interstitial fluid pressure in rats measured with a modified wick technique, Microvasc. Res. 14 (1977) 27-36.

[71] H.J. Guthe, T. Nedrebo, O. Tenstad, H. Wiig, A. Berg, Effect of topical anaesthetics on interstitial colloid osmotic pressure in human subcutaneous tissue sampled by wick technique, PLoS ONE 7 (2012) e31332.

[72] C. Höfferer, D. Tutkur, C. Fledelius, C.L. Brand, T.J. Alsted, J. Damgaard, E. Nishimura, C.B. Jeppesen, S.I. Mautner, T.R. Pieber, F. Sinner, Open flow microperfusion: Pharmacokinetics of human insulin and insulin detemir in the interstitial fluid of subcutaneous adipose tissue, Diabetes Obes. Metab. 17 (2015) 121-127.

[73] I. Hansen, K. Hakansson, S. Polberger, N. Svenningsen, P. Svedman, Dermally non-invasive suctioning technique for painless serial sampling of interstitial fluid (isf) in newborn infants 1525, Pediatr. Res. 43 (1998) 261-261.

[74] P. Svedman, C. Svedman, Skin mini-erosion sampling technique: Feasability study with regard to serial glucose measurement, Pharm. Res. 15 (1998).

[75] H.K. Sun, C.T. Ong, A. Umer, D. Harper, S. Troy, C.H. Nightingale, D.P. Nicolau, Pharmacokinetic profile of tigecycline in serum and skin blister fluid of healthy subjects after multiple intravenous administrations, Antimicrob. Agents Chemother. 49 (2005) 1629-1632.

[76] D.E. Nix, S.D. Goodwin, C.A. Peloquin, D.L. Rotella, J.J. Schentag, Antibiotic tissue penetration and its relevance: Impact of tissue penetration on infection response, Antimicrob. Agents Chemother. 35 (1991) 1953-1959.

[77] S. Gupta, C. Ajith, A.J. Kanwar, B. Kumar, Surgical pearl: Standardized suction syringe for epidermal grafting, J. Am. Acad. Dermatol. 52 (2005) 348-350.

[78] S. Gupta, S. Shroff, S. Gupta, Modified technique of suction blistering for epidermal grafting in vitiligo, Int. J. Dermatol. 38 (1999) 306-309.

[79] G.D. Chisholm, P.M. Waterworth, J.S. Calnan, L.P. Garrod, Concentration of antibacterial agents in interstitial tissue fluid, Br. Med. J. 1 (1973) 569-573.

[80] J.S. Tan, A. Trott, J.P. Phair, C. Watanakunakorn, A method for measurement of antibiotics in human interstitial fluid, J. Infect. Dis. 126 (1972) 492-497.

[81] S. Jaiswal, S. Muthuswamy, Instability analysis of mosquito fascicle under compressive load with vibrations and microneedle design, Journal of Bionic Engineering 12 (2015) 443-452.

[82] K. Ita, Transdermal delivery of drugs with microneedles-potential and challenges, Pharmaceutics 7 (2015) 90-105.

[83] N.T. Nguyen, S.A. Shaegh, N. Kashaninejad, D.T. Phan, Design, fabrication and characterization of drug delivery systems based on lab-on-a-chip technology, Adv. Drug Del. Rev. DOI 10.1016/j.addr.2013.05.008(2013).

[84] R.F. Donnelly, T.R. Raj Singh, A.D. Woolfson, Microneedle-based drug delivery systems: Microfabrication, drug delivery, and safety, Drug Deliv. 17 (2010) 187-207.

[85] J. McCaffrey, R. Donnelly, H. McCarthy, Microneedles: An innovative platform for gene delivery, Drug Deliv. and Transl. Res. 5 (2015) 424-437.

[86] L. Engelke, G. Winter, S. Hook, J. Engert, Recent insights into cutaneous immunization: How to vaccinate via the skin, Vaccine DOI http://dx.doi.org/10.1016/j.vaccine.2015.05.012.

[87] C.G. Li, K. Lee, C.Y. Lee, M. Dangol, H. Jung, A minimally invasive blood-extraction system: Elastic self-recovery actuator integrated with an ultrahigh- aspect-ratio microneedle, Advanced Materials 24 (2012) 4583-4586.

[88] M.C. P.M. Wang, and M.R. Prausnitz, Minimally invasive extraction of dermal interstitial fluid for glucose monitoring using microneedles, Diabetes Technol. Ther. 7 (2005) 131-141.

[89] M.R. Prausnitz, M.G. Allen, I.J. Gujral, Microneedle device for extraction and sensing of bodily fluids, Google Patents, 2008.

[90] D. Li, H. Yu, X. Huang, F. Huang, X. Hu, K. Xu, Prediction of blood glucose using interstitial fluid extracted by ultrasound and vacuum, Optical Diagnostics and Sensing VII, SPIE, 2007, pp. 1-8.

[91] S. Mitragotri, M. Coleman, J. Kost, R. Langer, Analysis of ultrasonically extracted interstitial fluid as a predictor of blood glucose levels, J. Appl. Physiol. 89 (2000) 961-966.

[92] Y. Haixia, R.C. Roberts, L. Dachao, X. Kexin, N.C. Tien, A pdms interstitial fluid transdermal extraction tool, Nano/Micro Engineered and Molecular Systems (NEMS), 2010 5th IEEE International Conference on, 2010, pp. 1106-1109.

[93] H. Yu, D. Li, R.C. Roberts, K. Xu, N.C. Tien, A time-of-flight flow sensor for the volume measurement of trace amount of interstitial fluid, J. Micromech. Microeng. 22 (2012) 055009 (055007pp).

[94] E.V. Mukerjee, S.D. Collins, R.R. Isseroff, R.L. Smith, Microneedle array for transdermal biological fluid extraction and in situ analysis, Sens. Actuators A 114 (2004) 267-275.

[95] C.D. Chin, V. Linder, S.K. Sia, Commercialization of microfluidic point-of-care diagnostic devices, Lab Chip 12 (2012) 2118-2134.

[96] S. Haeberle, R. Zengerle, Microfluidic platforms for lab-on-a-chip applications, Lab Chip 7 (2007) 1094-1110.

[97] Y. Xia, G.M. Whitesides, Soft lithography, Annu. Rev. Mater. Sci. 28 (1998) 153-184.

[98] R. Kane, A. Stroock, N. Jeon, D.E. Ingber, G.M. Whitesides, Soft lithography and microfluidics, Optical Biosensors: Present and Future, FS Ligler and CA Rowe Taitt (editors), Elsevier Science, BV, Amsterdam, Netherlands DOI (2002) 571-595.

[99] B.P. Casavant, E. Berthier, A.B. Theberge, J. Berthier, S.I. Montanez-Sauri, L.L. Bischel, K. Brakke, C.J. Hedman, W. Bushman, N.P. Keller, D.J. Beebe, Suspended microfluidics, Proceedings of the National Academy of Sciences 110 (2013) 10111-10116.

[100] C.W. Oomens, D.H. van Campen, H.J. Grootenboer, A mixture approach to the mechanics of skin, J. Biomech. 20 (1987) 877-885.

[101] A.C. Guyton, H.J. Granger, A.E. Taylor, Interstitial fluid pressure, Physiol. Rev. 51 (1971) 527-563.

[102] R.G. Harrison, T.A. Massaro, Water flux through porcine aortic tissue due to a hydrostatic pressure gradient, Atherosclerosis 24 (1976) 363-367.

[103] R.T. Tregear, P. Dirnhuber, Viscous flow in compressed human and rat skin1, J. Invest. Dermatol. 45 (1965) 119-125.

[104] C.A. Wiederhielm, The interstitial space, Biomechanics: Its Foundations and Objectives DOI (1972) 273-286.

[105] T.H. da Costa, E. Song, R.P. Tortorich, J.-W. Choi, A paper-based electrochemical sensor using inkjet-printed carbon nanotube electrodes, ECS J. Solid State Sci. Technol. 4 (2015) S3044-S3047.

[106] S. Nantaphol, O. Chailapakul, W. Siangproh, A novel paper-based device coupled with a silver nanoparticle-modified boron-doped diamond electrode for cholesterol detection, Anal. Chim. Acta DOI http://dx.doi.org/10.1016/j.aca.2015.08.007(2015).

[107] U. Kiistala, The suction blister method for the in-vivo separation of epidermis from dermis in human skin (Doctoral Thesis), Helsinki (1976).

[108] B.J. Vermeer, F.C. Reman, C.M. van Gent, The determination of lipids and proteins in suction blister fluid, J. Invest. Dermatol. 73 (1979) 303-305.

[109] N. Rossing, A.-M. Worm, Interstitial fluid: Exchange of macromolecules between plasma and skin interstitium, Clin. Physiol. 1 (1981) 275-284.

[110] J. Cahill, J. Campbell, R. Crouch, S. Cumming, S. Harrison, K. Merlin, F. Peter, A comparison of cryotherapy and imiquimod for treatment of actinic keratoses: Lesion clearance, safety, and skin quality outcomes, J. Drugs Dermatol. 10 (2011) 1432-1438.

[111] N. Tomson, J. Sterling, I. Ahmed, J. Hague, J. Berth-Jones, Human papillomavirus typing of warts and response to cryotherapy, J. Eur. Acad. Dermatol. Venereol. 25 (2011) 1108-1111.

[112] A. Essalik, A. Dussault, J.E. Essalik, Non-invasive biomedical detection and monitoring systems, Google Patents, 2012.

[113] B. Stoeber, Microneedles: A solid-state interface with the human body, in: K. Iniewski (Ed.) Vlsi circuits for biomedical applications, Artech House Inc., Boston, 2008, pp. 145-163.

[114] M.R. Prausnitz, Microneedles for transdermal drug delivery, Adv. Drug Del. Rev. 56 (2004) 581-587.

[115] S.N. Thennadil, J.L. Rennert, B.J. Wenzel, K.H. Hazen, T.L. Ruchti, M.B. Block, Comparison of glucose concentration in interstitial fluid and capillary and venous blood during rapid changes in blood clucose levels, Diabetes Technol. Ther. 3 (2001) 357-366.

[116] Y. Yoon, J. Kim, K. Lee, H. Song, K. Yoo, G. Lee, J. Lee, A novel microneedle-based non- enzymatic glucose sensor for painless diabetes testing application, Solid-State Sensors, Actuators and Microsystems (TRANSDUCERS), 2011, pp. 2164-2167.

[117] F.D. Zimmermann S., Stoeber B., Flounders A.W., and Liepmann D., , A microneedle-based glucose monitor: Fabricated on a wafer-level using in-device enzyme immobilization, Solid-State Sensors, Actuators and Microsystems (TRANSDUCERS), , 2003, pp. 99-102.

[118] U.O. Häfeli, M.H.H. Ensom, T.K.L. Kiang, B. Stoeber, B.A. Chua, M. Pudek, V. Schmitt, Comparison of vancomycin concentrations in blood and interstitial fluid: A possible model for less invasive therapeutic drug monitoring, Clin. Chem. Lab. Med. 49 (2011) 2123-2125.

[119] R.K. Sivamani, B. Stoeber, D. Liepmann, H.I. Maibach, Microneedle penetration and injection past the stratum corneum in humans, J. Dermatolog. Treat. 20 (2009) 156-159.

[120] P.M. Wang, M. Cornwell, J. Hill, M.R. Prausnitz, Precise microinjection into skin using hollow microneedles, J. Invest. Dermatol. 126 (2006) 1080-1087.

[121] M. Yang, J. Zahn, Microneedle insertion force reduction using vibratory actuation, Biomed. Microdevices 6 (2004) 177-182.

[122] R.L. Anderson, J.M. Cassidy, Variations in physical dimensions and chemical composition of human stratum corneum, J. Invest. Dermatol. 61 (1973) 30-32.

[123] J. Sandby-Møller, T. Poulsen, H.C. Wulf, Epidermal thickness at different body sites: Relationship to age, gender, pigmentation, blood content, skin type and smoking habits, Acta Derm. Venereol. 83 (2003) 410-413.

[124] U. Jacobi, M. Kaiser, R. Toll, S. Mangelsdorf, H. Audring, N. Otberg, W. Sterry, J. Lademann, Porcine ear skin: An in vitro model for human skin, Skin Res. Technol. 13 (2007) 19-24.

[125] W. Meyer, Comparative histological and histochemical investigations in the skin of the wild boar, domestic pigs and miniature pigs, Archiv fuer tieraerztliche Fortbildung (Germany, FR) 9 (1986) 232.

[126] I. Gersh, H.R. Catchpole, The nature of ground substance of connective tissue, Perspect. Biol. Med. 3 (1960) 282-319.

[127] A. Dasgupta, G. Tso, L. Chow, Comparison of mycophenolic acid concentrations determined by a new petinia assay on the dimension exl analyzer and a hplc-uv method, Clin. Biochem. 46 (2013) 685-687.

[128] J.C. Weaver, Y.A. Chizmadzhev, Theory of electroporation: A review, Bioelectrochem. Bioenerg. 41 (1996) 135-160.

[129] Thermo Scientific, Nanodrop2000 reproducibility data sheet, http://www.nanodrop.com/Library/NanoDrop%202000%20Reproducibility%20Performance%20Data.pdf, (accessed 15/10/7).

[130] S.J. Konopka, B. McDuffie, Diffusion coefficients of ferri- and ferrocyanide ions in aqueous media, using twin-electrode thin-layer electrochemistry, Anal. Chem. 42 (1970) 1741-1746.

[131] S.C. Jacobson, R. Hergenroder, L.B. Koutny, R.J. Warmack, J.M. Ramsey, Effects of injection schemes and column geometry on the performance of microchip electrophoresis devices, Anal. Chem. 66 (1994) 1107-1113.

[132] J.H. Chang, N.C. Hogan, I.W. Hunter, A needle-free technique for interstitial fluid sample acquisition using a lorentz-force actuated jet injector, J. Controlled Release DOI (2015).

[133] J.M. Varghese, P. Jarrett, R.J. Boots, C.M. Kirkpatrick, J. Lipman, J.A. Roberts, Pharmacokinetics of piperacillin and tazobactam in plasma and subcutaneous interstitial fluid in critically ill patients receiving continuous venovenous haemodiafiltration, Int. J. Antimicrob. Agents 43 (2014) 343-348.

[134] C. Joukhadar, M. Frossard, B.X. Mayer, M. Brunner, N. Klein, P. Siostrzonek, H.G. Eichler, M. Müller, Impaired target site penetration of β -lactams may account for therapeutic failure in patients with septic shock, Crit. Care Med. 29 (2001) 385-391.

[135] D. Hutschala, K. Skhirtladze, A. Zuckermann, W. Wisser, P. Jaksch, B.X. Mayer-Helm, H. Burgmann, E. Wolner, M. Müller, E.M. Tschernko, In vivo measurement of levofloxacin penetration into lung tissue after cardiac surgery, Antimicrob. Agents Chemother. 49 (2005) 5107-5111.

[136] G.L. Trainor, The importance of plasma protein binding in drug discovery, Exp. Op. Drug Disc. 2 (2007) 51-64.

[137] M. Müller, A. dela Peña, H. Derendorf, Issues in pharmacokinetics and pharmacodynamics of anti-infective agents: Distribution in tissue, Antimicrob. Agents Chemother. 48 (2004) 1441-1453.

[138] M. Rybak, The pharmacokinetic and pharmacodynamic properties of vancomycin, Clin. Infect. Dis. 42 (2006) 35-39.

[139] M. Rybak, B. Lomaestro, J.C. Rotschafer, R. Moellering, W. Craig, M. Billeter, J.R. Dalovisio, D.P. Levine, Therapeutic monitoring of vancomycin in adult patients: A consensus review of the american society of health-system pharmacists, the infectious diseases society of america, and the society of infectious diseases pharmacists, Am. J. Health. Syst. Pharm. 66 (2009) 82-98.

[140] J.J. Schentag, Gentamicin dispositions and tissue accumulation on multiple dosing, J. Pharmacokinet. Biopharm. 5 (1977) 559-577.

[141] S.J. Jerome, Gentamicin tissue accumulation and nephrotoxic reactions, DOI (1978).

[142] T.K. Kiang, M.H. Ensom, A qualitative review on the pharmacokinetics of antibiotics in saliva: Implications on clinical pharmacokinetic monitoring in humans, Clin. Pharmacokinet. DOI 10.1007/s40262-015-0321-z(2015).

[143] L. Kagan, P. Gershkovich, A. Mendelman, S. Amsili, N. Ezov, A. Hoffman, The role of the lymphatic system in subcutaneous absorption of macromolecules in the rat model, Eur. J. Pharm. Biopharm. 67 (2007) 759-765.

[144] B.A. Chabner, J. Bertino, J. Cleary, T. Ortiz, A. Lane, J.G. Supko, D. Ryan, Chapter 61. Cytotoxic agents, in: L.L. Brunton, B.A. Chabner, B.C. Knollmann (Eds.) Goodman & gilman's the pharmacological basis of therapeutics, 12e, The McGraw-Hill Companies, New York, NY, 2011.

[145] I.-S. Song, N. Savaraj, Z.H. Siddik, P. Liu, Y. Wei, C.J. Wu, M.T. Kuo, Role of human copper transporter ctr1 in the transport of platinum-based antitumor agents in cisplatin-sensitive and cisplatin-resistant cells, Mol. Cancer Ther. 3 (2004) 1543-1549.

[146] T.C. Johnstone, S.J. Lippard, Improvements in the synthesis and understanding of the iodo-bridged intermediate en route to the pt(iv) prodrug satraplatin, Inorg. Chim. Acta 424 (2015) 254-259.

[147] A. Bhargava, U.N. Vaishampayan, Satraplatin: Leading the new generation of oral platinum agents, Expert Opin. Investig. Drugs 18 (2009) 1787-1797.

[148] J.O. McNamara, Chapter 21. Pharmacotherapy of the epilepsies, in: L.L. Brunton, B.A. Chabner, B.C. Knollmann (Eds.) Goodman & gilman's the pharmacological basis of therapeutics, 12e, The McGraw-Hill Companies, New York, NY, 2011.

[149] F. Girardin, Membrane transporter proteins: A challenge for cns drug development, Dialogues Clin. Neurosci. 8 (2006) 311-321.

[150] A.M. Krensky, W.M. Bennett, F. Vincenti, Chapter 35. Immunosuppressants, tolerogens, and immunostimulants, in: L.L. Brunton, B.A. Chabner, B.C. Knollmann (Eds.) Goodman & gilman's the pharmacological basis of therapeutics, 12e, The McGraw-Hill Companies, New York, NY, 2011.

[151] L.M. Shaw, M. Figurski, M.C. Milone, J. Trofe, R.D. Bloom, Therapeutic drug monitoring of mycophenolic acid, Clin. J. Am. Soc. Nephro. 2 (2007) 1062-1072.

[152] P.H. Hinderling, Red blood cells: A neglected compartment in pharmacokinetics and pharmacodynamics, Pharmacol. Rev. 49 (1997) 279-295.

[153] G. Filler, I. Mai, Limited sampling strategy for mycophenolic acid area under the curve, Ther. Drug. Monit. 22 (2000).

[154] E.K. Todorova, S.-H.S. Huang, M.C. Kobrzynski, G. Filler, What is the intrapatient variability of mycophenolic acid trough levels?, Pediatr. Transplant. DOI 10.1111/petr.12559(2015).

[155] B.A. Miller, E.A. Clements, Chapter 23. Pharmacology of antiarrhythmics, in: J.E. Tintinalli, J.S. Stapczynski, O.J. Ma, D.M. Cline, R.K. Cydulka, G.D. Meckler, T.A.C.o.E. Physicians (Eds.) Tintinalli's emergency medicine: A comprehensive study guide, 7e, The McGraw-Hill Companies, New York, NY, 2011.

[156] G.M. Currie, J.M. Wheat, H. Kiat, Pharmacokinetic considerations for digoxin in older people, Open Cardiovasc. Med. J. 5 (2011) 130-135.

[157] C. Gresham, D.E. Brooks, Chapter 186. Methylxanthines and nicotine, in: J.E. Tintinalli, J.S. Stapczynski, O.J. Ma, D.M. Cline, R.K. Cydulka, G.D. Meckler, T.A.C.o.E. Physicians (Eds.) Tintinalli's emergency medicine: A comprehensive study guide, 7e, The McGraw-Hill Companies, New York, NY, 2011.

[158] Medscape, http://www.medscape.org/, (accessed 15/10/7).

[159] L.L. Brunton, Goodman & gilman's the pharmacological basis of therapeutics, The McGraw-Hill Companies, New York, NY, 2011.

[160] X. Li, F. Wang, B. Xu, X. Yu, Y. Yang, L. Zhang, H. Li, Determination of the free and total concentrations of vancomycin by two-dimensional liquid chromatography and its application in elderly patients, J. Chromatogr. B. 969 (2014) 181-189.

[161] Y. Cao, J. Yu, Y. Chen, J. Zhang, X. Wu, Y. Zhang, G. Li, Development and validation of a new ultra-performance liquid chromatographic method for vancomycin assay in serum and its application to therapeutic drug monitoring, Ther. Drug. Monit. 36 (2014) 175-181.

[162] I.L. Tsai, H.-Y. Sun, G.-Y. Chen, S.-W. Lin, C.-H. Kuo, Simultaneous quantification of antimicrobial agents for multidrug-resistant bacterial infections in human plasma by ultra-high-pressure liquid chromatography-tandem mass spectrometry, Talanta 116 (2013) 593-603.

[163] M. Hagihara, C. Sutherland, D.P. Nicolau, Development of hplc methods for the determination of vancomycin in human plasma, mouse serum and bronchoalveolar lavage fluid, J. Chromatogr. Sci. 51 (2013) 201-207.

[164] R.T. Cass, J.S. Villa, D.E. Karr, D.E. Schmidt, Rapid bioanalysis of vancomycin in serum and urine by high-performance liquid chromatography tandem mass spectrometry using on-line sample extraction and parallel analytical columns, Rapid Commun. Mass Spectrom. 15 (2001) 406-412.

[165] K. Konig, U. Kobold, G. Fink, A. Leinenbach, T. Dulffer, R. Thiele, J. Zander, M. Vogeser, Quantification of vancomycin in human serum by lc-ms/ms, Clin. Chem. Lab. Med. 51 (2013) 1761-1769.

[166] V. Shah, K. Midha, J.A. Findlay, H. Hill, J. Hulse, I. McGilveray, G. McKay, K. Miller, R. Patnaik, M. Powell, A. Tonelli, C.T. Viswanathan, A. Yacobi, Bioanalytical method validation— a revisit with a decade of progress, Pharm. Res. 17 (2000) 1551-1557.

[167] M. Zhang, Determination of vancomycin in human plasma, bone and fat by liquid chromatography/tandem mass spectrometry, J. Anal. Bioanal. Tech. 5 (2014) 1-9.

[168] C. Cheng, S. Liu, D. Xiao, J. Hollembaek, L. Yao, J. Lin, S. Hansel, Lc-ms/ms method development and validation for the determination of polymyxins and vancomycin in rat plasma, J. Chromatogr. B. 878 (2010) 2831-2838.

[169] R. Cazorla-Reyes, R. Romero-Gonzalez, A.G. Frenich, M.A. Rodriguez Maresca, J.L. Martinez Vidal, Simultaneous analysis of antibiotics in biological samples by ultra high performance liquid chromatography-tandem mass spectrometry, J. Pharm. Biomed. Anal. 89 (2014) 203-212.

[170] B.M. Henriet T, Liquid chromatography–tandem mass spectrometry for simultaneous determination of ticarcillin and vancomycin in presence of degradation products. Application to the chemical stability monitoring of ticarcillin- vancomycin solutions, J. Chromatogr. Sep. Tech. 05 (2014) 1-6.

[171] N. Shibata, M. Ishida, Y. Venkata Rama Prasad, W. Gao, Y. Yoshikawa, K. Takada, Highly sensitive quantification of vancomycin in plasma samples using liquid chromatography– tandem mass spectrometry and oral bioavailability in rats, J. Chromatogr. B. 789 (2003) 211-218.

[172] I. Baranowska, A. Wilczek, J. Baranowski, Rapid uhplc method for simultaneous determination of vancomycin, terbinafine, spironolactone, furosemide and their metabolites: Application to human plasma and urine, Analyt. Sci. 26 (2010) 755-759.

[173] J. Rossmann, S. Schubert, R. Gurke, R. Oertel, W. Kirch, Simultaneous determination of most prescribed antibiotics in multiple urban wastewater by spe-lc-ms/ms, J. Chromatogr. B. 969 (2014) 162-170.

[174] S. Tamura, A. Ohike, R. Ibuki, G.L. Amidon, S. Yamashita, Tacrolimus is a class ii low-solubility high-permeability drug: The effect of p-glycoprotein efflux on regional permeability of tacrolimus in rats, J. Pharm. Sci. 91 (2002) 719-729.

[175] M.H. Ensom, D. Décarie, Stability of extemporaneously compounded levetiracetam in glass and plastic bottles and plastic syringes, Can. J. Hosp. Pharm. 68 (2015).

[176] M.H.H. Ensom, J. Kendrick, S. Rudolph, D. Decarie, Stability of propranolol in extemporaneously compounded suspensions, Can. J. Hosp. Pharm. 66 (2013) 118-124.

[177] E. Demetrius, Clinical use of tacrolimus (fk-506) in infants and children with renal transplants, Pediatr. Nephrol. 9 (1995) 487-494.

[178] D. Taormina, H.Y. Abdallah, R. Venkataramanan, L. Logue, G.J. Burckart, R.J. Ptachcinski, S. Todo, J.J. Fung, T.E. Starzl, Stability and sorption of fk 506 in 5% dextrose

injection and 0.9% sodium chloride injection in glass, polyvinyl chloride, and polyolefin containers, Am. J. Hosp. Pharm. 49 (1992) 119-122.

[179] D.D. Cunningham, J.A. Stenken, In vivo glucose sensing, John Wiley & Sons, Inc., Hoboken, NJ, USA, 2009.

[180] X.H. Yu, D.C. Li, R.C. Roberts, W.S. Liang, K.X. Xu, N.C. Tien, An integrated microfluidic system for interstitial fluid transdermal extraction, Solid-State Sensors, Actuators and Microsystems (TRANSDUCERS), 2011, pp. 4.

[181] T.K. Kiang, U.O. Häfeli, M.H. Ensom, A comprehensive review on the pharmacokinetics of antibiotics in interstitial fluid spaces in humans: Implications on dosing and clinical pharmacokinetic monitoring, Clin. Pharmacokinet. 53 (2014) 695-730.
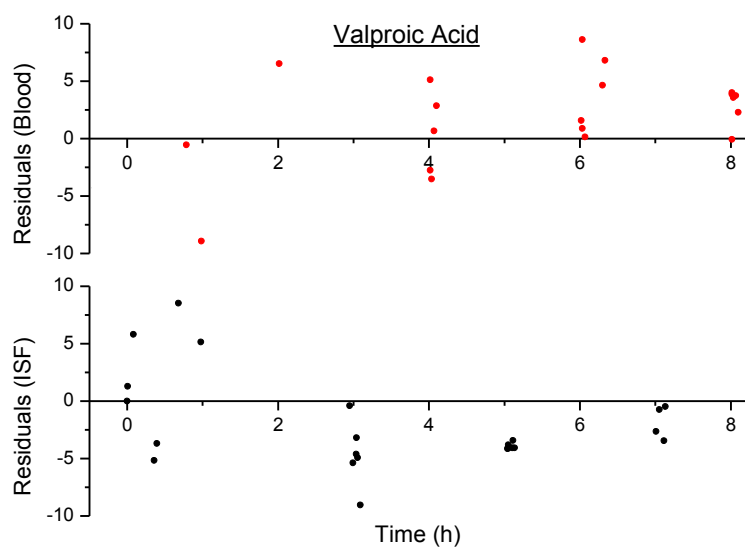
Appendix

This is a collection of residual plots for the compartmental analyses in chapter 3.3.
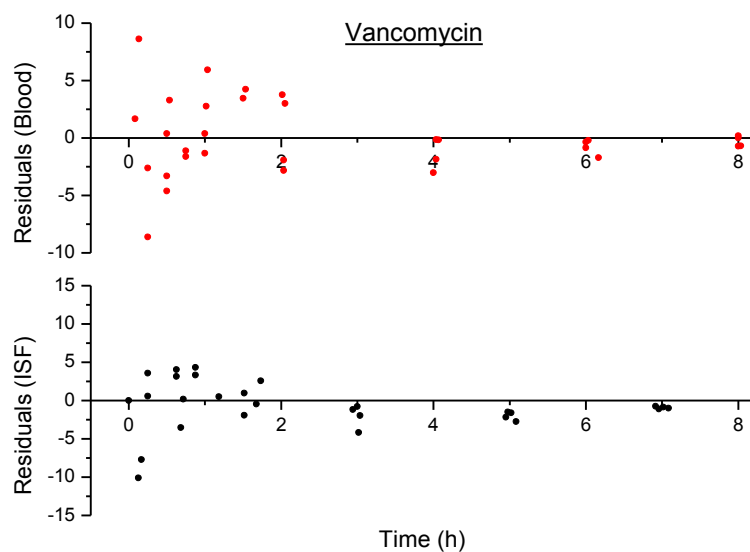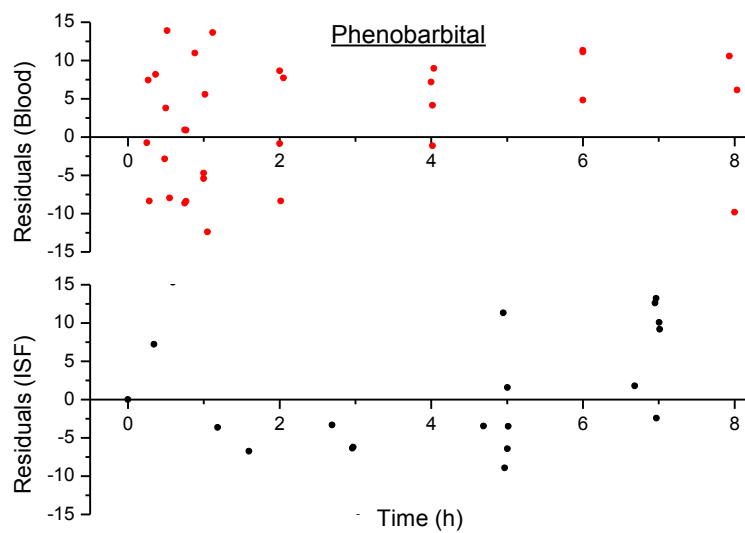

Figure 75. Residuals (model-predicted concentrations minus measured concentrations) plotted against time for vancomycin.
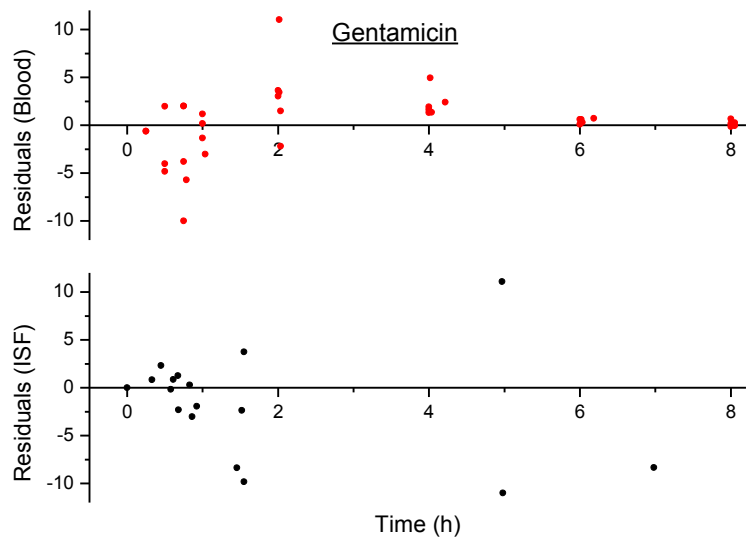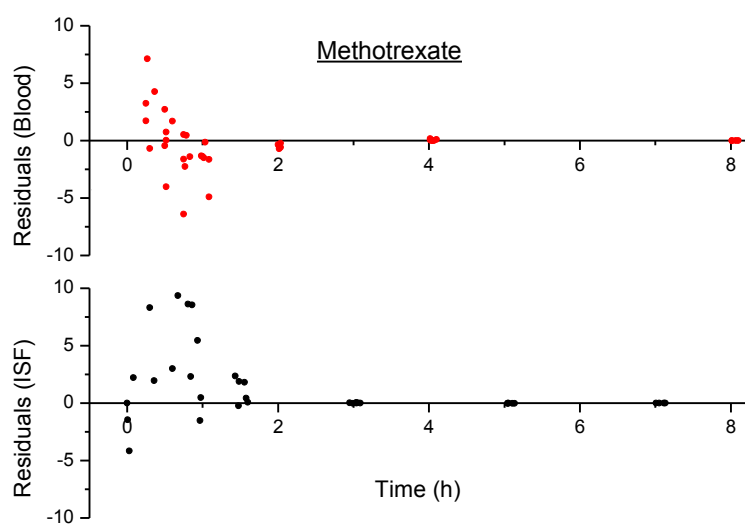

Figure 76. Residuals (model-predicted concentrations minus measured concentrations) plotted against time for gentamicin.
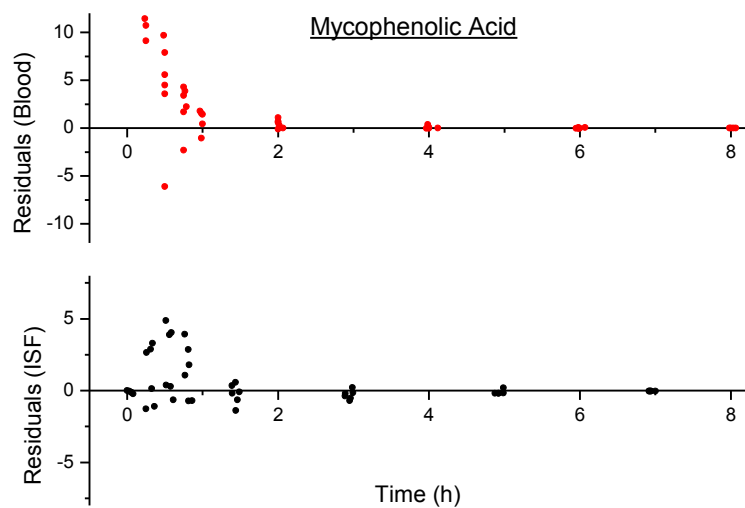
Figure 77. Residuals (model-predicted concentrations minus measured concentrations) plotted against time for valproic acid.
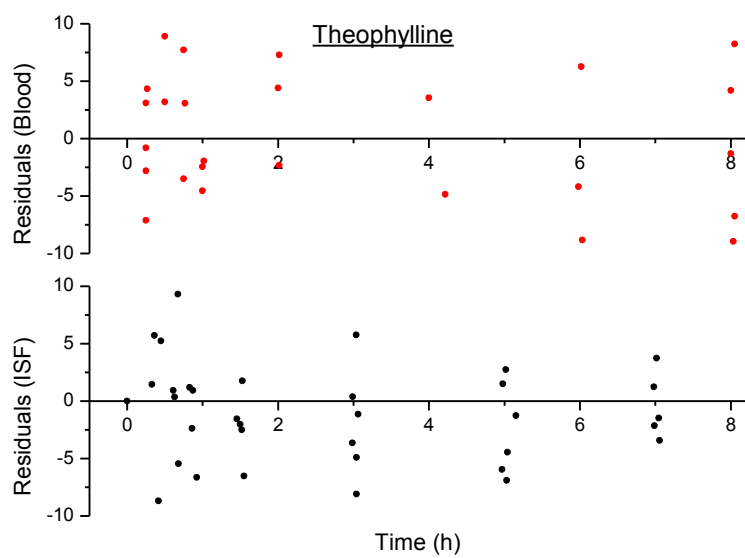

Figure 78. Residuals (model-predicted concentrations minus measured concentrations) plotted against time for phenobarbital.
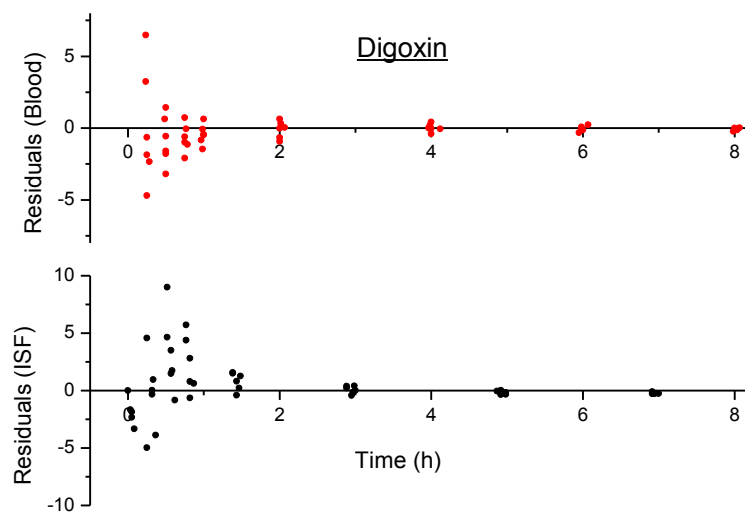
Figure 79. Residuals (model-predicted concentrations minus measured concentrations) plotted against time for methotrexate.

Figure 80. Residuals (model-predicted concentrations minus measured concentrations) plotted against time for mycophenolic acid.

Figure 81. Residuals (model-predicted concentrations minus measured concentrations) plotted against time for theophylline.

Figure 82. Residuals (model-predicted concentrations minus measured concentrations) plotted against time for digoxin.